Dynamic Response of Small Turbine Flowmeters in Pulsating Liquid Flows

Volume 1

Submitted for the Degree of Doctor of Philosophy

Betty Lee

Department of Systems Engineering

Brunel University

September 2002

Abstract

The dynamic response of turbine flowmeters in low pressure gas flows (i.e. where the rotational inertia of the fluid is negligible) is well understood and methods for correcting meter signals for a lack of response are available. For liquid flows there has been a limited amount of experimental work on the response of meters to step changes but no reports have been found of the response of meters to sinusoidally pulsating flows.

"Small" turbine meters are expected to behave differently from "large" meters for a number of reasons: a smaller meter would generally have: (1) a larger percentage of tip clearance leakage flow; (2) less fluid momentum between the meter blading; and, (3) less fluid friction forces on the effective surface area. In this research, arbitrarily, meters up to size 25 mm were defined as small; and within this study, meters of size 6 mm to 25 mm were investigated.

The aim of the research was to investigate and to understand the response of small turbine meters to pulsating liquid flows and to provide methods for correction. Three approaches were used: (1) application of an existing theoretical model of turbine meter behaviour; (2) an experimental investigation of meter performance in pulsating flows; and (3) simulation of flow behaviour through one selected meter using CFD and extending the simulation to predict the rotor dynamics and, hence, the response of this meter to specified cases of pulsating flow.

A theoretical model developed by Dijstelbergen (1966) assumes frictionless behaviour and that flow is perfectly guided by meter blading through the rotor and that fluid within the rotor envelope rotates as a "solid body". Results from this theoretical model applied for pulsating flows showed that there was likely to be positive error in predicted mean flow rate (over-registration) and negative error for predicted values of the amplitude of the pulsations (amplitude attenuation). This behaviour is due to the fundamental asymmetry between flows with increasing and decreasing angle of attack relative to the meter blades, throughout a pulsation cycle.

This qualitative behaviour was confirmed by experimental work with meters up to size 25mm working with pulsation frequencies up to 300 Hz. For low frequency pulsations

(below 10 Hz), the over-registration errors were within the limits of specified meter accuracy. At higher frequencies and larger pulsation amplitudes, the largest over-registration observed was 5.5 % and amplitude attenuation could be as large as 90 %. The dependence of these errors on both the flow pulsation amplitude and frequency were investigated. The theoretical model was also used as a basis for generating correction procedures, to be applied to both the mean flow and the pulsation amplitude measurements.

The results from the CFD simulation showed qualitative good agreement with the experimental data. The same kind of meter error trends were observed and it was shown to provide a better correlation with the experimental trends than the theoretical model derived from Dijstelbergen. From the CFD simulation, the causes of over-registration and amplitude attenuation in turbine flowmetering were understood through the investigation of rotor dynamics coupled with fluid behaviour around meter blading within the pulsation cycle. The CFD results were used to evaluate fluid angular momentum flux and to review the validity of the assumption that fluid within the rotor "envelope" rotated as a solid body.

For the case investigated, whilst the assumption that flow is perfectly guided is not inappropriate, the volume of fluid assumed to rotate as a "solid body" was found to be significantly less than the rotor envelope volume.

Acknowledgements

I would like to take this opportunity to express my deepest gratitude to Prof. Colin Clark for his excellent technical supervision during the course of this project. I must also thank him for his valuable comments, support, and motivation in the completion of the thesis; and I am also very thankful for his advice and enormous encouragement throughout the difficult periods of my Ph. D.

I would also like to thank Dr. Robert Cheesewright for his valuable contribution into my experimental work. His enormous input, helpful suggestions and comments on the work made a significant difference to my understanding of the methodology and correction procedure that was implemented on the meter indicated reading.

I am also very grateful to Dr. Jerry Ismael for his greatest interest in my CFD work. His tremendous contribution, support, encouragement and comments on the work made an immense difference not only to my understanding of the various practical analyses achieved from the CFD modelling results, but also to the achievement of further improvement of the theoretical model that has been used in the present research work.

I would also like to thank the departmental technicians, in particular Mr. Paul Chapman for their help in setting up and making changes to the flow rig used in this work. My thanks also go to my helpful and friendly colleague Douglas Bisset, Daniel Hamilton, Carola Konig and Humphrey Pasley.

I am also indebted to my parents for their greatest support, loving and care; and my brother for his persistent encouragement in the completion of the thesis. I would also like to thank my dearest friends (too many to include) for their incredible moral support.

This thesis is dedicated to Cherry Lee (1988-2001) and also to my mum and dad.

Publications relating to this work

The following paper is attached in this thesis in Appendix E.

Lee, B., Cheesewright, R. and Clark, C. The dynamic response of turbine flowmeters in liquid flows. Fluid Control, Measurement and Visualization (FLUCOME) 2000 Symposium, Canada. (2000) August.

Contents

Table of Figures

Table of Tables

Nomenclature

Acronyms

C	corrected meter data
E	experimental meter data
P	predicted meter data
rms	root mean square
S	CFD simulated meter data
URF	under relaxation factor

Subscripts

a	actual reading
abs	absolute
c	case
h	hub
in	inlet
m	meter indicated reading
max	maximum
min	minimum
out	outlet
pk-pk	peak-to-peak
r	radius at measurement point
rel	relative
s	CFD simulated meter indicated reading
t	tip
0	zero flow condition

Symbols

α_p	relative pulsation amplitude
β_i	blade incidence angle ($=\beta_r - \phi_{in}$)
β_r	blade angle at radius, r
γ_m	mean flow angle
ε	energy dissipation rate

η	blade deviation factor
θ	angle, angular position of the blade relative to the pick-up
λ	ratio of inertias, $(=I_f / I_R)$
μ	dynamic viscosity
μ_t	effective viscosity
ν	kinematic viscosity
ρ	density
φ	peak-to-peak flow pulsation amplitude
ϕ	relative flow angle
ω	rotational speed
A	area, annular area
AA	amplitude attenuation error, $\left(=\frac{\varphi_a - \varphi_m}{\varphi_a} \times 100\%\right)$
$d\boldsymbol{A}$	elemental area vector
b	meter response parameter, $\left(=I_R / \rho \bar{r}^2\right)$
B	hub height, dimensionless response parameter
$\boldsymbol{B}$	body force
c	length of chord
C_D	drag coefficient
C_f	skin friction coefficient
C_L	lift coefficient
D	drag
e	voltage response
F	dimensionless flow, $\left(=\dot{V}_m / \overline{\dot{V}_a}\right)$
f_b	blade passing frequency
F_f	total fluid force acting at $\bar{r}$
f_p	pulsation frequency
F_x	force acting in x-direction
F_y	force acting in y-direction
$H(t)$	unit step function
I_f	inertia of fluid
I_R	inertia of rotor

K	meter calibration factor
k	turbulence kinetic energy
L	lift
N	number of blades
OR	over-registration error, $\left(= \frac{\overline{\dot{V}_m} - \overline{\dot{V}_a}}{\overline{\dot{V}_a}} \times 100\% \right)$
P	pressure
P_v	vapour pressure of the liquid
Δp	differential pressure
$\bar{r}$	root mean square radius
Δr	differential radius
Re	Reynolds number
ΔR	differential resistance
s	blade spacing
t	time
T	torque, period
T_B	bearing retarding torque
t_c	time constant
T_d	driving torque
T_f	fluid drag
T_b	rotor hub fluid drag torque
T_m	magnetic pickup retarding torque
T_N	net torque
T_n	non-fluid drag
T_r	resistance drag torque
T_t	blade tip clearance drag torque
T_w	hub disc friction drag torque
$\overline{U}$	mean velocity
$\langle \overline{U} \rangle$	phase mean velocity
U_b	blade velocity
U'	fluctuating velocity
U_∞	freestream velocity
U_x	velocity in axial direction

U_r	velocity in radial direction
U_θ	velocity in θ direction
$\dot{V}$	volume flow rate
$\overline{\dot{V}}$	mean volume flow rate
W_b	relative velocity at the hub
x_i	time series of values of actual volume flow
y_i	time series of values of meter indicated volume flow

Chapter 1 Introduction

In this chapter the historical background to flow measurement will be introduced. The occurrence of pulsating flows will be discussed and a definition of the particular pulsating flow condition in this research will be reviewed. Finally, a qualitative description of a turbine flowmeter will be given and a number of representative industrial applications will be outlined.

1.1 Flow Measurement — An Historical Perspective

1.1.1 From the Egyptian Period until now

From the construction of the Egyptian water irrigation systems for agriculture purposes, and reservoirs and massive canal systems designed to prevent floods in China in 1500 B.C., to the rationing of water by the Romans for fiscal benefits, evidence of flow measurement can be found in the engineering feats achieved by civilisations through different eras of human history. (Bean 1966)

The first recorded understanding of fluid dynamics occurred in ancient Greece. Aristotle (384-322 B.C.) established the basic concept of "fluid dynamic drag"; Archimedes (287-212 B.C.) recognised the elementary principles of "buoyancy" and "pressure gradient" over a length of fluid in motion (Rouse 1963). A later era of fluid mechanics started in the Renaissance period, Leonardo Da Vinci (1452 – 1519) being the first to show any quantitative understanding of fluid dynamics. He gave the first mathematical description of "continuity"; observed and sketched many basic flow phenomena, and suggested designs for a hydraulic pump (Anderson 1998).

The beginning of the eighteenth century is marked by the "Age of enlightenment", during which scientists made huge advances in scientific knowledge. Isaac Newton (1642-1727) having already proven the existence of gravitational force and stated the three laws of motion, introduced new approaches to scientific enquiry which encouraged many scientists to follow. Daniel Bernoulli (1700-1782) unleashed the ideas of "hydrodynamics" on the world. Euler (1707 – 1783) and Venturi (1746 – 1822), further developed these ideas into

what is now known as Hydrodynamics. During the same period, the discovery of a force associated with linear motion in a rotating reference frame was made by Gaspard Gustave de Coriolis (1792-1843).

These provided the fundamental basis for many flowmeters developments. There were first the positive displacement meters, propeller type meters, and then the differential pressure meters represented by venturi tubes or thin-plate orifices, etc. More recent developments are the Magnetic flowmeter (1950's) (Baker 2000); the Ultrasonic Doppler flowmeter and Ultrasonic "transit time" flowmeter (1950's to 1960's) (Baker 2000), and the Coriolis mass flowmeter (1953) (Wilson 1991).

During the last twenty years, flowmeter accuracies have been improved incrementally, including the use of microprocessors and sensors, and for some meters (e.g. Coriolis mass flowmeter), there has been a move towards using digital signal processing.

1.1.2 Pulsating flow measurement and the occurrence of pulsating flows

The history of pulsating flow measurement research is as old as the history of industrial flow measurement (Mottram 1992). There are papers reporting the difficulties of making accurate flow measurement in the presence of pulsation dating back to the 1920s (Oppenheim and Chilton 1955), when reciprocating steam engines and compressors were producing low frequency, high amplitude flow pulsations.

In the same period, pressures have grown significantly towards achieving ever higher standards of flow measurement accuracy. Thus the interest in understanding pulsation effects on flowmeters and reducing metering errors due to pulsation has increased.

However, the characteristic of typical industrial pulsating flow behaviour has changed progressively, apart from applications using low frequency diaphragm and reciprocating pump, mostly it consists of a high frequency and low amplitude pattern. This is mainly due to the advent of rotary positive displacement machines. Also, the proliferation of automatic flow control systems which include components (e.g. valves and regulators), which may be driven into oscillations, thus producing flow pulsations which can affect the associated flowmeter.

According to BS ISO TR 3313 (1998), pulsations may be induced in the following machines, pipeline fittings, and operations:

(i) Rotary or reciprocating positive displacement engines, compressors, blowers and pumps.

(ii) Vibrations, particularly at resonance, of pipe runs and flow control equipment.

(iii) Periodic actions of flow controllers, e.g. valve 'hunting' and governor oscillations.

(iv) Flow separation within pipe fittings, valves, or rotary machines (e.g. compressor surge).

(v) Hydrodynamic oscillations generated by geometrical features of the flow system and multiphase flows (e.g. slugging). Vortex shedding from bluff bodies such as thermometer wells, trash grids, or vortex-shedding flowmeters fall into the former category.

(vi) Flow-metering calibration systems, e.g. rotodynamic pump blade passing effects and the effects of rotary positive-displacement flowmeters.

Whenever factors such as those indicated above are present, there is the possibility of flow pulsation occurring. It should also be appreciated that pulsation can travel upstream as well as downstream and thus possible pulsation sources could be on either side of the flowmeter installation. However, amplitudes may be small and, depending on the distance from pulsation source to flowmeter, may be attenuated by compressibility effects, in both liquids (and associated pipework) and gases, to undetectable levels at the flowmeter location. Pulsation frequencies range from fractions of a Hertz to a few hundred Hertz; pulsation amplitudes relative to mean flow vary from a few percent to 100% or larger. At low percentage amplitudes the question arises of discrimination between pulsations and turbulence effects.

1.2 Definition of Pulsating Flow in this Research

The particular flow condition considered in this study is sinusoidal pulsating flow. Pulsating flow is a type of unsteady flow in which there is regular cyclic variation in volume flow rate superimposed on a constant time average flowrate (Mottram 1992).

For example, a piston pump operates on the basis of transporting volumes of fluid in a pulsating manner, as shown in Figure 1. 1. In this example, the piston pump consists of two valves and one piston chamber box. The reciprocating piston is driven back and forth by a rotating mechanism, this discharges the fluid when it is driven forward (A) and raises the fluid into the chamber when it is driven backward (B). Hence, in any period of time, the flow output from the pump would be varying cyclically against the time average mean flowrate as shown in Figure 1. 1.

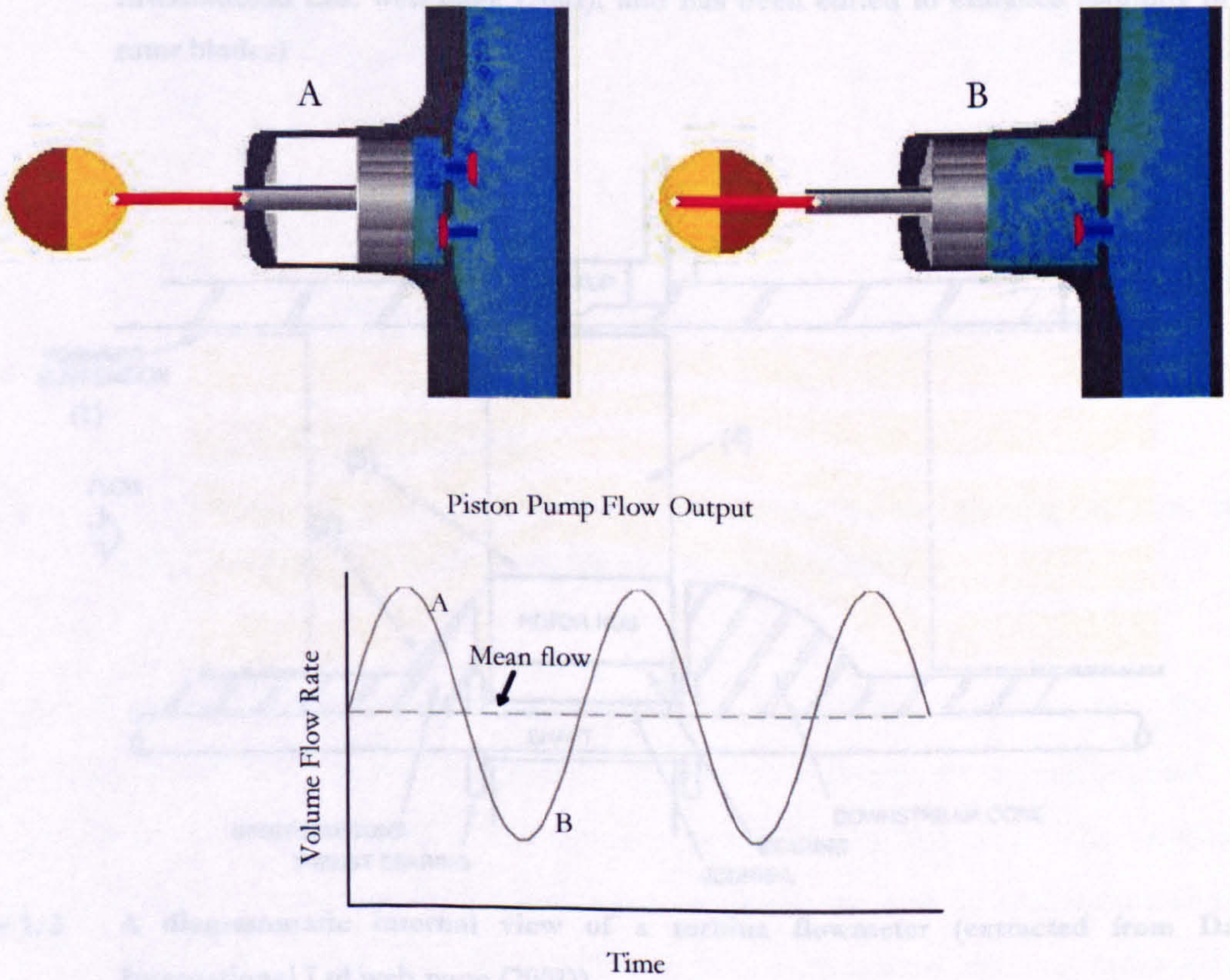

Figure 1. 1 Internal view of a typical piston pump in motion and its flow output (picture is extracted from The Animated Software Company web page (2001), and has been edited to enhance visibility)

1.3 The Turbine Flowmeter and its Industrial Applications

1.3.1 Description of operation

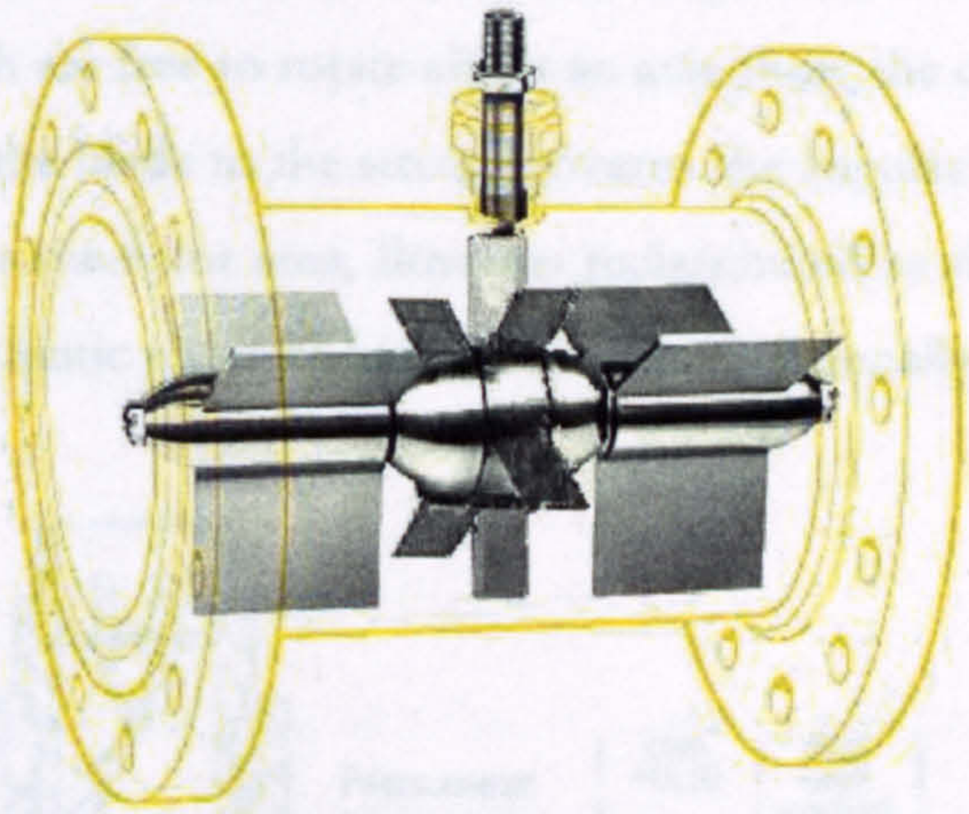

Figure 1. 2 **A photographic internal view of a turbine flowmeter (extracted from Daniel International Ltd. web page (2001), and has been edited to enhance visibility of the rotor blades)**

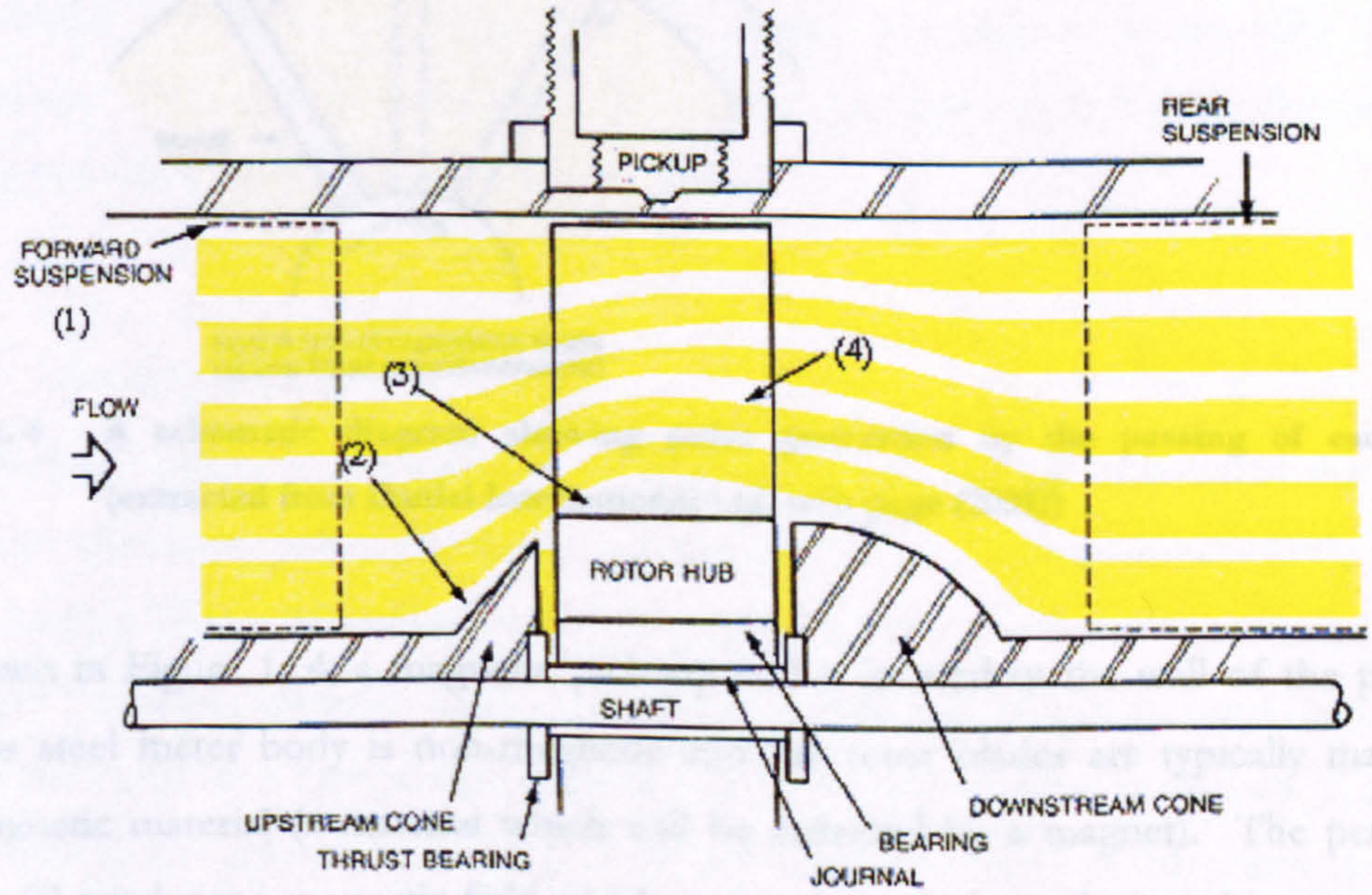

Figure 1. 3 **A diagrammatic internal view of a turbine flowmeter (extracted from Daniel International Ltd web page (2001))**

Some time prior to 1790 Reinhard Woltman invented the first propeller-type current meter which after centuries of utilisation, has been developed into the turbine flowmeter, as

shown in Figure 1. 2. An internal view of a typical turbine meter is shown in Figure 1. 3, it generally consists of multi-bladed rotor running between bearings. The forward and rear suspensions act as flow straighteners so that fluid motion through the meter is parallel to the meter centre line. Flowing fluid enters the turbine through the forward suspension, as shown at (1). When it encounters the cone at (2), the stream is deflected outward, causing the velocity to increase and a slight static pressure drop at (3). Fluid flow impinges upon the turbine blades which are free to rotate about an axis along the centre line of the turbine housing. The angle of the blade to the stream governs the angular velocity, at a given flow rate. As the fluid leaves the rotor area, flow has redistributed as shown at (4). Velocity is reduced slightly and the static pressure has increased proportionally.

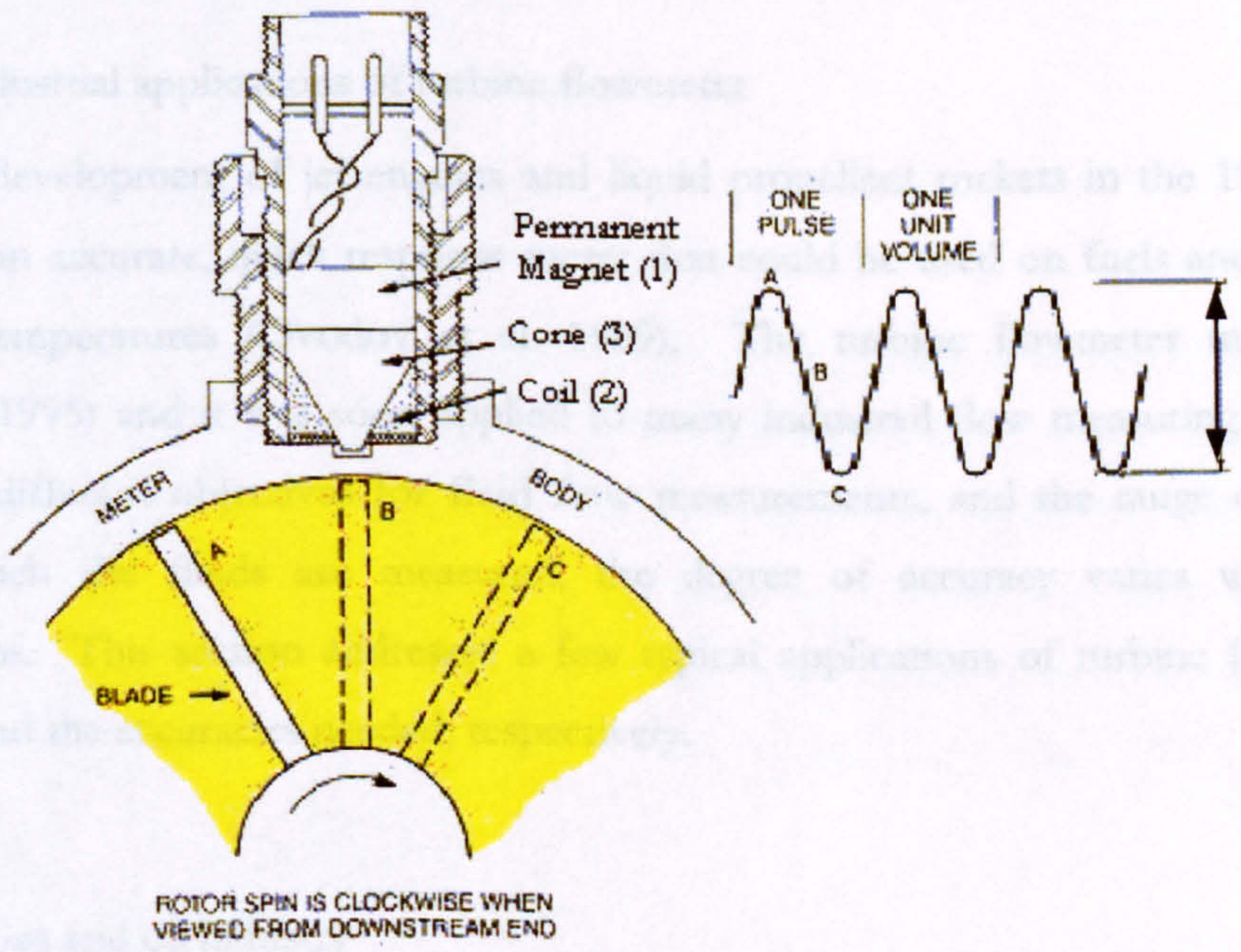

Figure 1. 4 A schematic diagram showing pulse generation by the passing of each blade (extracted from Daniel International Ltd. web page (2001))

As shown in Figure 1. 4, a magnetic pick–up coil is located in the wall of the pipe, the stainless steel meter body is non-magnetic and the rotor blades are typically made of a paramagnetic material (a material which will be attracted by a magnet). The permanent magnet (1) produces a magnetic field which passes through the coil (2) and is concentrated to a small point by the cone (3). The magnetic field is deflected when a turbine blade (shown at A) is moving into close proximity to the cone point, thus causing a voltage to be generated in the coil. This voltage decays as the blade passes under the cone point (B), but gradually builds back up in the opposite polarity as the blade moves towards point (C),

which causes the magnetic field to deflect in the opposite direction. Thus as each blade passes the cone, it produces a separate and distinct voltage waveform. The frequency of these waves is linearly proportional to the angular (rotational) velocity of the rotor, which is directly proportional to the fluid velocity and, thus, to the volume flowrate. The amplitude of the waves will vary in proportion to blade velocity but is not considered in the measurement process. Each wave is counted as a discrete event (pulse) and signal processing may be used to generate a pulse train output from the meter. Turbine meter output is rated in pulses per gallon, pulses per litre, or other standard engineering units. Though magnetic pickups are common, optical fibres and microwave techniques are used as well (Baker 1989).

1.3.2 Industrial applications of turbine flowmeter

With the development of jet engines and liquid propellant rockets in the 1950's, a need arose for an accurate, quick response meter that could be used on fuels and oxidizers at extreme temperatures (Ovodov et al. 1989). The turbine flowmeter met this need (Madison 1995) and it was soon applied to many industrial flow measuring applications. With the different objectives for fluid flow measurements, and the range of conditions under which the fluids are measured, the degree of accuracy varies with different applications. This section addresses a few typical applications of turbine flowmeters in industry and the accuracies needed, respectively.

1.3.2.1 Gas and oil industry

The dominant metering device used in the natural gas and oil industry is the turbine flowmeter (Birkhead 1985), (Bronner and McKee 1991), (Tiemstra et al 1991), (McKee 1992), (Mullen 1994), (Minemura et al. 1996), (Rowell 1996). In many applications such as in nuclear reactor systems, fossil-fuel power plants, oil refineries, and natural gas production fields and compressor stations, the flow may contain pulsations (Lee et al. 1975). For fiscal measurements such as meters used in services to the public, especially those for fuel gas and oil, governments lay strict regulations for their use and correctness, for tax purposes. When consideration is given to the value of liquid flowing through a custody transfer meter, it becomes apparent that seemingly microscopic improvements in accuracy amount to significant money amounts. For instance, a 10-inch turbine meter is metering at about 1000 m^3 per hour of crude oil, that is equivalent to approximately

£103000 per hour at current price (Unit Conversion web page 2001), (BBC News Online web page 2001), (Universal Currency Converter web page 2001), a +0.5% shift in accuracy represents a financial leak of over £510 per hour. These applications have resulted in efforts to reduce the magnitudes of metering uncertainties down to ±0.1% (Berto 1997).

In large scale power generation, it is general practice to carry out calibration tests of operating units and these tests involve the metering of water, steam, air, oil and fuel gas. Along with the steady increase in the size of power stations are the demands for increasing efficiency (Bean 1966), and hence the need to determine and then reduce the magnitudes of metering uncertainty, usually a minimum requirement of ±5% (Osha Federal Register web page 1994). This need arises from both the increasing cost of fuel and minimising environmental impact.

1.3.2.2 Processing industry

In the pharmaceutical industry, the production of drugs relies on mixing or dosing the right amount of chemicals accurately. High accuracy of the amounts delivered is always required in quality control of the products. Therefore for batch-flow applications, the flowmeter is required to have a short response time. In some applications, the batch time can be as short as of the order of 100 ms. Some small liquid turbine meters are known to have response time in the order of milliseconds (Cheesewright and Clark 1997), hence turbine meters might be suitable for this application.

In the processed food industry, EEC regulations require that the amount of a product sold has to be printed on the packaging. If one hundred grams of product is intended to be sold to the customers, then the customers will expect 100 grams or more of the products but nothing below 100 grams. Since the delivery of liquid products is usually driven by pumps and measured by flowmeters for the batch flow amount required, and then controlled by valves, the pulsation effects from pumps may cause uncertainties in metering the product. Therefore manufacturer(s)* always include a small amount of surplus in order to ensure every product sold complies with the law. Obviously, this is not a very cost

---

* Personal communication with Seaby, R. Group Technical Services Manager, Northern Foods Corporation, UK. (1998) March.

effective method for mass-production; however, if the accuracy in metering of pulsating flows can be improved, it will benefit the manufacturing company by saving on the cost of product.

1.3.2.3 Aerospace application

McCoy (1994) suggested that the comparatively faster response time of turbine flowmeters in liquid flows is of particular benefit in aerospace applications where it is essential to obtain rapid feedback on fuel flow rates for the control of engine performance. For instance, an aerospace manufacturer prototyping a new helicopter may need to test the performance of an orifice or pump, or to monitor engine heating under various flight conditions (McCoy 1994). In addition, turbine meters can withstand the extreme g forces encountered during the flight of military or other high-performance aircraft (Gannon 1994). Therefore, it is of interest to study the dynamic response of small turbine flowmeters to pulsating liquid flows for which it would be desirable for the meter to have a response time of 10 ms (corresponding to 100 Hz) or less.

1.3.2.4 Cryogenic industry

DeFeo J. W. (1992) reported that turbine meters are very widely used for flow measurements of cryogenic fluids. Applications of these measurements include cryogenic propellant loading for launching satellite and rockets (NASDA web page 1999), (The National Space Society web page 1997), and liquid nitrogen custody transfer as a commodity in both bio-medical and food preservation (Gruskos 1985). In a NASA sponsored flowmeter evaluation program (Alspach et al 1966), the performance results of some cryogenic turbine flowmeters were determined. The program found that several cryogenic turbine flowmeters were capable of an accuracy up to ±0.5% in steady flow. However, the work of Ovodov et al's (1989) on liquid nitrogen indicated problems of predicting transient behaviour without knowing the dynamic characteristics of the meter.

Chapter 2 Responsiveness of Differing Flowmeter Techniques to Pulsating Flow Conditions, Problem Definition, Aims and Objectives of this Study

Some meters are known to produce inaccuracies as a result of flow pulsations (e.g. pressure differential flowmeters), for some meter types the levels of pulsation induced errors are not fully known, namely the turbine flowmeters. This chapter gives a review on the dynamic response of some of these meters, this will be followed by a brief description of the problems encountered when the turbine flowmeter is subjected to pulsating flows. Finally the aims and objectives of this study will be detailed at the end.

2.1 Review of the Responsiveness of different types of Flowmeter to Pulsating Flow Conditions

2.1.1 Pressure differential flowmeters

Pressure differential flowmeters are volume flowrate devices in which the differential pressure produced by flow passing through a localised geometric constriction is sensed by a secondary device. By application of the Bernoulli equation, an idealised non-linear relationship is developed as shown in the equation below:

$$\Delta p = \text{Constant} \times \dot{V}^2 \qquad \textbf{Eq. 2. 1}$$

where Δp is the differential pressure and $\dot{V}$ is the volume flow rate. The main types are Orifice Plate, Venturi Meters and Nozzles. These devices were established in the early 20th century and numerous investigators have characterized aspects of their behaviour in pulsating flow (Deschere 1952), (Hall 1952), (Zarek 1966), (Gajan et al. 1992).

There are three main problem areas in using these devices for pulsating flow measurement: firstly, the non-linearity of the flowrate/differential pressure relationship — commonly known as the square root error; secondly, the accurate measurement of the dynamic

differential pressure (Clark 1992); thirdly, the temporal inertia effect. The first problem affects the indicated mean flow reading as the square root of the averaged differential pressure was used to infer the mean flowrate. The influence of the inertia of the fluid appears in the relation between the pulsation amplitude and differential pressure. This effect is due to the fact that a component of the differential pressure is required to accelerate the fluid with respect to time in addition to that required for the convective acceleration through the orifice, (Mottram 1992), (Gajan 1992).

2.1.2 Vortex flowmeter

The vortex meter is a volumetric flowmeter and the device consists of a bluff body within a circular pipe. Above a certain Reynolds number, vortices are shed alternately from each side of the bluff body, the frequency of shedding being proportional to flow velocity. The optimum width of the bluff body is about 25-30 percent of the pipe diameter, and the vortex shedding behind the body is greatly stabilised by two plates attached to the pipe wall (Baker 1989). The meter employs a natural fluid oscillation in its mode of operation (Baker and Deacon 1984) and the shedding frequency is detected by a sensor. If the approaching flow itself contains a flow pulsation, some interference between the two types of fluid oscillation takes place, particularly if their frequencies are similar. Mottram (1992) has described that, under some conditions, the vortex shedding process is liable to "lock-on" to the pulsation frequency, and when this happens the flow meter ceases to respond to changes in mean flow velocity and very significant metering errors may result.

2.1.3 Electromagnetic flowmeter

When a fluid carrying ions flows through a transverse magnetic field in a non-magnetic tube, voltages and currents are generated in the fluid due to the motion. Measurement of the potential difference between two electrodes mounted in the meter wall will provide an indication of mean velocity over the pipe cross-section, but may be subjected to the influence of some velocity profile effects in the pipe. The correct design of the pipe and magnetic coils is essential to achieve a flowmeter which is little affected by upstream disturbance (Ginesi 1991).

Electromagnetic flowmeters can respond to pulsating flow, (e.g. as used for medical applications) (Ross 1971). The measurement frequency bandwidth depends upon the frequency of meter excitation and upon the subsequent signal processing.

2.1.4 Ultrasonic flowmeter

The 'time of flight' flowmeter makes use of the difference in the time required for sound to travel a given distance in the flow. The difference in the time of transit between transducers of upstream and downstream pulses of ultrasound is used to obtain the flow velocity in the tube. This flowmeter is an inertia-less device having no moving parts and offering no obstruction to flow. This kind of meter has been successfully used for the measurement of pulsations in blood flow (Peronneau et al 1971).

In order to determine flow rate accurately, it is necessary to know the true average velocity over the pipe cross-section. Velocity distribution is a function of the Reynolds number (Re); as velocity distribution varies in a pipe due to pulsation effects, the relationship between measured velocity at a localised region and overall average velocity varies (McShane 1974), (Hakansson and Delsing 1994).

2.1.5 Coriolis flowmeter

The Coriolis flowmeter is essentially an oscillating pipe segment(s) conveying fluid and the measuring principle is based on the Coriolis force resulting from the linear velocity of fluid passing through an oscillating system. Operation of this meter is largely independent of pressure, temperature and viscosity (Baker 1994).

Vetter and Notzon (1994) showed that small U-tube Coriolis meters were disrupted by pulsations at the Coriolis mode frequency, with the potential for very large errors. In other words, pulsations cause forced oscillations of the measuring tube. If the pulsation frequency coincides with the basic resonant frequency (drive frequency) or with other resonant frequencies of the measuring tube, then the tube may oscillate with relatively large amplitudes, and measurement errors may then occur.

The relatively short time constants, from 0.01s to 0.1s, given by most of the meter manufacturers, suggest that most meters might be expected to correctly measure the time

histories of flows with pulsations at frequencies up to 20 to 30 Hz. However, Cheesewright and Clark (2000) showed that when some meters were subjected to low frequency pulsations (at 2 Hz to 40 Hz), though meter indicated mean flow readings were unaffected, significant pulsation amplitude attenuations, in the region of 50 % to 90 %, were experienced.

2.1.6 Turbine flowmeter

Turbine flowmeters are essentially instruments for metering steady flows, but it is often argued that their responsiveness makes them suitable for metering flows in which a degree of unsteadiness is present (Atkinson 1992). A comprehensive review of the dynamic response of the meter will be detailed in Chapter 4, whilst a brief description is given in this section.

Generally, the responsiveness of a turbine flowmeter is dependent on the design of the meter, particularly the inertia of the rotor, and upon the inertia of the fluid inside the rotor envelope which in turn depends upon the density of the fluid. The influence of density is such that in general, a meter is better able to follow any unsteadiness in liquid flows than in gas flows, because the density of the fluid is closer to that of the rotor (Baker 2000), and this has an effect on the value of time constant for different fluid medium turbine flowmeters. For example, if a meter is capable of running either in gas or liquid, since the density of water is around 1000 times higher than the density of air at 1 bar, then for a small meter, a typical value of the time constant might be in the order of 1 ms for water and 1 s for air. For natural gas, in the national grid at 300 bar pressure, then the meter response would be closer to that with a liquid passing through it, than to a low-pressure gas. This is explained in more detail in Chapter 4.

2.2 Problem Definition

Some of the situations leading to flow pulsation, which are described in Section 1.1.2, will cause approximately sinusoidal pulsation. Hence, assuming pure sinusoidal pulsation exists in a flow system, then the time dependent volume flowrate, $\dot{V}_a$ (as shown in Figure 2. 1), can be expressed algebraically in the following form:

$$\dot{V}_a = \overline{\dot{V}_a}(1+\alpha_p \sin 2\pi f_p t) \qquad \textbf{Eq. 2. 2}$$

Where $\overline{\dot{V}_a}$ is the mean flowrate,

α_p is the relative pulsation amplitude, $(=\varphi_a / 2\overline{\dot{V}_a})$, φ_a is the peak-to-peak flow pulsation, and

f_p is the pulsation frequency, $(=1/T)$, T is the period of pulsation.

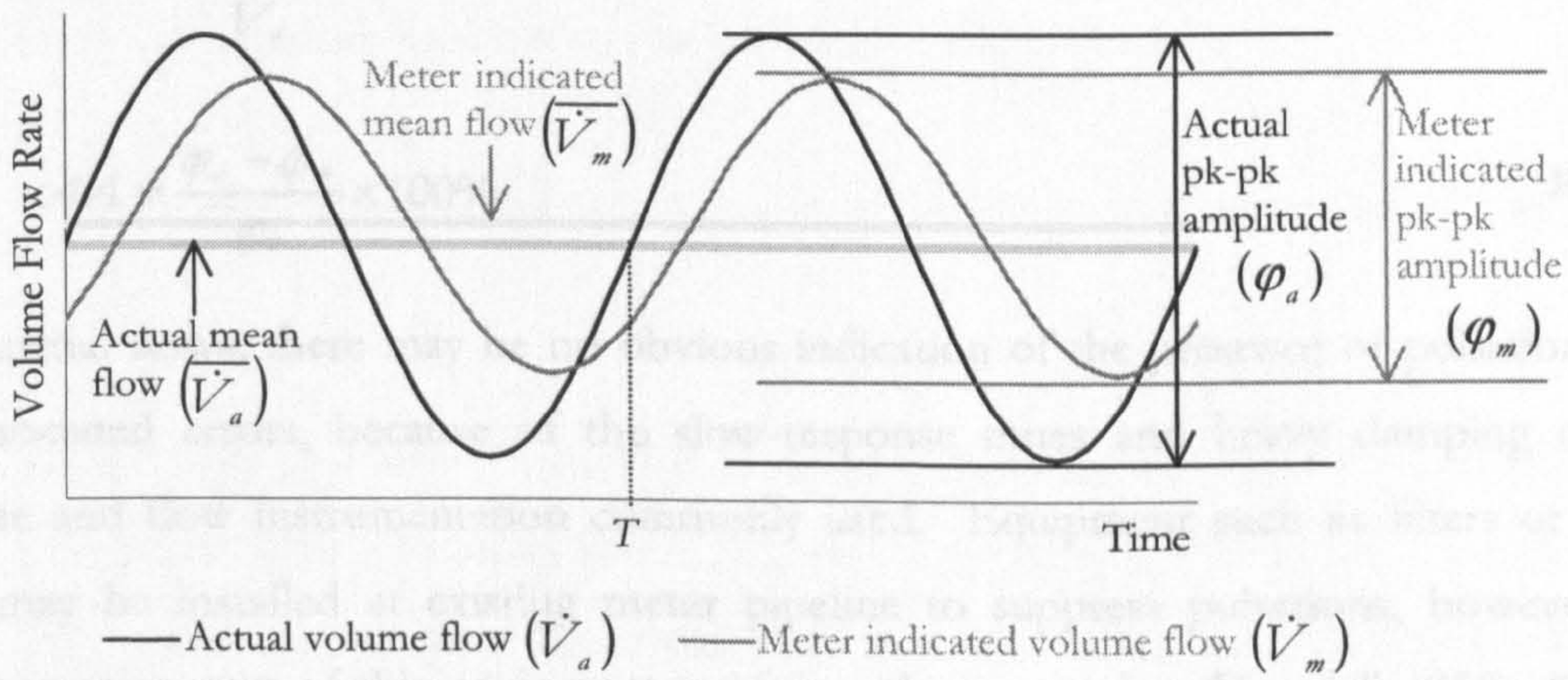

Figure 2. 1 Consequence of pulsating flow in turbine meter indicated reading

According to BS ISO TR 3313 (1998), when a turbine flowmeter is operating within a pulsation cycle, the inertia of the rotor (and possibly of the fluid contained within the rotor envelope) can cause the rotor speed to lag behind the steady state condition in an accelerating flow and to exceed it in a decelerating flow. When the flow is accelerating, the rotor takes time to respond to it; when the flow is decelerating, the fluid contained within the rotor envelope and the rotor might still be rotating at a comparatively faster rate, hence the influence of a decelerating flow is greater than that of an accelerating one so that the mean speed of a flowmeter subjected to pulsation can be greater than that corresponding to the mean flowrate.

A combination of these effects causes two commonly known problems in turbine flowmetering, which are illustrated in Figure 2. 1. Firstly the mean flow indicated, $\overline{\dot{V}_m}$, is higher than that which would occur with the corresponding actual mean flow, $\overline{\dot{V}_a}$; secondly there is a difference between the peak-to-peak pulsation amplitude indicated by the meter, φ_m, and the actual peak-to-peak pulsation amplitude, φ_a. These two effects are commonly termed "over-registration", *OR*, and "amplitude attenuation", *AA*, respectively. "Over-registration", *OR*, is defined by the indicated mean flow rate minus the actual mean flow rate as a percentage of the actual mean flow rate; and "amplitude attenuation", *AA*, is defined by the peak to peak variation of the actual flow rate minus the peak to peak variation of the indicated flow rate as a percentage of the peak to peak variation of the actual flow rate. In extreme cases over-registration error can be as high as 60% for gas flow meter (Cheesewright et al. 1996). These effects are expressed algebraically as follows:

$$OR = \frac{\overline{\dot{V}_m} - \overline{\dot{V}_a}}{\overline{\dot{V}_a}} \times 100\% \qquad \textbf{Eq. 2. 3}$$

$$AA = \frac{\varphi_a - \varphi_m}{\varphi_a} \times 100\% \qquad \textbf{Eq. 2. 4}$$

In industrial flows, there may be no obvious indication of the presence of pulsation, and the associated errors, because of the slow-response times and heavy damping of the pressure and flow instrumentation commonly used. Equipment such as filters or surge tanks may be installed at existing meter pipeline to suppress pulsations, however the implementation cost of this equipment is often rather expensive (Dowdell 1953), (Sparks 1966).

If the meter does not rapidly follow the flow rate, and the metering time is short, then erroneous mean flow measurements as well as time varying flow measurements could occur (Liu 1962). Thus the ability of a turbine flowmeter to respond rapidly to transient flow conditions is an important characteristic. Over the last thirty years, many investigators have studied the performance characteristics of turbine flowmeters in liquid and gas flows (Dijstelbergen 1966), (McKee 1992), (Atkinson 1992), (Cheesewright et al. 1996), (Cheesewright and Clark 1997). However, there is not a great deal of experimental evidence on the dynamic response of small turbine flowmeters in pulsating liquid flows.

2.3 The Aims and Objectives of this Study

The research aims are to investigate the effects of pulsating liquid flows upon the accuracy of small turbine meters and to make a contribution to the problem of reducing the errors introduced by pulsating flow conditions. The objectives for this research can be divided into 5 main parts;

(i) To review published literature, investigating conditions which are known to produce errors both in gas and liquid flow measurements and to identify techniques, mathematically and experimentally, which can either predict or remove the influence of pulsating effects in liquid flow measurements.

(ii) To predict any flow measurement errors in both mean and pulsating components when a turbine flowmeter is subjected to pulsating liquid flow, by using the knowledge gained from the review of published literature.

(iii) To perform a series of tests on a range of flowmeters, of sizes from 6 mm to 25 mm.

(iv) To develop and apply signal processing techniques capable of quantifying the errors, and then correcting for the errors by applying the knowledge gained from the review of published literature, such as published models for meter reading correction.

(v) To develop a Computational Fluid Dynamics (CFD) model to investigate the coupling between the flow and the rotor dynamics during unsteady flow, through integration of pressure (from skin friction) over the blade surfaces, the instantaneous resulting torque acting on the blades can then be determined and, hence, the corresponding motion of the rotor can be predicted. In addition to visualising flow behaviour around the blades, the simulation will allow independent evaluation of the assumptions underlying the techniques used to correct meter errors.

Chapter 3 Turbine Flowmeter in Steady Flow

Though the aim of this research is to investigate the performance of turbine flowmeter in pulsating liquid flow, some fundamental issues of meter accuracy in steady flow must be recognized first. Theories leading to the equation of motion of turbine flowmeter in steady flow are presented. Finally, a summary of the variables affecting the turbine flowmeter performance characteristics is detailed.

3.1 Turbine Flowmeter Performance Characteristics

To represent the performance of a turbine flowmeter, a few characteristic terms (Gannon 1994a) are commonly used and are outlined in this section. A typical performance curve is shown in Figure 3. 1:

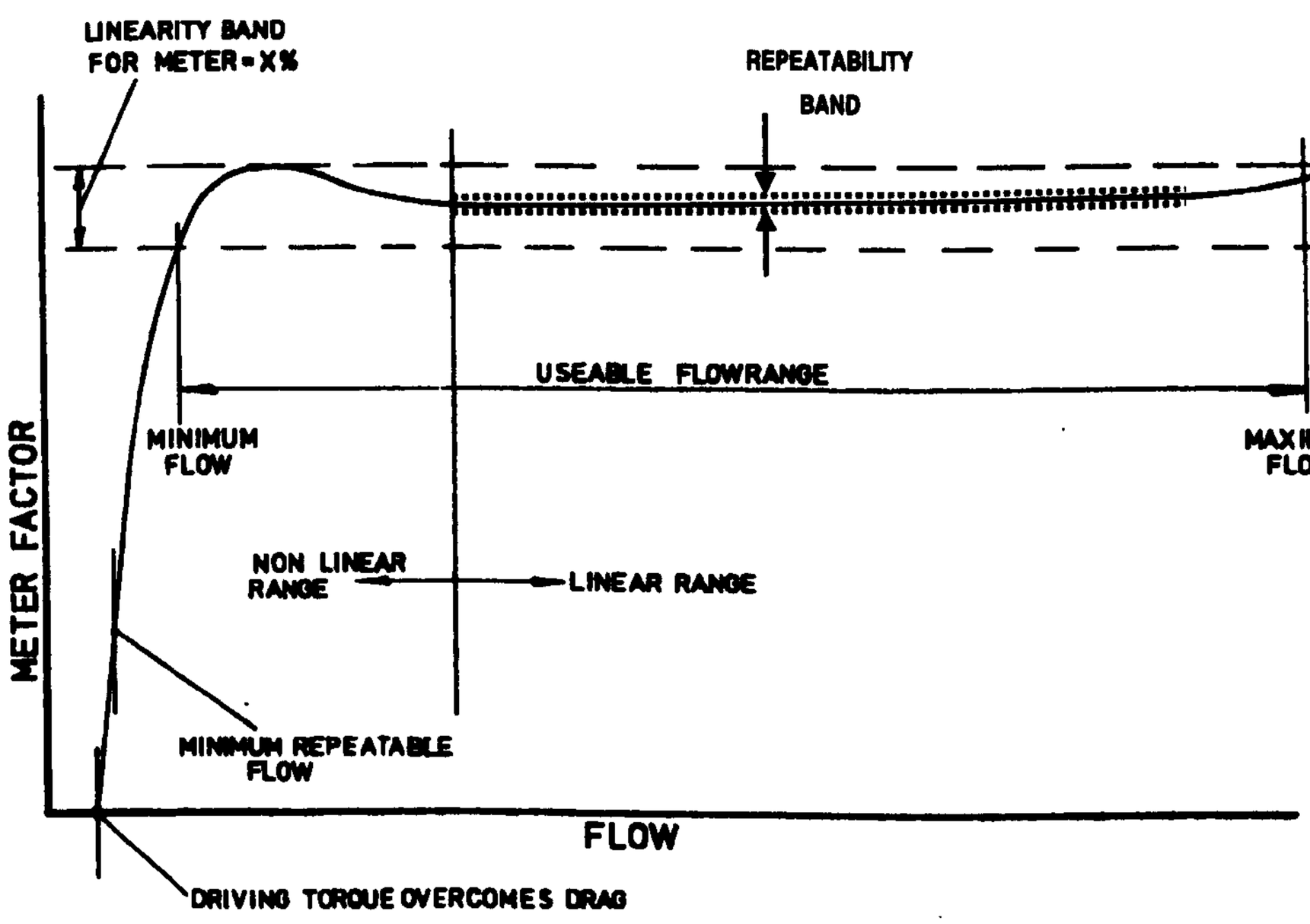

Figure 3. 1 A typical performance curve

3.1.1 K-factor

The factor, K, is the number of output pulses the flowmeter produces per unit of volume throughput. Hence, K is also the pulse frequency per unit of volume flow rate, expressed algebraically as shown in the equation shown below:

$$K = f_b / \dot{V} \qquad \textbf{Eq. 3. 1}$$

Where f_b is the blade passing frequency of the flowmeter operating at a given volume flow rate, $\dot{V}$.

3.1.2 Linearity and linear range

The turbine flowmeter is a nominally linear device over a specified flow range. Variations in linearity are stated as the maximum percentage deviation from the average K-factor. Linear range is the minimum to maximum flow range (typically 1 to 10) over which the K-factor is constant within specified limits.

3.1.3 Repeatability

Repeatability is the allowable percentage deviation from the stated K-factor in repeated tests. It is a measure of the output constancy under a given set of flow conditions. Repeatability errors of turbine flowmeters are many times smaller than the linearity errors (Gannon 1994b).

3.2 Theory: Equation of Motion of the Rotor in Steady Flow

3.2.1 Simple (ideal) model

According to Baker (2000), a well-designed turbine rotor will generally have helical blades to match the axial and tangential velocity of the rotor at each radial position. Ideally these will cut smoothly through the flow in a perfect helix, i.e. the fluid entering and leaving the blade at the blade angle. In the diagram below, U_x is the ideal (uniform) inlet axial velocity; U_b is the ideal blade velocity at the point considered, at radius r, and the blade angle at the point considered is β_r. U_{rel} is the ideal relative velocity of the fluid passing over the blade at this point. Clearly, U_b and U_{rel} both vary with the radius of the blade.

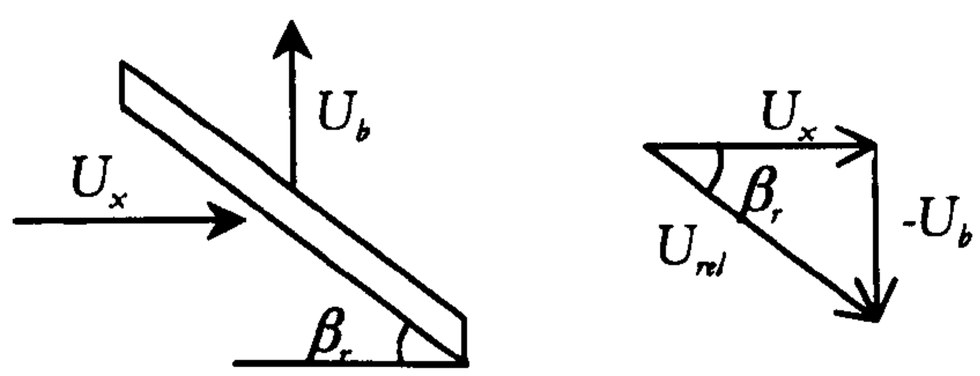

Figure 3. 2 Simple (ideal) vector diagram

Using the basic velocity diagram shown in Figure 3. 2, the inlet velocity can be derived as:

$$U_x = U_b / \tan \beta_r \qquad \textbf{Eq. 3. 2}$$

Where $U_b = \omega r$, ω is the angular velocity of the turbine rotor. If N is the total number of blades of that rotor, and f_b is the measured frequency of blade passing, then $\omega = 2\pi f_b / N$. Upon substitution of U_b, the value of f_b can be inferred from U_x as shown in the following equation:

$$f_b = N \tan \beta_r U_x / 2\pi r \qquad \textbf{Eq. 3. 3}$$

As can be seen from Eq. 3. 3, with no variation in axial velocity across the annulus, the value of β_r changes with radius to accommodate the profile across the pipe. Therefore, the correct blade angle distribution will be,

$$\tan \beta_r / r = \text{constant} \qquad \textbf{Eq. 3. 4}$$

In general, the blade angle is held between 20° and 50° to the flow.

However, friction must exist and the whole equation of motion of rotor would become quite complex in a realistic situation, whether friction is due to fluid motion or mechanical influence. The next section reviews the various friction parameters that would exist in a turbine meter system.

3.2.2 Zero net torque condition in steady flow

For a turbine flowmeter in steady motion, the net torque, T_N, acting on the rotor must be zero, that is:

$$T_N = T_d - T_r = 0 \qquad \textbf{Eq. 3. 5}$$

Where T_d is the driving torque and T_r is the resistance drag torque. The resistance drag torque is a sum of fluid drags (see Figure 3. 3) and non-fluid (mechanical) drags which the rotor encounters when rotating

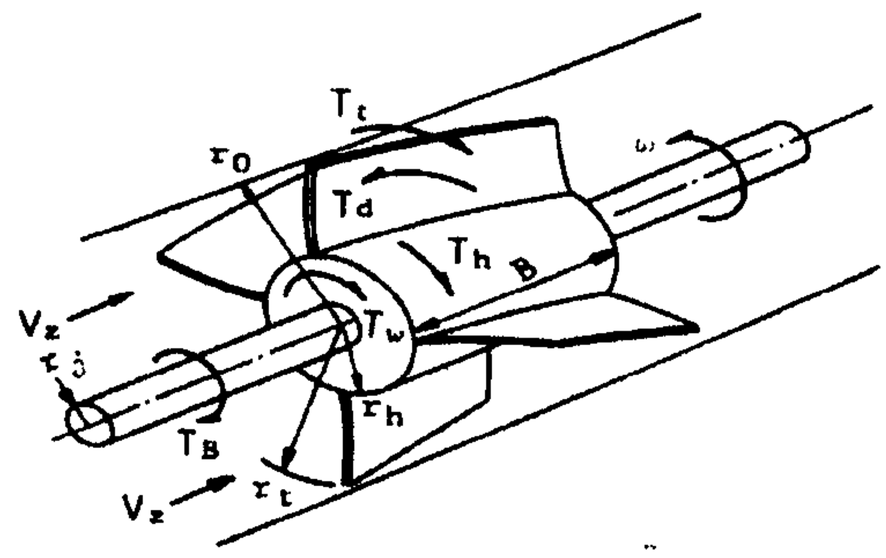

Figure 3. 3 Various torque terms in a turbine flowmeter when in motion

(Tsukamoto and Hutton 1985)

Tsukamoto and Hutton (1985) and Cheesewright and Clark (1996) gave components of the resistance drag torque and these are listed below;

T_t — blade tip clearance drag torque (Tsukamoto and Hutton 1985);

T_B — bearing retarding torque (Tsukamoto and Hutton 1985);

T_w — hub disc friction torque (Tsukamoto and Hutton 1985);

T_b — rotor hub fluid drag torque (Tsukamoto and Hutton 1985); and,

T_m — magnetic pickup retarding torque (Cheesewright and Clark 1996).

Hence T_r is mathematically expressed as:

$$T_r = T_t + T_B + T_w + T_b + T_m \qquad \textbf{Eq. 3. 6}$$

According to Baker (1993), torque could be obtained from a mathematical representation as shown below:

$$Torque = ShearStress \times area \times radius \times f(Re) \qquad \textbf{Eq. 3. 7}$$

At sufficiently high speed, Tsukamoto and Hutton (1985) gave the first three terms on the right of Eq. 3. 6 to be approximately proportional to ω^2. For instance, the equation for bearing drag was:

$$T_B = \pi\rho(r_j\omega)^2 \times r_j^{\,2} \times B \times f(\mathrm{Re}_b) \qquad \textbf{Eq. 3. 8}$$

Where ρ is the fluid density; r_j is the radius of journal bearing; B is the hub height; and Re_b is the local Reynolds number based on the radial clearance of the bearing. From the work of Tsukamoto and Hutton (1985), the dependence on angular velocity, ω, ranges from $T \propto \omega$ to $T \propto \omega^{1.8}$. At low speeds the dependence was in the range ω to $\omega^{1.5}$, whilst at high speeds the dependence was from $\omega^{1.75}$ to $\omega^{1.8}$.

For the hub fluid drag, Tsukamoto and Hutton (1985) expressed it as:

$$T_b = A_b \times r_b \times \sin\beta_b \times (\rho/2) W_b^{\,2} \times f(\mathrm{Re}_b) \qquad \textbf{Eq. 3. 9}$$

Where A_b is the total surface area of the hub (excluding the parts which are attached to the blades); r_b is its radius; β_b is blade angle at the hub and W_b is the relative velocity at the hub.

Cheesewright and Clark (1996) stated that the magnetic pick-up drag, T_m, would be more significant in gas flows, where the rotational inertia of the fluid passing through the meter was negligible. They investigated the effect of T_m on a range of small turbine meters (6mm to 15mm) in gas flow. From the same calibration tests done on the same meter with and without the presence of pick-up, it was found that the magnitude of T_m was most significant at meter starting up from rest, and it would decrease as the flowrate increased. Hence, they gave the simplest model of T_m as shown below:

$$T_m = T_{m,0} \sin(N\theta) \qquad \textbf{Eq. 3. 10}$$

Where $T_{m,0}$ is the torque that the rotor has to overcome to start rotating from rest, N is the number of blades, and θ is the measure of the angular position of the blade relative to the pick-up (note that $\omega = d\theta/dt$). Though the effect would vary from different design and

material, it was also concluded that $T_{m,0}$ generally increased as the meter size decreased, within the products of any particular manufacturer.

It is worth noting that, depending upon the effect the researcher is trying to demonstrate, the derivation of the net torque condition (as described in Eq. 3. 5) can vary. For instance, some researchers ignored the blade fluid drag component (e.g. Jepson and Bean 1969) and some ignored the magnetic pick-up drag component (e.g. Xu 1992b).

For the evaluation of the driving torque, T_d, researchers have used either the momentum approach or the application of airfoil theory. In the momentum approach, the driving torque is expressed in terms of a change in the angular momentum of the fluid passing through the blade row in a cascade of blades. In the airfoil approach, lift and drag coefficients are used to determine the fluid forces acting on a differential-area element of the blade, and then integration from blade root to tip is performed to obtain the driving torque. The following sections review these approaches in detail.

3.2.3 Rotor driving torque evaluation – "Momentum" model (based on Cascade theory)

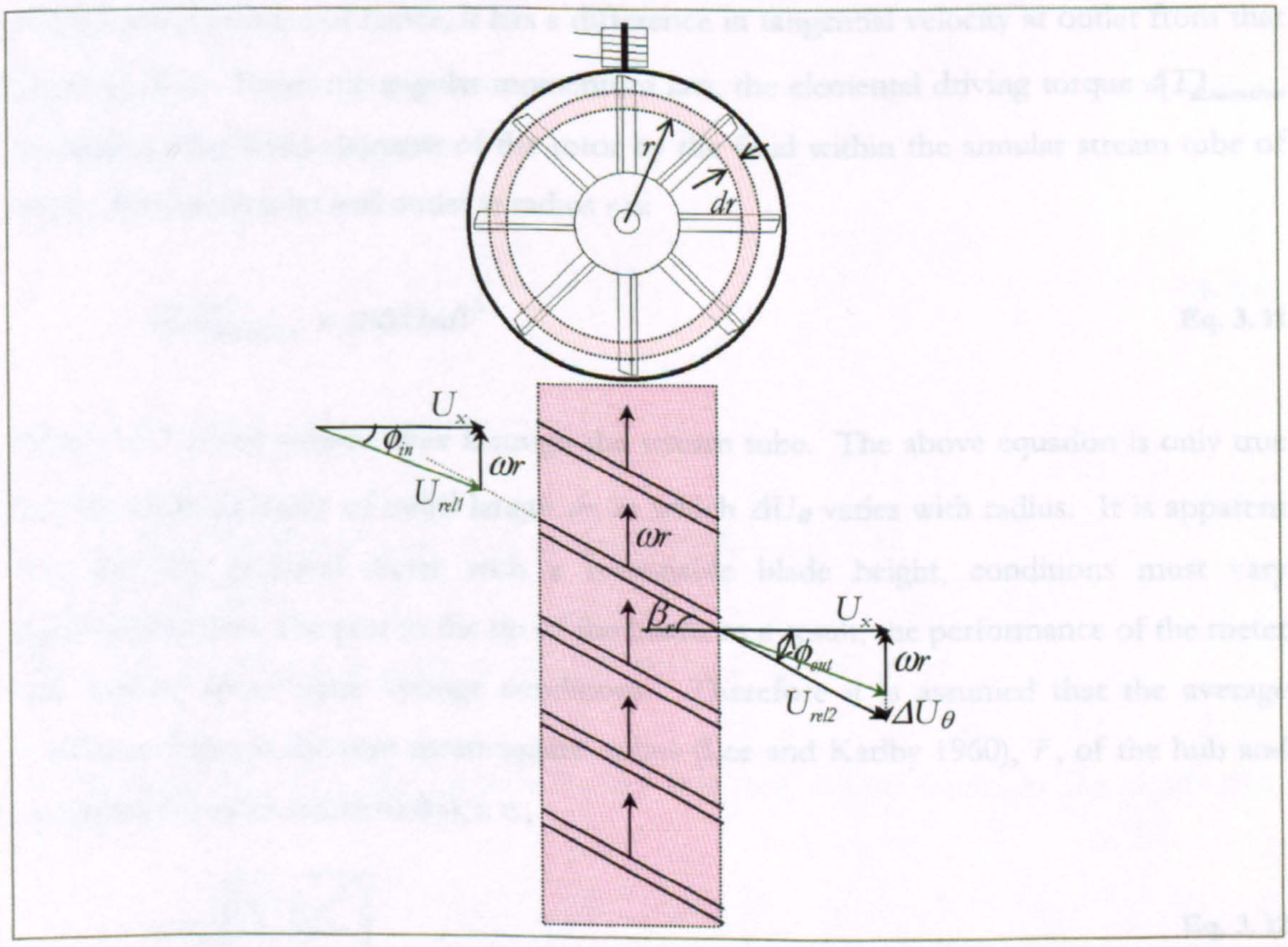

Figure 3. 4 Velocity vector diagram for a cascade based upon a general radius, *r* (steady flow model)

Cascade theory (eg. Lee and Karlby (1960), Lee et al. (1975) and Minemura et al. (1996)) is a model to solve the motion of rotor in a 2-dimensional aspect. Since the rotor of the turbine flowmeter is an axial flow type, a cascade is developed on a cylindrical stream surface with an infinitesimally small thickness dr at some radius, r, of the blade. This produces an infinite array of blades, as shown in Figure 3. 4, with β_r being the blade angle at r.

Consider the turbine being steadily rotated in a synchronous condition by the fluid having the velocity diagrams for blade elements at radius r shown in Figure 3. 4. The inlet fluid velocity U_x is assumed to be uniformly distributed due to the inlet flow straightener and neglecting the presence of a boundary layer. The inlet velocity angle, ϕ_{in}, is not the same as the blade angle β_r; this hypothesis is based upon the numerical work results obtained by Thompson and Grey (1970) on a 50mm meter, that the zero net torque situation happens when the blade incidence angle, $\beta_i = \beta_r - \phi_{in}$ (positive incidence direction assumed, Baker 2000), is at around 0.08°.

The outlet flow angle, ϕ_{out}, is assumed to be aligned with the blade angle β_r at the measurement point, and hence, it has a difference in tangential velocity at outlet from that at entry, ΔU_θ. From the angular momentum law, the elemental driving torque $d[T_d]_{momentum}$ induced on the blade elements of the rotor by the fluid within the annular stream tube of width dr between inlet and outlet at radius r is:

$$d[T_d]_{momentum} = \rho r \Delta U_\theta d\dot{V} \qquad \textbf{Eq. 3. 11}$$

Where $d\dot{V}$ is the volume flow through the stream tube. The above equation is only true for the blade elements of radial length dr, in which ΔU_θ varies with radius. It is apparent that for any practical meter with a reasonable blade height, conditions must vary considerably from the root to the tip of the blade; as a result, the performance of the meter will depend upon some average conditions. Therefore it is assumed that the average condition exists at the root mean square radius (Lee and Karlby 1960), $\bar{r}$, of the hub and tip radius; (r_b and r_t respectively), i. e.,

$$\bar{r} = \sqrt{\left(\frac{r_b^{\,2} + r_t^{\,2}}{2}\right)} \qquad \textbf{Eq. 3. 12}$$

With the further assumption that the blade-tip clearance is small in comparison with the length of the blade, now summing over the entire cross-section, resultant driving torque, $[T_d]_{momentum}$ becomes

$$[T_d]_{momentum} = \rho \dot{V} \bar{r} [\Delta U_\theta]_{\bar{r}} \qquad \textbf{Eq. 3. 13}$$

where $[\Delta U_\theta]_{\bar{r}}$ is the difference in outlet tangential velocity at mean radius $\bar{r}$.

From the vector triangle shown at outlet in Figure 3. 4, since $\phi_{out} = \beta_r$ at the measurement point, let r be $\bar{r}$ and we have

$$[\Delta U_\theta]_{\bar{r}} = (U_x \tan \beta_{\bar{r}}) - (\bar{r}\omega) \qquad \textbf{Eq. 3. 14}$$

Now Eq. 3. 13 becomes:

$$[T_d]_{momentum} = \rho \dot{V} \bar{r} [(U_x \tan \beta_{\bar{r}}) - (\bar{r}\omega)] \qquad \textbf{Eq. 3. 15}$$

Since $U_x = \dot{V}/A$, A being the actual mean cross-sectional area of the effective annular flow passage at the rotor blades:

$$[T_d]_{momentum} = \rho \dot{V}^2 \bar{r}^2 \left[\left(\frac{\tan \beta_{\bar{r}}}{\bar{r}A} \right) - \left(\frac{\omega}{\dot{V}} \right) \right] \qquad \textbf{Eq. 3. 16}$$

This type of model has two assumptions:

(i) The outlet flow angle is the same as the blade angle

(ii) Mean geometric parameters of rotor are used for evaluation.

Hence, from the momentum approach, the zero net torque condition for steady flow would be:

$$T_N = [T_d]_{momentum} - T_r = \left\{ \rho \dot{V}^2 \bar{r}^2 \left[\left(\frac{\tan \beta_{\bar{r}}}{\bar{r}A} \right) - \left(\frac{\omega}{\dot{V}} \right) \right] \right\} - T_r = 0 \qquad \textbf{Eq. 3. 17}$$

3.2.4 Rotor driving torque evaluation – "Airfoil Theory" model

Blows (1980) used an alternative approach to solve for the driving torque; he used lift and drag coefficients to characterise the cascade behaviour as shown in Figure 3. 5:

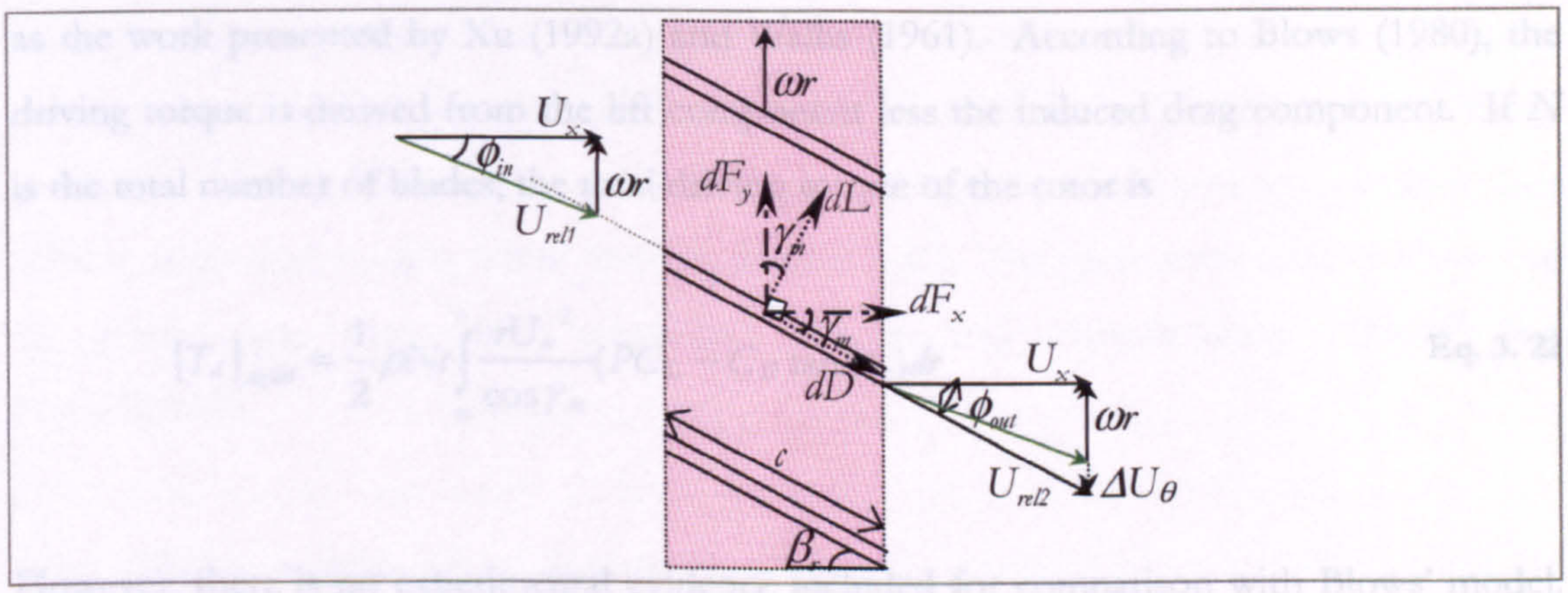

Figure 3. 5 Hydrodynamic forces of blade for a general radius, *r* (steady flow model)

A blade element of length *dr*, at radius *r*, experiences aerodynamic forces when the fluid goes through. The lift force, *L*, is a component of the total aerodynamic force on the blade, which is perpendicular to the direction of the oncoming fluid seen from a reference frame moving with the blade. The drag force, *D*, is another component of the total aerodynamic force on the blade, which is parallel to the direction of the oncoming fluid (Massey 1988).

The lift and drag forces are given per unit length of the blade by

Lift Force, $$dL = dF_y \cos\gamma_m + dF_x \sin\gamma_m$$ **Eq. 3. 18**

Drag Force, $$dD = dF_x \cos\gamma_m - dF_y \sin\gamma_m$$ **Eq. 3. 19**

And the lift and drag coefficients, C_L and C_D respectively are as follows:

$$C_L = \frac{L}{\frac{1}{2}\rho c P (U_x/\cos\gamma_m)^2}$$ **Eq. 3. 20**

$$C_D = \frac{D}{\frac{1}{2}\rho c (U_x/\cos\gamma_m)^2}$$ **Eq. 3. 21**

where c is the chord, γ_m is the mean flow angle, C_L is the lift coefficient, C_D is the drag coefficient and P is the factor which allows for the change in C_L between an isolated aerofoil and a cascade. Full derivation of the terms (PC_L) can be found in Baker (1993), and the values of C_L and C_D can be obtained from available numerical modelling data such as the work presented by Xu (1992a) and Wallis (1961). According to Blows (1980), the driving torque is derived from the lift component less the induced drag component. If N is the total number of blades, the total driving torque of the rotor is

$$[T_d]_{airfoil} = \frac{1}{2}\rho N c \int_{r_h}^{r_t} \frac{rU_x^{\,2}}{\cos\gamma_m}(PC_L - C_D \tan\gamma_m)dr \qquad \textbf{Eq. 3. 22}$$

However, there is no experimental evidence included for comparison with Blows' model. Also, Jepson and Bean (1969) and Thompson and Grey (1970), both published papers which show a very similar equation with a slightly different constant (P). For instance, Jepson and Bean's equation (1969) neglected the component of drag forces, based on the assumption that the rotor space/chord ratio is greater than unity where the cascade effect could be ignored.

This type of model has two assumptions:

(i) The outlet flow angle is the same as the blade angle

(ii) Increasing the blade number should give a proportional increase in torque, but increasing the blade number will eventually result in changes in the lift and drag coefficients used in the numerical integration, in which the coefficient values are usually based on empirical data. Also, Xu's (1992a) theoretical results showed that both the lift and drag coefficients vary significantly from the blade hub to tip. In the hub section, the cascade space is small, so both lift and drag forces are very much lower than those at the tip section (Xu 1992a).

Hence, from the airfoil approach, the zero net torque condition for steady flow would be:

$$T_N = [T_d]_{airfoil} - T_r = \left[\frac{1}{2}\rho N c \int_{r_h}^{r_t} \frac{rU_x^{\,2}}{\cos\gamma_m}(PC_L - C_D \tan\gamma_m)dr\right] - T_r = 0 \qquad \textbf{Eq. 3. 23}$$

3.3 Factors affecting the Accuracy of Turbine Flowmeter in Steady Liquid Flow

Accurate flow measurement using a turbine flowmeter requires knowledge and control over every parameter which may influence its performance (Nicholl 1977). A number of researchers have published reviews on the different variables affecting the driving torque, such as the effects of velocity profile, retarding torques, blade interference and meter geometry. This section reports some of these well known parameters and outlines their effects on the various drag terms listed in Section 3.2.2. The parameters reviewed here can be divided into three main categories: "design and manufacturing"; "fluid" and "installation".

3.3.1 Design and manufacturing variables

3.3.1.1 Blade – edge effects

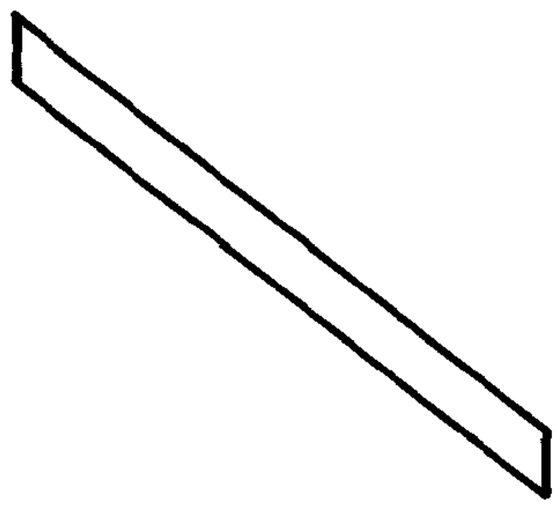

Figure 3. 6 A two dimensional representation of a rotor blade

Most turbine blades are manufactured as the sharp edge type as shown in Figure 3. 6, and this has a direct influence on the meter calibration, as it alters the effective blade angle and hence the angle of attack. Also, if burrs exist on the blade surface, it may change the effective blade area. Nicholl (1977) indicated that a chamfered blade edge meter would drop the K factor by about 0.6% as compared to a normal sharp edge meter. He also reported that a maximum of 7% increase in the K factor could be recorded if "sufficiently large burrs" were present on the blade edges (both leading and trailing). "Note that the burrs were artificially produced for this test and that it is unlikely that burrs of such a size would be present on a final rotor assembly" (Nicholl (1977)). The actual size of the burrs, or the relative size of burrs to blade size, was not stated in his paper. The linearity error could deteriorate to ± 0.6% as opposed to ±0.2% for the normal blade without burrs.

3.3.1.2 Surface finish of the rotor blades

One of the several resisting torques that the turbine meter has to overcome is the fluid drag through the blades. For large meters, the fluid drag is more significant than the mechanical drag effects of the bearings. Blade fluid drag consists of pressure and skin friction drags where the latter depends on both the Reynolds number and surface finish. Nicholl (1977) showed that a polished blade surface would drop the K factor curve by 0.5%, with linearity unaffected.

3.3.1.3 Tip clearance

Tan and Hutton (1971) highlighted the importance of leakage flows in the tip clearance. They indicated that the change in velocity profile was most significant near the wall. A meter with a small tip clearance showed a drop in meter factor with decreasing flowrate since there was an increase in the negative angle of attack towards the tips of the blades, with a resulting rise in drag. Conversely a large tip clearance meter responded to the relatively higher velocity at the blade tip and hence comparatively raised the driving torque, resulting in a higher meter factor. Their findings agreed with the investigation on the radial distribution of incidence angle by Salami (1984), where he found that the blade tip sections in the fully developed upstream flow acted as a pump. "This pumping action gives big torque and energy losses which must be overcome by the inner part of the blade acting as a turbine. An increase in tip clearance leads to a decrease in the pumping action region near the blade tip section, and hence results in a rise in meter factor." (Tsukamoto and Hutton 1985)

3.3.2 Fluid variables

3.3.2.1 Viscosity

Variation in the viscosity of the passing fluid will not only affect the upstream velocity profile, but also the various drag losses through the meter (Nicholl 1977). As viscosity increases the boundary layer tends to remain laminar from the leading edge. Hence, to maintain equilibrium due to varying viscous effect on the blade, the angle of attack changes which in turn affects the K-factor. The usual effect of viscosity on the performance characteristics is to decrease the linear range (Watson 1977).

3.3.2.2 Effect of temperature on the density of the fluid

Altering the temperature of the passing fluid will alter its viscosity, and for gases, density will also change. Changes in fluid density will change the meter K-factor since the available torque for the rotor of a turbine meter is directly proportional to the fluid density (Nicholl 1977), as can be seen in Eqs. 3.16 and 3.22.

3.3.3 The effect of installation variables

3.3.3.1 Upstream flow condition and swirl

According to Shafer (1962), turbine meters can be influenced to a varying extent by the upstream flow pattern. Jepson and Bean (1969) produced data indicating a shift in meter K-factor of about +2% for a change in velocity profile from turbulent to flat. However, this was for a meter with a small hub-to-tip ratio. Tan and Hutton (1971) observed that meters with a larger hub-to-tip ratio are less sensitive to profile. Salami (1984) confirmed that a commercial meter with a hub-to-tip ratio of about 0.5 and a tip clearance of 10% was almost insensitive to changes from uniform to turbulent profile. The particular upstream disturbance which has the greatest influence on meter accuracy, is rotational flow or swirl. It will change the angle of attack between the fluid and the turbine blades with a resultant effect upon turbine speed at a constant flow rate. Salami (1985) showed that a typical change of K factor value due to swirl would be about 2.5% per degree of swirl. One common practice to minimise swirl is to install a flow straightening section in the upstream pipework or within the meter, upstream of the rotor.

3.3.3.2 Cavitation

Cavitation is the phenomenon of a liquid boiling due to locally low pressure. With the onset of cavitation, the *K*-factor of the turbine meter begins to rise (Kalivoda 1998). The curve will rise because the vapour is usually moving at a high velocity and keeps the rotor moving as if the entire flow was the process liquid. The release of vapour can be minimised by maintaining sufficient back pressure immediately downstream (approximately four pipe diameters) of the meter. For low vapour pressure liquids, a recommended formula for calculating this required back pressure is(BS 6169: Part2: 1984):

$$P_{min} = 2\Delta P + 1.25 P_v \qquad \textbf{Eq. 3. 24}$$

where P_{min} is the minimum allowable back pressure downstream of the meter, ΔP is the pressure drop across the meter at maximum flow rate, and P_v is the absolute vapour pressure of the liquid at maximum operating temperature.

Chapter 4 Turbine Flowmeter in Unsteady Flow

This chapter will start by reviewing existing theoretical models which characterise the motion of the meter rotor in unsteady gas and liquid flows; the factors which influence the performance of the meter in unsteady flow will be then identified.

When the behaviour of the meter under unsteady conditions is considered, two different aspects need attention. First, the transient response of the instrument to "step" changes is important when it is to be used in control loops (e.g. in batch flow operation), and secondly the behaviour in response to large-amplitude pulsations should be evaluated. Hence the latter part of this chapter covers these two aspects based on the previous work published on the rotor behaviour: for the step response in liquid flows; and the response to pulsating flow, for both gas, and liquid flows.

4.1 Theory: Equation of Motion of the Rotor in Unsteady Flow

Following on from the steady flow equation reviewed in Section 3.2, if the flow is pulsating sinusoidally in time with relative pulsation amplitude of α_p, the time dependent actual volume flow rate, $\dot{V}_a(t)$, is given by $\dot{V}_a(t) = \overline{\dot{V}_a}(1 + \alpha_p \sin 2\pi f_p t)$ and $\alpha_p = \varphi_a / 2\overline{\dot{V}_a}$ (as stated in Section 2.2). When the meter is subjected to $\dot{V}_a(t)$, the rotor responds and rotates with angular velocity $\omega(t)$, and the meter indicated volume flow rate, $\dot{V}_m(t)$, can then be evaluated. It is of interest to investigate this time dependent response of the meter to the driving flow rate, i.e., what is the relationship between the true flow $\dot{V}_a(t)$ and the meter indicated flow $\dot{V}_m(t)$.

To investigate the motion of the rotor in unsteady flow, researchers have used various methods such as aerofoil theory (Ower 1937), (Grey 1956), and the change in angular momentum of the fluid upon entering and leaving the rotor zone (Dijstelbergen 1966), (Atkinson 1992), (Cheesewright et al 1994). (See Section 3.2 for details)

In the following theoretical description of dynamic response, the momentum approach is used.

Clarification:

The following theory assumes that the meter has zero resisting torque and hence there will be zero driving torque under steady flow conditions, i.e. Eq. 3. 16 now becomes:

$$[T_d]_{momentum(steady)} = \rho U_x A\bar{r}(U_x \tan\beta_{\bar{r}} - \omega\bar{r}) = 0 \qquad \textbf{Eq. 4. 1}$$

This implies that $U_x \tan\beta_{\bar{r}} = \omega\bar{r}$, i.e. the relative velocities at both the entrance and exit are aligned with the blade angle in steady flow condition.

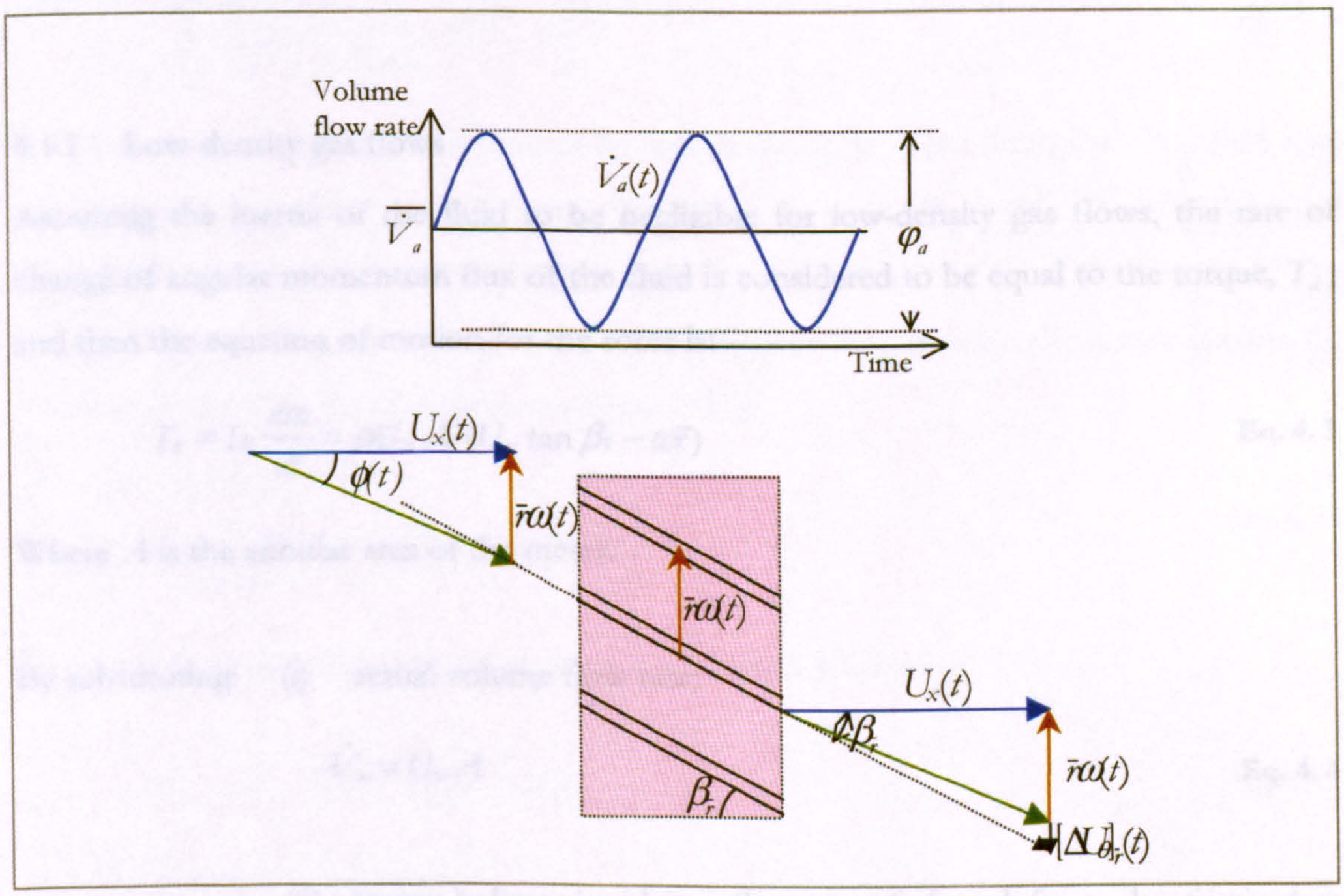

Figure 4. 1 Velocity vector diagram for the mean radius, $\bar{r}$ (unsteady flow model)

For a typical meter rotor, since the angle of the blade varies with radius to accommodate the velocity profile across the pipe, it is therefore assumed that the average flow condition around the blade exists at the root mean square radius, $\bar{r}$ (as mentioned in Section 3.2.3). The same assumption applies here and the cascade diagram shown in Figure 4. 1 is for the root mean square radius $\bar{r}$, with the helix blade angle $\beta_{\bar{r}}$ at this radius. From the velocity

vector diagrams shown, the incidence angle of the fluid entering the rotor zone changes periodically due to the pulsating axial velocity, i.e. $U_x(t)$, which is assumed to be uniformly distributed due to the inlet flow straightener and neglecting the presence of a boundary layer. Note that this incidence angle is assumed to be zero if the meter is operating under steady flow condition. The fluid leaving the rotor is assumed to have become aligned with the blade angle, and hence, has a difference in tangential velocity at outlet from that at entry, $[\Delta U_\theta]_{\bar{r}}(t)$. Assuming the average condition exists on the mean radius, $[\Delta U_\theta]_{\bar{r}}(t)$ would be given by:

$$[\Delta U_\theta]_{\bar{r}}(t) = [U_x(t)\tan\beta_{\bar{r}}] - [\bar{r}\omega(t)] \qquad \textbf{Eq. 4. 2}$$

In the following sections, we replace the notation for $\dot{V}_a(t)$, $\dot{V}_m(t)$, $\omega(t)$, $U_x(t)$ and $[\Delta U_\theta]_{\bar{r}}(t)$ by $\dot{V}_a$, $\dot{V}_m$, ω, U_x and $[\Delta U_\theta]_{\bar{r}}$ respectively, for convenience.

4.1.1 Low-density gas flows

Assuming the inertia of the fluid to be negligible for low-density gas flows, the rate of change of angular momentum flux of the fluid is considered to be equal to the torque, T_d, and then the equation of motion for the rotor is:

$$T_d = I_R \frac{d\omega}{dt} = \rho U_x A\bar{r}(U_x \tan\beta_{\bar{r}} - \omega\bar{r}) \qquad \textbf{Eq. 4. 3}$$

Where A is the annular area of the meter.

By substituting: (i) actual volume flow rate;

$$\dot{V}_a = U_x A \qquad \textbf{Eq. 4. 4}$$

(ii) meter indicated volume flow rate (inferred from the frictionless rotor assumption made under steady flow condition);

$$\dot{V}_m = A\omega\bar{r} / \tan\beta_{\bar{r}} \qquad \textbf{Eq. 4. 5}$$

(iii) the response parameter;

$$b = I_R / \rho\bar{r}^2 \qquad \textbf{Eq. 4. 6}$$

The equation of motion for the rotor (Ower 1937), (Grey 1956) can now be presented as:

$$b\frac{d\dot{V}_m}{dt} = \dot{V}_a^{\,2} - \dot{V}_a\dot{V}_m \qquad \textbf{Eq. 4. 7}$$

In the absence of any geometrical information for determining the value of the response parameter, b, we can obtain the value of b from a step response test of the meter. Rearranging Eq. 4. 7:

$$\frac{b}{\dot{V}_a^{\,2} - \dot{V}_a\dot{V}_m}d\dot{V}_m = dt \qquad \textbf{Eq. 4. 8}$$

Integrating to find the response time, t_R, required for the rotor to accelerate from a speed corresponding to the initial flow $\dot{V}_a - \Delta\dot{V}_a$; to that of the final flow $\dot{V}_a$; where $\Delta\dot{V}_a$ is the size of the step change:

$$\int_{\dot{V}_a-\Delta\dot{V}_a}^{\dot{V}_a}\left(\frac{b}{\dot{V}_a^{\,2} - \dot{V}_a\dot{V}_m}\right)d\dot{V}_m = \int_0^{t_R} dt \qquad \textbf{Eq. 4. 9}$$

It is obvious that the integration cannot be carried out to its upper limit, since it would take a mathematically infinite time to reach this limit. In order to avoid this difficulty, it is customary to compute the time required to reach a fraction $[1-(1/e)]$ of the imposed step, where e is the base of natural logarithms. This required time is called the time constant, t_c. The upper limit may thus be rewritten (Grey 1956):

$$\int_{\dot{V}_a-\Delta\dot{V}_a}^{\dot{V}_a-\left(\frac{1}{e}\Delta\dot{V}_a\right)}\left(\frac{b}{\dot{V}_a^{\,2} - \dot{V}_a\dot{V}_m}\right)d\dot{V}_m = \int_0^{t_c} dt \qquad \textbf{Eq. 4. 10}$$

For a step increase, the analytical solution is (Atkinson 1992):

$$\dot{V}_m = \dot{V}_a - \Delta\dot{V}_a \exp[-t/t_c] \qquad \textbf{Eq. 4. 11}$$

The time constant t_c is given by

$$t_c = \frac{b}{\dot{V}_a} \qquad \textbf{Eq. 4. 12}$$

Plotting $\ln[(\dot{V}_a - \dot{V}_m)/\Delta\dot{V}_a]$ against t produces a straight line (Atkinson 1992) whose gradient is equal to $-1/t_c$. Measurement of the gradient then yields a value for b as the steady flow after the step, $\dot{V}_a$, is known.

4.1.2 High-density gas flows and liquid flows

Dijstelbergen (1966) argued that Eq. 4. 7 was only valid for low-density gas flows because the inertia of the fluid in the rotor envelope was not included; his analysis was based on investigating the time constant when the flow was reduced to zero. If the flow was reduced by a step to zero, then, from the definition of t_c in Eq. 4. 12, the rotor would theoretically behave as having an infinite time constant and thus continue to rotate at its initial speed. In practice secondary effects such as bearing friction and viscosity would damp out the speed of the rotor.

Indeed, Cheesewright and Clark (1997) showed that, when a step to zero flow was applied, the time constant was very large compared with the one for step to non-zero flow; this will be explained later in Section 4.3.2. When the turbine flowmeter is subjected to a step to zero flow in high-density fluid, the time constant generally appears to be considerably less than that which occurs in gas flow (Dijstelbergen 1966). For these reasons, Dijstelbergen attempted to distinguish the rotor response in low-density and high-density time-varying flows.

For the derivation of the equation of motion, consider the rate of change in angular momentum between a radial plane at the entrance of the rotor and a corresponding plane at the rotor exit. The resulting torque, however, acts not only on the rotor but on the fluid between these two planes as well. In other words, the "gas equation" is only valid when the moment of inertia of the medium between the rotor blades is negligibly small compared with the inertia of the rotor.

When the turbine meter is subjected to a step change to zero flow, the rotor is running down under its own inertia; there will be a body of fluid rotating with the turbine blades and the predominant resistance will be due to a "disc friction" between this fluid and the surrounding fluid (Cheesewright et al. 1996). Hence, for the case of high-density fluid flow, Dijstelbergen (1966) suggests that the total angular momentum will be the sum of that of the rotor and the liquid that it carries round. The torque required to accelerate both the rotor and the fluid surrounding it can be expressed as:

$$T_d = I_R \frac{d\omega}{dt} + \left[I_f \frac{d(\omega - U_x \tan \beta_{\bar{r}} / \bar{r})}{dt} \right] \qquad \textbf{Eq. 4. 13}$$

Since T_d is also equated to the change of angular momentum flux (Eq. 4. 3), the "high-density fluid equation" now becomes:

$$I_R \frac{d\omega}{dt} + \left[I_f \frac{d(\omega - U_x \tan \beta_{\bar{r}} / \bar{r})}{dt} \right] = \rho U_x A \bar{r} (U_x \tan \beta_{\bar{r}} - \omega \bar{r}) \qquad \textbf{Eq. 4. 14}$$

Through substitutions of Eq(s). 4. 4, 4. 5 and 4. 6 into Eq. 4. 14, Dijstelbergen (1966) revised the equation of motion of the rotor for the liquid flowmeter as follows:

$$b(1 + \frac{I_f}{I_R}) \frac{d\dot{V}_m}{dt} + \dot{V}_m \dot{V}_a = \dot{V}_a^2 + b \frac{I_f}{I_R} \frac{d\dot{V}_a}{dt} \qquad \textbf{Eq. 4. 15}$$

If the ratio of inertias I_f / I_R is termed as λ, then the above equation can be written as follows:

$$b(1 + \lambda) \frac{d\dot{V}_m}{dt} + \dot{V}_m \dot{V}_a = \dot{V}_a^2 + b\lambda \frac{d\dot{V}_a}{dt} \qquad \textbf{Eq. 4. 16}$$

According to Cheesewright and Clark (1997), the above equation explains the prediction of that, for $t \leq 0$, when $\dot{V}_m = \dot{V}_a$ the fluid passes straight through the turbine without ever having any component of angular velocity, whereas any condition involving $\dot{V}_m \neq \dot{V}_a$ implies that if the fluid leaving the turbine is aligned with the exit angle of the blades, then it must have a component of angular velocity. Since there are no external torques, conservation of angular momentum can only be satisfied by an exchange of angular momentum between the rotor and the fluid.

As mentioned before, the value of b (response parameter) in Eq. 4.16, can be obtained from geometry by using Eq. 4. 6, $\left(b = I_R / \rho \bar{r}^2\right)$; and if it is assumed that only the fluid within the rotor envelope contributes to I_f, then, by treating this part of fluid as a solid body, the value of λ can also be obtained from geometry.

However, if a better estimation of $\lambda (= I_f / I_R)$ is needed, the value of $b(1 + \lambda)$ could be obtained from a step response test of the meter. Subsequent to the work published by Dijstelbergen, Cheesewright and Clark (1997) modified Dijstelbergen's approach to produce a formal mathematical solution to Eq. 4. 16, for a flow subjected to a step change

from $\dot{V}_a$ to $\dot{V}_a - \Delta\dot{V}_a$. According to Cheesewright and Clark (1997), the flow indicated by the meter, $\dot{V}_m$, will then be as shown below (assuming the leaving fluid is aligned with the exit blade angle):

$$\dot{V}_m = \dot{V}_a - H(t)\Delta\dot{V}_a\left\{1-\exp\left[-\frac{\dot{V}_a-\Delta\dot{V}_a}{b}\left(\frac{1}{1+\lambda}\right)t\right]\right\} \qquad \textbf{Eq. 4. 17}$$

where $H(t)$ is a unit step function at t = 0. Rearranging:

$$\frac{\dot{V}_m-\dot{V}_a}{\Delta\dot{V}_a} = \exp\left[-\frac{\dot{V}_a-\Delta\dot{V}_a}{b}\left(\frac{1}{1+\lambda}\right)t\right]-1 \qquad \textbf{Eq. 4. 18}$$

Thus the empirical representation assumes that when a 'step' change in flow is applied to a turbine, the whole response to the 'step' is exponential with the time constant given by the meter characteristics and the true flow rate after the 'step':

$$\left[t_c = b(1+\lambda)/\left(\dot{V}_a-\Delta\dot{V}_a\right)\right] \qquad \textbf{Eq. 4. 18a}$$

By using the above equation, a numerical value of the time constant can be obtained by plotting $\ln\left[\left(\dot{V}_m-\dot{V}_a\right)/\Delta\dot{V}_a\right]$ against t. The quantity $b(1+\lambda)$ could then be obtained from the slope since $\dot{V}_a-\Delta\dot{V}_a$ (the steady flow after the step) is known. With the value of b obtained from geometry, a better estimation of λ could then be made from the step test.

According to Cheesewright and Clark (1997), in practical situations true step changes are impossible and Eq. 4. 17 can only be considered as a mathematical solution rather than a practical solution, as the flow must separate off the blade. The following paragraph explains this flow separation phenomenon, taken from Cheesewright and Clark (1997).

"The maximum rate at which the volume flowrate imposed on the meter can be changed depends only weakly on the characteristics of the meter, being primarily dependent on the forces and pressures in the external device that produces the change. The exchange of angular momentum between the rotor and the fluid is controlled by the forces of interaction between the turbine blades and the fluid, and for fast, externally imposed, changes in flowrate, the rate at which the exchange proceeds will not be dependent on the

rate of change of flow. This conclusion implies that there is likely to be a short period immediately following a "step change" in the flowrate when Eq. 4. 16 is not strictly applicable. In physical terms, this is likely to correspond to the fluid leaving the turbine at an angle other than the exit angle of the blades. Equally, it seems probable that this corresponds to stall and flow separation when the problem is looked at in terms of blade dynamics, as in the work of Jepson (1964)." (Cheesewright and Clark 1997).

Both of the above models, ("low-density gas" and "high-density fluid"), are based upon a number of assumptions: (1) the fluid is perfectly guided between the blades, (2) the fluid is aligned with the blade angle when it leaves the rotor zone; and (3) the rotor is frictionless, i.e. other resistance torques mentioned in Section 3.2.4 are negligible. The first two cases will be reviewed in Chapter 8 to determine the details of fluid behaviour around the blade in pulsating flow.

4.1.3 Resistance torques included in the "Gas Equation"

In previously stated theories, regardless of whether the flow was steady or unsteady, the flow was always assumed to be aligned with the blade angle at the rotor exit. In Section 3.2.3., when resistance torques are not negligible, the flow was assumed to enter the rotor zone at a different angle to the blade angle, but it becomes aligned with the blade angle when it leaves. An alternative assumption that could be used is that the relative flow enters the rotor zone at the blade angle, but leaving at a different angle to the blade angle. This would be based on the argument of some fluid deflection at outlet, due to the limited fluid guidance ability of the rotor blading (Lee and Evans 1970).

Hence, even if a steady flow is assumed to be entering at the blade angle, there would now be a difference in tangential velocity at the outlet if the flow is deflected. This hypothesis leads back to the existence of resistance torques in the steady flow condition. The driving torque T_d is slightly modified into the following form to account for the fluid deflection due to resistance torques (Lee et al. 1975):

$$T_d = \rho U_x A \bar{r} \frac{(U_x \tan \beta_{\bar{r}} - \omega \bar{r})}{1+\eta} \qquad \textbf{Eq. 4. 19}$$

Where η is the blade deviation factor. It represents the percentage loss of fluid deflection at outlet due to the limited fluid guidance capacity of the rotor blading (Lee and Evans

1970). For perfectly guided flow, i.e. if the relative flow leaves at the blade angle, η would be zero. Lee and Evans (1965) gave $\eta = 0.2$ (cf. Lee and Evans 1970) as used in the above equation, based on the comparison of theoretical analysis with experimental data on meter accuracy.

To account for resistance torques for unsteady flow conditions, the transient equation (Lee et al. 1975) is

$$I_R \frac{d\omega}{dt} = T_d - T_r \qquad \textbf{Eq. 4. 20}$$

Lee et al. (1975) gave an equation for T_r:

$$T_r = T_f + T_n \qquad \textbf{Eq. 4. 21}$$

Where T_f is the fluid drag and T_n is the non-fluid drag, assumed constant. Lee et al assumed that T_f could be replaced by a corresponding total fluid force, F_f, acting at the root mean square radius of the rotor, i.e.

$$T_f = \bar{r}F_f \qquad \textbf{Eq. 4. 22}$$

Introducing a dimensionless fluid drag coefficient C_f for F_f using rotor tangential velocity $\bar{r}\omega$ at the blade section at radius, $\bar{r}$:

$$C_f = \frac{F_f}{(\rho/2)A(\bar{r}\omega)^2} \qquad \textbf{Eq. 4. 23}$$

If T_n is assumed to be constant, through substitutions of Eq(s). 4. 21, 4. 22 and 4. 23 into Eq. 4. 20, Lee et al (1975) then obtained:

$$I_R \frac{d\omega}{dt} = \rho U_x A\bar{r}\frac{(U_x \tan\beta_{\bar{r}} - \omega\bar{r})}{1+\eta} - \frac{(\rho A\bar{r}^3 C_f \omega^2)}{2} - T_n \qquad \textbf{Eq. 4. 24}$$

Then, through substitutions of Eq(s). 4. 4, 4. 5 and 4. 6 into the above equation, Lee et al's equation is now modified into the following form:

$$b(1+\eta)\frac{d\dot{V}_m}{dt} = \dot{V}_a^2 - \dot{V}_a\dot{V}_m - \frac{(1+\eta)C_f \tan\beta_{\bar{r}}}{2}\dot{V}_m^2 - \frac{(1+\eta)AT_n}{\tan\beta_{\bar{r}}\rho\bar{r}} \qquad \textbf{Eq. 4. 25}$$

4.1.4 Resistance torques included in the "High-Density Fluid Equation"

The same procedure could be taken here to include resistance torques for Eq. 4. 14:

$$I_R \frac{d\omega}{dt} + \left[I_f \frac{d(\omega - U_x \tan \beta_{\bar{r}} / \bar{r})}{dt} \right]$$
$$= \rho U_x A \bar{r} \left(\frac{U_x \tan \beta_{\bar{r}} - \omega \bar{r}}{1+\eta} \right) - \frac{\left(\rho A \bar{r}^3 C_f \omega^2 \right)}{2} - T_n \qquad \textbf{Eq. 4. 26}$$

Using the same substitutions as before, the above equation becomes:

$$b(1+\eta)(1+\lambda)\frac{d\dot{V}_m}{dt} - b(1+\eta)\lambda\frac{d\dot{V}_a}{dt}$$
$$= \dot{V}_a^{\,2} - \dot{V}_a \dot{V}_m - \frac{(1+\eta) C_f \tan \beta_{\bar{r}}}{2} \dot{V}_m^{\,2} - \frac{(1+\eta) A T_n}{\tan \beta_{\bar{r}} \rho \bar{r}} \qquad \textbf{Eq. 4. 27}$$

All notations are as previously stated.

Now Eq. 4. 27 more closely represents the real rotor behaviour when the meter is subjected to pulsating liquid flow. However, there has been no experimental evidence to validate this equation and most of the published work from previous researchers (reviewed in the next section) were usually based on the frictionless equations stated in Section 4.1.1 and 4.1.2.

Therefore, it was considered that a Computational Fluid Dynamics (CFD) model would allow the investigation of the coupling between the flow and the rotor dynamics during unsteady flow. If the CFD model could correlate with experimental results, subsequently, an evaluation could be made to show the difference between Eqs. 4. 16 (without friction) and 4. 27 (with friction). As a result of the lack of correlation between experimental results, to be reviewed in Chapter 8, the inclusion of resistance torques in the "High-Density Fluid Equation" was not fully evaluated analytically.

4.2 Performance Characteristics in Unsteady Flow

4.2.1 Response parameter, *b*

The response parameter (b) of a turbine flowmeter determines how quickly the meter responds to changes in the flow rate and it depends upon: the inertia of the rotor (I_R), the density of the fluid and the geometry ($\bar{r}$ — the root mean square radius between the blade hub and blade tip) of the rotor. The mathematical expression is as given in Eq. 4. 6: $b = I_R / \rho \bar{r}^2$, usually expressed in the unit of m^3.

4.2.2 The influence of fluid density

As mentioned in Section 2.1.6, the dynamic response of the meter depends upon the density of the fluid. The most common distinctive features for gas turbine meters are the large hub and small blades designed to create a high flow velocity and a high torque on the rotor (Baker 1993). As explained in Section 4.1, in low-density gas flows, the angular momentum of the gas is treated as negligible compared with that of the rotor. If high frequency pulsations are present, particularly in gas flows, then the meter's lack of responsiveness will cause it to over-register the mean flow rate as described in Section 2.2. Because liquids have a higher dynamic viscosity than gases, the shear stress applied to the blades by liquid flow is also more significant than gas flow.

4.2.3 Ratio of inertias

The ratio of the fluid inertia enclosed within the rotor envelope, I_f, to the rotor inertia, I_R, is represented by $\lambda = I_f / I_R$. This is another parameter which contributes to the response characteristics, as described in Section 4.1.2, it is particularly important to the meter operating in pulsating liquid flow. The term I_f is calculated by assuming the fluid is perfectly guided between the rotor blades, and, hence, that it can be treated as a solid body within the rotor envelope.

4.2.4 Time constant

The transient response of turbine flowmeters may be loosely characterised by the time constant of the meter (including the rotor and the coupled fluid) when a step change is applied to the fluid flow. If an instantaneous increase were to occur in the flow rate, the rotor will accelerate from a speed corresponding to the original flow rate, to a speed corresponding to the new flow rate. The time required to accelerate the rotor to approximately 63% of the change in speed is regarded as the time constant, t_c. The smaller the time constant, the faster the rotor response to change in flow. Typical values vary with: the size of the meter; the associated inertia of the rotor and inertia of the fluid; and the blade angle employed (Watson 1977). In addition, time constant is flow rate dependent, with $\dot{V}$ being the steady flow rate after the step: $\left[t_c = b/\dot{V}\right]$ for low density gas flows; or $\left[t_c = b(1+\lambda)/\dot{V}\right]$ for high density fluid flows.

According to BS ISO TR 3313 (1998):

(i) For flowmeters in the range of 2.54 cm (1 in) to 10.16 cm (4 in) in diameter, for measuring gases flowing at near atmospheric pressure, typical time constants are of the order of 1 s.

(ii) For flowmeters in the range from 1.91cm (3/4 in) to 5.08 cm (2 in) in diameter, for measuring water, typical time constants are of the order of 1 ms.

It is thus apparent that errors due to pulsation are much more likely to be significant with flowmeters measuring low pressure gases than with flowmeters measuring liquids.

4.3 Step Change in High-Density Fluid Flows

This section reports the different phenomena observed in experiments to investigate: "step from zero flow", "step to zero flow" and "step change in flow". For applications in batch flow measurement, the process involves the start up and shut down of valves or pumps, hence the combinational effect of "step from zero flow" and "step to zero flow" on turbine flowmetering is of particular importance. On the other hand, in other applications such as aerospace, the dynamic response of small liquid turbine meters is of particular importance when the meter is to be used in the fuel flow control loops. Cheesewright and Clark (1997) quoted that the latest specification in control systems for aircraft gas turbine engines required a guaranteed frequency response up to two hundred Hertz.

4.3.1 Step from zero flow

Grey (1956) used potential flow theory to estimate the lift forces acting on a single blade during a speeding up process (drag forces were assumed to be negligible). He gave numerical values of the time constant (t_c) for a range of meter sizes for liquid flows and showed that in the range of meter diameters, 12-150mm, for the flow range of 5 to 50 gal/min (approximately 0.38×10^{-3} m^3/s to 3.8×10^{-3} m^3/s), the values was in the range of 1-9ms; he also showed that the time constant decreased with increasing flow rate. Further, Grey suggested that an increase in blade angle would lead to an increase in the time constant.

Higson (1964) reported an investigation on the transient response of a single 20 mm liquid flowmeter designed for use in metering aircraft fuel in the flow range 8 gal/hr to 80 gal/hr (approximately 0.01×10^{-3} m^3/s to 0.1×10^{-3} m^3/s). Using water as the test liquid, within the specified flow range, his experiments showed that for a step change from zero, t_c is between 6-110 ms. He also observed that the time constant decreased with increasing flow rate. For the rotor to return to equilibrium, it took approximately $4t_c$. However, Higson neglected friction effects such as the bearing friction for this evaluation of t_c.

Jepson (1964) commented that Grey's theoretical approach was inappropriate: firstly, it neglected the reductions in lift and drag coefficients due to the finite spacing of the blades; secondly it neglected the effect of stall and flow separation, due to the high values of

incidence over the initial part of the speeding-up process. Hence, Jepson (1964) formed an equation to calculate the change in rotor speed for a step increase in the flow rate starting from zero, in which the torque was calculated from lift and drag coefficients. His theoretical results for response time agreed closely with those obtained by Higson. Similarly, Jepson also assumed that: bearing and other non-aerodynamic drags could be neglected, and that the exit angle was the same as the blade angle.

However, later, Jepson (1967) questioned the accuracy of the experimental results obtained by Higson. Higson used the peak voltages generated as each rotor blade passed an inductive pick-up coil to measure the transient speed. The meter tested by Higson had only three blades, so that for the flow rates investigated, the probe could record a maximum of only two peak-to-peak voltages before the 63% rise time was reached. Therefore, inaccuracies would have occurred in estimating the time constant due to the small number of data points.

As a result, Jepson (1967) developed a new experimental system to overcome the difficulty of low-bladed rotors, by fixing a small, ancillary, perforated drum to the rotor, a miniature photoelectric cell being used to indicate the meter's position after applying the step-input in flow. The perforated drum had 12 holes, so in one revolution, 12 pulses would be emitted from the photocell. His investigations were based on 2 open-channel water meters, one had two blades, and the other had three blades. His experimental results showed that the measurement of time constants, in both air and water, were to an accuracy of better than ±3% compared with method of using the rotor alone.

4.3.2 Step to zero flow

In a step change to zero flow, as Baker (1993) suggested, the fluid between the blades will be subject to some re-circulation, but will essentially be carried around by the rotor, and so will exact much lower retarding forces (due to viscous friction from the surrounding stationary fluid) than those which Jepson (1967) showed for the accelerating rotor.

The step response tests reported by Cheesewright and Clark (1997) did not include start-up from zero but they did include steps to zero, and in that case, it was demonstrated that the

whole mechanism of the response was different because the forces on the turbine rotor are dominated by disk friction effects rather than by fluid dynamic forces on the blades.

4.3.3 Step change in flow

Shafer (1962) obtained a range of time constant values (2-5 ms) by imposing large steps (around 40% to 80% of the meter flow range) for 3 different designs of 12mm liquid meters, the liquid that he used in the investigation had a density of 760 kg/m^3.

Cheesewright and Clark (1997) carried out step tests on small (6-12.5mm) turbine flowmeters using water, and all the tests showed a generally exponential response to the step. Under small step changes, the time constants were of the order of a few milliseconds, which agreed well with the work by Higson and Jepson, respectively. Also, Cheesewright and Clark implemented the mathematical equation (Eq. 4. 17) described in Section 4.1.2. into their experimental data, and by using the value of b estimated from rotor geometry (which compared well to the value obtained from air step tests on the same meter), the experimental results then allowed an estimation of λ, which was approximately 1 for one of the meters investigated.

4.4 Pulsation Effects

Flow pulsations may be induced in many machines, pipeline fittings and control operations used in industries, and these cause a tendency to over-registration of mean flow, *OR*, and amplitude attenuation, *AA*, in turbine flowmetering. The response of a turbine flowmeter to flow pulsation is discussed here. It can range from the ability to follow the pulsation almost perfectly (medium to large flowmeters in liquid flows) to an almost total inability to follow the pulsation (small to medium flowmeters in gas flows with moderate to high frequencies of pulsation). This latter condition is the worst case for a turbine flowmeter installation because not only does the flowmeter output not show significant pulsation but if the flow pulsation is of significant magnitude, the apparently steady flowmeter output will not be a correct representation of the mean flow.

4.4.1 Low-density gas flows

Lee et al. (1975) obtained the effect of sinusoidal pulsations by using a normalised form of Eq. 4. 25. They validated their theoretical results on a single 100-mm turbine meter of pulsation frequency not higher than 18 Hz and pulsation amplitude of 10 % to 100 %. The theoretical values of over-registration error agreed well with the experimental values at the lower range of pulsation amplitudes. However, at pulsation amplitudes of 75% or higher, the theoretical values tend to under-estimate the experimental values (by as high as a discrepancy of 20% of the experimental over-registration error). Lee et al explained that this was due to the appearance of non-uniform inlet velocity profile as pulsation amplitude increased, whereas a uniform velocity profile was assumed in the theoretical approach. They also reported an experimental error of mean flow reading as high as 60% for pulsation amplitude of 75 % or higher.

McKee (1992) investigated the over-registration errors of both a single- and a two rotor 100 mm turbine meters of pulsation frequencies ranging from 1 to 75 Hz at pressure pulsation amplitudes not higher than 20%. A maximum of 1.5% of error was observed from his experiment.

Atkinson (1992) developed a software tool to predict the over-registration error of a turbine meter in pulsating gas flow. The tool is based on the equation of motion of the gas flowmeters $b\left(d\dot{V}_m/dt\right)=\dot{V}_a^{\,2}-\dot{V}_a\dot{V}_m$ (Eq. 4. 7).

Assuming that any pulsations in the flow are regular and approximately sinusoidal, use of the software tool involves recording the turbine meter output signal and then calculating a correction factor. If the flow $\dot{V}_a=\overline{\dot{V}_a}(1+\alpha_p\sin 2\pi f_p t)$ in which pulsations are periodic with period T and the mean flow rate is $\overline{\dot{V}_a}$, then the following dimensionless variables are defined:

$$T=2\pi f_p t \qquad \textbf{Eq. 4. 28}$$

$$F=\dot{V}_m/\overline{\dot{V}_a} \qquad \textbf{Eq. 4. 29}$$

$$B=2\pi b f_p/\overline{\dot{V}_a} \qquad \textbf{Eq. 4. 30}$$

Eq. 4. 7 is now normalised into the following form

$$B\frac{dF}{dT}+F(1+\alpha_p\sin T)=(1+\alpha_p\sin T)^2 \qquad \textbf{Eq. 4. 31}$$

Since the pulsation was assumed to be a pure sinusoidal waveform, Atkinson found F as a function of T. Integrating $F(T)$ numerically over the interval $\Delta t = T$, a dimensionless mean meter reading F was obtained and the over-registration error, OR, given by:

$$OR=F(T)-2\pi \qquad \textbf{Eq. 4. 32}$$

Atkinson produced a look-up table relating the amplitude and frequency of the pulsations in the meter output signal to the amplitude of the pulsations in the actual flow and hence to the meter error. However the look-up table provided was limited (Cheesewright et al. 1996) in its range of amplitudes of the actual flow, because solutions to Eq. 4. 7 for $\dot{V}_m$ as

a function of $\dot{V}_a$ were double valued at high amplitudes, which for some conditions is a quadratic with two positive, real, roots.

As a summary of Atkinson's findings, factors governing the magnitude of the error are the flow rate, frequency and waveform of the pulsations, as well as the time constant of the rotor. Correction factors obtained by this method were checked experimentally by Cheesewright et al (1996), and it was found that Atkinson's tool was effective with pulsating-induced errors as high as 50%, with correction possible to an accuracy of better than ±2%.

4.4.2 High-density gas flows and liquid flows

A literature survey revealed the only experimental study on liquid flow effects was published by Dowdell and Liddle (1953) and their results did not show any significant over-registration error. They tested three water meters in the size range of 6-in to 8-in with pulsation frequency not higher than 132.5 cycles per minute (around 2 Hz), in which trivial errors under this kind of pulsating conditions would be expected for larger size meters. Moreover, they did not measure the actual flow pulsations to which the meter was subjected; hence, the results were not conclusive.

According to BS ISO TR 3313 (1998), there has not been any experimental validation of the Dijstelbergen's equation for liquid flows. Dijstelbergen (1966) has published data, using Eq. 4. 16, for the theoretical pulsation error for square wave flow pulsation of different amplitude, frequency and mark/space ratio, but it is difficult to generalize his results and there has been no experimental confirmation of them.

Hence, this research will investigate further the applicability of Eq. 4. 16 (frictionless rotor approach) and Eq. 4. 27 (with friction included), either theoretically (by the use of computer simulation) or experimentally, for sinusoidal pulsating flow in small turbine flowmeters. The next chapter will outline the methodologies undertaken during the course of this research program.

Chapter 5 Research Methodology and Preliminary Theoretical Work

Having reviewed the existing theoretical models for the motion of the rotor, the following chapters cover the three main avenues that have been used to investigate the behaviour of small turbine flowmeters under pulsating liquid flows: theoretical, experimental, and numerical modelling using Computational Fluid Dynamics (CFD) simulation. It is anticipated that the undesirable effects of pulsation on accuracy of mean flow measurement can be understood and appropriate action can be taken to correct for metering errors.

5.1 Research Methodology

5.1.1 Theoretical method

A theoretical approach for prediction of the meter behaviour when it is under pure sinusoidal pulsating flow is presented in Section 5.2. Similar to the method used by Atkinson in pulsating gas flows, but including fluid inertia, by using the equations reviewed in Section 4.1.2, this approach is based on the assumptions that the outlet flow angle is aligned with the blade angle; and there are negligible resistance torques such as bearing drag and electromagnetic pick-up torque.

One of the advantages of conducting such work is that a preliminary indication of the range of errors and pulsation amplitude attenuations can be predicted. Identification of the relevant parameters and their effects would facilitate understanding of experimental results.

5.1.2 Experimental method

There appears to be no experimental work of significance relating to meter response to pulsating liquid flows in the open literature.

The experimental program is described in Chapter 6, the responses of a number of small turbine flowmeters to (sinusoidally) pulsating flow have been evaluated. These results are

then compared with the prediction from the theoretical model (in Chapter 7) and these comparisons also allow insight into possible procedures for the correction of metering errors (Chapter 7).

5.1.3 Numerical method

Numerical modelling of physical blade (and associated rotor) dynamics is of importance, mainly because it allows modelling of effects of velocity misalignment with blade angles and the resulting flow separation. Chapter 8 presents the work undertaken towards the development of a Computational Fluid Dynamic (CFD) model of unsteady turbine flowmeter response.

The numerical solutions obtained through CFD represent the values of the physical variables of the fluid field. An advantage of carrying out such work is that the flow around the blade area can be visualized and understood at different time steps within a pulsating cycle. By integration of pressure over the blade surfaces, the instantaneous resulting torque acting on the blades can then be determined and, hence, the corresponding motion of the rotor (by use of Eq. 4.16) can be predicted . Another objective of this work is to investigate the relationship between the values of rotational inertia of fluid, I_f, the pulsation frequencies, f_p and relative pulsation amplitude, α_p. The dynamic performance from the simulation model will then be compared with the results of experimental meter tests.

5.2 Turbine Flowmeter Dynamic Response Prediction by using Theoretical Model

The theories of dynamic meter response reviewed in the last Chapter gave a background to this theoretical model. Atkinson used the normalised frictionless "gas equation" (Eq. 4. 31) to predict meter errors for gas turbine meters when subjected to sinusoidal (in time) pulsations. As reviewed in Section 4.4.1., Atkinson normalised the frictionless "gas equation" into the form shown in Eq. 4. 31. Atkinson produced a look-up table relating the amplitude and frequency of the pulsations in the meter output signal to the amplitude of the pulsations in the actual flow and hence to the meter error. The same approach is taken here to attempt prediction of metering errors for liquid turbine meters using the Dijstelbergen's frictionless "high-density fluid equation" (Eq. 4. 16). The following sections review the procedures taken to accomplish this.

5.2.1 Normalisation of the frictionless "high-density fluid equation"

As stated in Section 4.1.2, the frictionless "high-density fluid equation" (Eq. 4. 16) is:

$$b(1+\lambda)\frac{d\dot{V}_m}{dt}+\dot{V}_m\dot{V}_a=\dot{V}_a^{\,2}+b\lambda\frac{d\dot{V}_a}{dt}$$

Assuming the pulsation is a pure sinusoid, with α_p and f_p being the imposed relative pulsation amplitude and pulsation frequency respectively, and if the mean flow rate is $\overline{\dot{V}_a}$, then the actual time dependent flow $\dot{V}_a$ is equal to $\overline{\dot{V}_a}(1+\alpha_p \sin 2\pi f_p t)$. Similar to the normalisation parameters that Atkinson used (See Section 4.4.1.), the following dimensionless variables are defined as: $T=2\pi f_p t$ (Eq. 4. 28), $F=\dot{V}_m/\overline{\dot{V}_a}$ (Eq. 4. 29) and $B=2\pi b f_p/\overline{\dot{V}_a}$ (Eq. 4. 30) respectively. Through substitution of these variables, the frictionless "high-density fluid equation" is now normalised into the following form:

$$B(1+\lambda)\frac{dF}{dT}+F(1+\alpha_p \sin T)=(1+\alpha_p \sin T)^2+B\lambda\alpha_p \cos T \qquad \textbf{Eq. 5. 1}$$

The above equation can be solved numerically by using Mathematica (Version 4.0.1) and from the resulting *F(T)*, a simulated meter output can be obtained. Hence for any relative pulsation amplitude and pulsation frequency, if the values of the actual mean flow rate ($\overline{\dot{V}_a}$), b and λ are known, the meter over-registration error (*OR*), and amplitude attenuation (*AA*) can be predicted, and this is explained in the following paragraphs.

Over-registration error

Having obtained the solution of *F(T)*, an integration of the solution could be carried out over the interval $\Delta T=2\pi$, and the dimensionless mean meter reading $\overline{F}$ can be expressed as shown below:

$$\overline{F} = \frac{\overline{\dot{V}_m}}{\overline{\dot{V}_a}} = \left[\int_x^{x+2\pi} F(T).dT \right] \Big/ 2\pi \qquad \textbf{Eq. 5.2}$$

Therefore the over-registration error (Eq. 2.3) can be evaluated as,

$$OR = \left(\frac{\overline{\dot{V}_m}}{\overline{\dot{V}_a}} - 1 \right) \times 100\% = \left(\overline{F} - 1 \right) \times 100\% \qquad \textbf{Eq. 5.3}$$

Amplitude attenuation

By finding the maximum and minimum value of *F(T)*, the dimensionless meter indicated amplitude is:

$$F_{\max} - F_{\min} = \frac{\varphi_m}{\overline{\dot{V}_a}} \qquad \textbf{Eq. 5.4}$$

Where φ_m is the peak to peak amplitude of the meter reading. Since the peak to peak amplitude of the actual pulsation, φ_a, is known as $2\alpha_p \overline{\dot{V}_a}$ (See Section 2.2), the amplitude attenuation (Eq.2.4) can then be evaluated as,

$$AA = \left(1 - \frac{\varphi_m}{\varphi_a} \right) \times 100\% = \left(1 - \frac{(F_{\max} - F_{\min})}{2\alpha_p} \right) \times 100\% \qquad \textbf{Eq. 5.5}$$

5.2.2 Estimation of $b(=I_R/\rho\bar{r}^2)$ and $\lambda(=I_f/I_R)$

In all the work on the response of turbine meters in gas flows (Grey 1956, Atkinson 1992), the response parameter, b, has been determined experimentally from step response tests. However, such tests are much more difficult in water because the step must be much faster and the dynamic pressures involved are much larger. The only published reports of step tests in water were those by Cheesewright and Clark (1997), which included data for two of the meters used in this research program. For one of these meters Cheesewright and Clark also reported values of b obtained by calculation from step tests with the meter in air flow and values of b obtained by calculation from engineering drawings of the meter rotor by using Eq.4. 6, $b=I_R/\rho\bar{r}^2$. The data suggested that adequate estimates of the value of b can be obtained from drawings of a meter rotor, as the geometrical estimate of one meter compared well to the value obtained from air step tests on the same meter. If only the fluid contained within the envelope of the meter rotor is assumed to contribute to I_f, the value of ratio of inertias, λ, can also be obtained from the geometry. This approach was used here to obtain estimates of b and λ for those meters which had not been subjected to step response tests.

Of the five meters that were available for testing in this research program (Section 6.1). Meter B (12 mm 3-bladed) and meter D (12 mm 6-bladed) were selected for this theoretical modelling. This is because both meters are nominally of the same size and both can be operated on the same flowrate (within their linear ranges). However, due to geometrical differences, the values of b, I_R, I_f and λ are not the same for both meters, therefore a comparison could be made from the prediction to see the resulted effects of using these different values under the same flow condition.

Furthermore, meter D has double the number of blades of meter B. This condition can also provide some insight into how reliable the model is, since it is based on the assumption that flow is fully guided between blades, the flow is expected to be less guided in a lower-bladed rotor, therefore the predictions made for meter B (3-bladed) may be less accurate then the ones made for meter D (6-bladed). The effect of this condition from the theoretical prediction can be compared with experimental data obtained later on.

A solid modelling program called Solidworks (Version 98plus) allows for the calculation of the mass properties of any created geometry within the program, hence, drawings of rotor and casing were created by using Solidworks and then both the inertia of rotor, I_R, and inertia of fluid (assumed as solid contained with the rotor envelope), I_f, were obtained from this program. Note that except for meter C (detailed drawing available, see Appendix A), all of the rotor geometries were measured using a computer controlled contact co-ordinate measuring machine (Mitutoyo model FN005); resolution was quoted to 0.001 mm. The following table shows the parameters obtained from Solidworks for all five meters:

Meter (Nominal size mm/ blade number)	Linear Flowrange (10^{-3} m^3/s)	I_R ($\times 10^{-9}$ kg m^2)	I_f ($\times 10^{-9}$ kg m^2)	$b = I_R/\rho\bar{r}^2$ ($\times 10^{-7}$ m^3)	$\lambda = I_f/I_R$	$b(1+\lambda)$ ($\times 10^{-7}$ m^3)
A (6 mm / 3)	0.025 - 0.4	2.185	4.068	2.850	1.862	8.16
B (12 mm / 3)	**0.14 - 1.67**	**8.894**	**30.542**	**5.123**	**3.434**	**22.71**
C (12 mm / 5)	0.015 - 0.092	4.528	5.887	4.474	1.300	10.29
D (12 mm / 6)	**0.04 - 0.4**	**6.900**	**4.851**	**4.855**	**0.703**	**8.27**
E (25 mm / 5)	0.44 - 4.4	206.6	411.0	34.18	1.989	67.98

Table 5.1 Various parameters obtained from Solidworks

In the above table, $\bar{r}$ represents the root mean square radius and all other notations are as before. For each meter, with the knowledge of b, ranges of dimensionless B values could be found for various pulsation frequencies (f_p) and mean flow rates ($\overline{\dot{V}_a}$), by using Eq. 4. 30: $B = 2\pi b f_p / \overline{\dot{V}_a}$. Take meter B for example, if f_p is 10 Hz and $\overline{\dot{V}_a}$ is 0.292×10^{-3} m^3/s, the value of B would be equal to: $2\pi b f_p / \overline{\dot{V}_a} = 0.4893$.

With a fixed value of $\overline{\dot{V}_a}$ equals to 0.292×10^{-3} m^3/s, values of λ and B for meter B and meter D, respectively, were input into Eq. 5. 1, and the equation was then solved for a range of α_p and f_p, using Mathematica. This yielded values of $F(T)$ from which predicted values of over-registration error and amplitude attenuation were determined. The following two sections review the prediction results from this model for both meters, for a range of f_p below maximum possible pulsation frequency (see Section 6.2) and a range of α_p up to 50% (this is a value chosen arbitrarily aiming to predict the effects); according to BS ISO TR 3313 (1998), as mentioned in Section 1.1.2, pulsation amplitudes relative to mean flow can vary from a few percent to 100% or larger.

5.2.3 Prediction of over-registration error

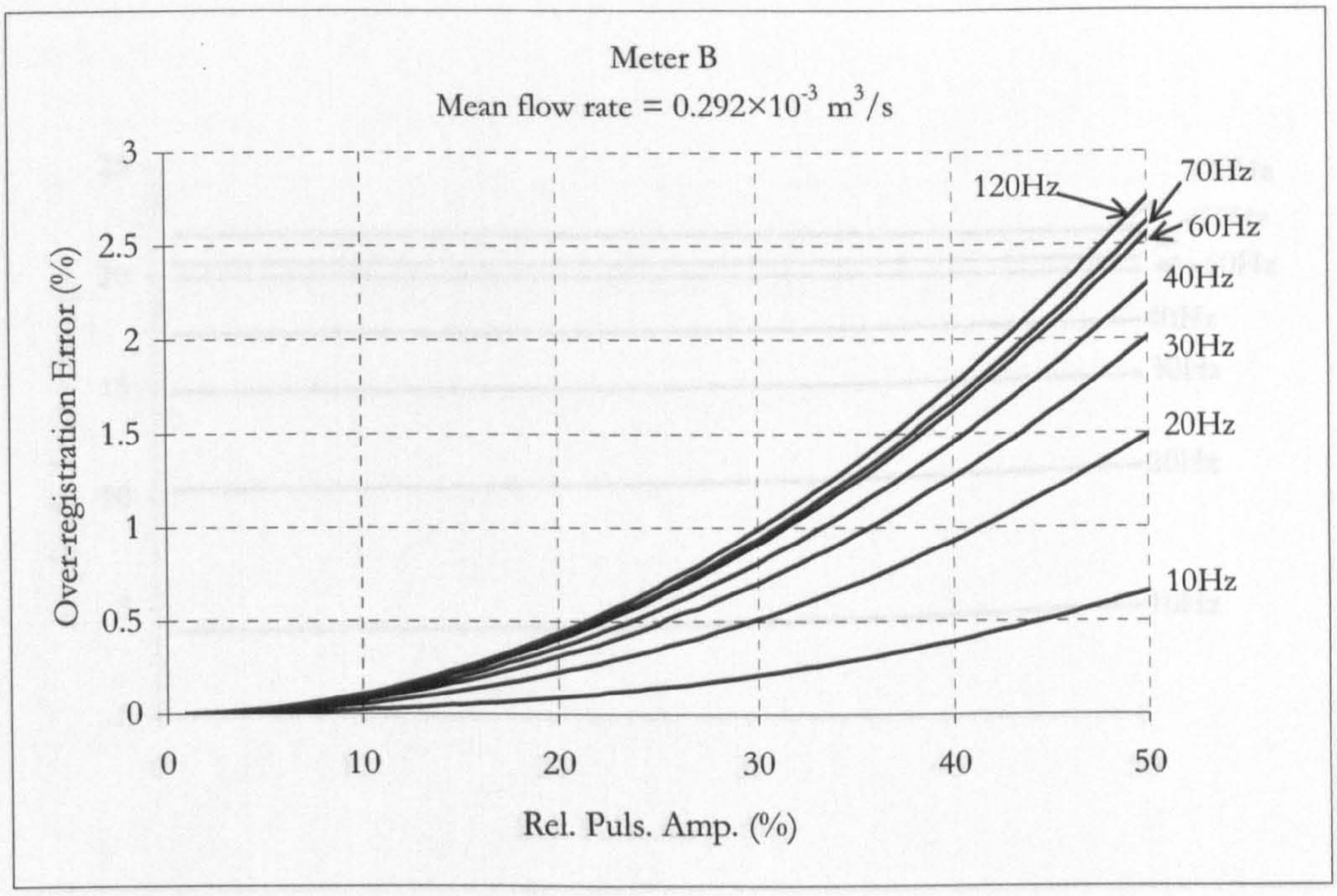

Figure 5.1 Meter B (3-bladed): Prediction of over-registration errors with differing pulsation amplitudes and pulsation frequencies

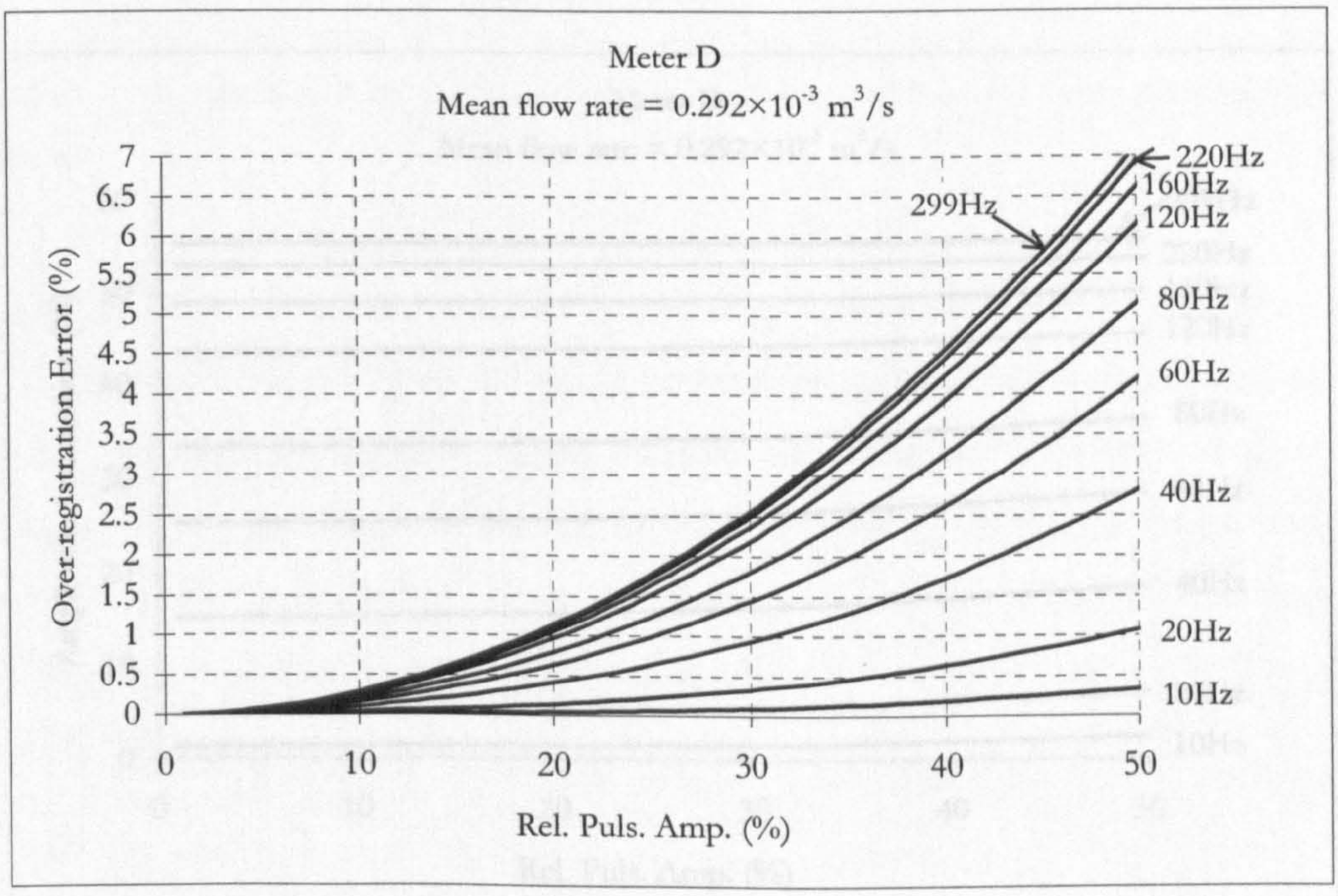

Figure 5.2 Meter D (6-bladed): Prediction of over-registration errors with differing pulsation amplitudes and pulsation frequencies

5.2.4 Prediction of amplitude attenuation

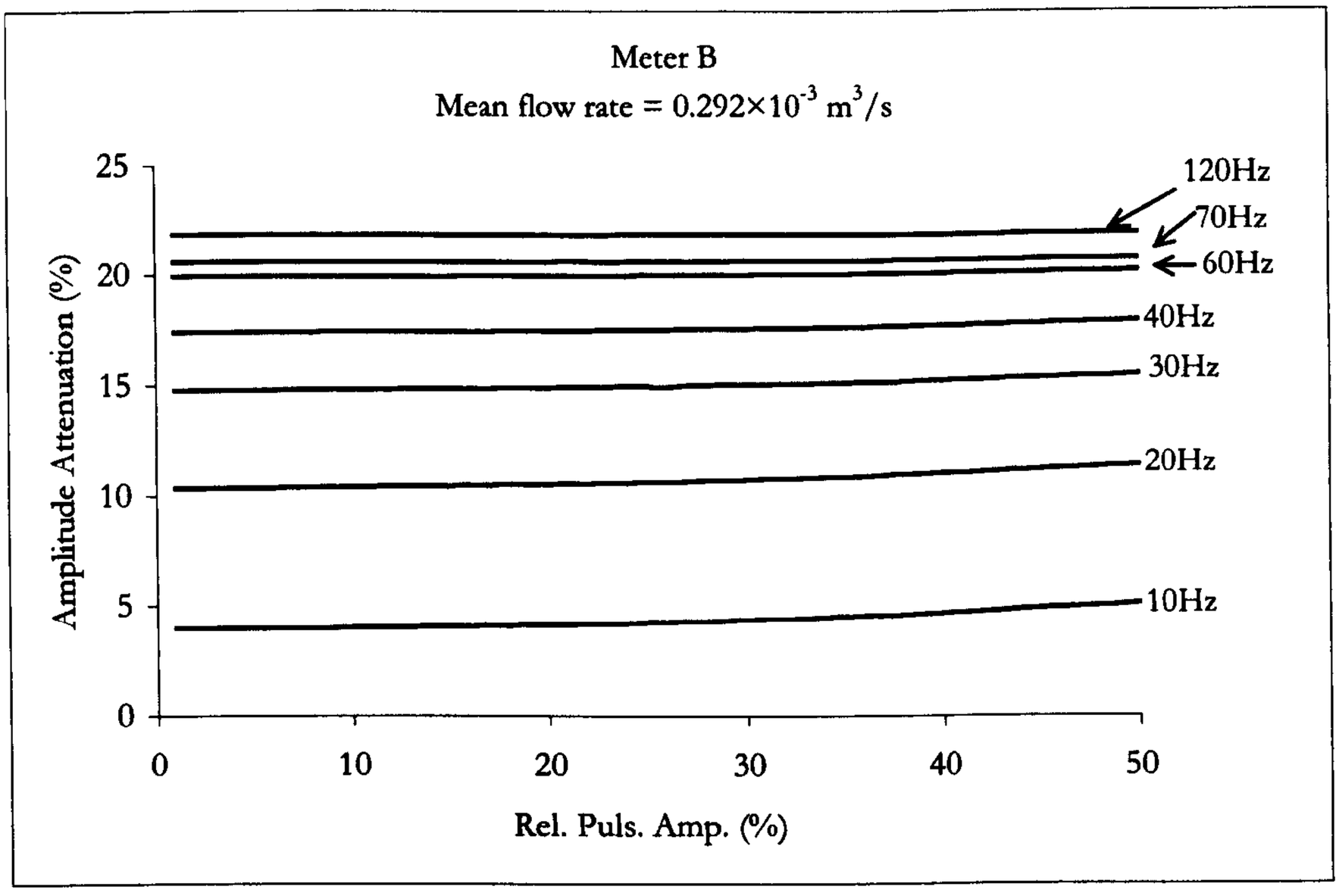

Figure 5.3 Meter B (3-bladed): Prediction of amplitude attenuations with differing pulsation amplitudes and pulsation frequencies

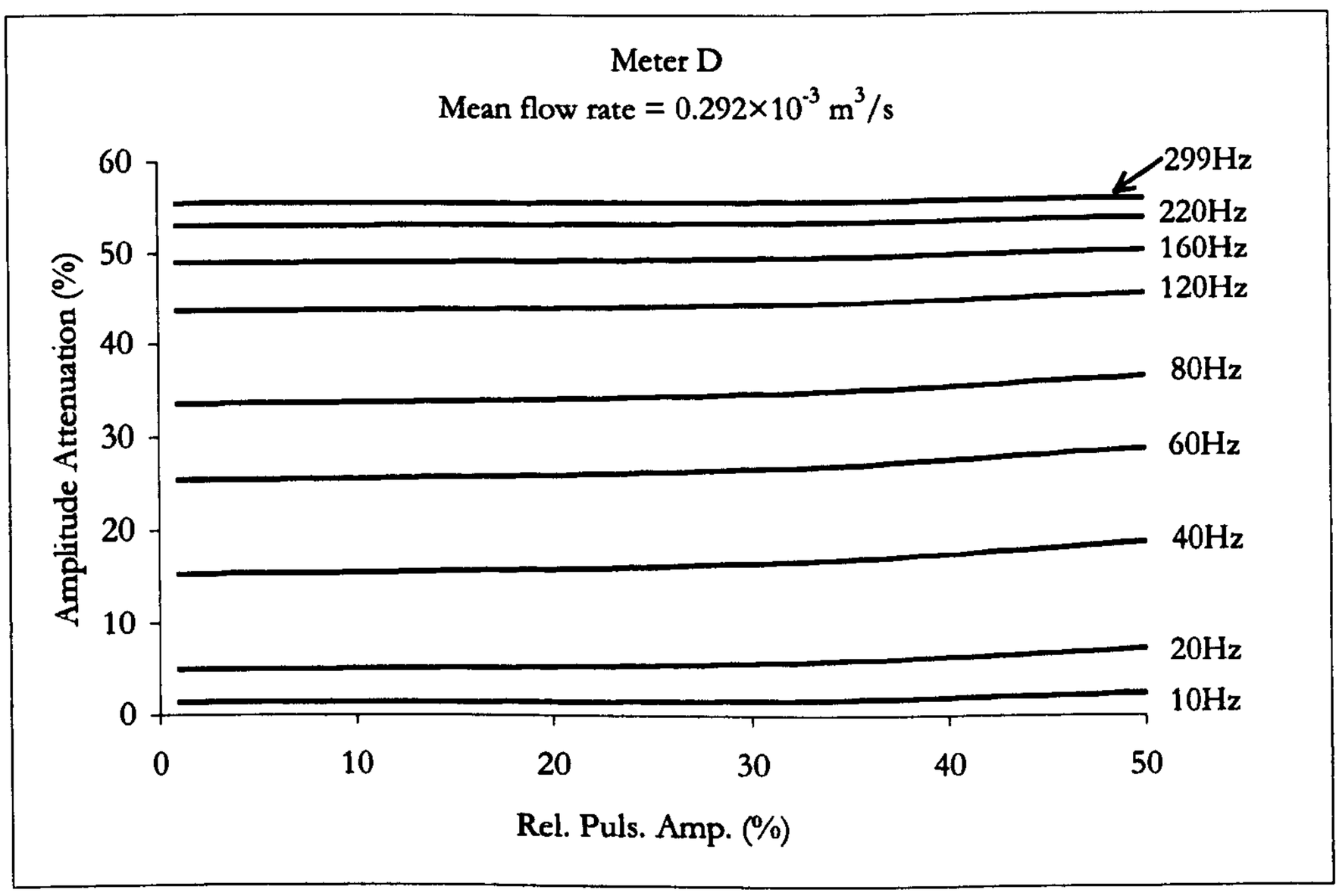

Figure 5.4 Meter D (6-bladed): Prediction of amplitude attenuations with differing pulsation amplitudes and pulsation frequencies

Since the amplitude attenuation mainly varies with pulsation frequencies, by taking the average of amplitude attenuation at each frequency, Figures 5.3 and 5.4 can be re-plotted as shown below:

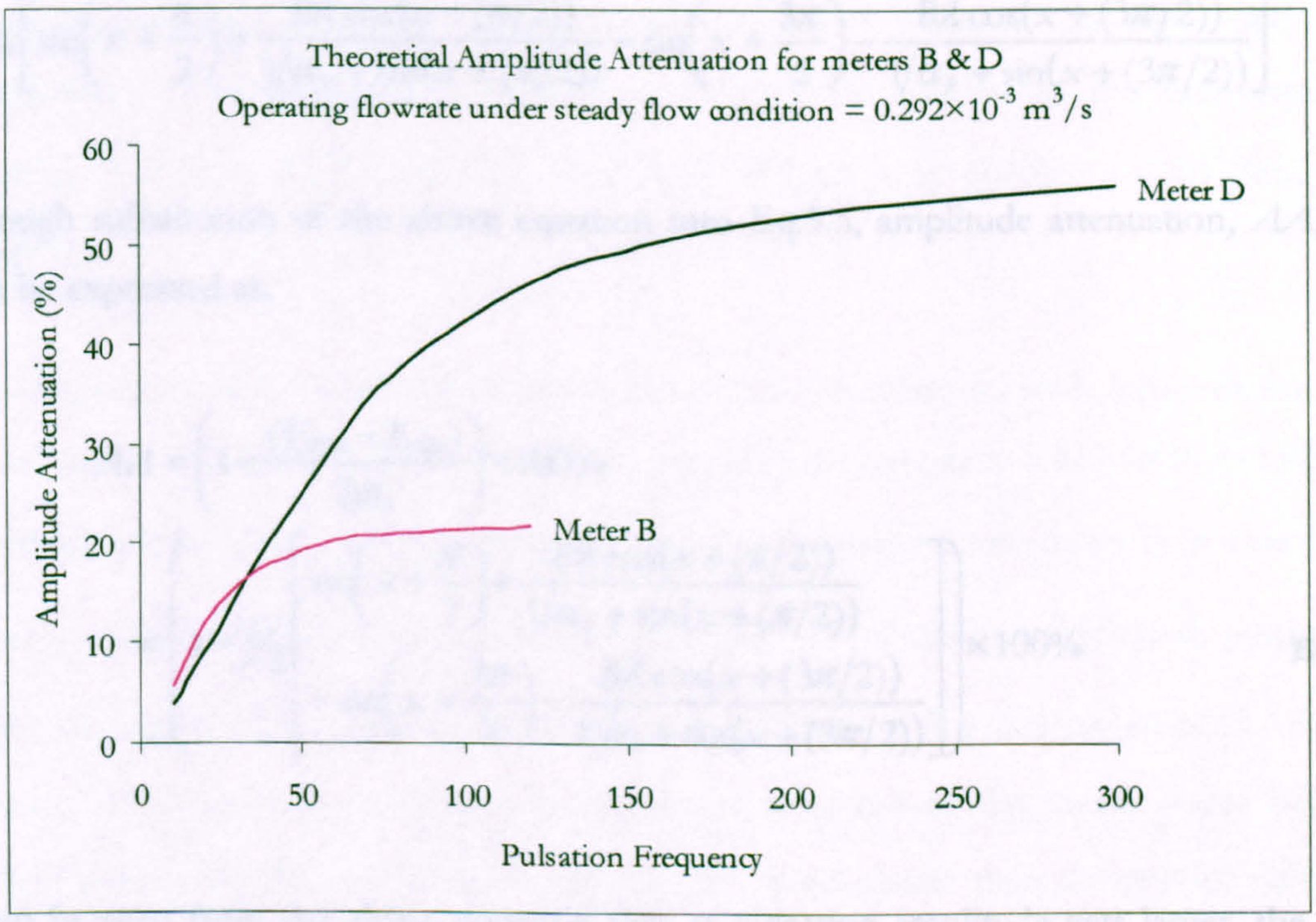

Figure 5.5 Meters B & D: Prediction of amplitude attenuations with differing pulsation frequencies

For both meters the predictions are qualitatively similar, the over-registration errors increase with both the imposed pulsation frequencies and pulsation amplitudes; and the amplitude attenuations increase with pulsation frequencies but only slightly with amplitudes. This phenomenon can be explained by using Eq. 5.1 in which the main contributor to the evaluation of the peak-to-peak amplitude of $F(T)$ is when the term $dF/dT=0$, this condition happens at the time interval $T=x+\pi/2$ and $x+3\pi/2$ within a sinusoidal pulsation cycle. Hence the maximum and minimum values of $F(T)$ is:

$$F_{\max} = \left(1+\alpha_p \sin\left(x+\frac{\pi}{2}\right)\right)+\frac{\alpha_p B\lambda \cos(x+(\pi/2))}{1+\alpha_p \sin(x+(\pi/2))} \qquad \textbf{Eq. 5.6}$$

$$F_{\min} = \left(1+\alpha_p \sin\left(x+\frac{3\pi}{2}\right)\right)+\frac{\alpha_p B\lambda \cos(x+(3\pi/2))}{1+\alpha_p \sin(x+(3\pi/2))} \qquad \textbf{Eq. 5.7}$$

Therefore, the dimensionless meter peak-to-peak amplitude is given by,

$$F_{max} - F_{min} =$$

$$1+\alpha_p \sin\left(x+\frac{\pi}{2}\right)+\frac{\alpha_p B\lambda\cos(x+(\pi/2))}{1+\alpha_p \sin(x+(\pi/2))}-1-\alpha_p \sin\left(x+\frac{3\pi}{2}\right)-\frac{\alpha_p B\lambda\cos(x+(3\pi/2))}{1+\alpha_p \sin(x+(3\pi/2))}$$

$$=\alpha_p\left[\sin\left(x+\frac{\pi}{2}\right)+\frac{B\lambda\cos(x+(\pi/2))}{1/\alpha_p+\sin(x+(\pi/2))}-\sin\left(x+\frac{3\pi}{2}\right)-\frac{B\lambda\cos(x+(3\pi/2))}{1/\alpha_p+\sin(x+(3\pi/2))}\right]$$

Through substitution of the above equation into Eq.5.5, amplitude attenuation, AA, can then be expressed as:

$$AA=\left(1-\frac{(F_{max}-F_{min})}{2\alpha_p}\right)\times 100\%$$

$$=\left(1-\frac{1}{2}\left[\begin{array}{l}\sin\left(x+\frac{\pi}{2}\right)+\frac{B\lambda\cos(x+(\pi/2))}{1/\alpha_p+\sin(x+(\pi/2))}\\ -\sin\left(x+\frac{3\pi}{2}\right)-\frac{B\lambda\cos(x+(3\pi/2))}{1/\alpha_p+\sin(x+(3\pi/2))}\end{array}\right]\right)\times 100\% \qquad \textbf{Eq. 5.8}$$

It can be seen from the above equation that as pulsation amplitude gets larger, the term $(1/\alpha_p)$ in the denominators tends to become comparatively insignificant and the amplitude attenuation is then predominantly dependent upon $B\lambda=\left(2\pi bf_p/\overline{\dot{V}_a}\right)\lambda$. The term $\lambda(=I_f/I_R)$ is assumed to be constant; the value of b is rotor geometrical dependent and fluid density dependent (Eq. 4.6), therefore for any pulsating flow about a mean of $\overline{\dot{V}_a}$, the amplitude attenuation is predominantly dependent on pulsation frequency f_p.

5.2.5 Summary of the prediction results

Under steady flow condition, the uncertainty quoted by manufacturers for these two meters used here is ±0.5% of full scale (over the linear range of the meters). For the largest pulsation amplitude of 50%, both meters are predicted to have over-registrations in the mean flow above pulsation frequency of 10 Hz (meter B) and 20 Hz (meter D), and significant amplitude attenuations are also predicted for both meters above these frequencies.

In addition, from the above figures, it can be seen that the errors predicted for meter B are less than the ones for meter D for pulsation frequency of 40Hz upwards. For example, at 60 Hz and 50% imposed relative pulsation amplitude, the over-registration errors predicted for meter B and meter D are 2.5% and 4% respectively; and at the same imposed pulsation, the amplitude attenuations predicted for meter B and meter D are 20% and 28% respectively. This occurrence contradicts to theory by considering the time constant equation $\left[t_c = b(1+\lambda)/\left(\dot{V}_a - \Delta\dot{V}_a\right)\right]$ (Eq. 4.18 a) and it is detailed in the following paragraph.

As shown in Table 5.1, since the response parameters (b) estimated by Solidworks for both meters are of very close value (ratio of b for meter B to meter D is 5.123:4.855 = 1.05 : 1), therefore, for the same pulsation frequency (f_p), and same volume mean flow rate ($\overline{\dot{V}_a}$), the values of the dimensionless parameter B ($= 2\pi b f_p / \overline{\dot{V}_a}$) calculated for both meters are almost the same. The only significant difference of input to Eq. 5. 1 would be λ. As can be seen from Eq. 4. 18 a, when λ increases, the response of the meter would become slower. Since λ for meter B is approximately five times greater than the one for meter D, (ratio of λ for meter B to meter D is 3.434:0.703 = 4.89 : 1), it would be expected that the dynamic response of meter B to be worse than meter D.

However, the model used here is based on the assumptions that the rotor is frictionless, the flow is perfectly guided, the fluid inside the rotor envelope is rotating as a solid body (for the evaluation of $\lambda = I_f / I_R$); and, there is a purely sinusoidal pulsation. Hence, these predictions can only give a guideline of what ranges of over-registration errors and amplitude attenuations may be expected for meters B and D if operated under those pulsation frequencies and amplitudes.

The next chapter, Chapter 6, reviews the experimental results of the dynamic response for all of the meters. Then in Chapter 7, a comparison of the theoretical data with experimental data will be made for meters B and D, and hence the applicability of this model will be evaluated.

Chapter 6 Experimental Investigation into the Dynamic Response of Turbine Flowmeter

This chapter covers a key aspect of the research project. Before any analysis of flowmeter signals under pulsating conditions could be performed, a test rig capable of inducing these conditions, and data acquisition systems capable of recording all relevant information were required. A detailed test program was undertaken to identify which flow conditions are likely to produce meter errors within experimental limitation. Finally the results will be reviewed.

6.1 Experimental Equipment

6.1.1 Test meters

Five meters were selected for this research program, their characteristics are given in the table below;

Meter	Manufacturer	Nominal Size (mm)	r_h/r_t Ratio	Blade Number	Experimental K-factor (P/10^{-3} m^3)	Linear Flowrange (10^{-3} m^3/s)
A	Euromatic	6	0.4	3	1608	0.025 - 0.4
B	Euromatic	12	0.4	3	520.3	0.14 - 1.67
C	Bestobell	12	0.67	5	9016.9	0.015 - 0.092
D	Bestobell	12	0.5	6	2614	0.04 - 0.4
E	ATS	25	0.33	5	186.6	0.44 - 4.4

Table 6. 1 Characteristics of Meters

(r_t: tip radius, r_h: hub radius)

Photographic views of rotors of meter A, B, D and E are shown in Figure 6. 1. Rotor A and B were given as spares by the manufacturer, the given drawings are presented in Appendix A. Drawings of meter D and E were unobtainable; hence it was necessary to dismantle the meter housing so that measurements of the meter geometry could be taken. This information was required for the evaluation of the meter response parameter value, *b* (see Section 5.2). A detailed drawing of meter C (see Appendix A) was available; hence it has not been dismantled. Rotor A, C and E are mounted onto the shaft by ball race

bearings fitted inside the hub, whereas rotor D has a solid hub which uses journal bearings. The bearings are made from stainless steel allowing use for corrosive liquid applications. The races are open, with no lubricant, the process fluid is used to lubricate the bearings.

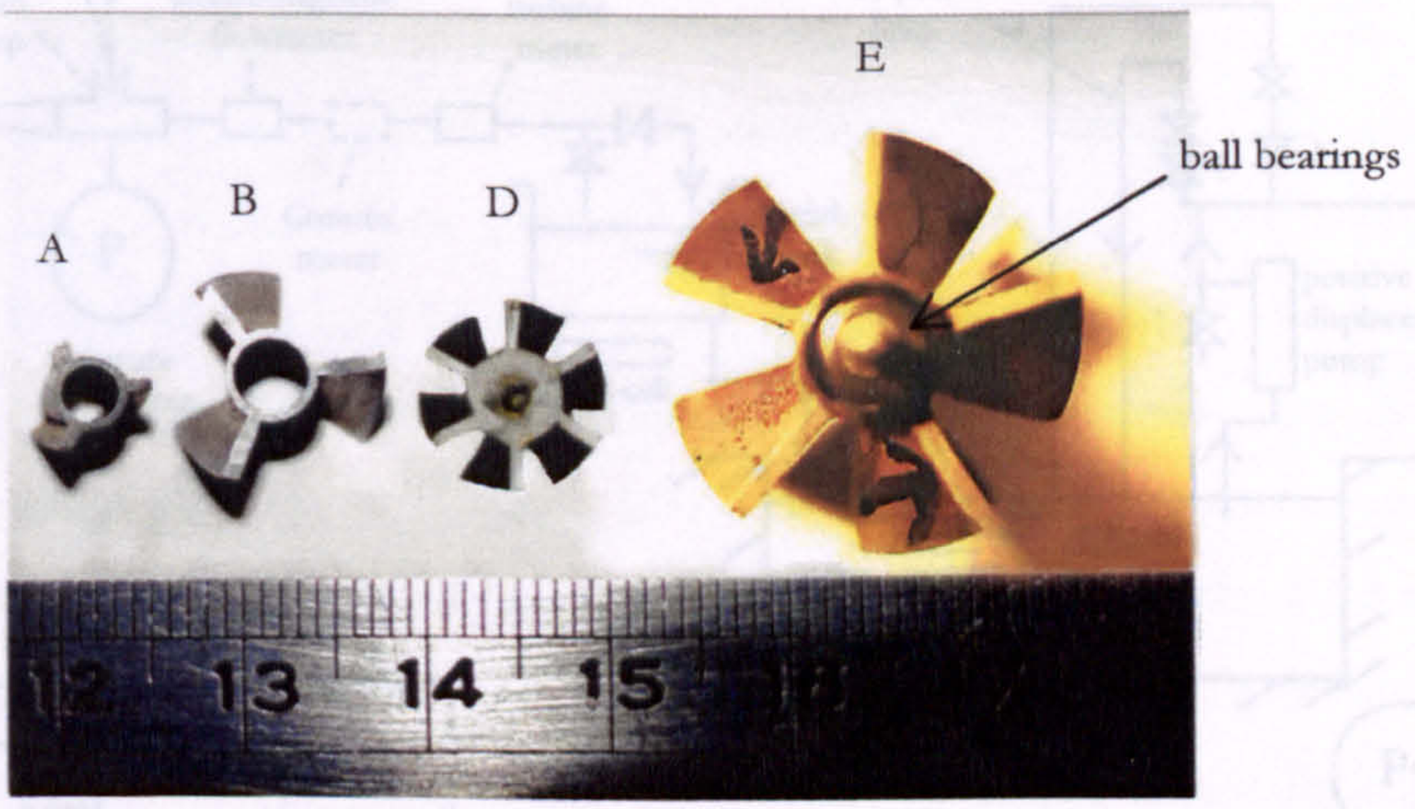

Figure 6. 1 Photographic view of rotors

A typical meter assembly is shown in Figure 6. 2, it can be seen that the rotor is held in position in the flowmeter body (1) by two spirolox rings (3 and 7) located upstream and downstream.

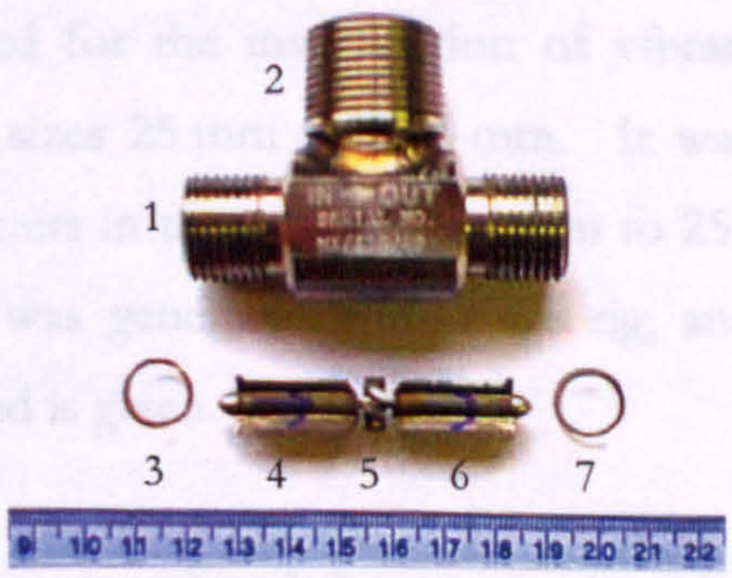

1. Meter body
2. Pick-up housing
3. Upstream spirolox ring
4. Upstream flow straightener
5. Rotor
6. Downstream flow straightener
7. Downstream spirolox ring

Figure 6. 2 Photographic view of Meter D Assembly

All of the meter bodies have screw threads at both ends for piping fixtures. The screw threads of meters A, B, C and D are suitable for 12 mm diameter pipe fixtures; meter E screw threads are suitable for 25mm diameter pipe fixtures. However, the diameter of the internal casing of meter A is nominally 6 mm, hence, the screw threads of this particular meter are truncated from 12 mm to 6 mm, thus having an exceptionally larger thickness (approx. 3mm thick) compare to other meters (See Appendix A).

6.1.2 The flow rig

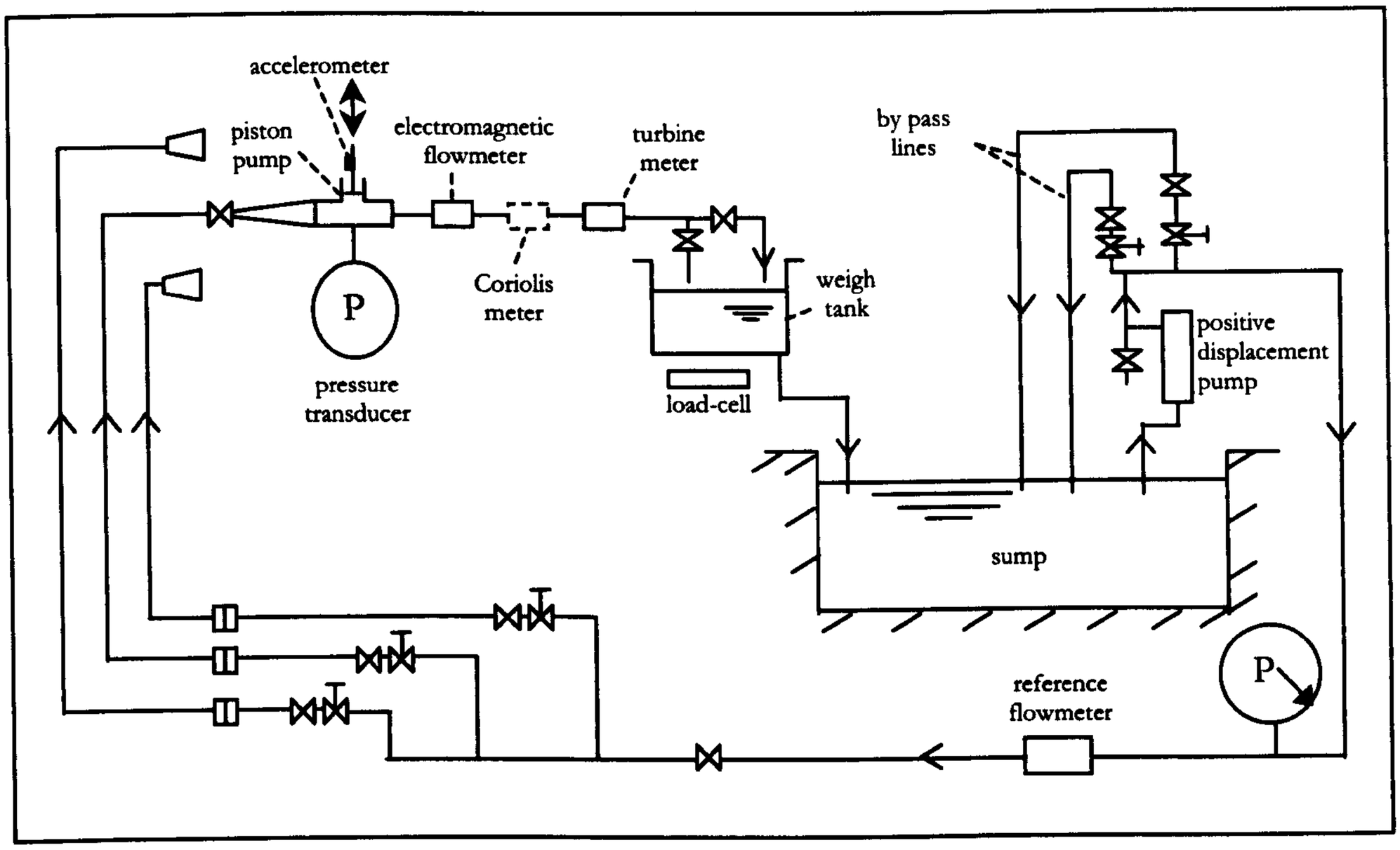

Figure 6. 3 A schematic diagram of the flow rig

A schematic diagram of the water flow test rig is shown in Figure 6. 3, this flow rig was initially designed for the investigation of vibration and pulsation effects upon Coriolis flowmeters of sizes 25 mm and 76 mm. It was modified to allow pulsation testing of turbine flowmeters in the size range 6 mm to 25 mm. The following paragraphs describe how the flow was generated within the rig, and a description of the function of each component used is given.

Steady flow was produced by a positive displacement pump with a helical rotor (Monopump model CE064MS1R3/H421) driven at a fixed speed of 700 rpm. The pump intake was fed from a sump holding in excess of 30 m^3 of water. The required flow rate through the test meter was attained by adjusting the fraction of pump outflow diverted through two bypass lines. This provided the nominal meter flow rates, required for the present tests, of 0.095×10^{-3} m^3/s to 1.75×10^{-3} m^3/s.

An electromagnetic flowmeter (Endress & Hauser model PROMAGF) provided a secondary flow rate reference, the flow rate was monitored visually, but not logged. The positive displacement pump produced a steady flow condition except for very small

fluctuations at approximately 11.5 Hz and 23 Hz due to the driving rotor having two lobes. However, the magnitude of these pulsations was very small compared with the sinusoidal pulsations produced by the purpose built piston pump.

A piston pump, developed by modifying an existing diaphragm pump, was situated approximately 10 pipe diameters upstream of the test meter. The piston chamber diameter was 25.4 mm. An accelerometer was mounted onto the piston rod to sense the piston motion. The pump was driven by a Gearing and Watson electromagnetic actuator (model GW100B) and power amplifier (model SS600PA) to produce sinusoidal flow pulsations over a frequency range of 5 Hz to 300 Hz. The amplitude of the pulsations was varied within the limit imposed by the maximum actuator force of 600 N and the need to avoid cavitation. A Hewlett Packard model 3325A signal generator with a high-precision quartz clock, accurate to within ±5 μHz, was used as an external frequency source for the power amplifier, enabling flow pulsation frequencies to be controlled with high resolution and high stability. The waveform output from the signal generator generally had a low level of harmonic distortion so that the meter was usually not subjected to pulsations with more than one frequency component. However, it was observed that there was some harmonic distortion produced in the flow output waveform at low pulsation frequencies of 5 Hz and 10 Hz (See Figure 6. 6 and Figure 6. 10).

In order to ensure that a very high fraction of the flow pulsation was added to the downstream flow (through the test meter), it was necessary that there was much higher impedance upstream of the pulsator than downstream of it. For this reason, the mean flow component was supplied at an upstream pressure of 20 bar. Accordingly, the positive displacement pump required a drive of 30 kW; the rate of fluid temperature increase was limited to less than 1°C/hour by the sump volume being greater than 30 m^3.

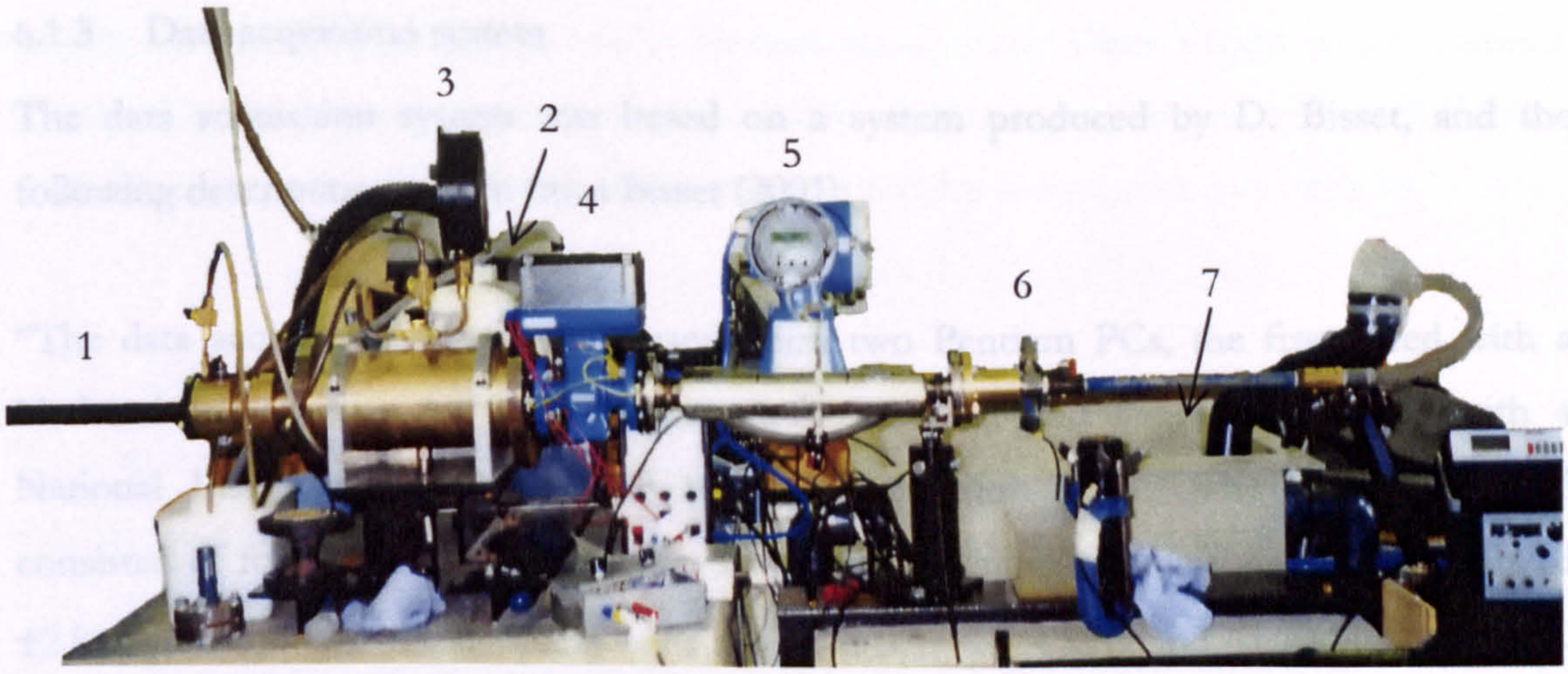

Figure 6. 4 Part of the Flow Rig

A photographic view of the following parts of the rig is given in Figure 6. 4. An appropriate length of a relatively small-bore tube (1) dropped the pressure from 20 bar to 2 bar at the location of the piston pump (2), a pressure gauge (3) was used to monitor this back pressure. Pulsation amplitudes were restricted to ensure that the minimum pressure within the pulsation cycle remained above atmospheric pressure.

The piston pump was connected to the main flow line through a T-piece, a short distance upstream of a second electromagnetic flowmeter (4). The pulsation flow waveform was obtained from this commercially available electromagnetic (EM) 1" flowmeter, (Krohne model IFM4010K/D/6). Usage of other devices to give independent measurement of the pulsation flow waveform were attempted as well, such as a Coriolis meter (5) and a hot-film anemometer; results of the usage of these devices will be reviewed in Section 6.1.4.

The turbine meter (6) under test was placed downstream of the electromagnetic flowmeter and the outlet from the meter was fed to a weigh tank (7). Continuously timed gravimetric collection using the weigh tank mounted on an Avery-Berkel L105 load-cell provided a primary flow rate standard with a measurement uncertainty of ±0.1%. An electromagnetic pick-up on the meter generated a signal each time a turbine blade passes and this signal was amplified and digitised.

6.1.3 Data acquisition system

The data acquisition system was based on a system produced by D. Bisset, and the following description is taken from Bisset (2001):

"The data acquisition system was based upon two Pentium PCs, the first fitted with a National Instruments AT-2150C data acquisition card and the second fitted with a National Instruments AT-MIO-16E-10 data acquisition card. The AT-2150C card consisted of four 16-bit, simultaneously sampled A/D input channels with input limits of ±2.828 volts and various sampling rates available between 4 kHz and 51.2 kHz. The AT-2150C card provides adequate anti-aliasing protection. The AT-MIO-16E-10 card consisted of eight 12-bit A/D input channels with software-selectable input limits and sampling rates up to 100 kHz."

"A 16-bit A/D process contains 65536 discrete voltage levels. Each time a measurement occurs, the nearest of these values to the input signal is taken as the measurement, the difference being known as the quantisation error. If a signal was very much smaller than the input limits, then it would cover a very small number of the discrete voltage levels. As a result, quantisation error would be much greater and the overall quality of digitisation would be very poor. Alternatively, if a signal was larger than the input limits, then any portion of the signal outside these limits would be clipped. To prevent these problems from occurring when using the AT-2150C card, Fylde instrumentation amplifiers (model 351UA) and potential divider circuits were used to scale input signals to the card input limits. The software-selectable input limits of the AT-MIO-16E-10 card removed the need for use of these procedures on that card."

Typically the signals from the turbine flowmeter were recorded on both cards: the AT-2150C card was used to record signals with a high sampling rate over a shorter period of time (for example 32 kHz for 5 seconds); and the AT-MIO-16E-10 card was used to record signals with a low sampling rate over a longer period of time (for example 4 kHz for 30 seconds). Other signals, such as the accelerometer, Krohne EM meter and pressure signals were recorded using the AT-MIO-16E-10 card.

LABVIEW (V. 5.1) graphical programming software was used for data acquisition. There were some programs readily available, (originally written by D. Bisset who worked on

turbine flowmeters previously), to use for data acquisition. These programs were written around the data acquisition subroutines provided so that continuous records of A/D data could be stored. LABVIEW software was again used for subsequent data analysis.

6.1.4 Independent measurement of flow pulsation amplitude

There are various techniques available to determine the flow pulsation characteristics. A few techniques have been attempted during experimentation, thermal anemometry, a Coriolis mass flowmeter, and an electromagnetic flowmeter. A final decision of using the electromagnetic flowmeter as a reference source was made, and this section explains why this device is superior to others for the purpose of this research.

6.1.4.1 Thermal anemometry

A hot-film anemometer was considered to be a potential device to indicate the flow pulsation waveform of the flow. It is a point velocity technique, in which flow pulsation amplitude and waveform can only be estimated. The r.m.s. value of the fluctuating velocity component can be determined by using a true r.m.s. flowmeter to measure the fluctuating component of the linearized anemometer output voltage. The general relationship between the response of a hot-film anemometer and the point velocity at the pipe is:

$$\left[\left(e^2 - e_0{}^2\right)/\Delta R\right] = Constant \times U_{probe}{}^{1/n} \qquad \textbf{Eq. 6. 1}$$

Where e is the voltage response of the hot-wire anemometer at the time of measurement, e_0 is the voltage response at zero flow; ΔR is the difference between the probe resistance at fluid temperature and the set probe resistance (chosen to allow for an nominal 10% overheat); U_{probe} is the velocity at the probe and n is the exponent associated with the forced convective heat transfer. Assuming uniform velocity profile along the pipe, Eq. 6. 1 becomes:

$$\left[\left(e^2 - e_0{}^2\right)/\Delta R\right] = Constant \times \dot{V}^{1/n} \qquad \textbf{Eq. 6. 2}$$

Where $\dot{V}$ is the volume flow rate which could be indicated by a turbine meter operating under steady flow condition. The value of n can be determined by plotting

$\ln\left[\left(e^2 - e_0{}^2\right)/\Delta R\right]$ against $\ln[\dot{V}]$, which should produce a straight line whose gradient is equal to $1/n$.

Figure 6. 5 shows the hot-film anemometer experimental response, calibrated by using Meter B operating under steady flow conditions. It can be seen that the data points are widely scattered and it is difficult to find a line of best fit across the points. This may well be due to the fact that hot-film anemometer was very sensitive to the cleanliness of the fluid in the rig. According to BS ISO TR 3313 (1998), cleanliness of flow is very important; even nominally clean flows can result in rapid fouling of probes with a consequent dramatic loss of response. Hence the attempt of using this device to indicate the pulsation waveform was unsuccessful.

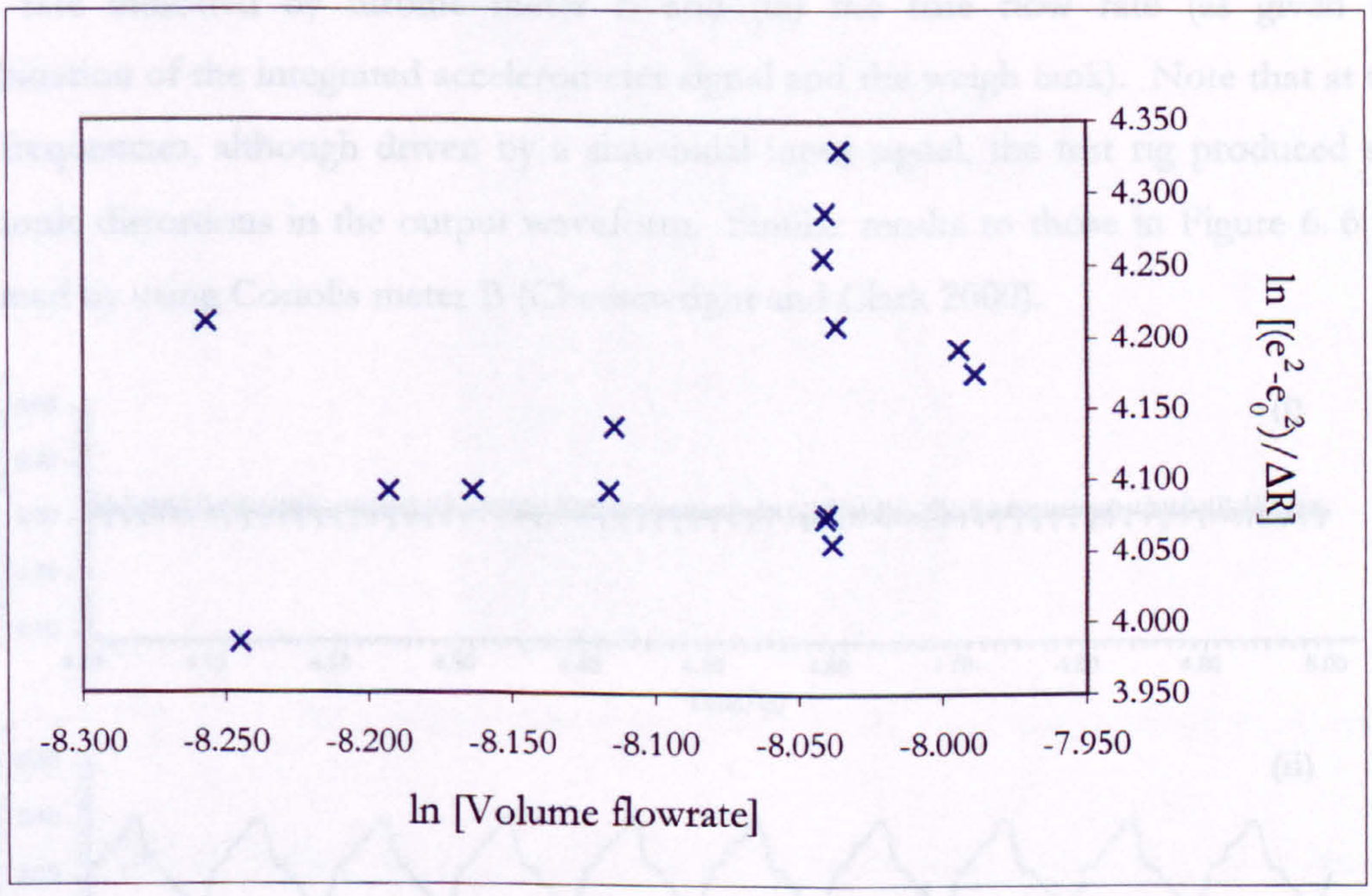

Figure 6. 5 **Response from hot-film anemometer plotted against indicated volumetric flowrate from Meter B**

6.1.4.2 Coriolis mass flowmeter

Two commercial Coriolis mass flowmeters (A and B) were available for use during the course of experimentation. Hence an attempt was made to use a Coriolis meter to measure the amplitude of the pulsations. Pulsation frequencies from 5 Hz to 40 Hz were investigated; it was immediately observed that, even at frequencies of 5 to 10 Hz, the amplitudes of pulsation which were indicated by the Coriolis meter were significantly smaller than those indicated by the turbine meters. Since any inertial effects on a turbine meter will always tend to cause it to under-indicate the pulsation amplitude, this implied that the dynamic response of the Coriolis meter was comparatively inferior to the turbine meter in this case.

Figure 6. 6 shows a comparison of: (i) the flow rate indicated by Coriolis meter A, (ii) the flow rate indicated by turbine meter B and (iii) the true flow rate (as given by a combination of the integrated accelerometer signal and the weigh tank). Note that at these low frequencies, although driven by a sinusoidal input signal, the test rig produced some harmonic distortions in the output waveform. Similar results to those in Figure 6. 6 were obtained by using Coriolis meter B (Cheesewright and Clark 2000).

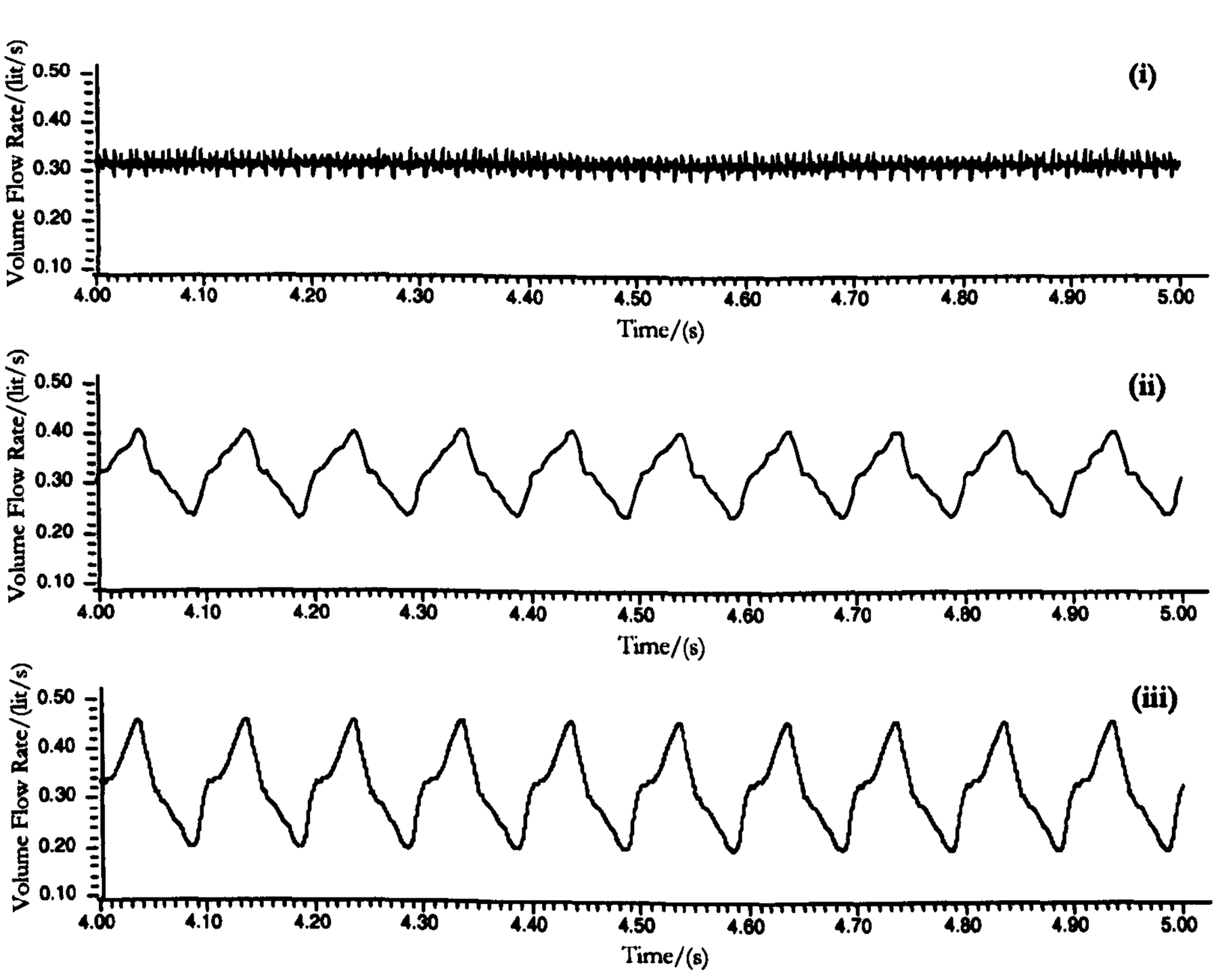

Figure 6. 6 Comparison of the flow rate time histories given by, (i) Coriolis meter A, (ii) turbine meter B, and (iii) piston pump motion + mean flow, pulsation frequency 10 Hz. (Extracted from Cheesewright and Clark 2000)

6.1.4.3 Electromagnetic flowmeter

According to BS ISO TR 3313 (1998), when the electromagnetic flowmeter is of the pulsed d.c. field type (likely maximum d.c. pulse frequency a few hundred hertz), there is the capability to resolve flow pulsation up to frequencies approximately five times below the excitation frequency. This technique is only suitable for liquids with an adequate electrical conductivity. It provides a measure of bulk flow pulsation, although there is some dependence upon velocity profile shape.

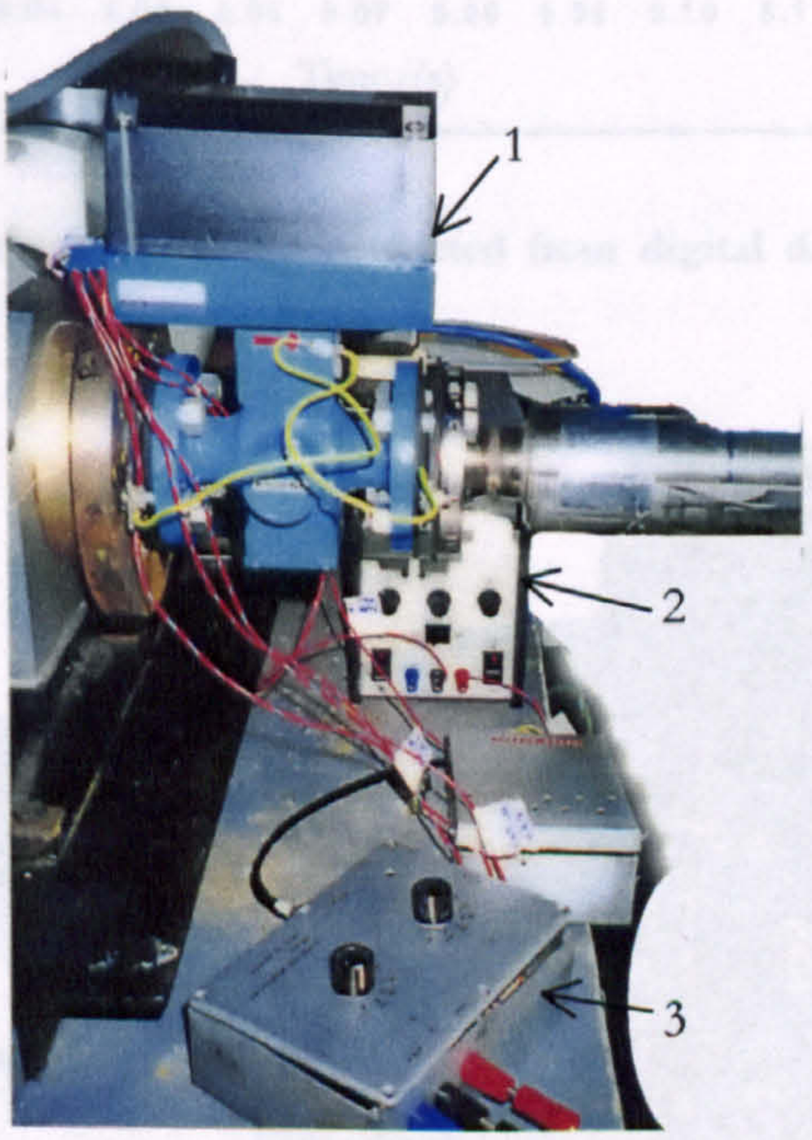

Figure 6. 7 Photographic view of the 1" Krohne EM meter and electronic equipment

As mentioned in Section 6.1.2, the EM meter (1) shown in Figure 6. 7 is a standard, commercially available meter (1" Krohne), but because the usual AC magnetic excitation would not permit the resolving of pulsatile flows above approximately 3 Hz, that excitation was replaced with a DC excitation from a 12 V source (2). The penalty for using DC excitation is the occurrence of shifting DC levels due to electrolytic action at the meter electrodes. To overcome this problem, the output from the meter was AC coupled to a high gain (10,000 to 150,000) amplifier (3), so that the final output from the modified meter represented only the pulsatile component of the time dependent flow rate. A typical EM signal is shown in Figure 6. 8. This procedure allowed pulsations to be recorded over a frequency range of 5 Hz to 300 Hz and thus avoided the frequency limitation that would have arisen from the conventional AC excitation of the meter. It can be seen that the

waveform produced by the EM flowmeter contained some relatively high-frequency noise components, so it was necessary to filter the signal at three times the pulsation frequency by using a digital low-pass filter (a virtual instrument available in LABVIEW).

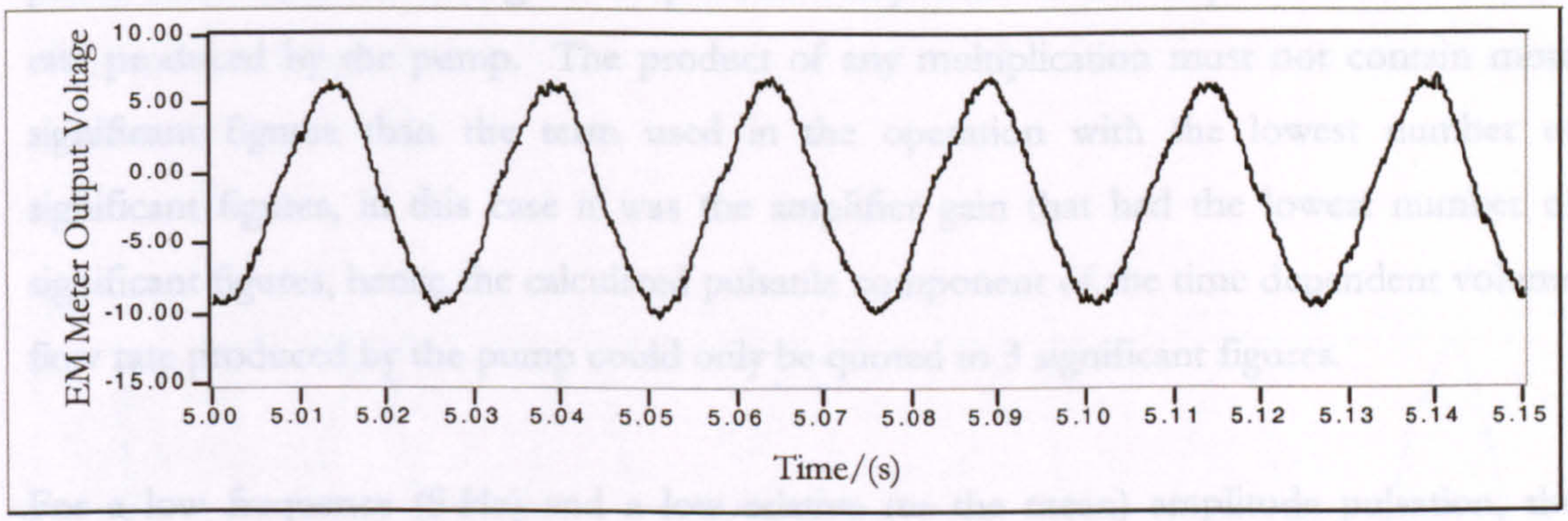

Figure 6. 8 EM meter output signal reconstructed from digital data, pulsation frequency 40 Hz

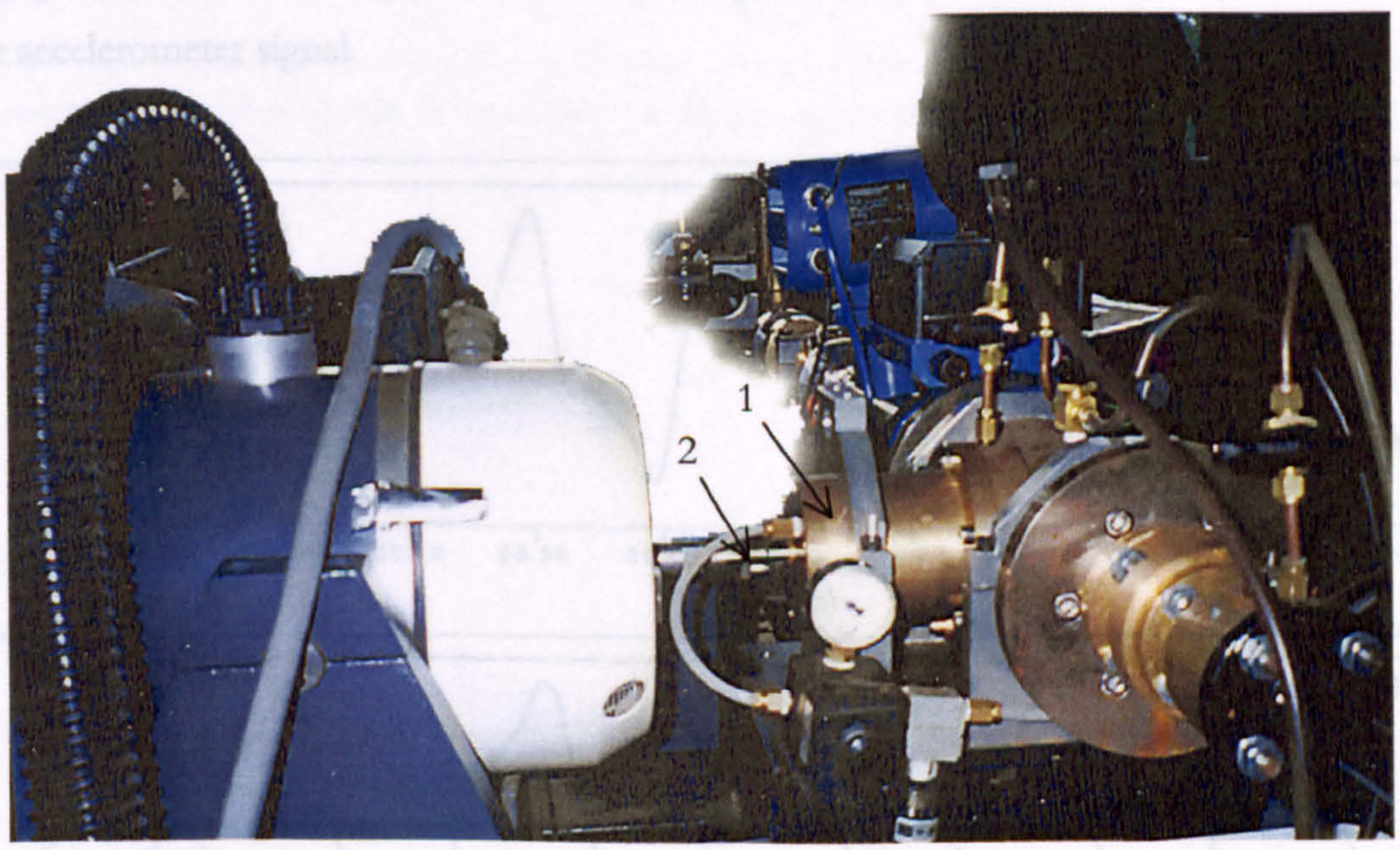

Figure 6. 9 Photographic view of the piston pump

The modifications to the EM flowmeter meant that the normal meter calibration was no longer applicable. The pulsatile output from the modified meter was calibrated with reference to the flow from the piston pump (1) as shown in Figure 6. 9. An accelerometer (2) was attached to the piston rod to sense the motion of this pump. The accelerometer output signal was amplified by a high-frequency response amplifier, in which the selectable gains were: 0.316*g*, 1.00*g*, 3.16*g* and 10.0*g* (to 3 significant figures), *g* being the standard gravitational acceleration constant, 9.807 m/s^2. Again, this signal contained some relatively

high-frequency noise components; hence the same low-pass filtering procedure (as was carried out in the processing of EM signal waveform) was conducted here. Integration of the filtered accelerometer signal gave the piston speed, and the multiplication of this by the piston cross-sectioned area gave the pulsatile component of time dependent volume flow rate produced by the pump. The product of any multiplication must not contain more significant figures than the term used in the operation with the lowest number of significant figures, in this case it was the amplifier gain that had the lowest number of significant figures, hence the calculated pulsatile component of the time dependent volume flow rate produced by the pump could only be quoted to 3 significant figures.

For a low frequency (5 Hz) and a low relative (to the mean) amplitude pulsation, the pulsation amplitude obtained from the accelerometer signal could be compared against that indicated by the turbine meter, assuming that inertia effects on the turbine meter were negligible, as shown in Figure 6. 10. This comparison confirmed the validity of the use of the accelerometer signal.

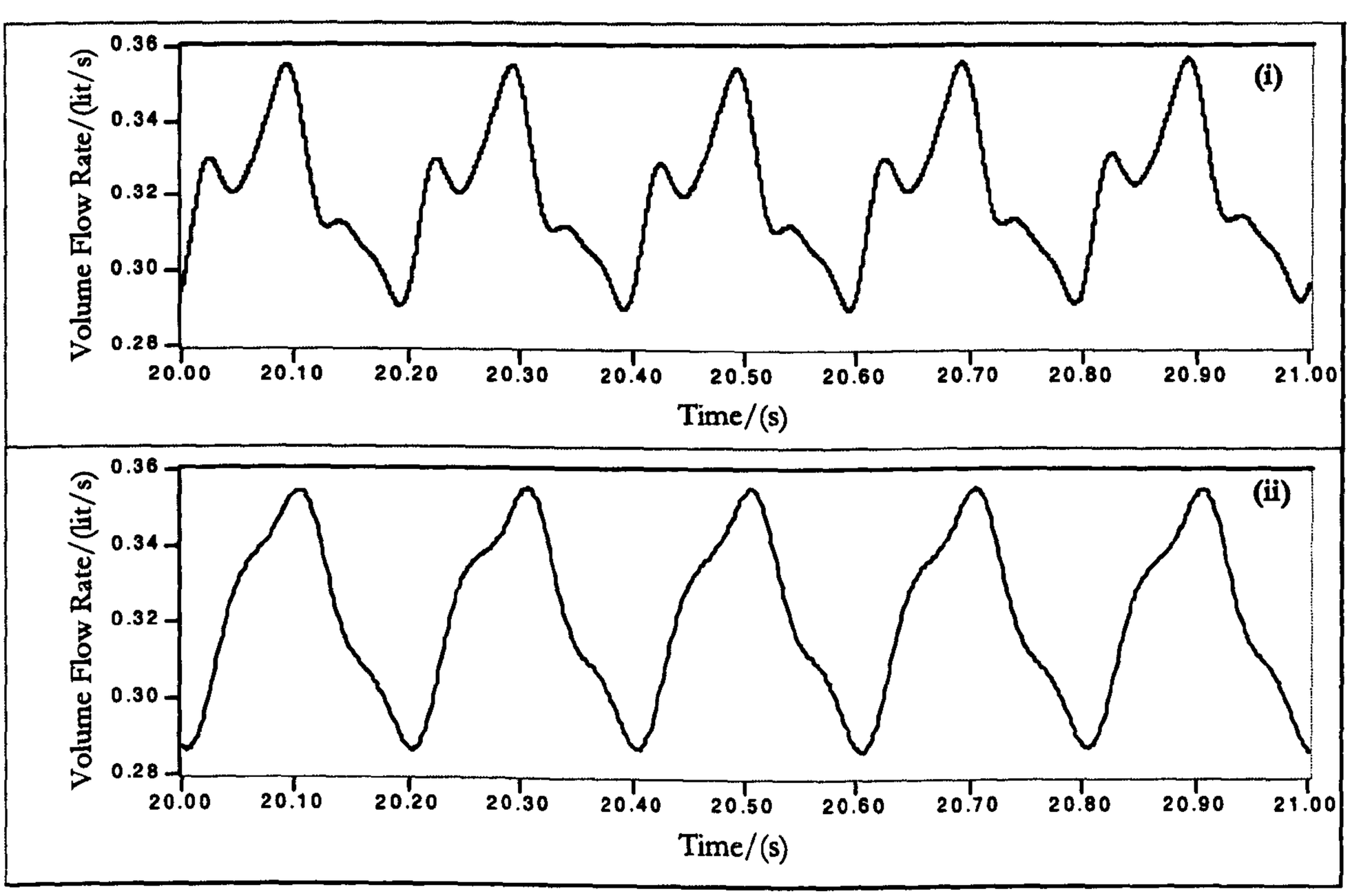

Figure 6. 10 **Comparison of the flow rate time histories given by, (i) piston pump motion (obtained from low-pass filtered and integrated accelerometer signal) + mean flow, (ii) turbine meter B, pulsation frequency 5 Hz.**

When the calibrated EM flow pulsation waveform is coupled with the mean flowrate value obtained from the weigh tank measurement, this will give an independent measurement of the pulsation flow as shown in Figure 6. 11. The repeatability of this pulsation calibration was better than 5% over a period of three days; further details are given in Section 6.2. Hence the electromagnetic flowmeter was chosen as the device to determine the flow pulsation characteristics.

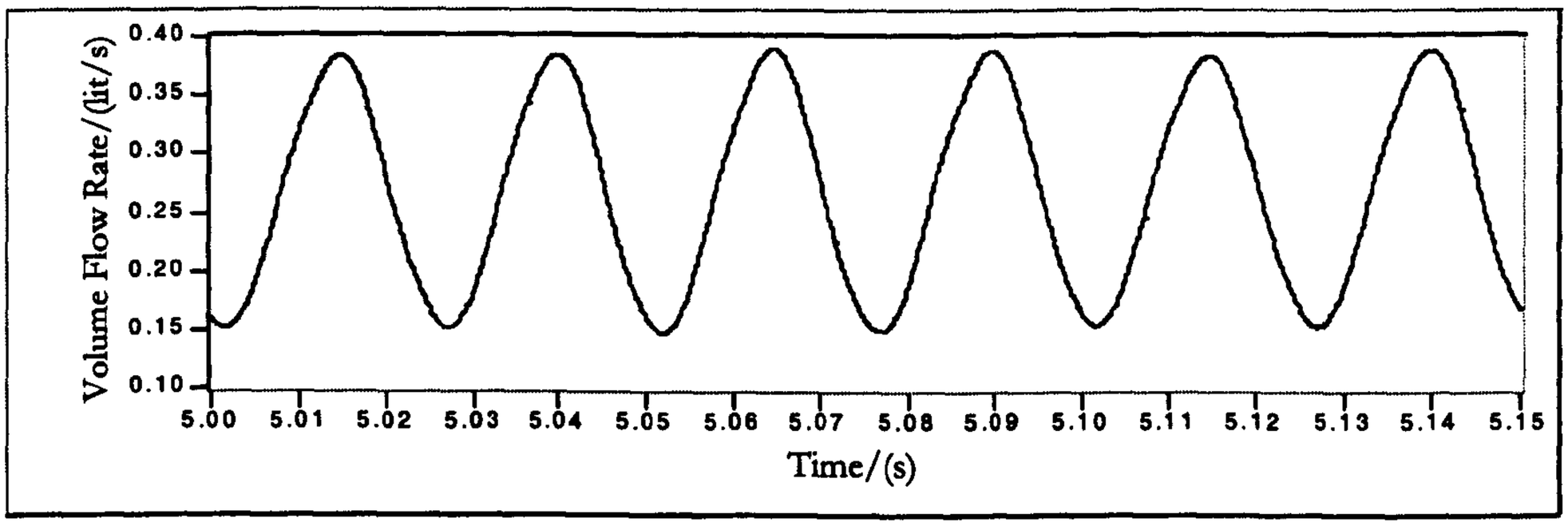

Figure 6. 11 Calibrated EM (+ mean flow) waveform processed for low-pass filtered waveform in Figure 6. 8

6.2 Planning and Preparation

6.2.1 Range of possible test conditions to be investigated

Meters (nominal size/mm)	Linear Flow range (10^{-3} m^3/s)	Operating Flow rate (10^{-3} m^3/s)	Corresponding Blade Passing Frequency (Hz)	Maximum Pulsation Frequency (Hz)	Corresponding Pipe Re. no. under steady flow situation	
					At upstream	Immediately after meter inlet
A (6)	0.025-0.4	0.095	154	60	1.01×10^4	1.87×10^4
B (12)	0.14-1.67	0.292	152	60	3.11×10^4	3.11×10^4
C (12)	0.015-0.092	0.095	866	300	1.01×10^4	1.01×10^4
D (12)	0.04-0.4	0.292	758	300	3.11×10^4	3.11×10^4
E (25)	0.44-4.4	1.740	317	120	9.07×10^4	9.07×10^4

Table 6. 2 Test conditions for each meter to be investigated

Five meters were tested and their characteristics and possible testing conditions are given in Table 6. 2. Each meter has its individual K-factor (see Table 6. 1), and with the specific linear operating flow rate chosen for experimentation, each meter rotates with a corresponding blade passing frequency. All of the meters were tested with pulsation frequencies ranging from 5 Hz up to a maximum frequency which varied from meter to meter, and which was dictated by the blade passing frequency produced by the mean flow rate. The reason for this limitation will be explained in detail in Chapter 6.3.

It can also be seen that the steady flow conditions for all meters at the specific operating flow rates are within the turbulent flow regime. However, it is worth noting that, since meter A has truncated screw threads (diameter changes from 12mm to 6mm) at both ends of the meter body, hence the abrupt contraction of flow will cause an increase of Reynolds no. from 1.01×10^4 at upstream to 1.87×10^4 immediately after the meter inlet. It is therefore of interest to see whether this sudden change in Reynolds no. would result in any variations in the meter error trends when comparing with the results from other meters.

For one meter, meter D, three different flowrates within its linear operating flow range (0.143×10^{-3} m^3/s, 0.191×10^{-3} m^3/s and 0.291×10^{-3} m^3/s) were investigated with the same imposed pulsation frequencies. The aim of this was to investigate any variations in the resulting meter errors corresponding to the change in mean flowrates.

6.2.2 Experimental procedure

After identification of the imposed maximum pulsation frequency of each meter for experimentation, the following general experimental procedure was undertaken:

1. Ensure that all equipment is switched on and is connected to the A/D input for data logging. This includes: back pressure transducer, test meter, Krohne EM meter, accelerometer and weigh tank load-cell.

2. Start the pump and ensure that the upstream supply pressure is set at 20 bar (this is monitored regularly throughout the experiment).

3. Check the input signals to the computer are of suitable amplitude (volts).

4. Record a set of data at zero flow, and then follow by a set of data under steady flow.

5. Weigh tank measurement should be taken at least every 5 minutes to monitor any changes in the set mean flowrate during the course of experiment.

6. Adjust the signal generator to give a fixed pulsation frequency of 5 Hz.

7. Vary the amplitude of the pulsations within the limit imposed by the maximum actuator force of 600 N and check the back pressure waveform to decide on the maximum allowed imposed force to avoid cavitation.

8. Start with the highest amplitude pulsation, and record the data. This step is to be repeated for medium amplitude pulsation and lowest amplitude pulsation. In the meantime, check the signals from both the accelerometer and EM flowmeter, switch the amplifier gain if necessary, to avoid the occurrence of signal clipping. Then record a set of data at steady flow.

9. Check the logged data after the first run. Repeat Steps 5-8 for another pulsation frequency.

10. Finish off with a set of data at zero flow.

6.2.3 EM signal calibration

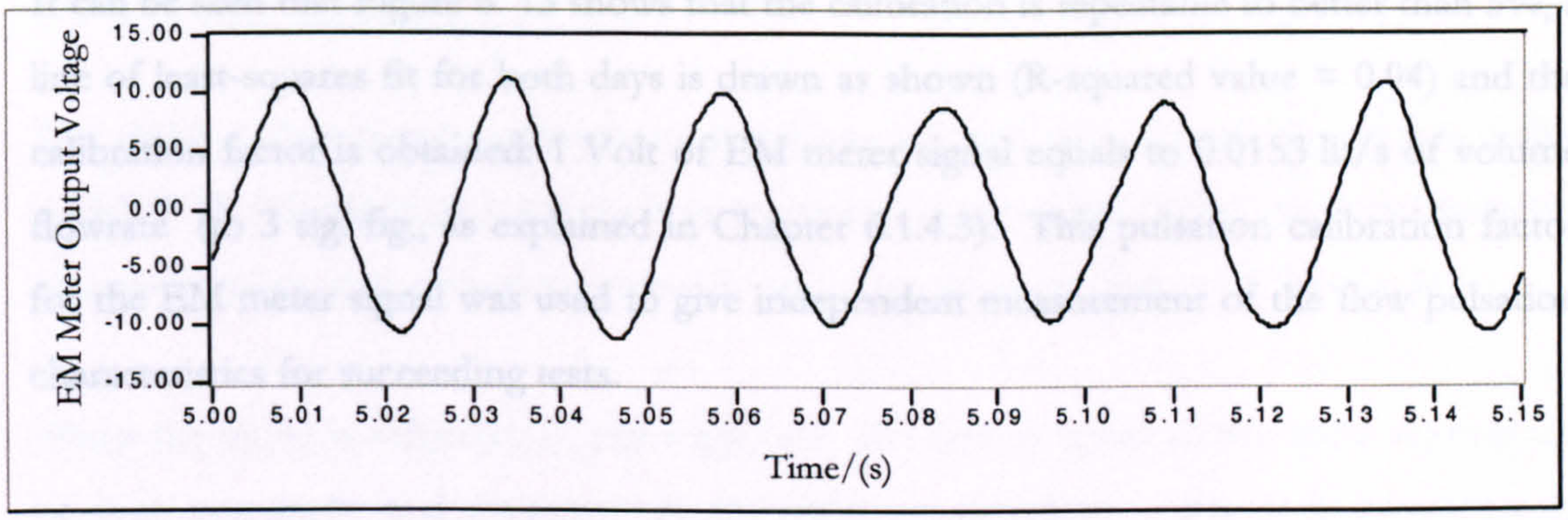

Figure 6. 12 Filtered EM meter signal, pulsation frequency 40 Hz

As mentioned in Chapter 6.1.4.3, it was decided to use the modified Krohne EM meter signal to give independent measurement of the operating pulsation amplitude for each flow test, in which this signal (as shown in Figure 6. 12) was calibrated against the accelerometer signal attached to the piston rod. Since the penalty for using the DC excitation is the occurrence of shifting DC levels due to electrolytic action at the meter electrodes, pulsation calibrations between the EM meter signal and accelerometer signal were carried out over a period of time to investigate the repeatability of the EM meter signal.

The output of the EM meter and accelerometer were measured over a range of pulsation frequencies from 5 Hz to 100 Hz. Figure 6. 13 shows the calibration results from tests over a period of three days.

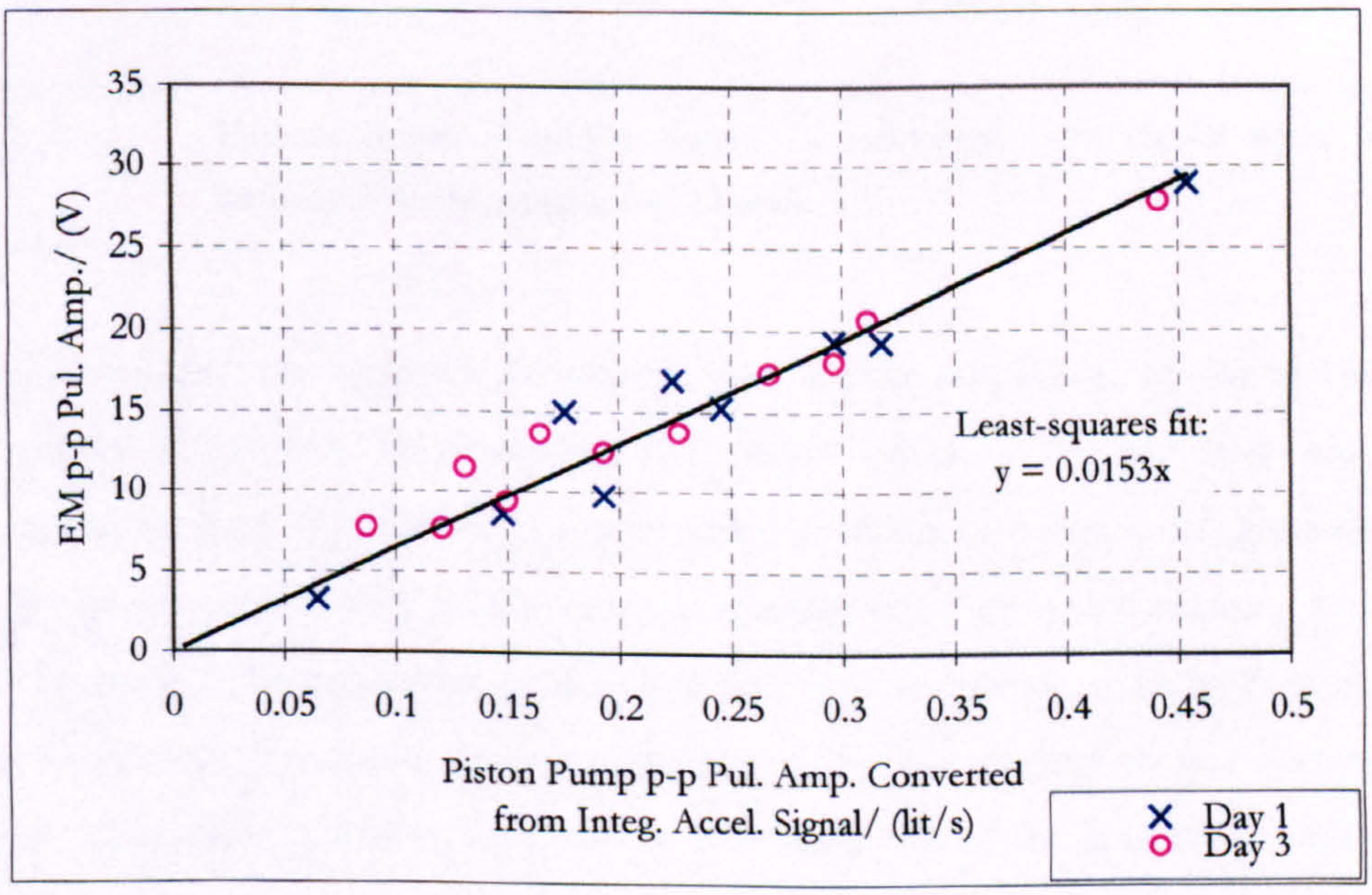

Figure 6. 13 Calibration results of the EM meter p-p pulsation amplitude plotted against the flow p-p pulsation amplitude from the piston pump

It can be seen that Figure 6. 13 shows that the calibration is repeatable to better than 5%, a line of least-squares fit for both days is drawn as shown (R-squared value = 0.94) and the calibration factor is obtained: 1 Volt of EM meter signal equals to 0.0153 lit/s of volume flowrate (to 3 sig. fig., as explained in Chapter 6.1.4.3). This pulsation calibration factor for the EM meter signal was used to give independent measurement of the flow pulsation characteristics for succeeding tests.

6.3 Turbine Data Processing

The digitised time history of the meter signal was analysed using virtual instruments within LABVIEW. This section describes how the meter output signal (Volts) produced from the electro-magnetic pick-up was processed to represent the meter indicated flow (in lit/s).

When the meter is subjected to pulsating flow, the output signal shows some modulation of both amplitude and frequency at the pulsation frequency. Figure 6. 14 shows an example of the digitised meter output signal for a pulsation flow test at pulsation frequency of 40 Hz; individual data points are not shown here due to the high resolution. This modulation characteristic at the pulsation frequency was observed for all other turbine flowmeters during testing, for example, as shown in Figure 6. 15. It can also be seen that not all of the test meters produced a signal that was sinusoidal, and the features of a sawtooth waveform was observed in this case.

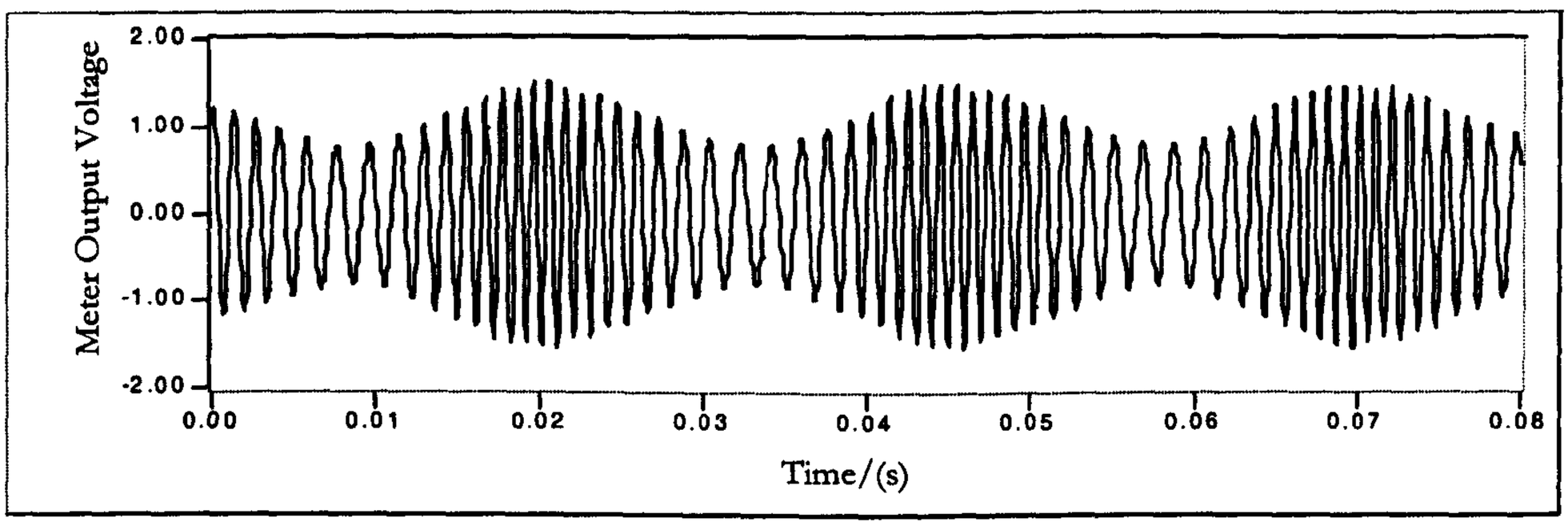

Figure 6. 14 **Turbine meter D output signal reconstructed from digital data, pulsation frequency 40 Hz, sampled at 22 kHz.**

It should be noted that only the frequency, but not the amplitude, of the meter output waveform is of interest for extracting the meter indicated volume flow rate. The conventional method of processing turbine meter signals is to convert the quasi-sinusoidal signal to a pulse signal with a pulse generated at either the + to – zero crossing or the – to + zero crossing. The reciprocal of the time between successive pulses is then the blade passing frequency. However, in the present work it was desired to test meters at the highest possible flow pulsation frequencies, and since one of the features of interest was the pulsation amplitude attenuation, this required a minimum of some 8 to 10 data points

per pulsation wave. This would have restricted the pulsation frequency to $1/8^{th}$ of the blade passing frequency.

It is clearly possible to generate pulses at both of the zero crossings in a given cycle of the signal from the pick-up, but consideration of the waveform displayed in Figure 6. 15 shows that the intervals between such pulses cannot be used to give two independent estimates of the blade passing frequency per signal cycle. The best that it is possible to do is to take the period between two successive – to + zero crossings and to associate that with the **average** blade passing frequency over that period, which can then be converted to volume flow rate (marked as "☎" in Figure 6. 16); and then to take the period between the two + to – zero crossings and to associate that with the average over that period (marked as "▲"). Thus it is possible to get twice as many data points per signal cycle, **but** successive data points are averages over (partially) overlapping periods. It is even possible to extend this process by identifying successive maxima (marked as "×") and successive minima (marked as "+"). Thus giving 4 data points per signal cycle, but each of the data points will be an average over a period of one signal cycle, with a 75% overlap between successive periods. Figure 6. 16 shows the flow waveform graph resulting from processing by using this technique for meter B (3-bladed) output signal in Figure 6. 15.

With this approach it is potentially possible to examine the meter response to flow pulsations at frequencies as high as $1/3^{rd}$ of the blade passing frequency. However, it must be noted that the identification of maxima and minima will be inherently less accurate than the identification of zero crossings. For some tests it was found that the data points thus generated were too inaccurate to be of value, so that it was necessary to revert to only 2 data points per signal cycle.

In the work of Cheesewright and Clark (1997) and Cheesewright et al (1998), it was shown that blade spacing unevenness would affect the meter output waveform and an algorithm was developed to correct meter signals due to this effect. The algorithm requires that a long data record is available, and that when the data record is truncated to a multiple of the number of blades, conditional averages for each of the physical inter-blade spaces should be identical. Difference between the conditional averages are used to estimate the unevenness of the blade spacing and then these estimates can be used to correct the data to an equivalent time history for evenly spaced blades.

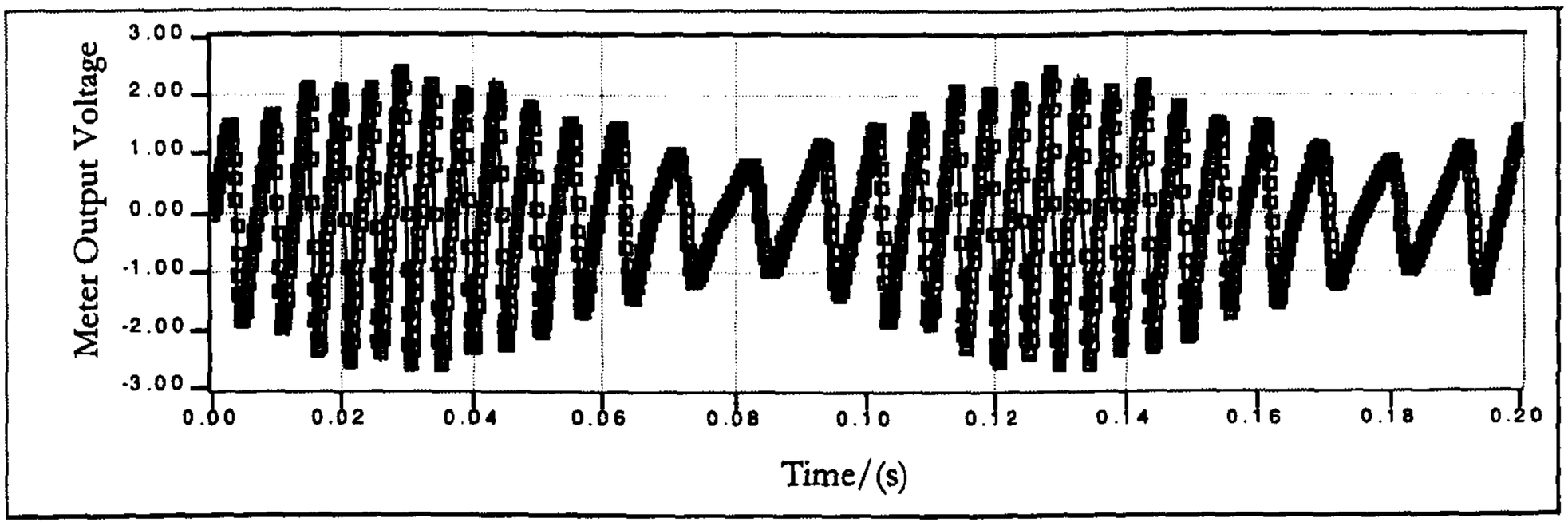

Figure 6. 15 **Turbine meter B (3-bladed) output signal reconstructed from digital data, pulsation frequency 10 Hz, sampled at 8 kHz.**

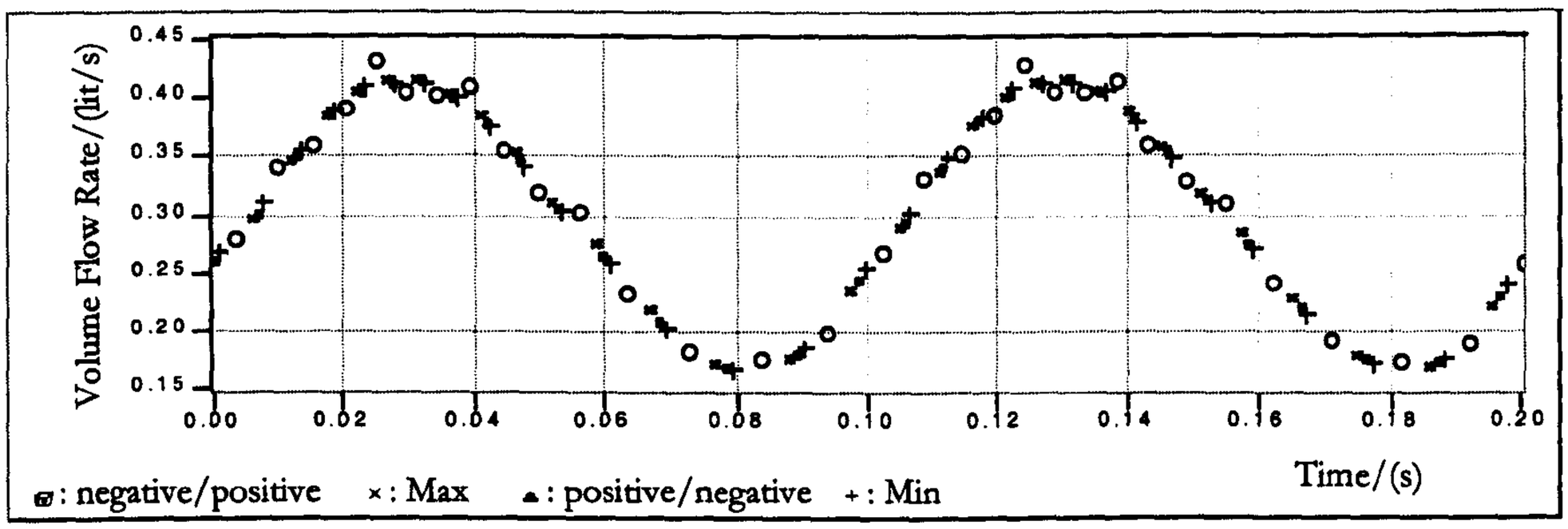

Figure 6. 16 **Flow waveform from processing by using four points per cycle technique for meter output signal shown in Figure 6. 15.**

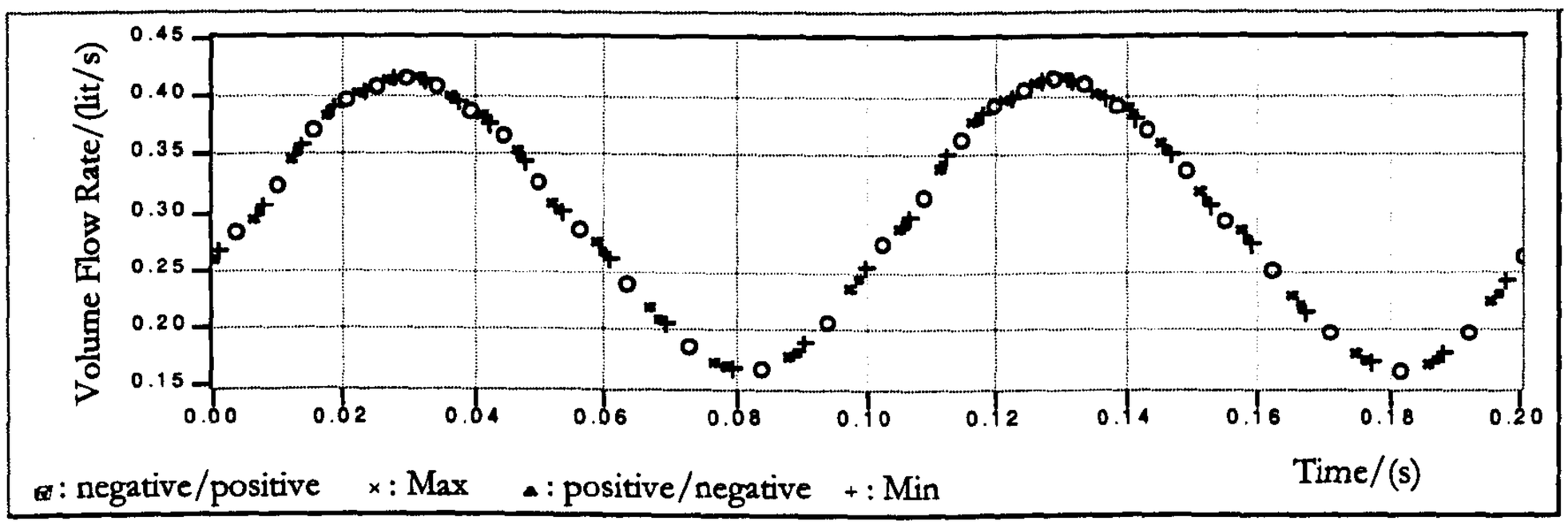

Figure 6. 17 **Flow waveform corrected for uneven blade spacing for waveform in Figure 6. 16.**

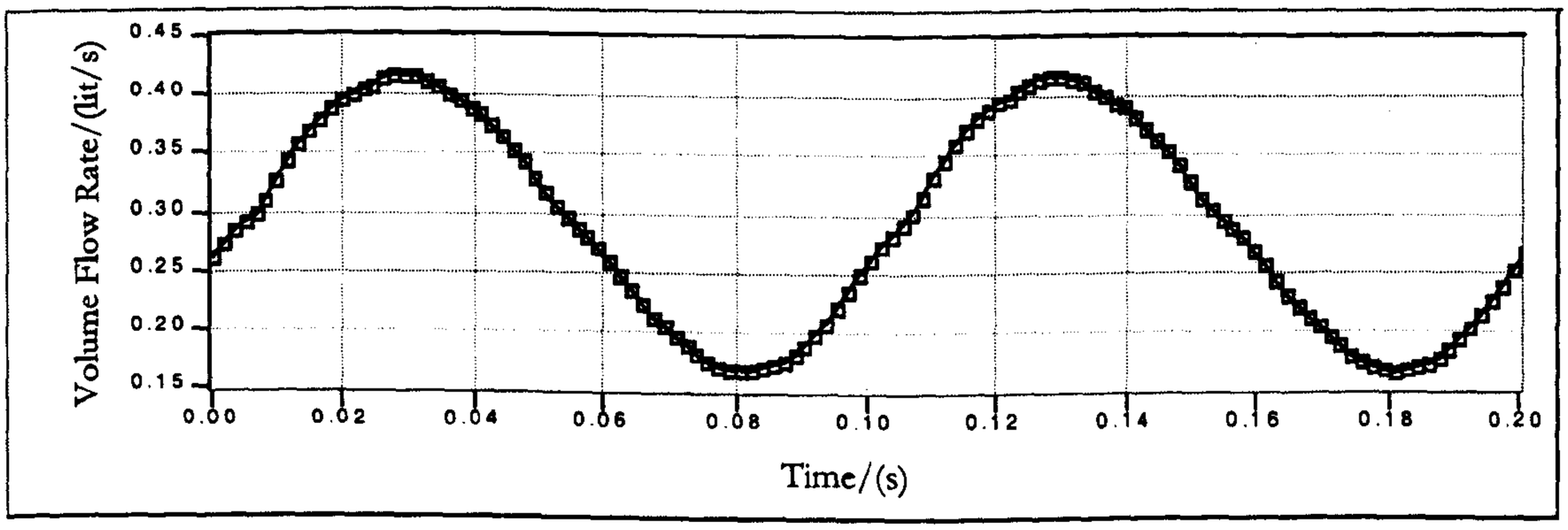

Figure 6. 18 **Flow waveform re-sampled for equal time intervals for waveform in Figure 6. 17.**

As can be seen in Figure 6.16, the occurrence of the irregularity of data points agrees well with the findings from Cheesewright et al (1998) in which it is clear that if there are small imperfections in the uniformity of spacing of the spacing of the turbine blades then this could produce fluctuations in the apparent flow rate. Therefore, the same correction algorithm is used here to improve for all meter signals due to unevenness of blade spacing. Figure 6. 17 shows an example of the flow waveform graph after the correction of uneven blade spacing for the flow waveform in Figure 6. 16.

It must also be noted, from Figure 6. 17, that the data points are not equally spaced in time; there is a greater concentration of data points during periods of high flow rate than during periods of low flow rate. Thus a simple average of all the estimates of the flow rate does not give a true mean flow rate; it is necessary, either to integrate the flow rate/time history or, as was done in the present work, to digitally re-sample the flow rate/time history at equal intervals of time. The resulting flow waveform is shown in Figure 6. 18.

From Figure 6. 18, information such as meter indicated mean flow value, $\overline{\dot{V}_m}$; and the indicated peak-to-peak pulsation amplitude, φ_m, can then be extracted. The following section will present results of all five meters tested as compared to the reference information extracted from the weigh tank (actual mean flowrate, $\overline{\dot{V}_a}$); and the EM meter signal (actual peak-to-peak pulsation amplitude, φ_a).

6.4 Experimental Results

This section presents a range of test results for each meter, showing the behaviour of meter output signal when it is subjected to pulsating flow. For each meter, the output flow after correction for blade-spacing unevenness under nominal steady flow condition will be shown first. Then a selection of meter output flow waveforms will be compared to the reference information given by the weigh tank (mean flow) and the EM meter signal (pulsating component). In the following description, the "actual flow" (▬) is inferred from the calibrated EM meter signal superimposed onto the mean flow as given by the weigh tank; and the "meter indicated flow" (—) is inferred from the turbine meter output signal either by the 2 points or 4 points per cycle technique. Individual data points are not shown as they may overlap each other.

It must be noted that the meter signals (after correction of blade-spacing unevenness) show small amplitude fluctuations even in steady flow situation. Hence a threshold value is required to distinguish the difference between steady and pulsating flow.

As stated in BS ISO TR 3313 (1998), the threshold value is calculated by the velocity amplitude of sinusoidal pulsation, $U'_{rms}/\overline{U}$. Hence, in terms of volume flow rate, this would be:

$$\dot{V}'_{rms}/\overline{\dot{V}} \qquad \textbf{Eq. 6. 3}$$

BS ISO TR 3313 (1998) stated that the threshold value for sinusoidal pulsation which will produce a systematic error of 0.1% in a turbine flowmeter is 3.5%, i.e. $\dot{V}'_{rms}/\overline{\dot{V}} = 0.035$. It can be seen that in the steady flow waveform graphs that are presented in the following sections, the evaluation of $\dot{V}'_{rms}/\overline{\dot{V}}$ for each meter is less than 0.035. Therefore, considering the manufacturers' quoted linearity for all meters is ±0.5%, the small amplitude fluctuations would not significantly increase the measurement uncertainty.

6.4.1 Meter A

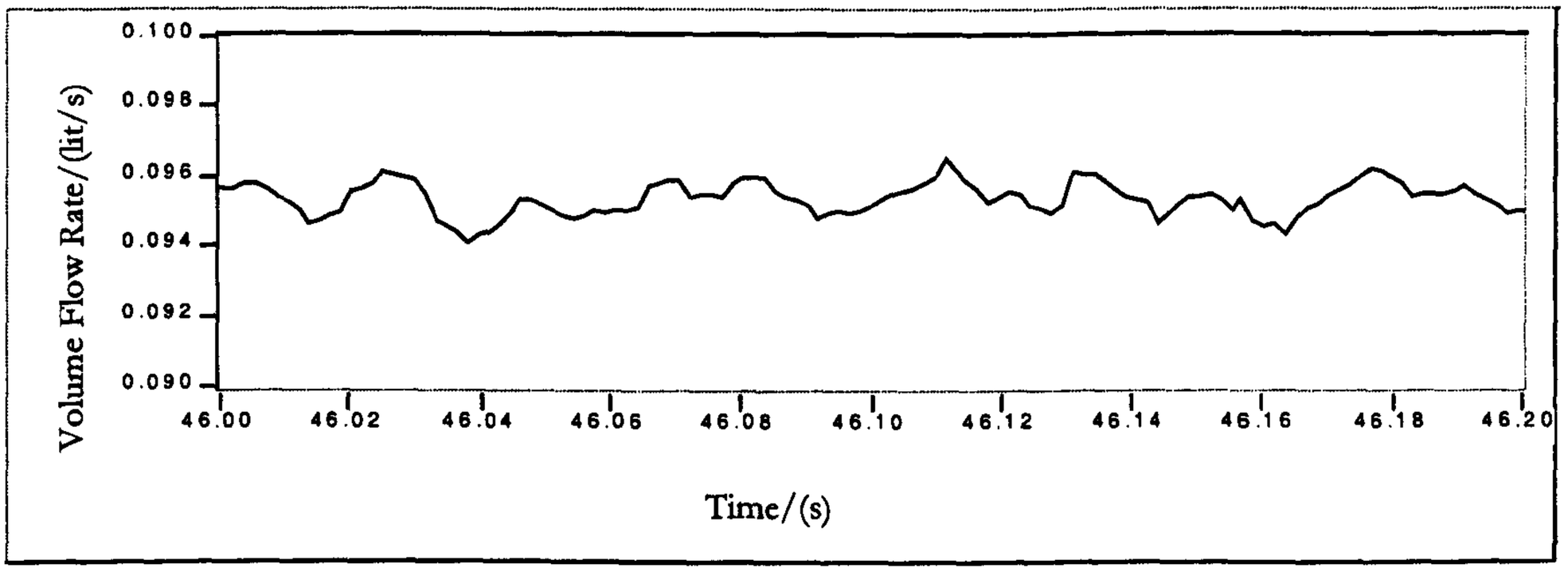

Figure 6. 19 **Meter A — Flow inferred from meter output signal after correction for blade-spacing unevenness under steady flow condition, volume flow rate = 0.095 × 10^{-3} m^3/s, $\dot{V}'_{rms}/\overline{\dot{V}}$ =0.000023.**

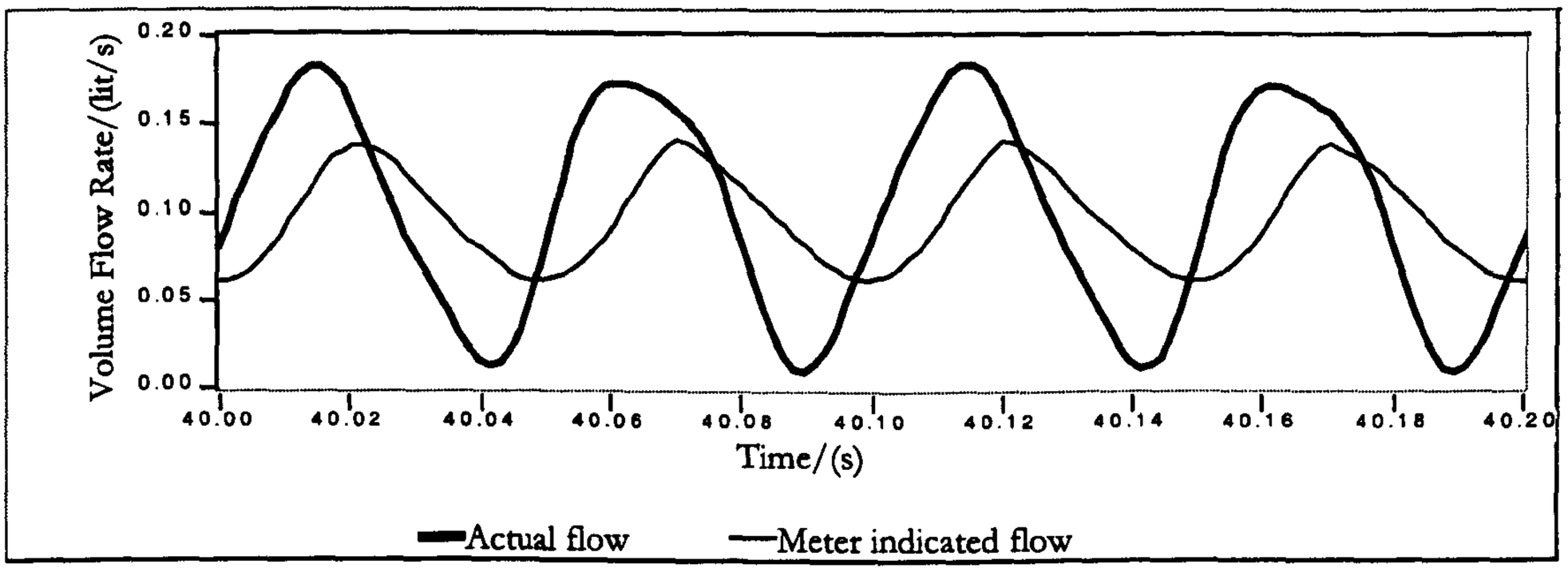

Figure 6. 20 **Meter A — Comparison of actual flow and meter indicated flow at 20 Hz imposed pulsation with 90% relative pulsation amplitude, mean volume flow rate = 0.095 × 10^{-3} m^3/s.**

6.4.2 Meter B

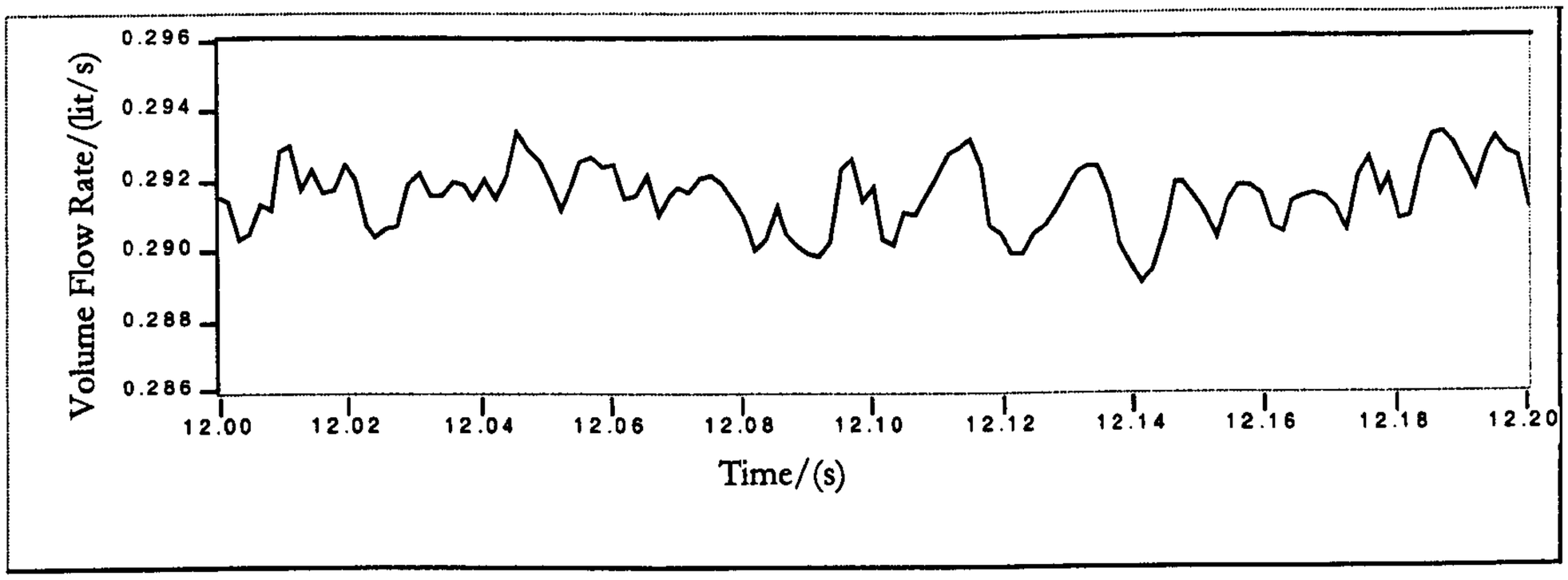

Figure 6. 21 **Meter B — Flow inferred from meter output signal after correction for blade-spacing unevenness under steady flow condition, volume flow rate = 0.292 × 10^{-3} m^3/s, $\dot{V}'_{rms}/\dot{V}$ =0.000005.**

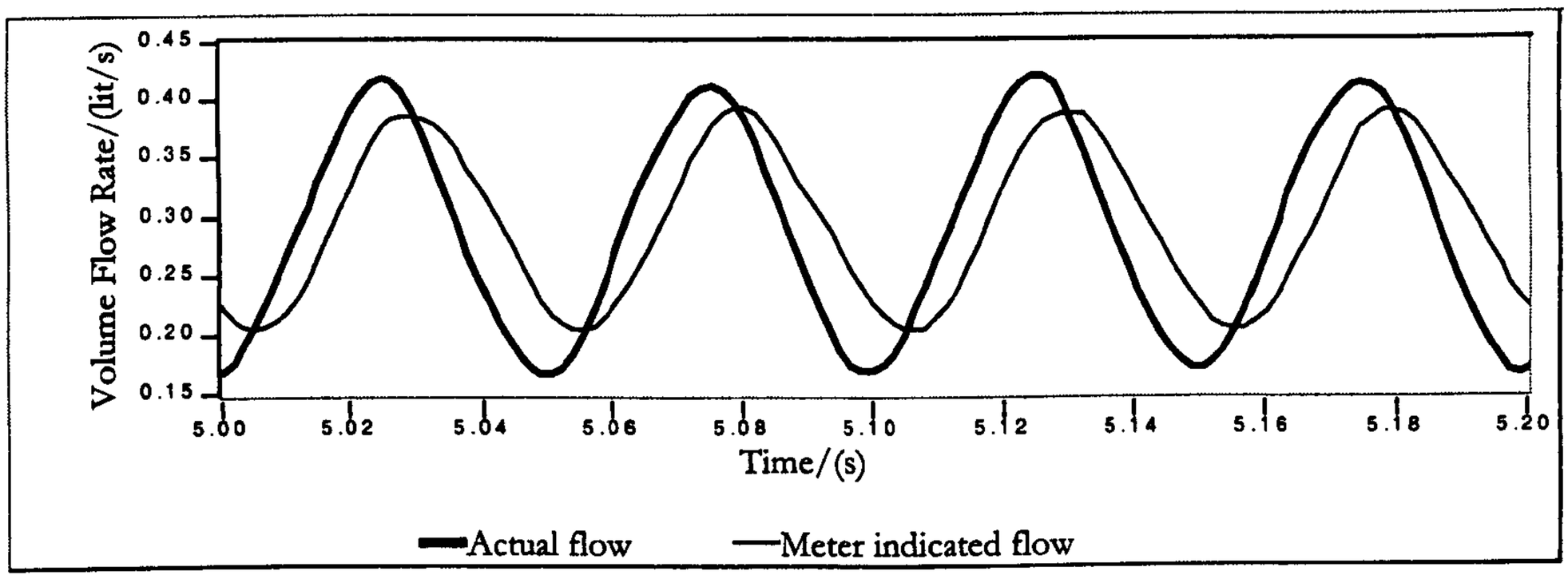

Figure 6. 22 **Meter B — Comparison of actual flow and meter indicated flow at 20 Hz imposed pulsation with 40% relative pulsation amplitude, mean volume flow rate = 0.292 × 10^{-3} m^3/s.**

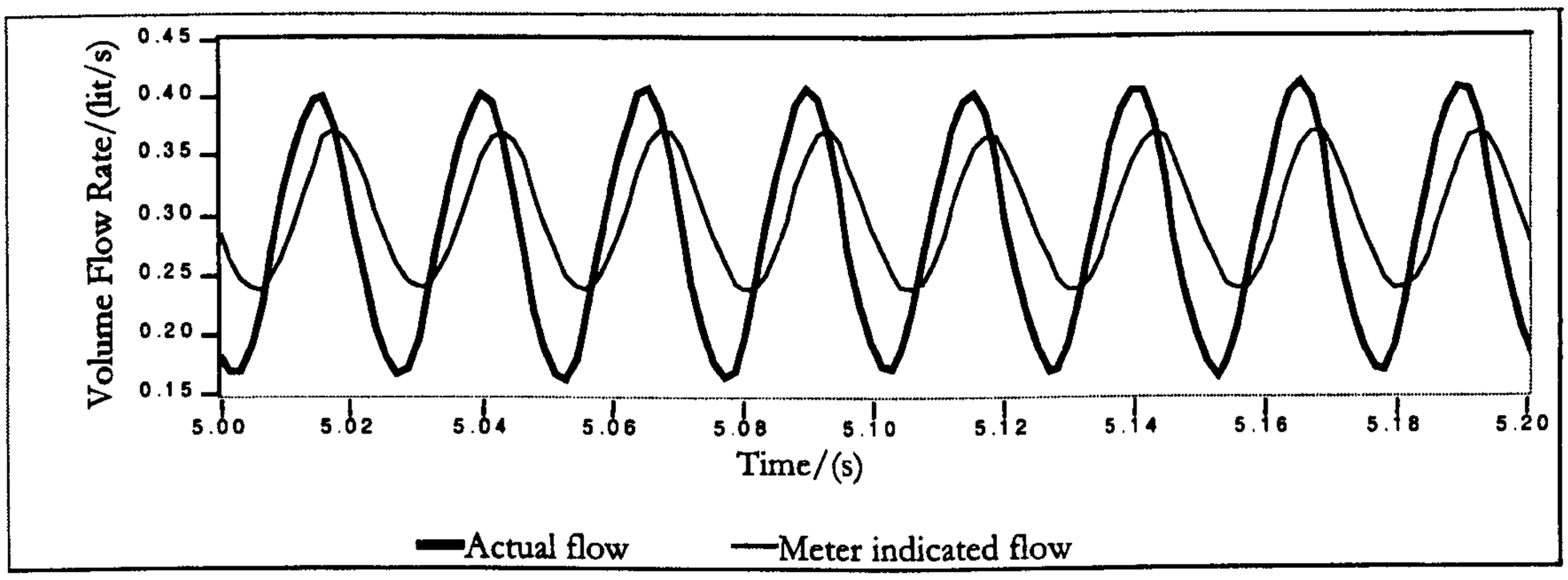

Figure 6. 23 **Meter B — Comparison of actual flow and meter indicated flow at 40 Hz imposed pulsation with 40% relative pulsation amplitude, mean volume flow rate = 0.292 × 10^{-3} m^3/s.**

6.4.3 Meter C

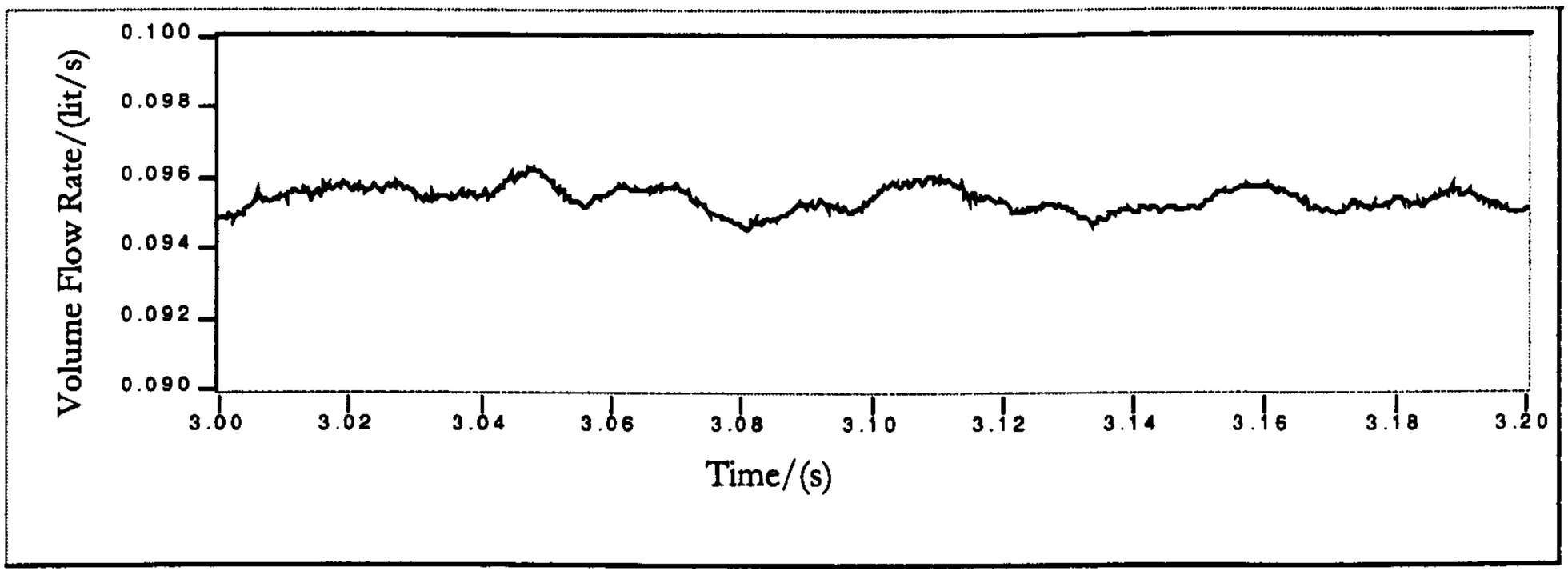

Figure 6. 24 **Meter C — Flow inferred from meter output signal after correction for blade-spacing unevenness under steady flow condition, volume flow rate = 0.095 × 10^{-3} m^3/s, $\dot{V}'_{rms}/\overline{\dot{V}}$ =0.00001.**

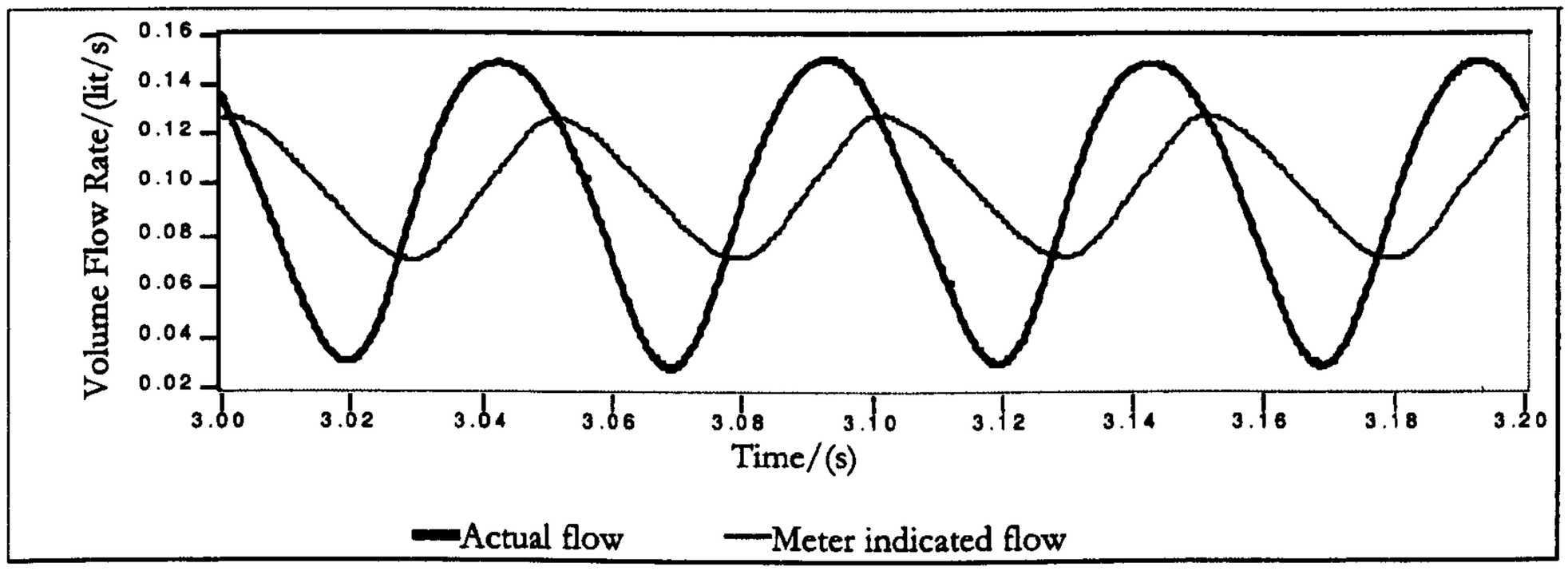

Figure 6. 25 **Meter C — Comparison of actual flow and meter indicated flow at 20 Hz imposed pulsation with 65% relative pulsation amplitude, mean volume flow rate = 0.095 × 10^{-3} m^3/s.**

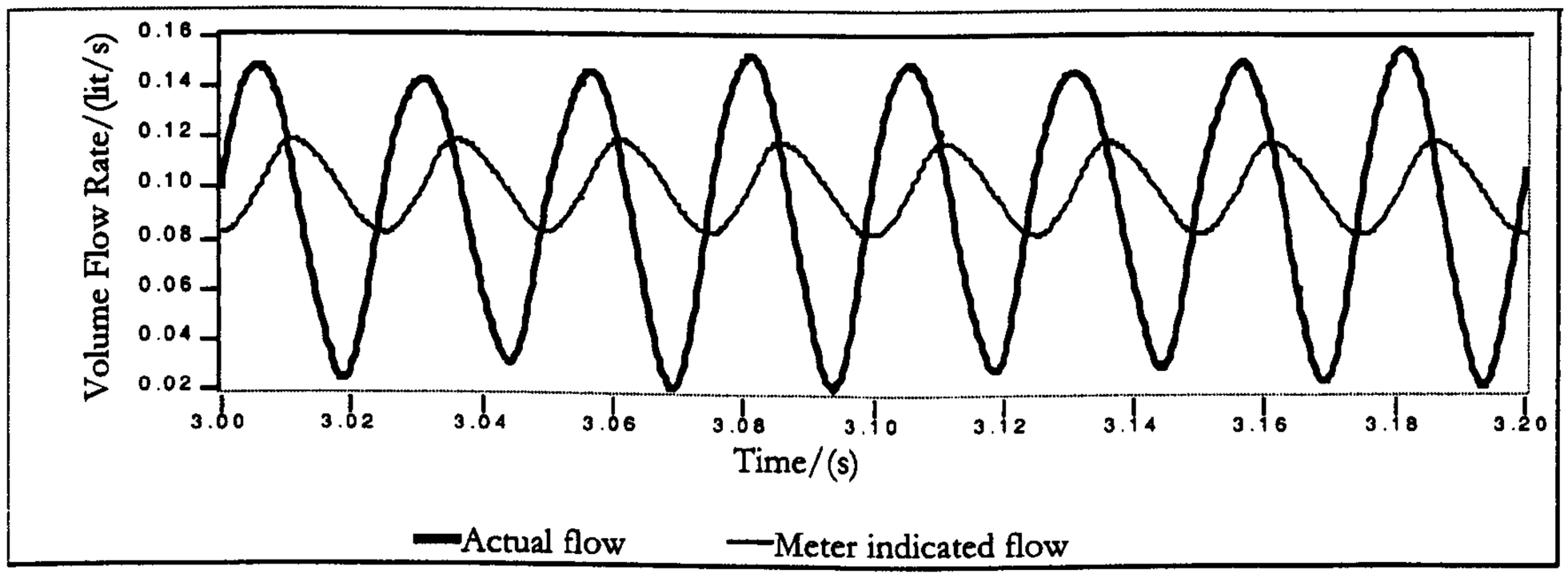

Figure 6. 26 **Meter C — Comparison of actual flow and meter indicated flow at 40 Hz imposed pulsation with 68% relative pulsation amplitude, mean volume flow rate = 0.095 × 10^{-3} m^3/s.**

6.4.4 Meter D

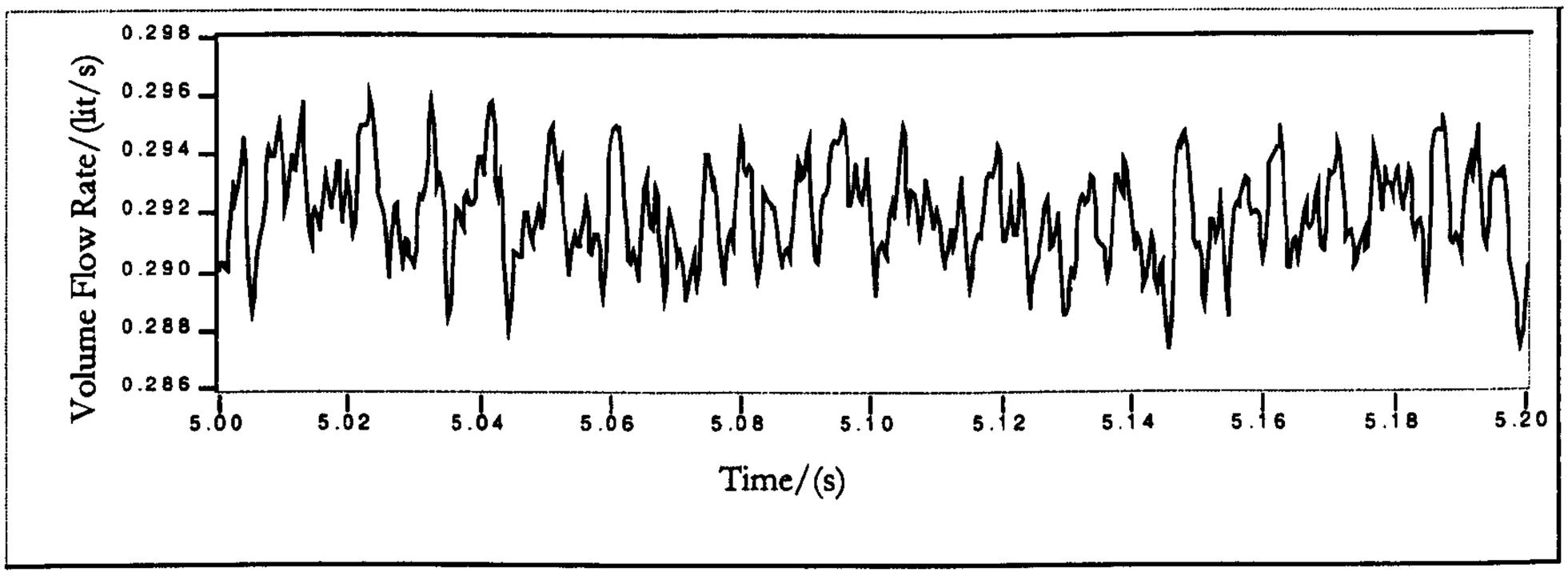

Figure 6. 27 **Meter D — Flow inferred from meter output signal after correction for blade-spacing unevenness under steady flow condition, volume flow rate = 0.292 × 10^{-3} m^3/s, $\dot{V}'_{rms}/\dot{V}$ =0.000015.**

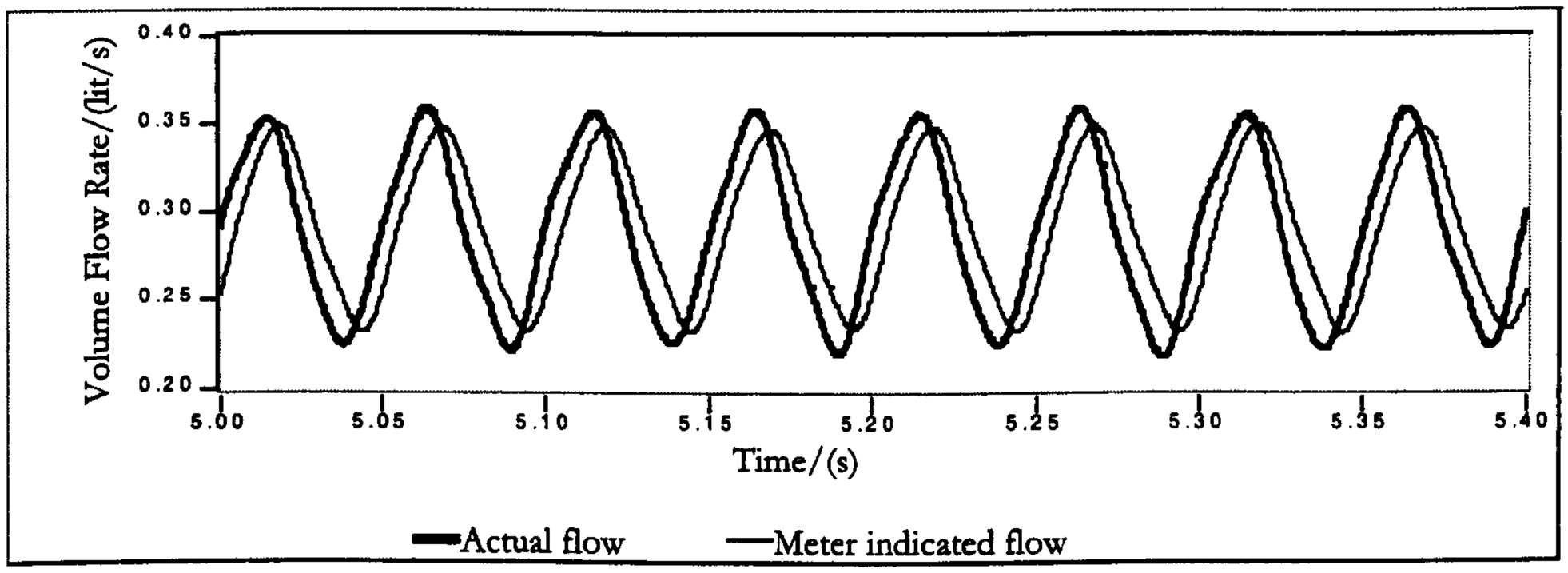

Figure 6. 28 **Meter D — Comparison of actual flow and meter indicated flow at 20 Hz imposed pulsation with 23% relative pulsation amplitude, mean volume flow rate = 0.292 × 10^{-3} m^3/s.**

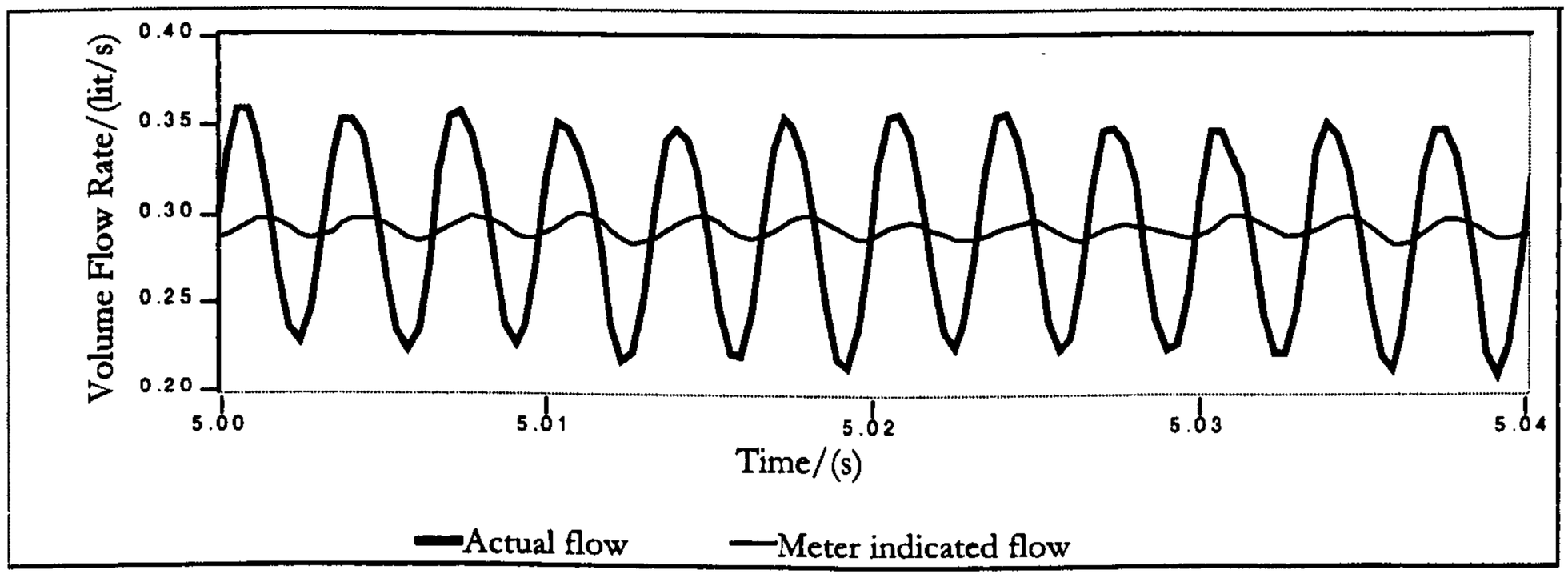

Figure 6. 29 **Meter D — Comparison of actual flow and meter indicated flow at 299 Hz imposed pulsation with 22% relative pulsation amplitude, mean volume flow rate = 0.292 × 10^{-3} m^3/s.**

6.4.5 Meter E

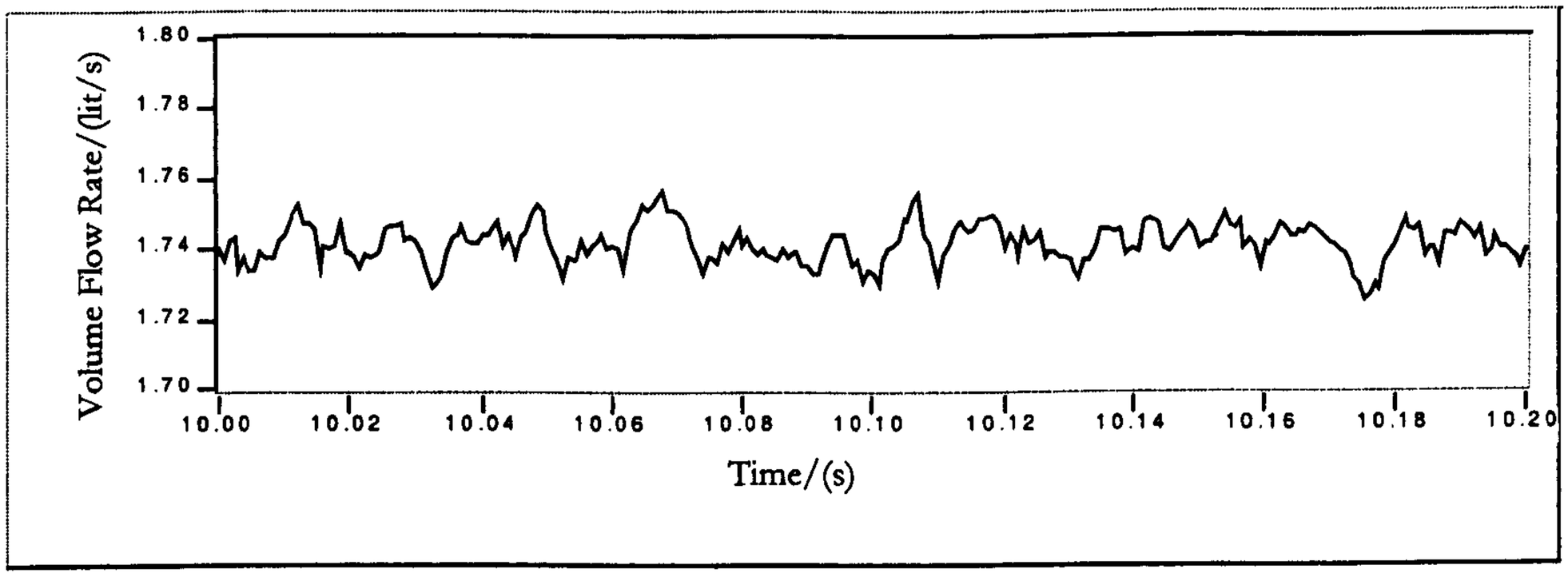

Figure 6. 30 **Meter E — Flow waveform inferred from meter output signal after correction for blade-spacing unevenness under steady flow condition, volume flow rate = 1.740 × 10^{-3} m^3/s, $\dot{V}'_{rms}/\overline{\dot{V}}$ =0.000006.**

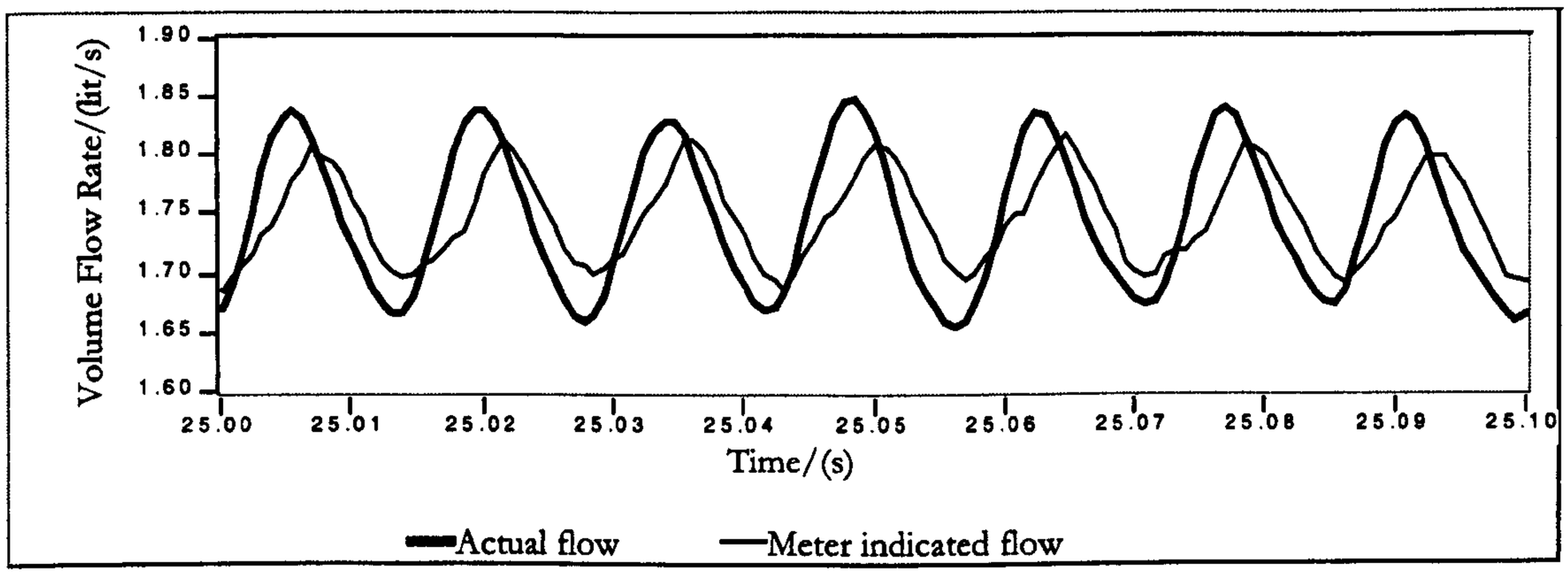

Figure 6. 31 **Meter E — Comparison of actual flow and meter indicated flow at 70 Hz imposed pulsation with 5% relative pulsation amplitude, mean volume flow rate = 1.740 × 10^{-3} m^3/s.**

It can be seen that all of the above selected pulsation tests show significant amplitude attenuation. And apart from meters D and E, significant over-registration in the indicated mean flow value can also be observed for the cases shown. The next section gives a summary of the whole series of tests for each meter.

6.5 Discussions of Experimental Results

This section presents the discussion of pulsation flow test results for each meter. The levels of over registration error, *OR*, and amplitude attenuation, *AA*, against the imposed pulsation frequencies and amplitudes will be analysed. As mentioned in Section 2.2, for the quantitative discussion of the meter behaviour, the parameters are defined as follows:

'Relative pulsation amplitude' (α_p) is defined by half of the peak to peak variation of the flow rate ($\varphi_a/2$) as a percentage of the mean flow rate ($\overline{\dot{V}_a}$);

$$\alpha_p = \frac{\varphi_a}{2\overline{\dot{V}_a}} \times 100\%$$

'Over-registration' (*OR*) is defined by the indicated mean flow rate ($\overline{\dot{V}_m}$) minus the true mean flow rate ($\overline{\dot{V}_a}$) as a percentage of the true mean flow rate, Eq. 2.3:

$$OR = \frac{\overline{\dot{V}_m} - \overline{\dot{V}_a}}{\overline{\dot{V}_a}} \times 100\%$$

'Amplitude attenuation' (*AA*) is defined by the peak to peak variation of the true flow rate (φ_a) minus the peak to peak variation of the indicated flow rate (φ_m) as a percentage of the peak to peak variation of the true flow rate, Eq. 2.4:

$$AA = \frac{\varphi_a - \varphi_m}{\varphi_a} \times 100\%$$

6.5.1 Over-registration errors

The results are presented from Figures 6.32 to 6.39. In assessing the significance of the values of the over-registration error, it must be noted that the uncertainty quoted by manufacturers for meters used in these tests is ±0.5% of full scale (over the linear range of the meters). The measured mean flow is obtained by a continuously timed gravimetric collection using a weigh tank mounted on an Avery-Berkel L105 load-cell giving an overall measurement uncertainty of ±0.1%. Hence, the error bars in over-registration graphs represent an error of: ±(0.5+0.1)=±0.6% (Morris 1991), associated with the measurement

of mean flow rate by the meter as compared to the weightank mean flow rate measurement.

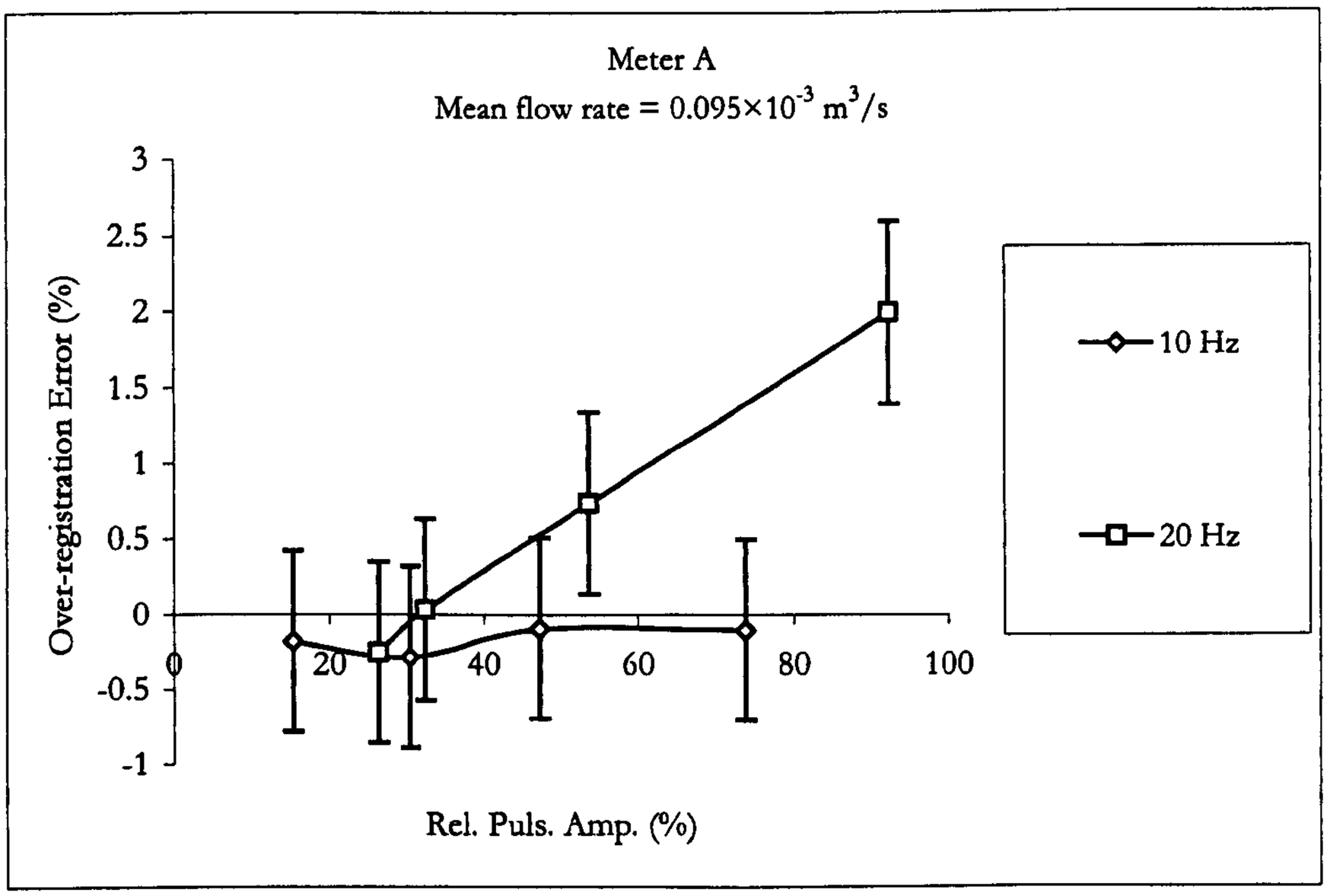

Figure 6. 32 Meter A — Over-registration errors with differing pulsation amplitudes and pulsation frequencies

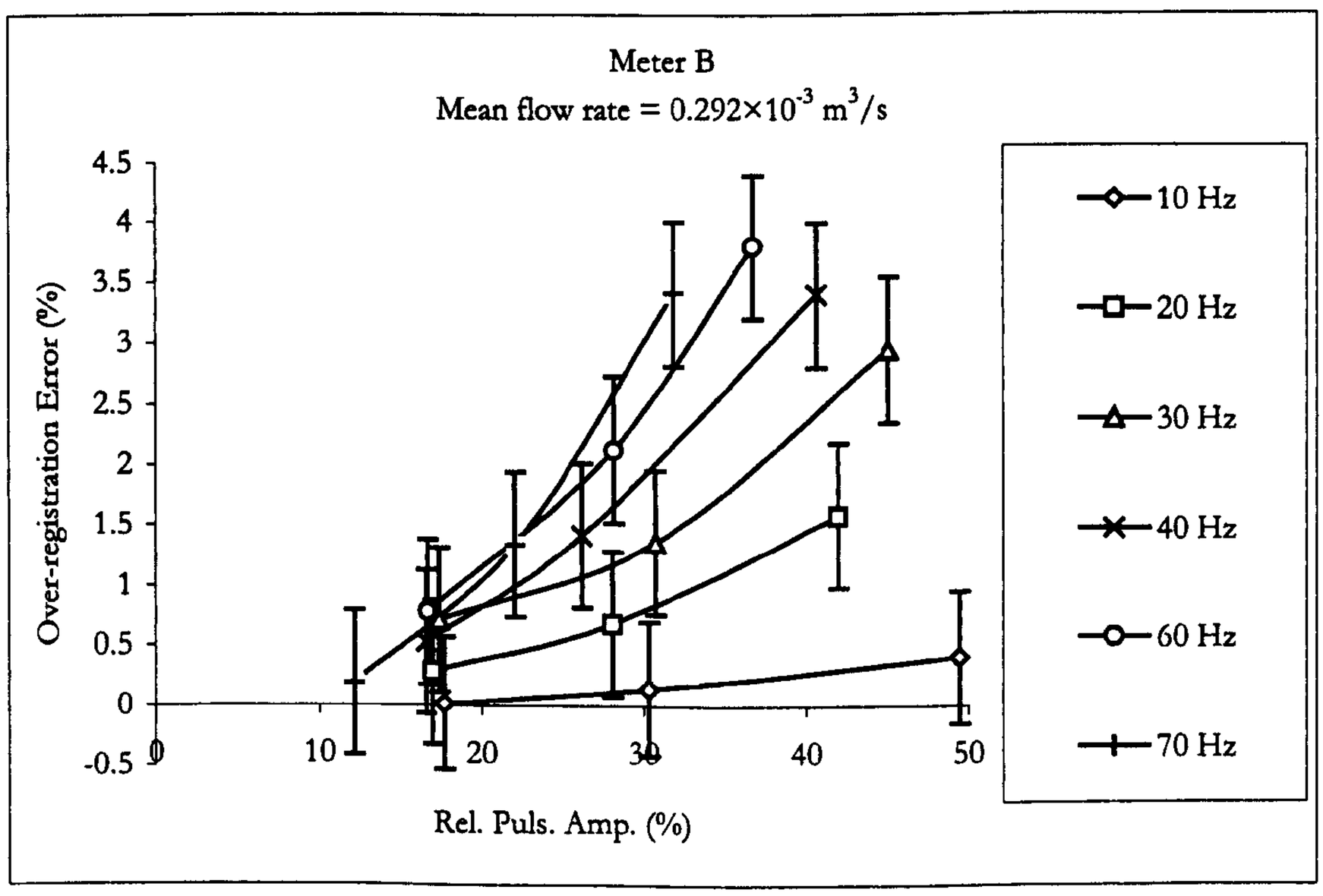

Figure 6. 33 Meter B — Over-registration errors with differing pulsation amplitudes and pulsation frequencies

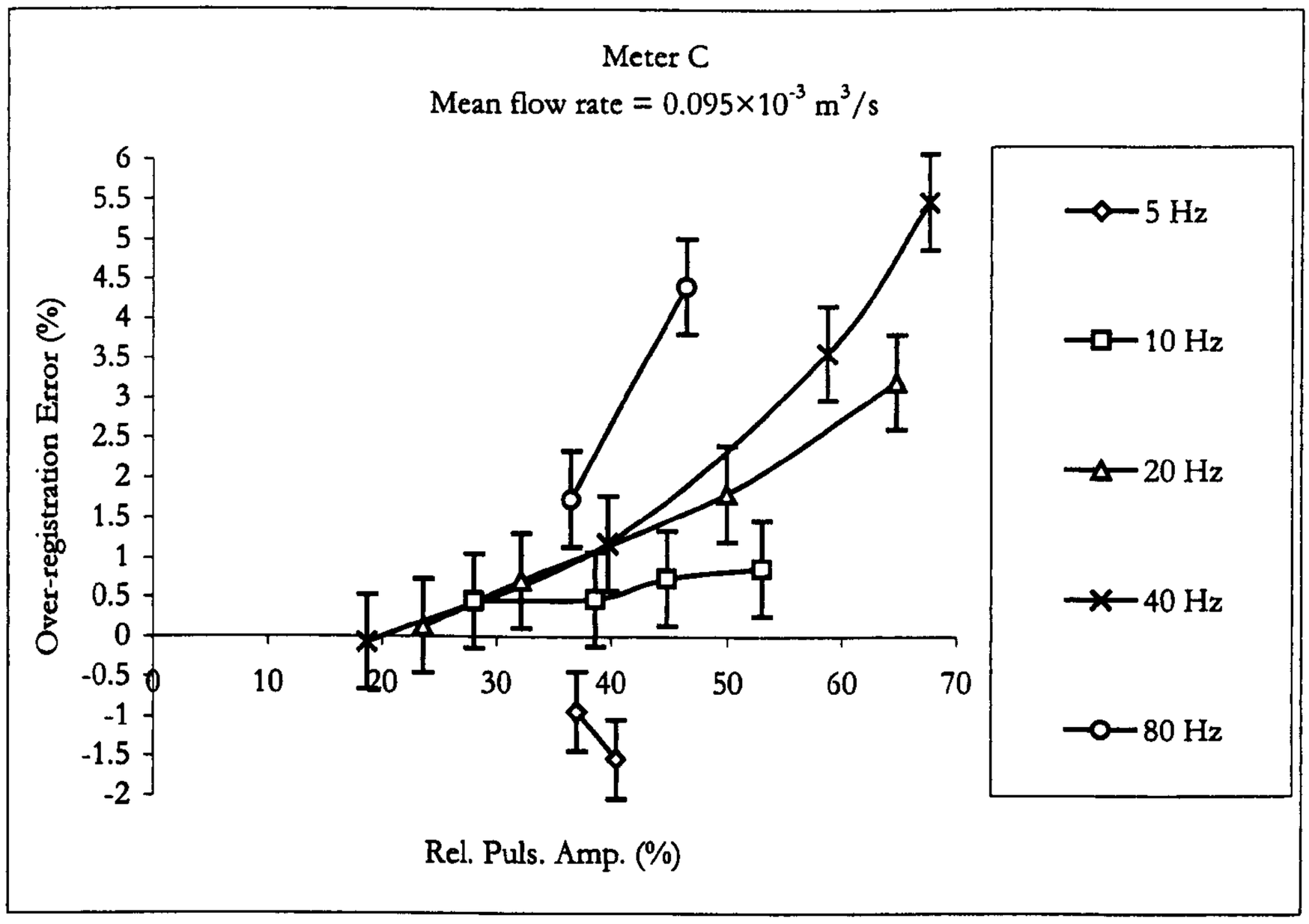

Figure 6. 34 Meter C — Over-registration errors with differing pulsation amplitudes and pulsation frequencies

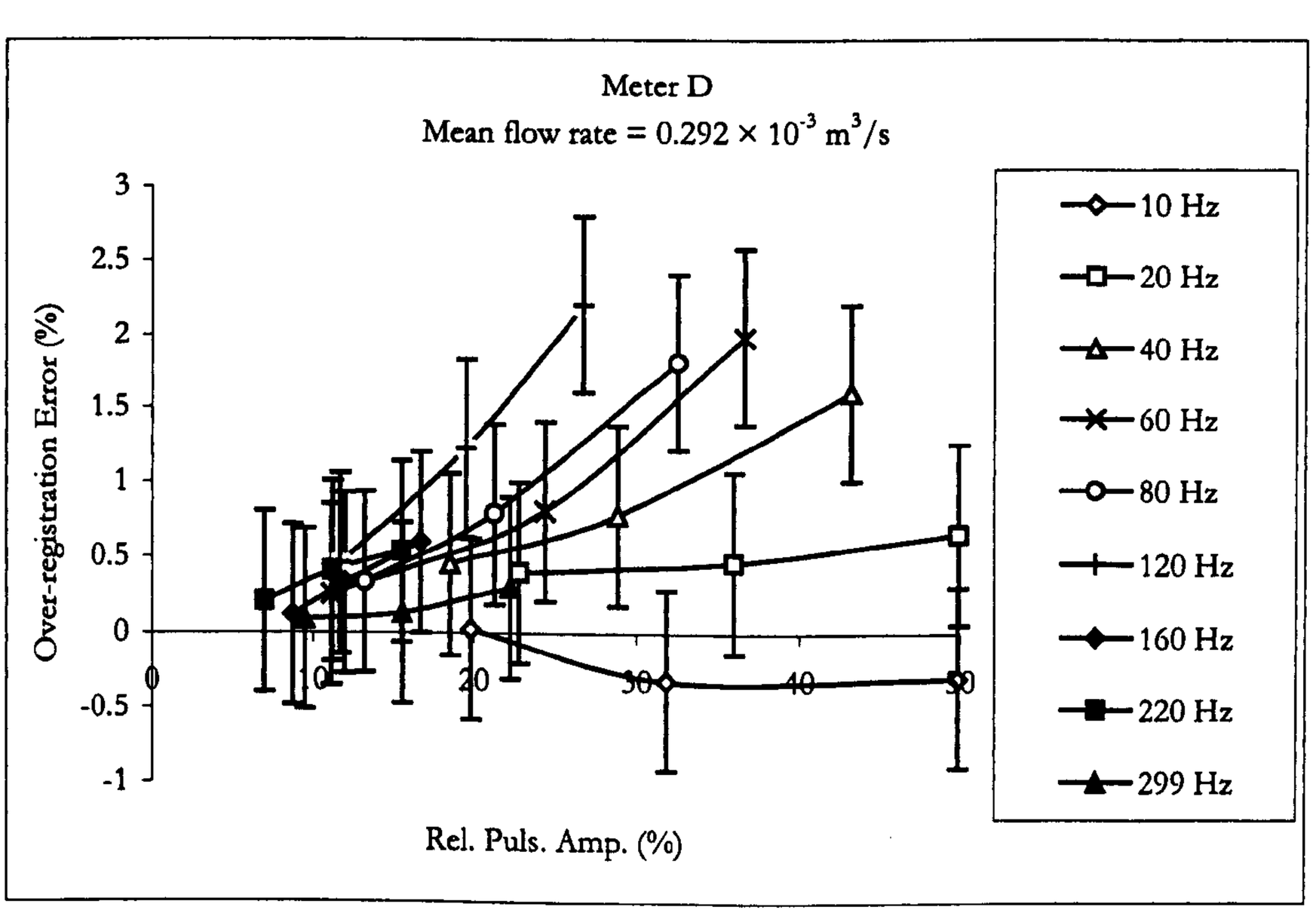

Figure 6. 35 Meter D — Over-registration errors with differing pulsation amplitudes and pulsation frequencies

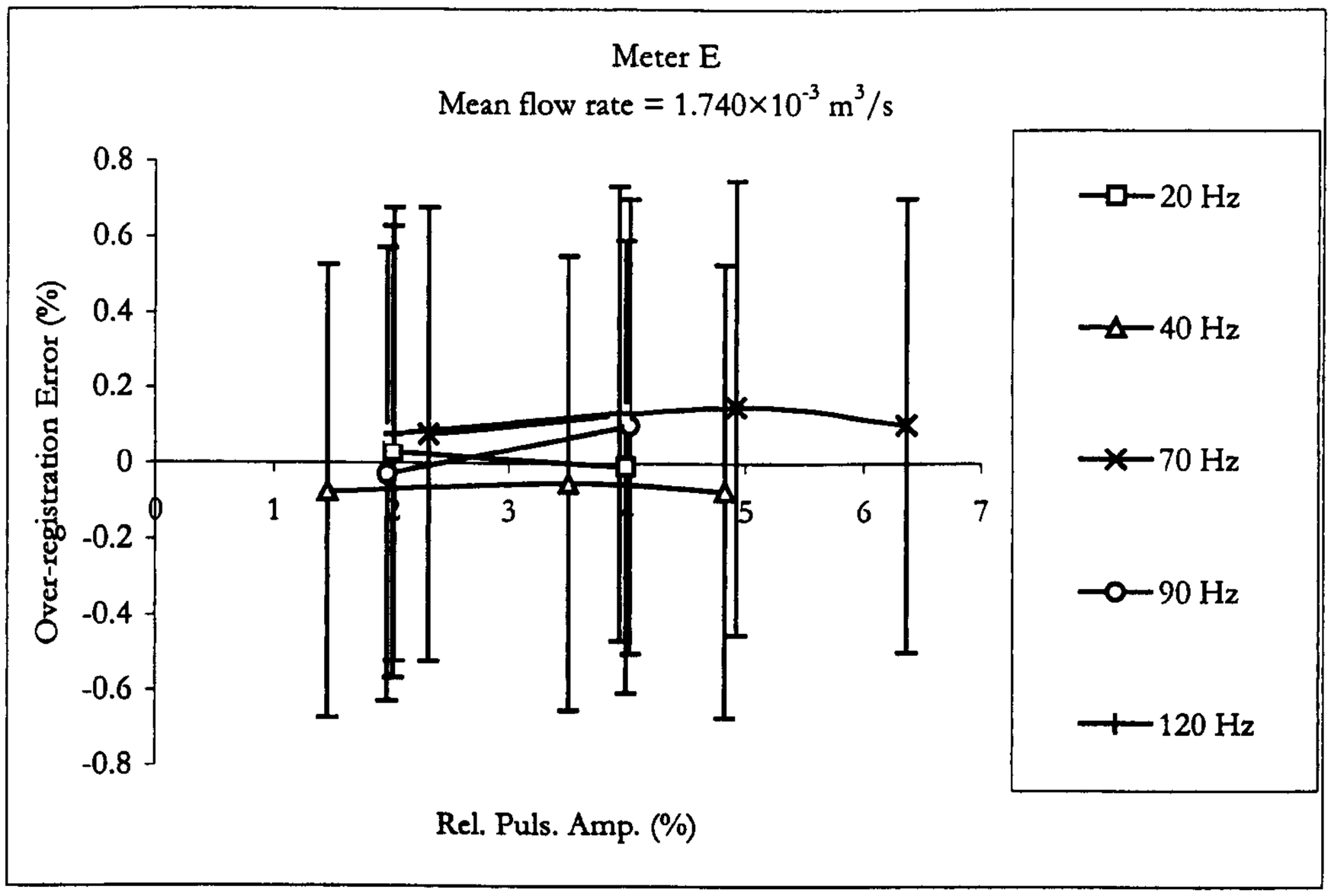

Figure 6. 36 Meter E — Over registration errors with differing pulsation amplitudes and pulsation frequencies

It can be seen from Figures 6. 32, 6. 33, 6. 34 and 6. 35 that the over-registration errors for meters A, B, C and D are qualitatively very similar — the over-registration error increased significantly with increasing pulsation frequency and increasing relative pulsation amplitude. As an example of the effects, for meter B, at 20 Hz pulsation frequency, the imposed relative pulsation amplitude ranged from 17% to 40%, the observed over-registration errors were 0.27% to 1.58%. For the same meter, at 40 Hz pulsation frequency and the same range of imposed pulsations, the over-registration errors were 0.53% to 3.40%. Graphical representations of these effects of 20 Hz and 40 Hz pulsation at 40% imposed pulsation amplitude are shown in Figure 6. 22 and 6. 23 respectively.

Furthermore, at the largest pulsation amplitudes, it can be observed that meters A, B, C, and D all experienced significant over-registration for pulsation frequencies above 20 Hz. The maximum over-registration observed was 5.5% (as shown in Figure 6. 34 and the graphical representation of this is shown in Figure 6. 26). Whilst at lower pulsation frequencies of 5 and 10 Hz, the pulsation induced errors depicted are negligible (as the results are in close proximity to the manufacturers' quoted uncertainty of ±0.5%). However, it must be noted that there was some harmonic distortion produced in the flow output waveform at these low pulsation frequencies (See Figure 6. 6 and Figure 6. 10),

therefore the negligible errors could be due to the deficiency of the flow rig in producing a true pulsation flow waveform.

For meter E, the results from investigated cases (as shown in Figure 6. 36) suggested that pulsation induced errors were insignificant considering the majority were close to the manufacturer's quoted uncertainty of ±0.5%. However, it should be noted that the imposed relative pulsation amplitudes which were examined for this meter were comparatively smaller than the other test cases for other meters.

For meter C, the negative errors resulted from the 5 Hz pulsation (Figure 6. 34) suggested that the meter under-registered the flow rate by about 1.5% at around 40% imposed pulsation amplitude. A possible physical explanation would be — during the pulsating cycle, there is a gradual reduction in flow, for instance at 5 Hz with 40% relative amplitude, 40% reduction in the volume flow rate would result in 40% reduction in the pipe flow velocity, (since volume flow rate=pipe cross-section area*velocity), therefore the pipe Reynolds number (calculated using steady flow condition) would also be reduced by around 40% ($Re = ud/\upsilon$) at the same rate, i.e. from around 10000 reduced to 6000, in which this value suggested that the meter is operating close to the transitional flow regime (<4000), Massey 1988. And when the flow is gradually increasing to the upper limit of 40%, the meter may be experiencing difficulty in responding to the change. When this intermittent turbulence phenomenon is repeated cyclically, the meter may therefore be "under-registering" the mean flow.

For one particular meter (D), the effects of flow pulsations were examined at three different operating flow rates within its linear range (which was determined under steady flow conditions): 0.143×10^{-3} m^3/s, 0.191×10^{-3} m^3/s and 0.291×10^{-3} m^3/s. Figures 6. 37, 6. 38 and 6. 39 show the over-registration errors of these tests at pulsation frequencies of 10 Hz, 20 Hz and 40 Hz respectively. The results suggested that the varying of the operating flow rates induced little effect on the over-registration errors, as each flow rate plot in each figure displayed similar trends. The maximum differentiation in these over-registration errors observed was 1.5% at 40 Hz pulsation frequency, with 40% imposed relative pulsation amplitude.

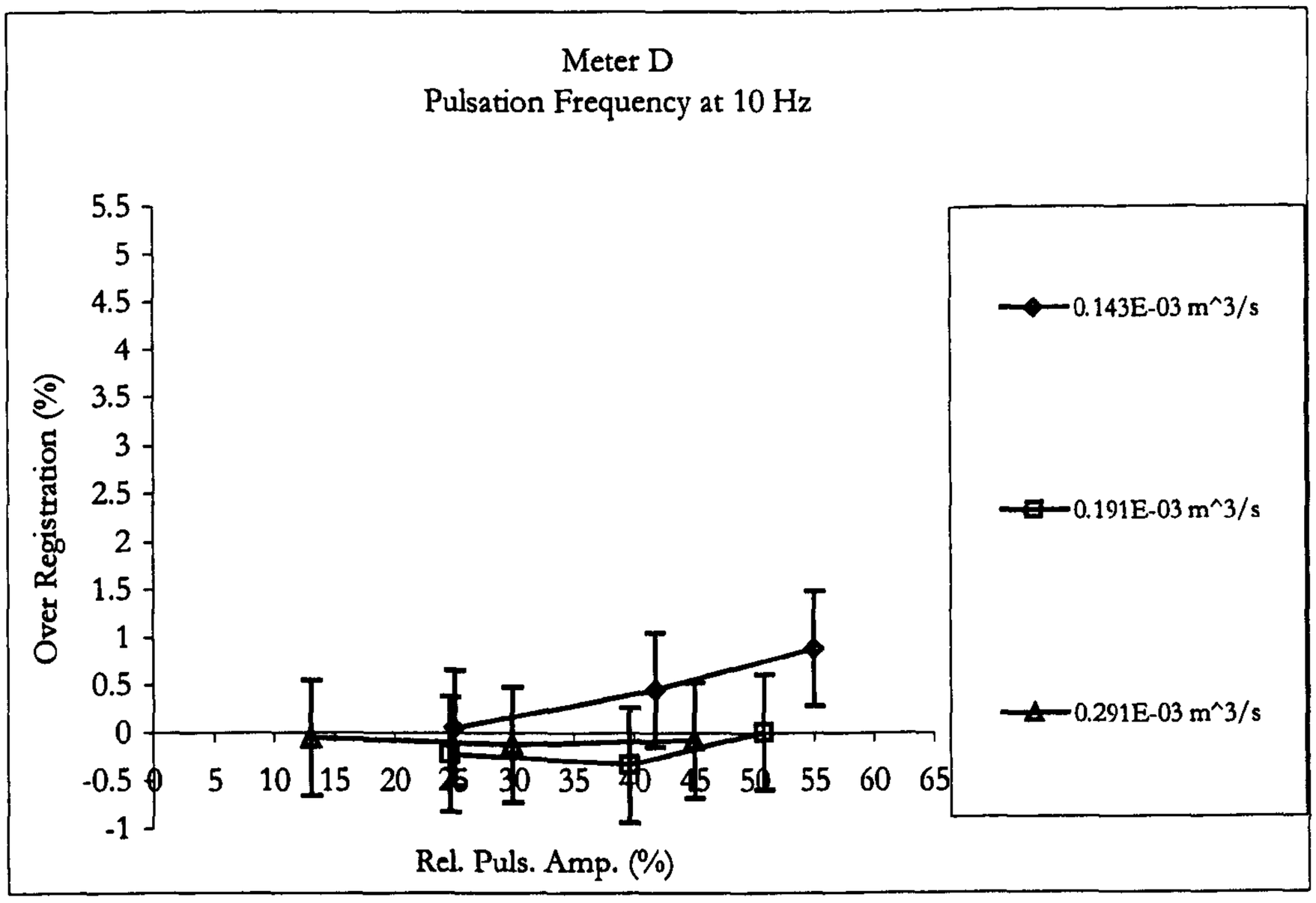

Figure 6. 37 Meter D — Over-registration errors with differing pulsation amplitudes and flow rates at 10 Hz pulsation frequency

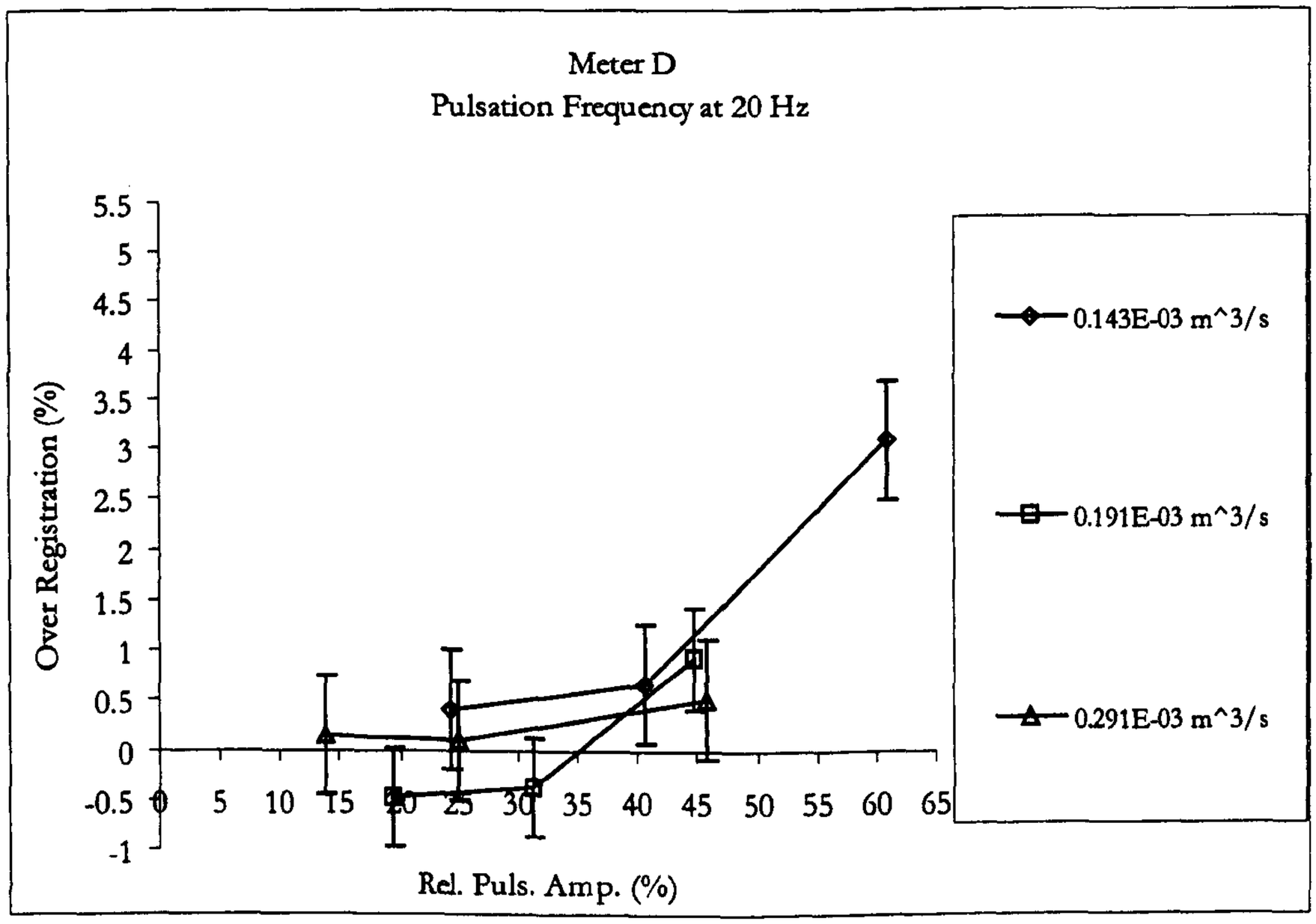

Figure 6. 38 Meter D — Over-registration errors with differing pulsation amplitudes and flow rates at 20 Hz pulsation frequency

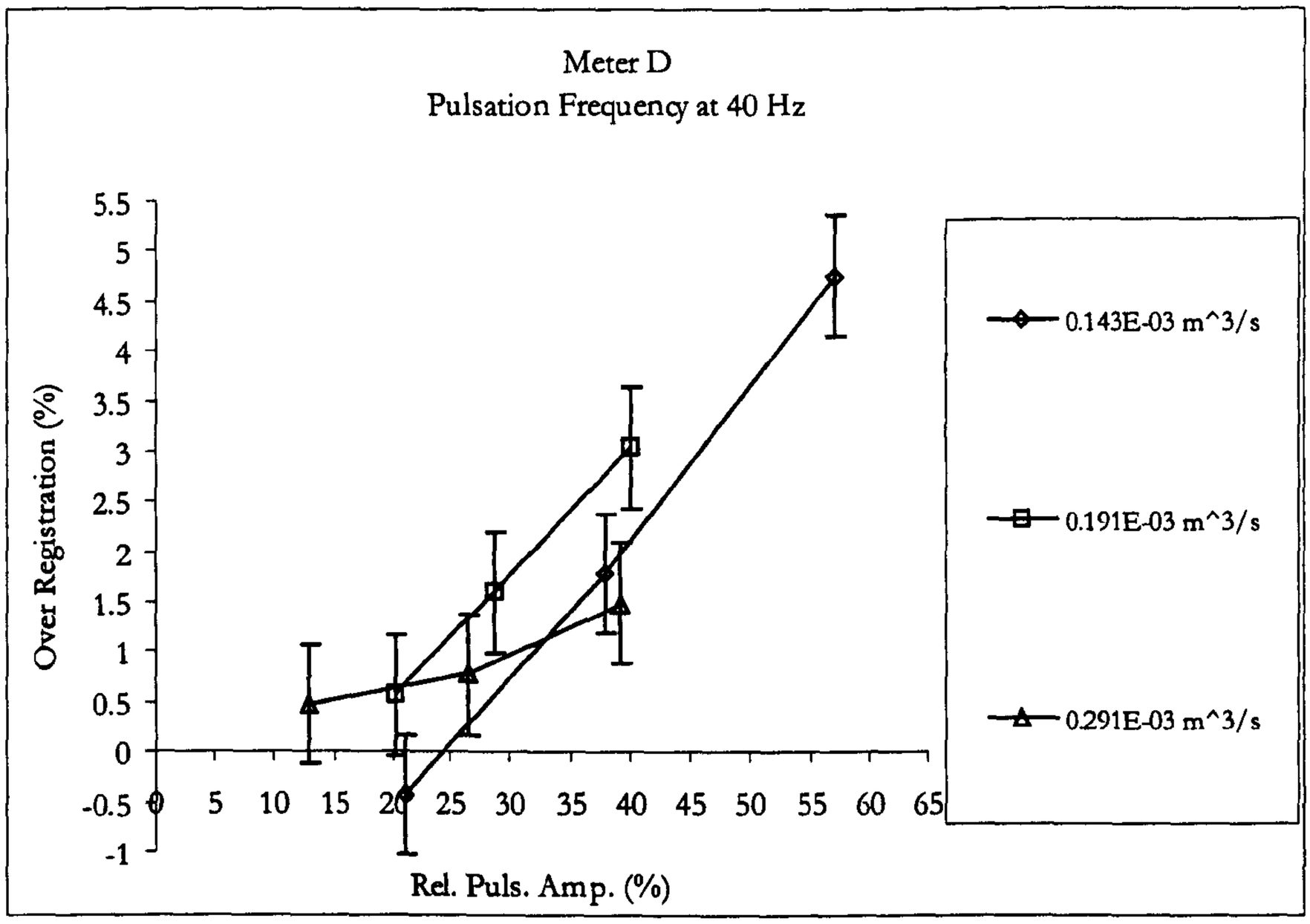

Figure 6. 39 Meter D — Over-registration errors with differing pulsation amplitudes and flow rates at 40 Hz pulsation frequency

6.5.1.1 Comparisons of over-registration between meters at "standard" pulsation cases

Since there was a 20 Hz pulsation frequency test for every meter, therefore a comparison of over-registration errors can be made on all the meters at 20 Hz. A summary of all the 20 Hz test results are given in Figure 6. 40. The error bars are not included as they may overlap each other.

At 20 Hz pulsation, it can be seen from Figure 6. 40, that there are different levels of over-registration error experienced by different meters. Apart from meter E, it can also be seen that there are no other meters which have been tested under the conditions below 7% of relative pulsation amplitude, therefore meter E will be excluded from any comparison being made from Figure 6. 40.

At 20 Hz with 40% imposed relative pulsation amplitude, meter A exhibits the best response; for the particular cases investigated, the ascending order of over-registration errors ranks from meters A, D, C and B. There are many factors affecting this order, such

as the meter size, mean flow rates and blade number, etc. A table summarising these factors is given below:

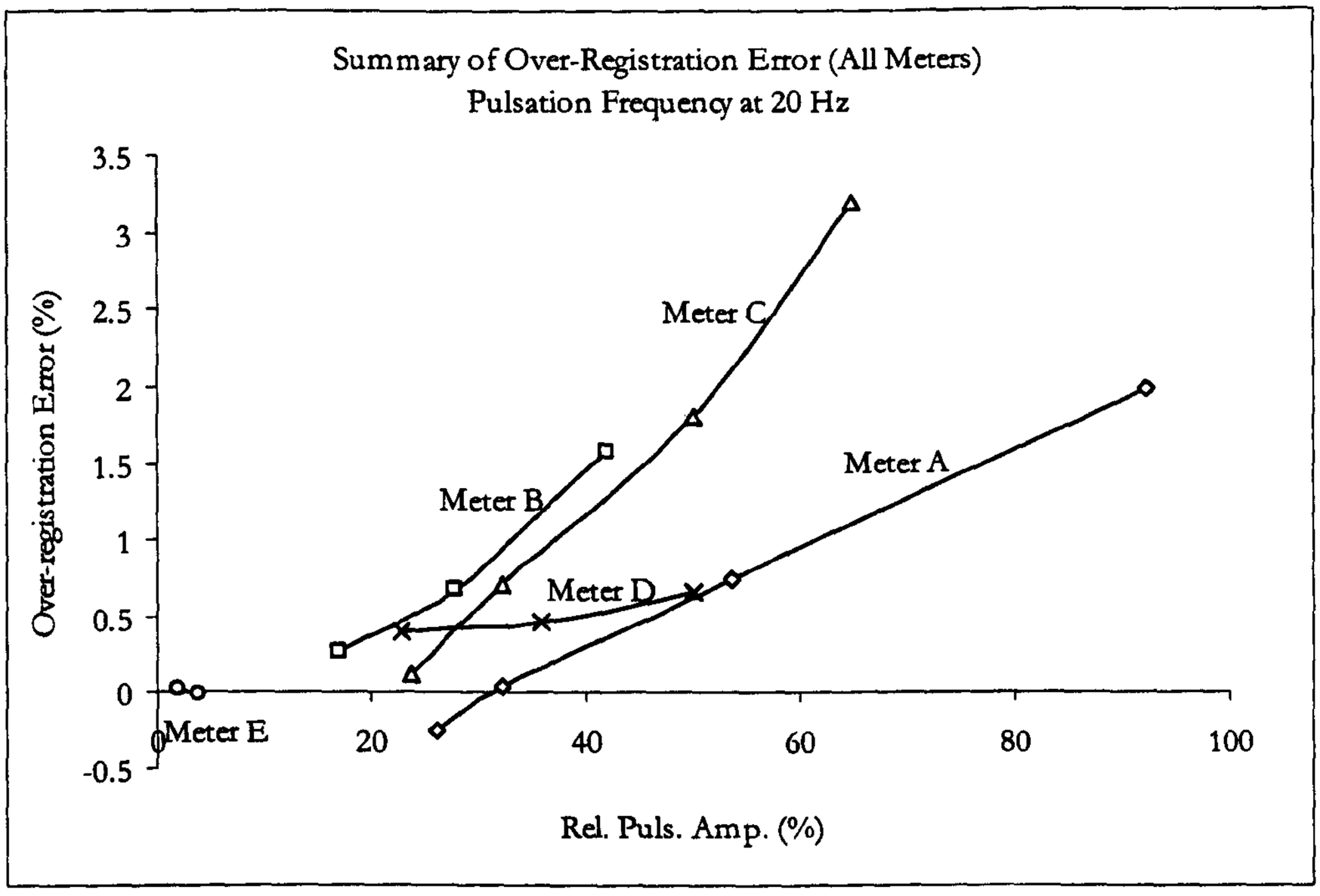

Figure 6. 40 A comparison of over-registration error for all meters at 20 Hz pulsation frequency

Rank (20Hz)	Meter	Nominal Size (mm)	Blade no.	r_b/r_t ratio	$b = \frac{I_R}{\rho \bar{r}}$ ($\times 10^{-7}$ m^3)	$\lambda = I_f/I_R$	$b(1+\lambda)$ ($\times 10^{-7}$ m^3)	Mean flow rate ($\times 10^{-3}$ m^3/s)	Ratio of lowest linear flow rate* to mean flow rate
Good	A	6	3	0.4	2.850	1.862	8.16	0.095	1 : 3.8
↕	D	12	6	0.5	4.855	0.703	8.27	0.292	1 : 7.3
↕	C	12	5	0.67	4.474	1.300	10.29	0.095	1 : 6.3
Bad	B	12	3	0.4	5.123	3.434	22.72	0.292	1 : 2.1

Table 6. 3 A summary of factors affecting meter indication of mean flow rate when subjected to 40% imposed relative pulsation amplitude at 20 Hz (based on comparison made in Figure 6. 40)

On the other hand, if excluding meter A, by comparing results at 40 Hz, another order can be observed. Figure 6. 41 shows the results obtained for meters B, C, D and E. Again, since no other meters, except for meter E, were tested under the conditions below 7% of

---

* The lowest linear flow rate value is given by manufacturers. (as stated in Table 6. 1).

imposed relative pulsation amplitude, therefore meter E will be excluded from any comparison being made from Figure 6. 41.

It can be seen that now meter C exhibits a better response than meter D to pulsation at 40 Hz with 40% imposed relative pulsation amplitude. The ascending order of over-registration errors ranks from meters C, D and B for the particular cases investigated. Similar to Table 6. 3, a table summarising the factors is given in Table 6. 4.

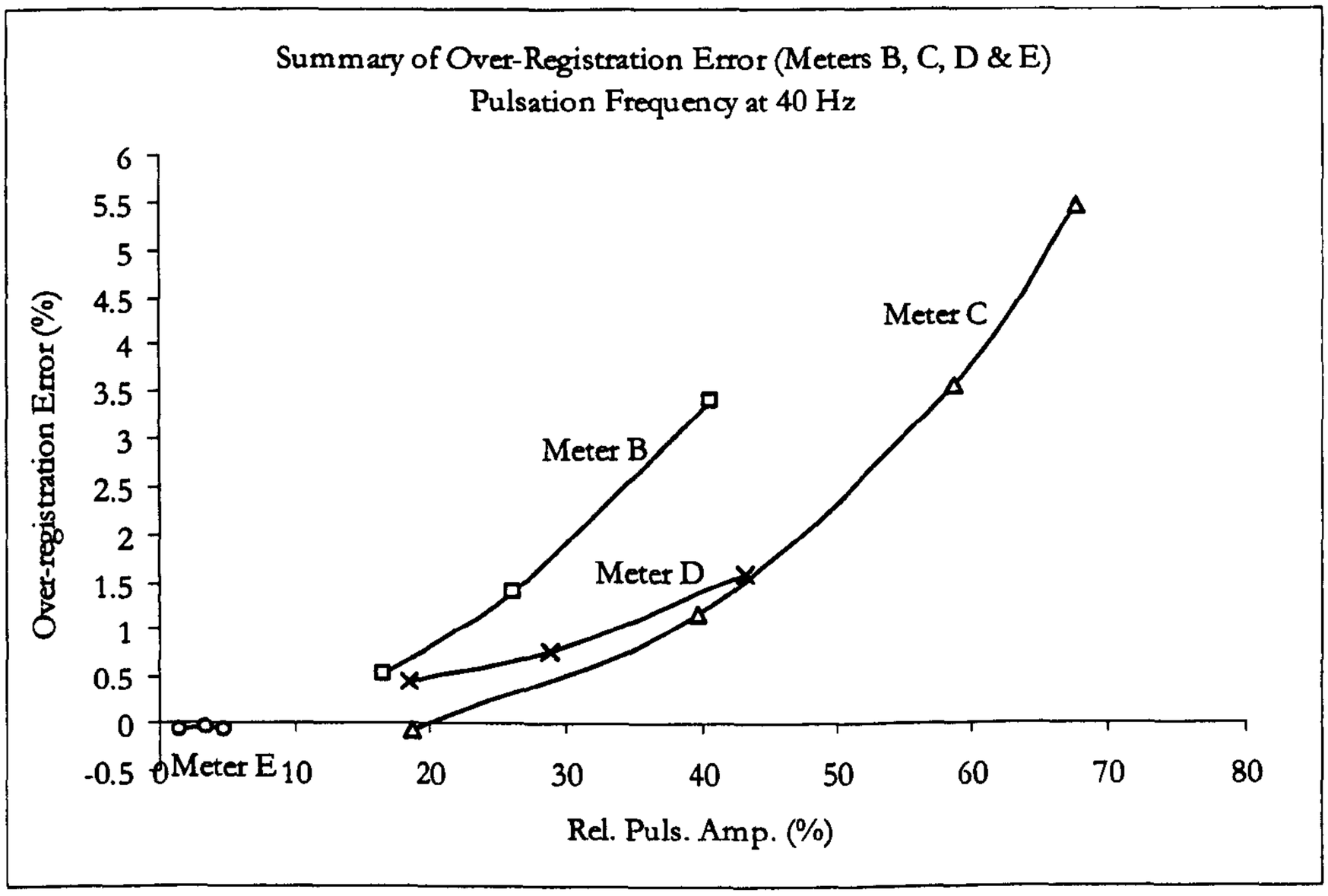

Figure 6. 41 A comparison of over-registration error for meters B, C, D and E at 40 Hz pulsation frequency

Rank (40Hz)	Meter	Nominal Size (mm)	Blade no.	r_b/r_t ratio	$b = \frac{I_R}{\rho \bar{r}}$ ($\times 10^{-7}$ m^3)	$\lambda = I_f/I_R$	$b(1+\lambda)$ ($\times 10^{-7}$ m^3)	Mean flow rate ($\times 10^{-3}$ m^3/s)	Ratio of lowest linear flow rate to mean flow rate
Good	C	12	5	0.67	4.474	1.300	10.29	0.095	1 : 6.3
↕	D	12	6	0.5	4.855	0.703	8.27	0.292	1 : 7.3
Bad	B	12	3	0.4	5.123	3.434	22.72	0.292	1 : 2.1

Table 6. 4 A summary of factors affecting meter indication of mean flow rate when subjected to 40% imposed relative pulsation amplitude at 40 Hz (based on comparison made in Figure 6. 41)

6.5.2 Amplitude attenuations

In assessing the significance of the values of the amplitude attenuation, it must be noted that the uncertainty quoted by manufacturers for meters used in these tests is ±0.5% of full scale (over the linear range of the meters). Since the peak to peak variation of the true flow rate is obtained from the EM flow waveform in which it was calibrated by reference to the flow from the piston pump with an estimated accuracy of ±5%. Hence, the error bars in amplitude attenuation graphs represent an error of: ±(0.5+5)=±5.5% (Morris 1991), associated with the measurement of pulsation amplitude by the turbine meter as compared to the value obtained from the EM flow waveform.

6.5.2.1 Against various relative pulsation amplitudes

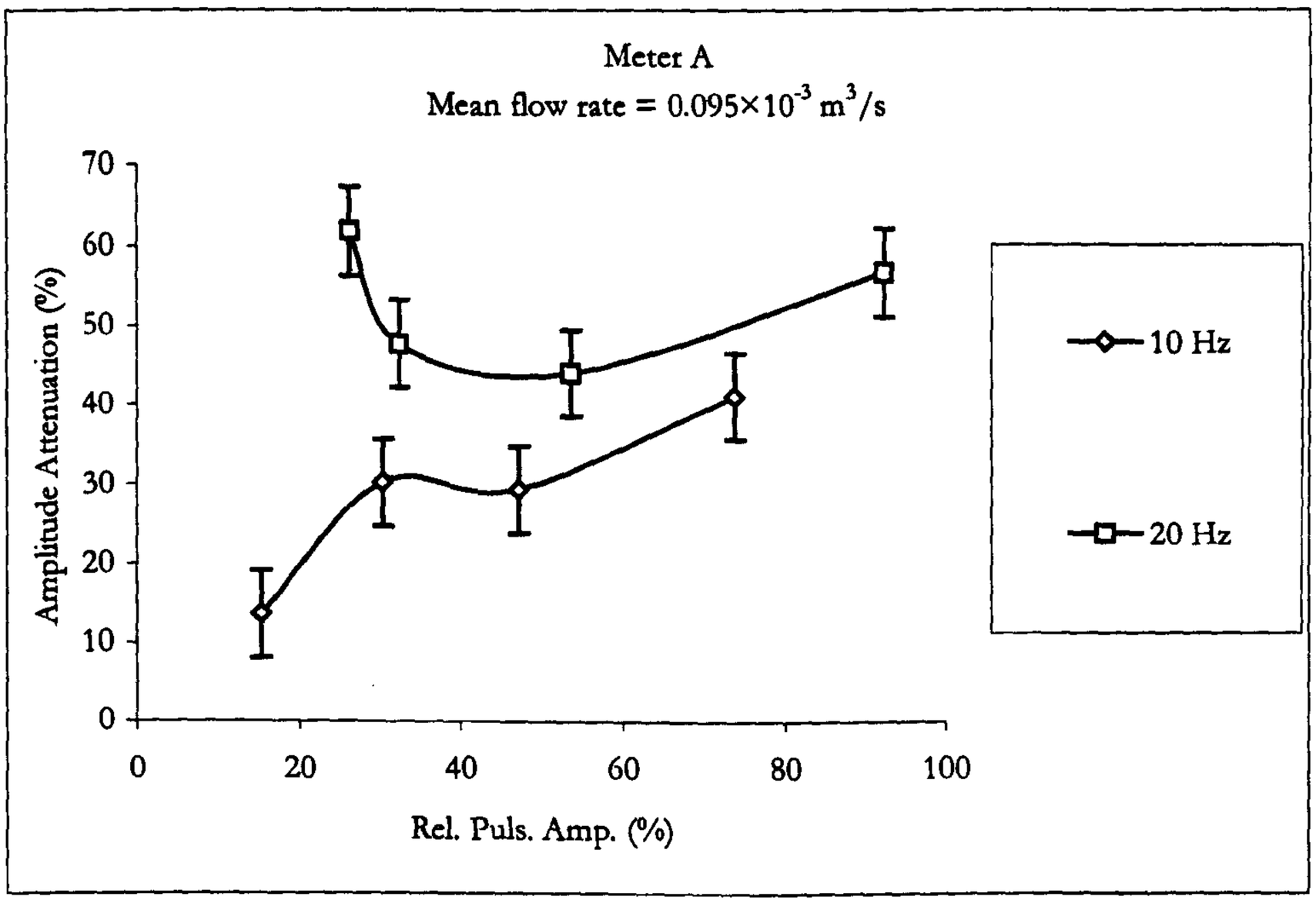

Figure 6. 42 Meter A — Amplitude attenuations with differing pulsation amplitudes and pulsation frequencies

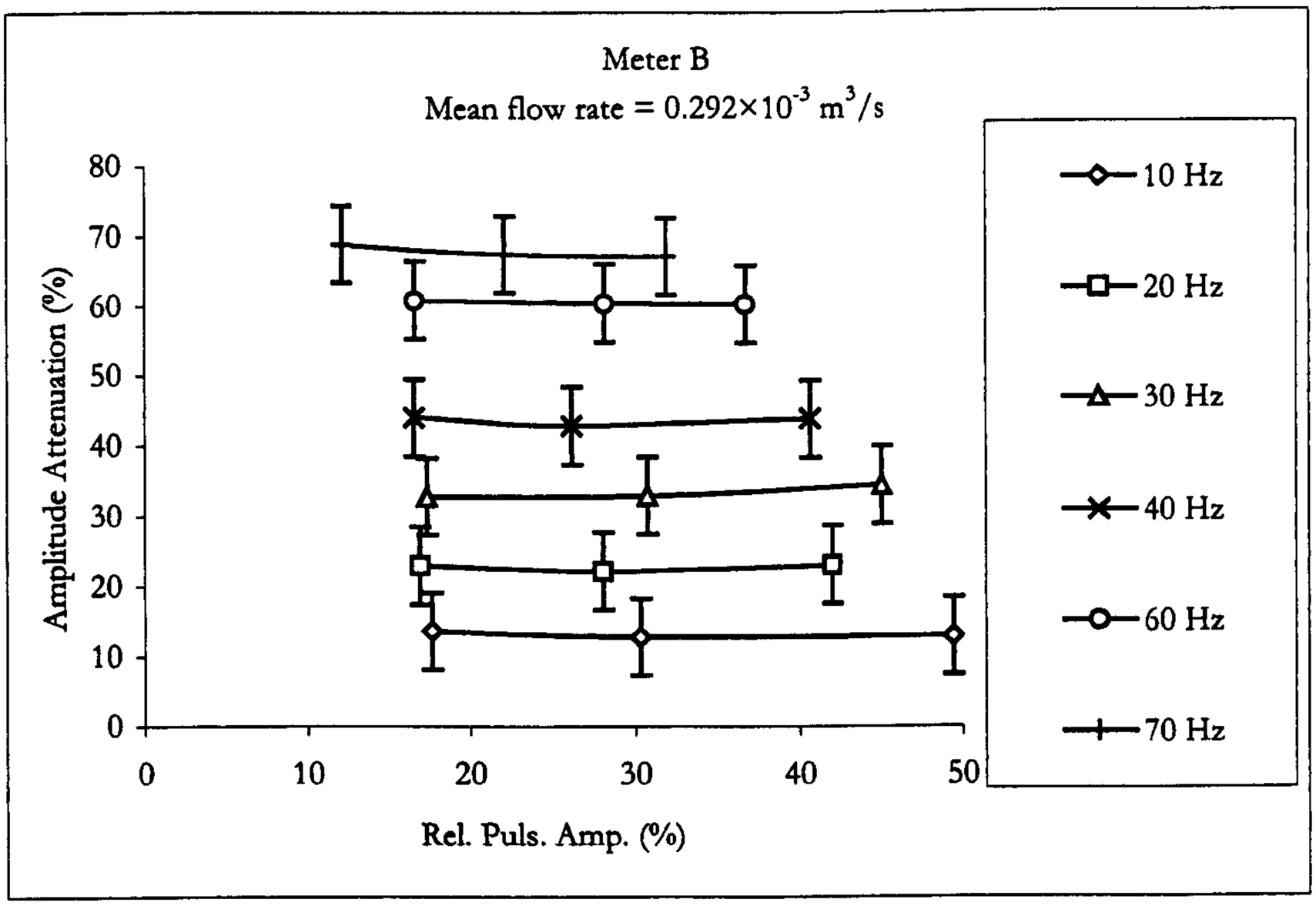

Figure 6. 43 Meter B — Amplitude attenuations with differing pulsation amplitudes and pulsation frequencies

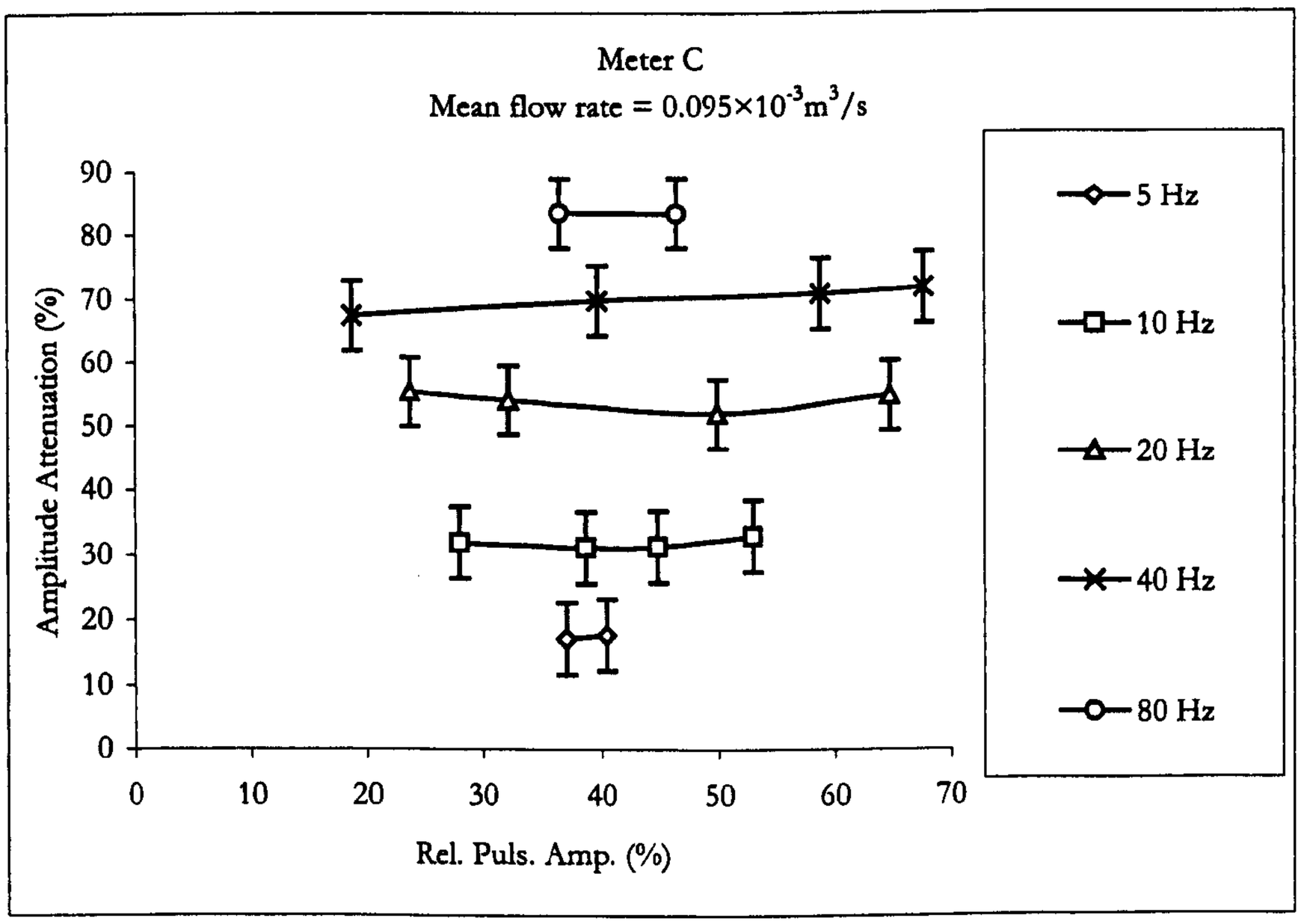

Figure 6. 44 Meter C — Amplitude attenuations with differing pulsation amplitudes and pulsation frequencies

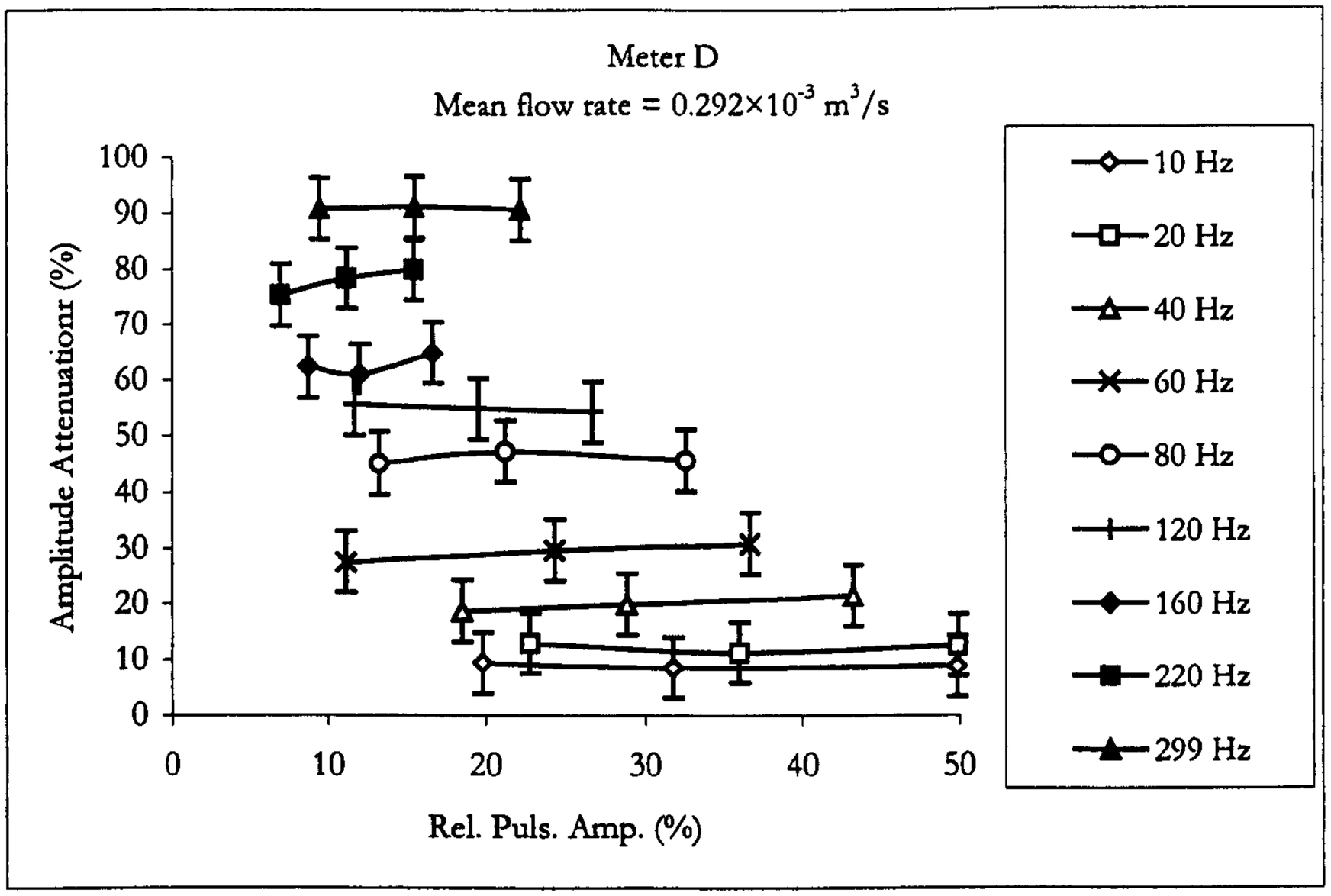

Figure 6. 45 Meter D — Amplitude attenuations with differing pulsation amplitudes and pulsation frequencies

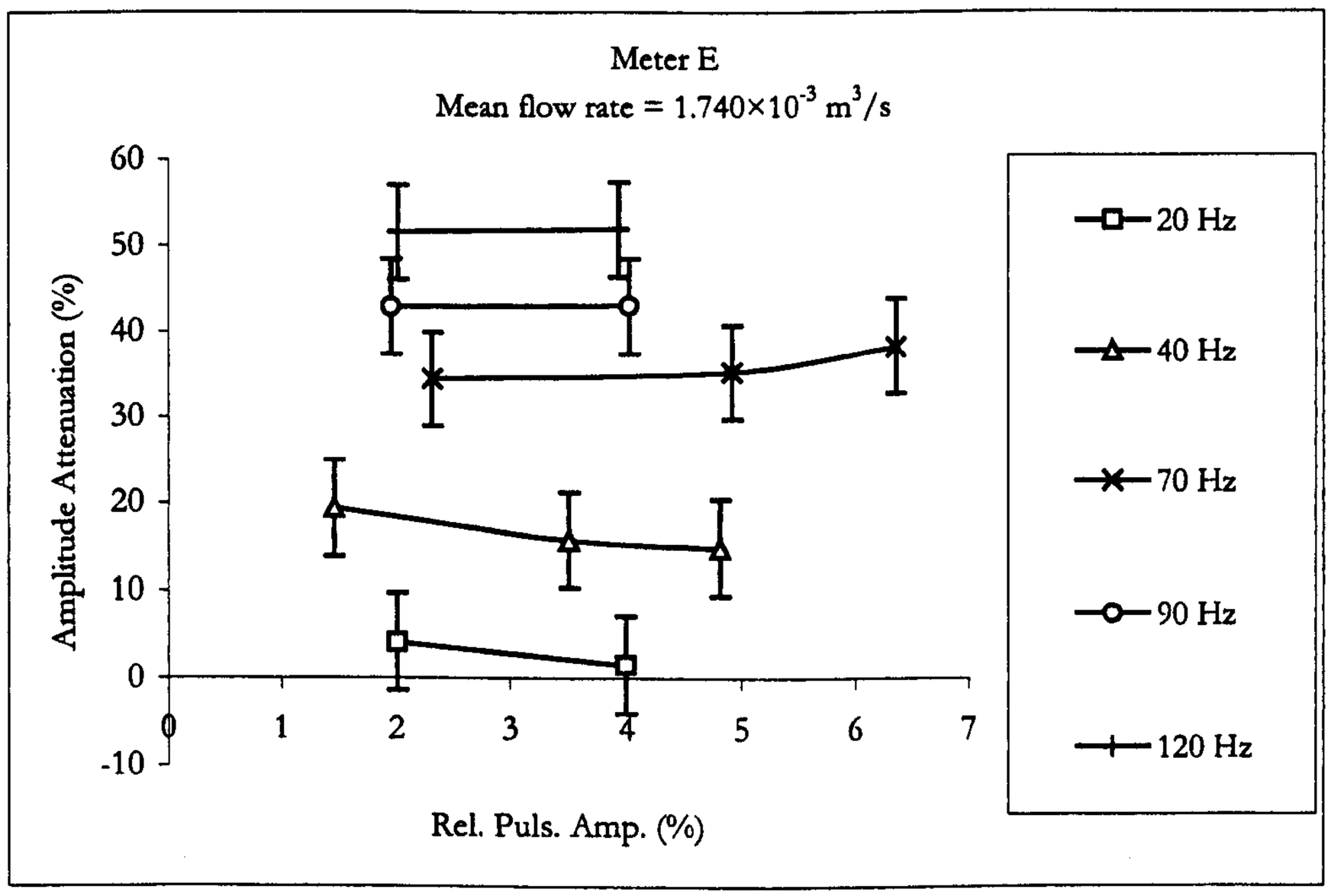

Figure 6. 46 Meter E — Amplitude attenuations with differing pulsation amplitudes and pulsation frequencies

It can be seen from the above figures that the errors in pulsation amplitude are generally much larger than over-registration errors. Except for meter A, the majority of amplitude

attenuations for all meters, are qualitatively very similar — the amplitude attenuation increased significantly with increasing pulsation frequency but attenuation was nominally independent of relative pulsation amplitude. As an example of the effects, for meter B, at 20 Hz pulsation frequency, the imposed relative pulsation amplitude ranged from 17% to 40%, the observed amplitude attenuations were between 22% and 23%. For the same meter, at 40 Hz pulsation frequency and the same range of imposed pulsations, the amplitude attenuations were between 43% and 44%. Graphical representations of these effects on meter B at 20 Hz and 40 Hz pulsation with 40% imposed pulsation amplitude are shown in Figures 6. 22 and 6. 23 respectively.

It is not apparent why there is a different trend observed for meter A (Figure 6. 42), this may be due to the abrupt contraction of flow at the meter inlet (as mentioned in Ch. 6.2.1). In which eddies generated between the vena contracta and the wall of the meter body immediately after the inlet (Massey 1998) may have disturbed the inlet flow profile, and when the flow characteristic is pulsatile, this may affect the meter response.

The majority of amplitude attenuations observed in each meter were higher than 10% for pulsation frequency above 10 Hz, and the maximum amplitude attenuation observed was 90% (as shown in Figures 6. 29 and 6. 45).

Again for meter D, the amplitude attenuations were examined at three different operating flow rates within its linear range (which was determined under steady flow conditions): 0.143×10^{-3} m^3/s, 0.191×10^{-3} m^3/s and 0.291×10^{-3} m^3/s. Figures 6 47, 6. 48 and 6. 49 show the amplitude attenuations of these tests at pulsation frequencies of 10 Hz, 20 Hz and 40 Hz respectively. At three different flow rates, the typical amplitude attenuation trend was observed for all pulsation frequencies. However, it can be seen that the amplitude attenuations at the tested frequencies are generally higher at the lowest flow rate, for example, in Figure 6. 49, at 40 Hz with 40% imposed relative pulsation amplitude, the amplitude attenuations were from 22% at the highest flow rate to 46% at the lowest flow rate.

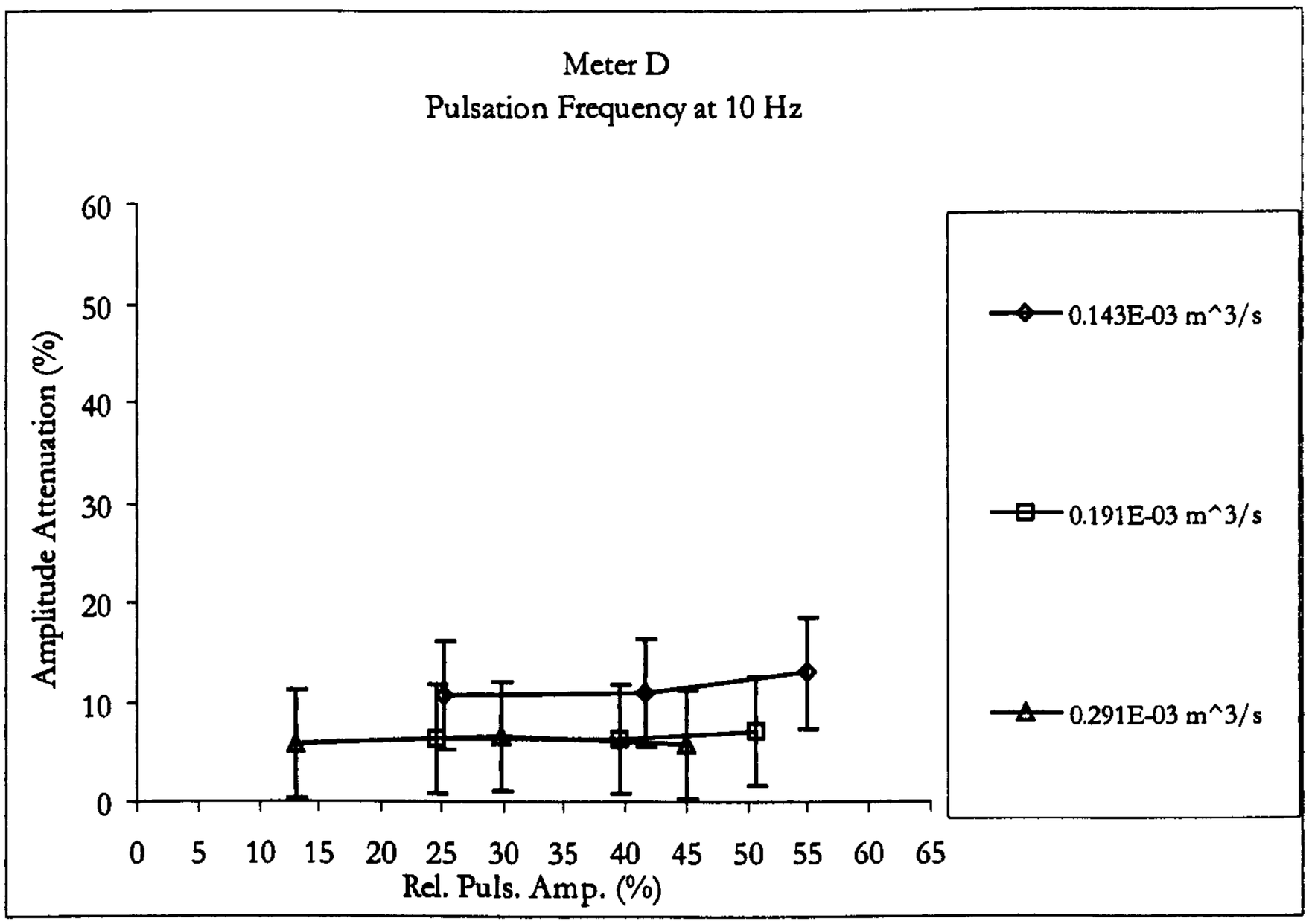

Figure 6. 47 Meter D — Amplitude attenuations with differing pulsation amplitudes and flow rates at 10 Hz pulsation frequency

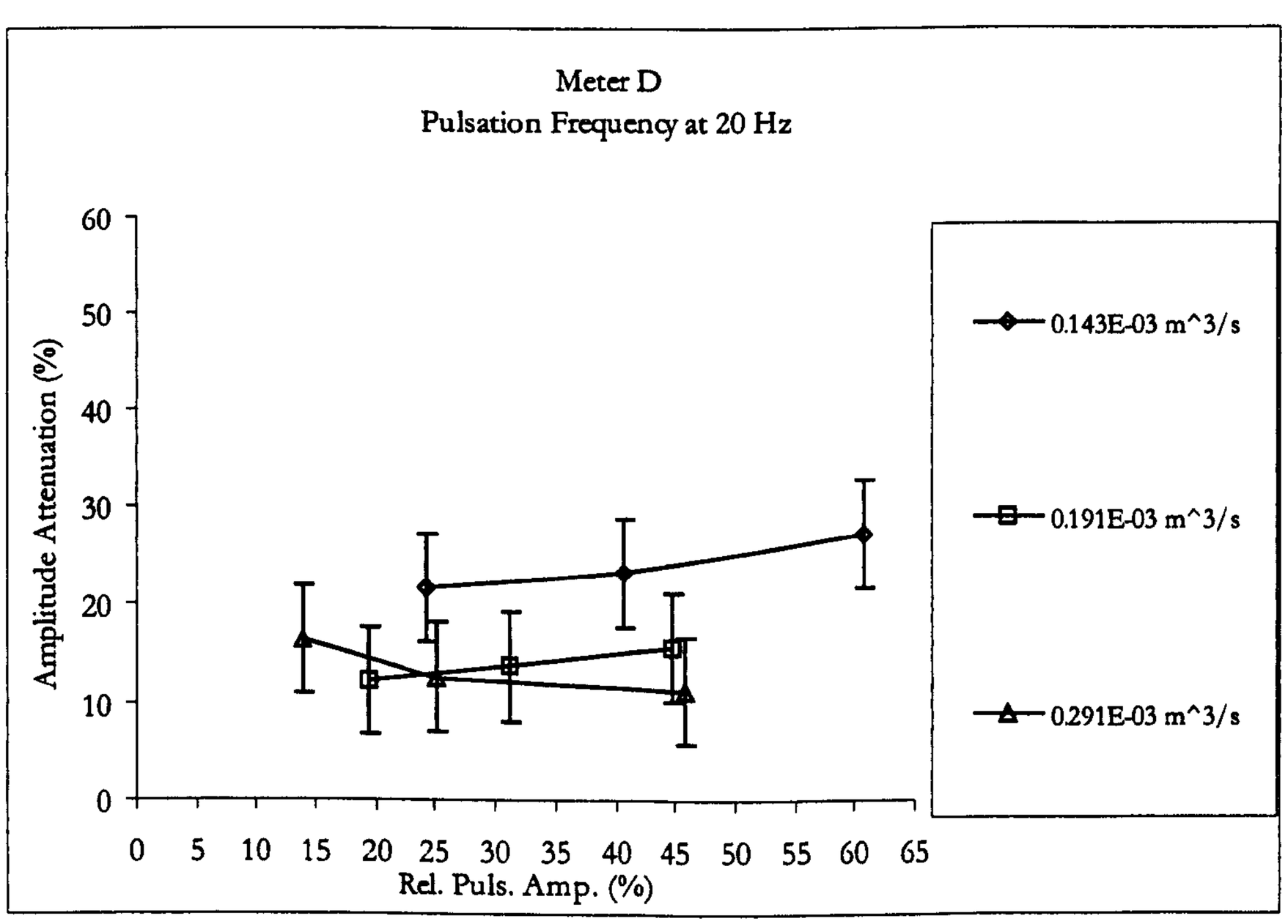

Figure 6. 48 Meter D — Amplitude attenuations with differing pulsation amplitudes and flow rates at 20 Hz pulsation frequency

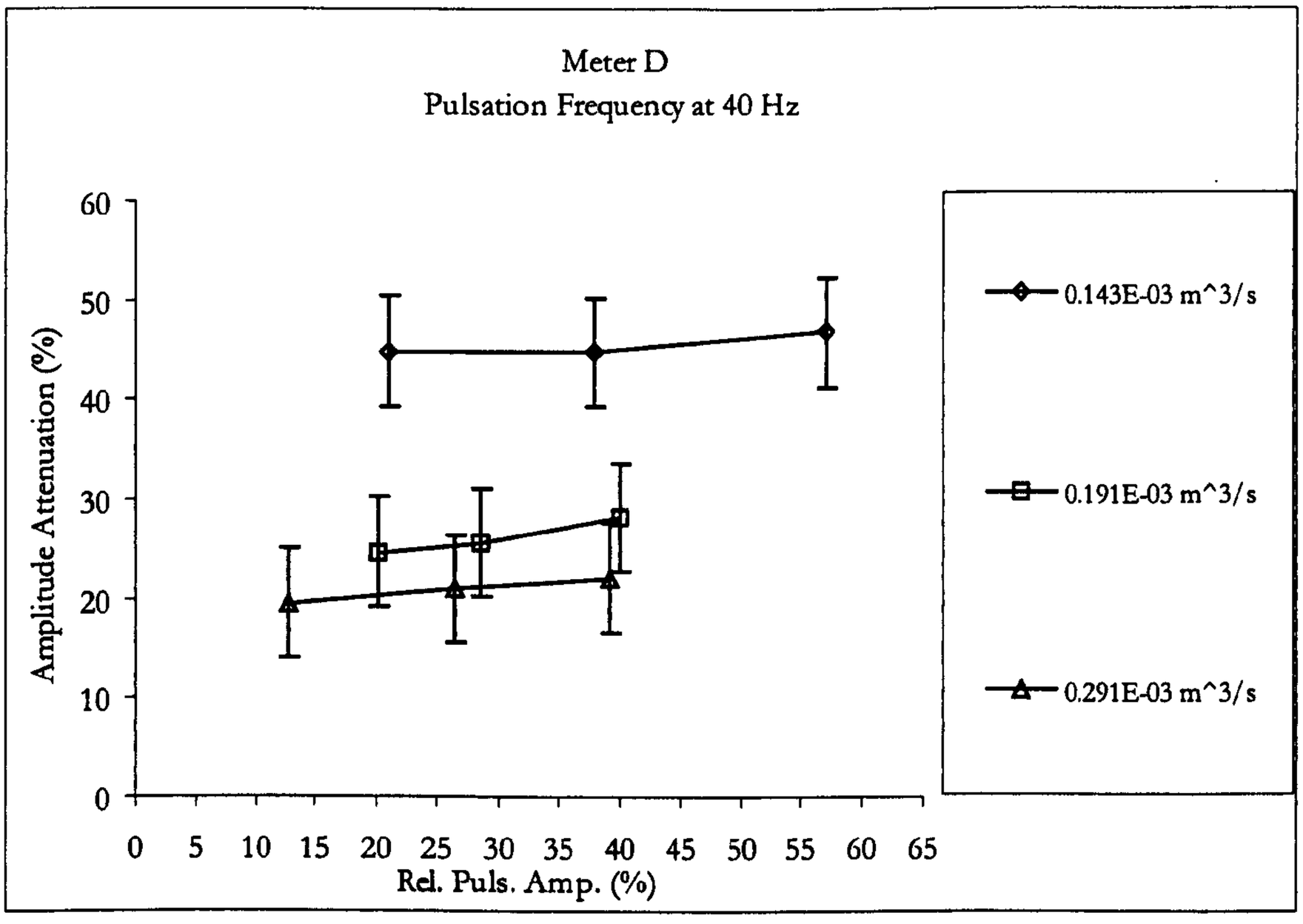

Figure 6. 49 Meter D — Amplitude attenuations with differing pulsation amplitudes and flow rates at 40 Hz pulsation frequency

6.5.2.2 Against various pulsation frequency

From the previous section, it is observed that the amplitude attenuations for all tested meters, except for meter A, have strong dependency on pulsation frequencies, but not on relative pulsation amplitudes.

Therefore it is useful to re-plot the results in a different manner; instead of plotting amplitude attenuation against relative pulsation amplitude, this section shows the results of amplitude attenuation against pulsation frequency. The error bars are excluded as they may overlap each other.

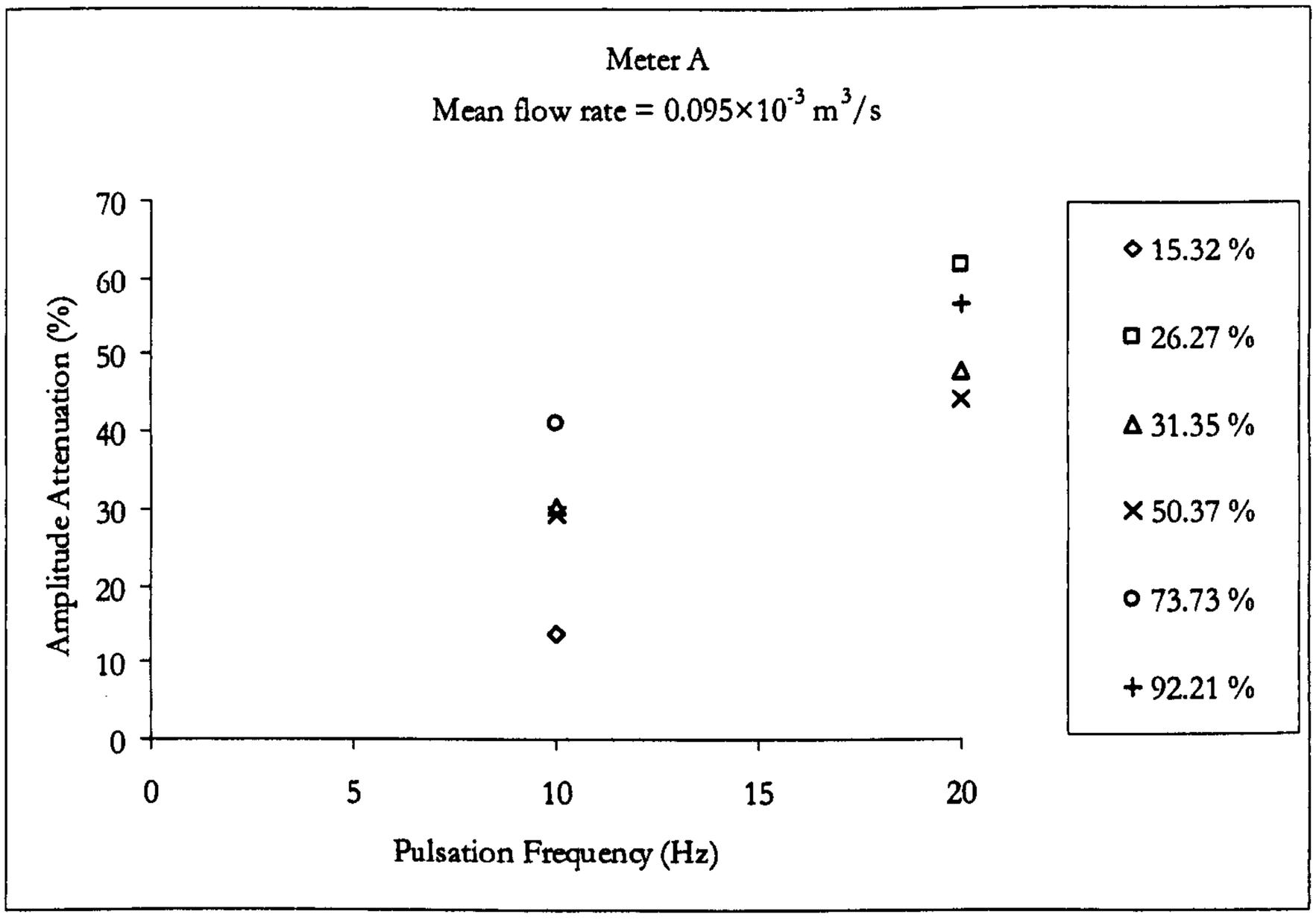

Figure 6. 50 Meter A — Amplitude attenuations with differing pulsation frequencies and pulsation amplitudes (re-plotted for results shown in Figure 6. 42)

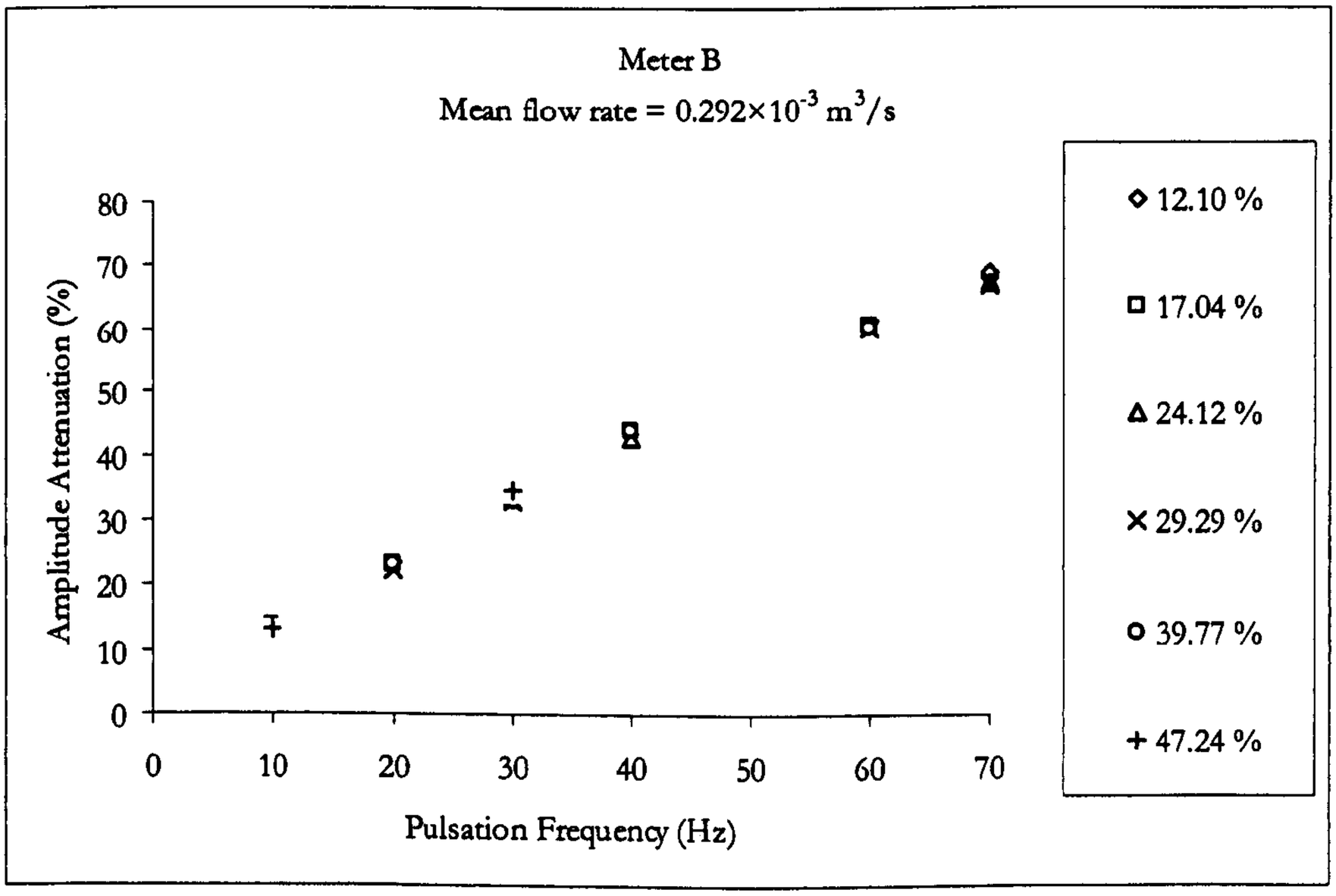

Figure 6. 51 Meter B — Amplitude attenuations with differing pulsation frequencies and pulsation amplitudes (re-plotted for results shown in Figure 6. 43)

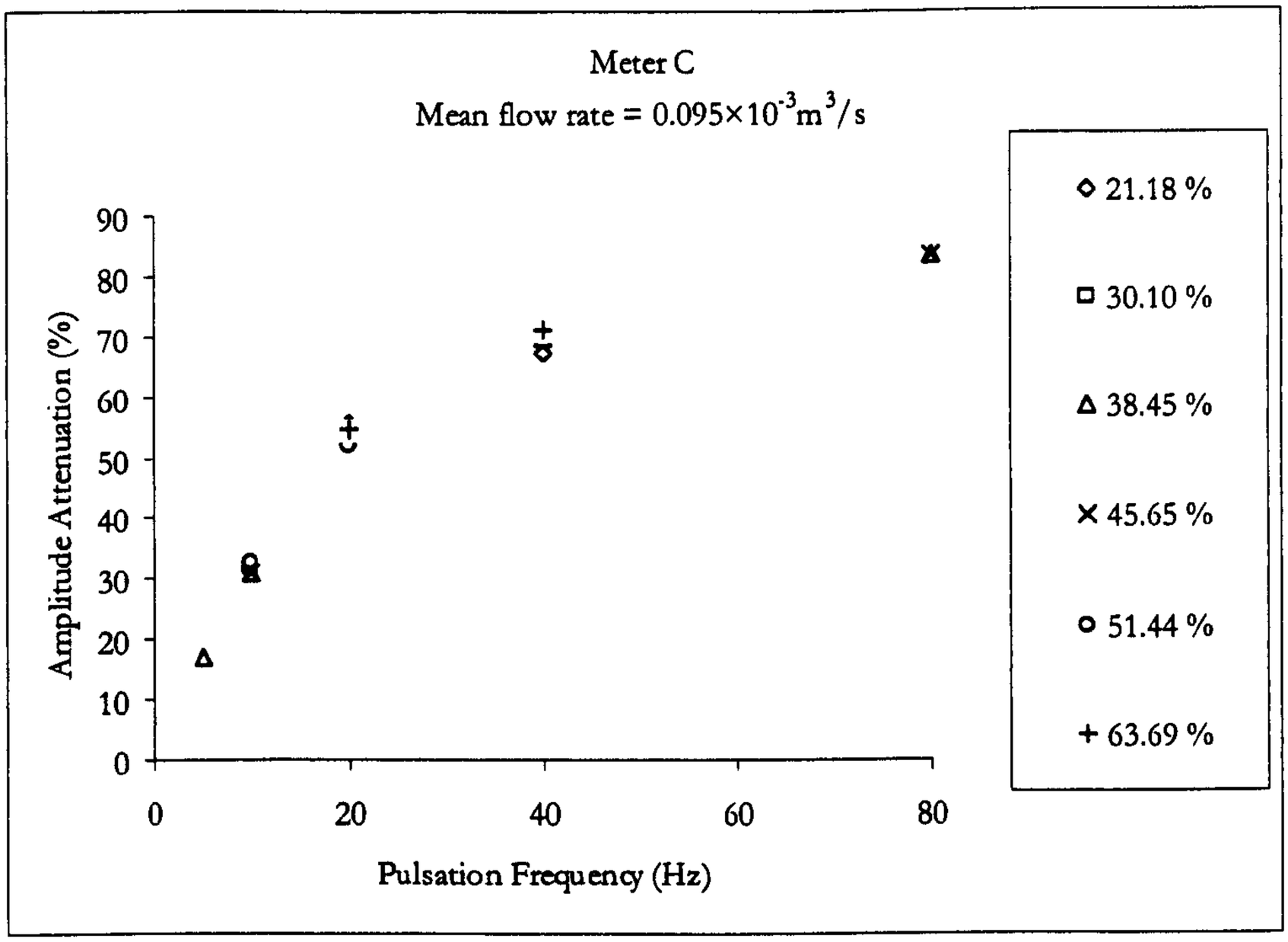

Figure 6. 52 Meter C — Amplitude attenuations with differing pulsation frequencies and pulsation amplitudes (re-plotted for results shown in Figure 6. 44)

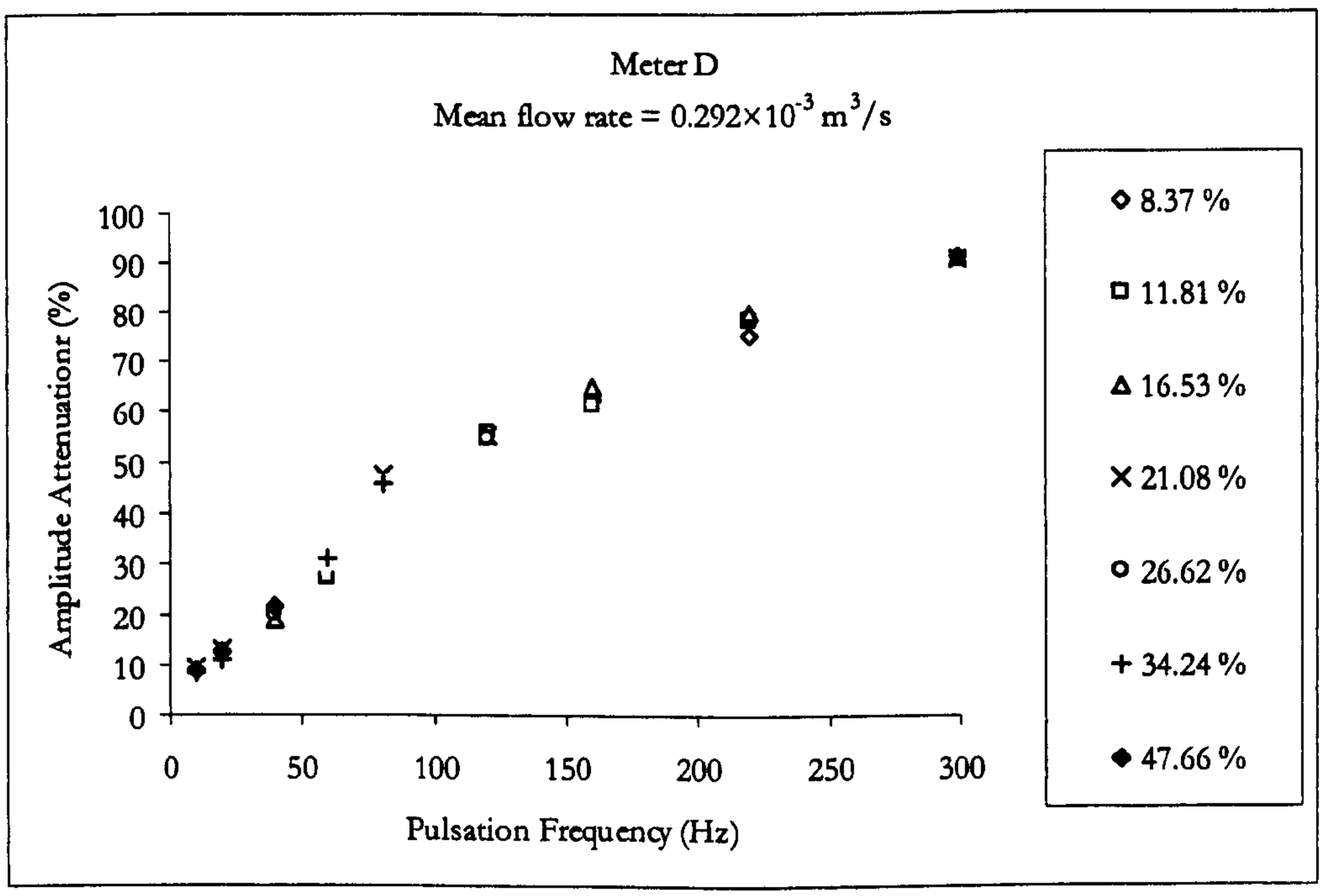

Figure 6. 53 Meter D — Amplitude attenuations with differing pulsation frequencies and pulsation amplitudes (re-plotted for results shown in Figure 6. 45)

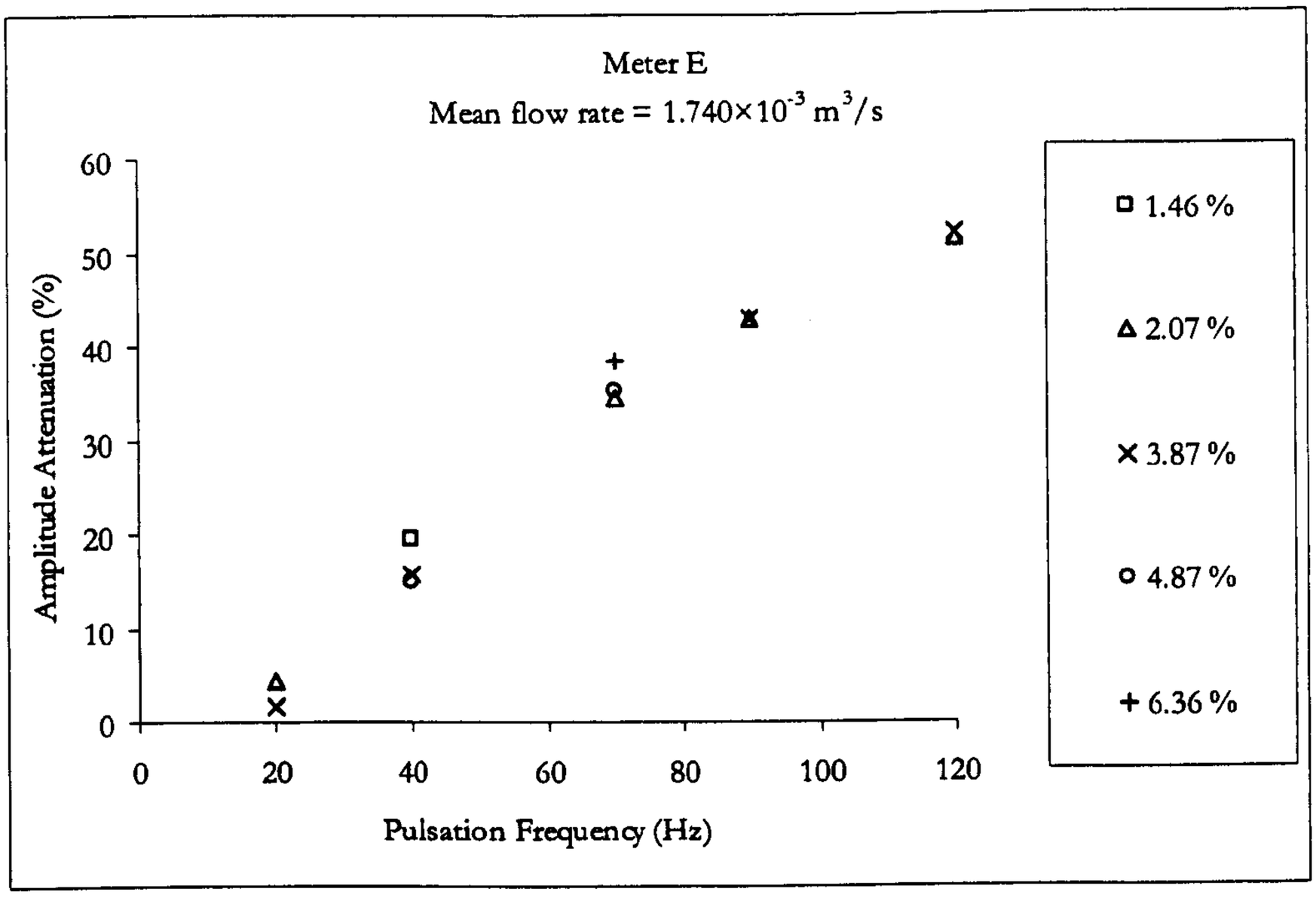

Figure 6. 54 Meter E — Amplitude attenuations with differing pulsation frequencies and pulsation amplitudes (re-plotted for results shown in Figure 6. 46)

6.5.2.3 Comparison of amplitude attenuation between meters at "standard" pulsation cases

Apart from meter A, all amplitude attenuation trends are qualitatively similar; it can be seen more clearly now that the increase of amplitude attenuation is strongly dependent on the increase of pulsation frequency, but not significantly dependent on the increase of relative pulsation amplitude, as predicted in Ch. 5.2.5. However, there are different scopes of dependency observed when the trends are compared with each other. To make this comparison more apparent, the trends of all meters have to be plotted on the same scale. Consequently, individual meter error plot has to be represented by using the arithmetic average meter error value for all pulsation amplitudes at each frequency. Figure 6. 55 shows the various meter error trends achieved by using this method.

It can be seen that there are some meters which can give better indication of pulsation amplitude than others, such as at 20 Hz, meter E is better able to follow the actual pulsation amplitude than others, and the ascending order of amplitude attenuation can be ranked from E, D, B, A and C.

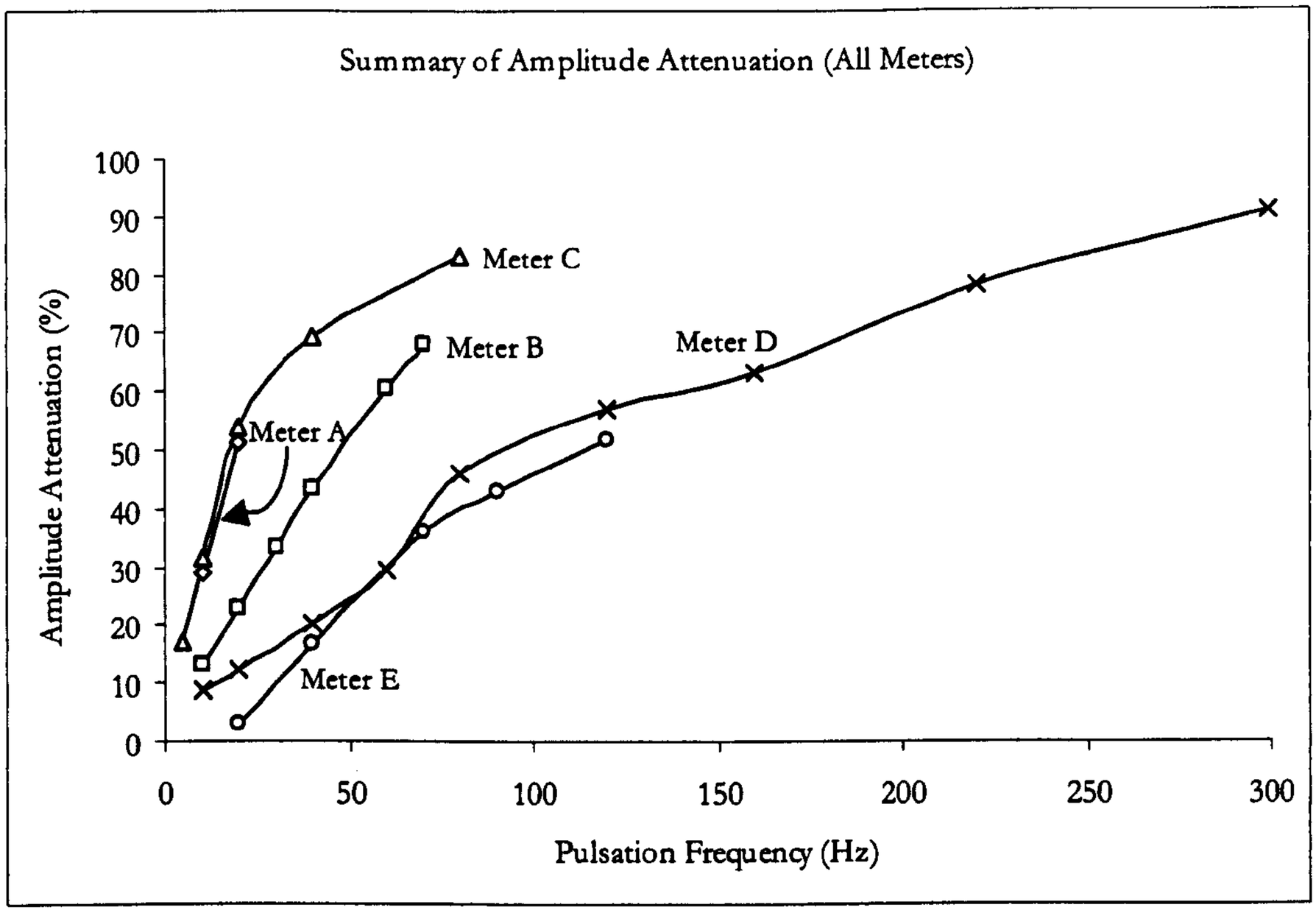

Figure 6. 55 A comparison of amplitude attenuation for all meters

Again, a summary of factors considered to be influential on meter results is given below:

Rank (20Hz)	Meter	Nominal Size (mm)	Blade no.	r_b/r_t ratio	$b = \frac{I_R}{\rho \bar{r}}$ ($\times 10^{-7}$ m^3)	$\lambda = I_f/I_R$	$b(1+\lambda)$ ($\times 10^{-7}$ m^3)	Mean flow rate ($\times 10^{-3}$ m^3/s)	Ratio of lowest linear flow rate to mean flow rate
Good	E	25	5	0.33	34.18	1.989	102.16	1.740	1 : 4.0
↑	D	12	6	0.5	4.855	0.703	8.27	0.292	1 : 7.3
↑	B	12	3	0.4	5.123	3.434	22.72	0.292	1 : 2.1
↑	A	6	3	0.4	2.850	1.862	8.16	0.095	1 : 3.8
Bad	C	12	5	0.67	4.474	1.300	10.29	0.095	1 : 6.3

Table 6. 5 A summary of factors affecting meter indication of pulsation amplitude for pulsation frequency at 20 Hz (based on comparison made in Figure 6. 55)

6.5.3 Summary of discussion

- In Tables 6. 3 and 6. 4, meter B is found to be the most affected meter on indicating the true mean flow when it is subjected to pulsating flow from the investigated cases (with 40% imposed relative pulsation amplitude at 20 and 40 Hz). However, in terms of amplitude attenuation, meter C is most affected for pulsation frequency below 20Hz (Table 6. 5).

- If the meters are rated in groups by different mean flow rate, for pulsation tests at 20 Hz with 40% relative pulsation amplitude, Figures 6. 40 and 6. 55 show that meter D is more responsive than meter B, similarly, meter A is better than meter C. Then the only factor that correlates with this observation is the value of $[b(1+\lambda)]_X$†, in which $[b(1+\lambda)]_D < [b(1+\lambda)]_B$ and $[b(1+\lambda)]_A < [b(1+\lambda)]_C$ (see Table 6. 3). Hence under the same flow condition, according to experimental observation, a meter with smaller value of $b(1+\lambda)$ gives better indication of the true flow than one with a larger value. This observation reflects what is expected from theory, as shown in Eq. 4. 18a, $\left[t_c = b(1+\lambda)/(\dot{V}_a - \Delta\dot{V}_a)\right]$, for the same value of $\dot{V}_a - \Delta\dot{V}_a$, and since $[b(1+\lambda)]_D < [b(1+\lambda)]_B$, the time constant of meter D would be smaller than meter B, hence rotor D takes less time than rotor B to response to change in flow. Similarly, the time constant of meter A would be smaller than meter C, since $[b(1+\lambda)]_A < [b(1+\lambda)]_C$.

- However, theoretical model predicted that meter B would be more responsive than meter D, contradicting the observation made from experimental results. As stated in Ch. 5.2.5, the theoretical model is based on the assumptions that the flow is perfectly guided between blades where no separation of flow is allowed, the rotor is frictionless and there is a purely sinusoidal pulsation. All of these assumptions would not exist in a real situation; hence this could be the reason that the results from theoretical predictions did not correlate with experimental results. More comparisons between these two results will be made in Section 7.1.

---

† $[b(1+\lambda)]_X$ is the specific value of $b(1+\lambda)$ for meter X.

6.5.4 Conclusions

New data have been obtained, which demonstrate the occurrence of over-registration and amplitude attenuation when a small turbine flowmeter is subjected to a pulsation liquid flow. Although the over-registration errors are within the limits of specified meter accuracy for low frequency pulsations, they may be significant for higher frequencies and larger pulsation amplitudes. The amplitude attenuation error is likely to be significant over a considerable range of amplitudes and frequencies and can be as large as 90%. Also the typical trends in over-registrations and amplitude attenuations remain unchanged with varying operating flow rates within the linear range.

For the pulsation cases investigated, the experimental data also demonstrate that a meter with a smaller value of $[b(1+\lambda)]$ would be more responsive to pulsating flow condition under the same mean flow rate.

The next chapter reviews the possible correction procedures investigated in order to rectify metering errors under pulsating liquid flow.

Chapter 7 Comparison of Experimental Results with Theoretical Results and Correction of Meter Reading

In this chapter, a comparison will be made for the meter dynamic response resulting from experimentation and from theoretical modelling (Section 5.2). Then, a technique for dealing with the correction of turbine meter readings will be given. This work resulted in the development of a correction model, and the resulting corrected data are then compared with experimental measurements.

7.1 Comparison of Experimental Results with Theoretical Results

Results based upon the theoretical model given by Eq. 5. 1 were used to predict the dynamic response for Meter B and Meter D (Section 5.2). A comparison of the experimental data with those produced from this model will allow evaluation of the applicability of this model.

7.1.1 Comparison of over-registration error

For Meter B, the correlation between theoretical results and experimental data is quite poor; apart from the 10 Hz pulsation case, the theoretical data tend to under-estimate the over-registration errors. For example, as shown in Figure 6. 33, the largest over-registration observed from experimental results is around 4% at a pulsation frequency of 60 Hz, 37% imposed relative pulsation amplitude. However from Figure 5. 1, it can be seen that the over-registration predicted under the same pulsating condition is less than 1.5%, this represents a discrepancy of 63% as compared to the experimental *OR* of 4%. For all of the cases compared, with the exception of the 10 Hz pulsation, the largest discrepancy between theoretical and experimental data is 71%. Graphical comparison of these errors are presented in Section 8.4.3., Figs 8.25 a and 8.25 c.

For Meter D, however, there is a better correlation between the theoretical data and experimental data except for pulsations at 10 Hz and 299 Hz. As shown in Figure 6. 35,

the largest over-registration observed from experimental results is around 2.2% at pulsation frequency of 120 Hz, with a 27% imposed relative pulsation amplitude. From Figure 5. 2, it can be seen that theoretically the over-registration predicted under the same pulsating condition is approximately 1.8%, hence the discrepancy is around 20%. The majority of the discrepancies between the two sets of data are around 20%.

7.1.2 Comparison of amplitude attenuation

For Meter B, at 70 Hz pulsation frequency, experimental data (in Figure 6. 41) show that the amplitude attenuations are around 68%; however, for the same f_p, the theoretical data (in Figure 5. 3) show that the attenuations are around 21%. The majority of the discrepancies are in the range of 50% to 70% between these data. Graphical comparison of these errors are presented in Section 8.4.3., Figs 8.26 a and 8.26 c.

Better correlation between experimental and theoretical data is found for Meter D. For instance, at 299 Hz pulsation frequency, the experimental amplitude attenuations (Figure 6. 43) observed are around 90%, whilst the theoretical ones are around 55% for the same f_p. Except for the 10 Hz pulsation frequency, the majority of the discrepancies between these data are in the range of 10% to 40%.

7.1.3 Summary of the comparisons

As mentioned in Section 5.2.1, the model used was based on the assumptions that the rotor is "frictionless", and the flow is perfectly guided between rotor blades. Then, due to the lower number of blades for Meter B, the predictions made for this meter would be expected to be less accurate than the results predicted for Meter D (6-bladed). This hypothesis is supported by the poorer correlation between experimental and theoretical data for Meter B than for Meter D.

Furthermore, as stated in Section 5.2.5, it was assumed that only the fluid contained within the envelope of the meter rotor contributes to I_f, hence the ratio of inertias (λ) calculated for Meter B was five times higher than for Meter D. This is because Meter B has a substantially larger annular space between the rotor body and casing than for Meter D (as

shown in Figure 6. 1). Hence, for this reason, Meter B was predicted to have a better response than Meter D for the same pulsating condition. However, experimental data showed that Meter D actually has a better response than Meter B. For example, the 60 Hz pulsation frequency, at around 35% imposed relative pulsation amplitude, predictions of over-registration error for Meter B and Meter D were 4% and 2% respectively; at the same imposed pulsation, the amplitude attenuations predicted for Meter B and Meter D are 60% and 30% respectively.

The above two observations implied that the values of λ or B that were used for Meter B were possibly too large in the theoretical model and hence the treatment of fluid contained within the rotor envelope as a "solid body" (see Section 5.2.2.) for Meter B was incorrect.

For a real meter, flow must separate off the blade surfaces due to boundary layer effects associated with misalignment with the blade angle, hence, there is a need to determine the appropriate values of b and λ for Meter B by an independent and experimental means based on step response tests.

The following section gives a brief description of the step response tests for Meter B and the results from these tests will be discussed.

7.2 Step Response Tests for Meter B

In Section 4.1.2, it was noted that following the work published by Dijstelbergen (1966), Cheesewright and Clark (1997) modified the "frictionless" liquid equation to produce a formal mathematical solution (Eq. 4. 17):

$$\dot{V}_m = \dot{V}_a - H(t)\Delta\dot{V}_a\left\{1-\exp\left[-\frac{\dot{V}_a-\Delta\dot{V}_a}{b}\left(\frac{I_R}{I_R+I_f}\right)t\right]\right\}$$

where $H(t)$ is a unit step function at t = 0. By using the above equation, a numerical value of the time constant can be obtained by plotting $\ln\left[\left(\dot{V}_m-\dot{V}_a\right)/\Delta\dot{V}_a\right]$ against t. The quantity $b\left(1+I_f/I_R\right)$ could then be obtained from the slope since $\dot{V}_a-\Delta\dot{V}_a$ (the steady velocity after the step) is known. Since instantaneous changes cannot occur, the above equation can only be considered to be a mathematical solution rather than a practical solution, as in a real device, the flow must separate off the blade (as mentioned in Section 4.1.2).

However, despite the uncertainty in the possible solution, it was decided to perform a step response test to attempt to find a better estimate of $b\left(1+I_f/I_R\right)$ for Meter B. The step response test method described in Cheesewright and Clark (1997) was used in this study and a description of the method, which was extracted from Cheesewright and Clark (1997), is shown in Appendix B. The same data acquisition programs built in Labview, as described in Section 6.1.3, were used here for obtaining turbine meter raw data; and the same data processing technique (described in Section 6.3) was used to process the subsequent meter data.

7.2.1 Step response test results

A total of 15 step tests were carried out on this meter. All the tests showed a qualitatively similar response to the step and Figure 7. 2 shows the variation of flow with time obtained from the meter output signal (in Figure 7. 1) for a typical step change in flow. It can be seen that the scarceness of the data points presented some difficulties in characterising the time-course of the change in the flow. This is mainly due to the fact that the significant changes in turbine speed, following a step change in the flow, took place within only two to three blade passings of the turbine rotor, as depicted from Figure 7. 2 that the time scale of step change was between 5.815 s to 5.83 s, it showed that the step took place just within

one revolution (Figure 7.1) since the rotor of Meter B is 3-bladed . It is also noted that the initial part of the step shows a rather different feature to the exponential one predicted by theory. The probable physical explanation of this effect is that at the moment after the initial "step change", the turbine rotor and a body of fluid enclosed within the rotor envelope may still be rotating in the speed just before the step, with the associated "disc friction" effect (Cheesewright and Clark 1997). Despite these limitations, an attempt to match the second part of the experimental step response curve to an exponential feature was made and the best-fit exponential curve was drawn as shown in Figure 7. 3.

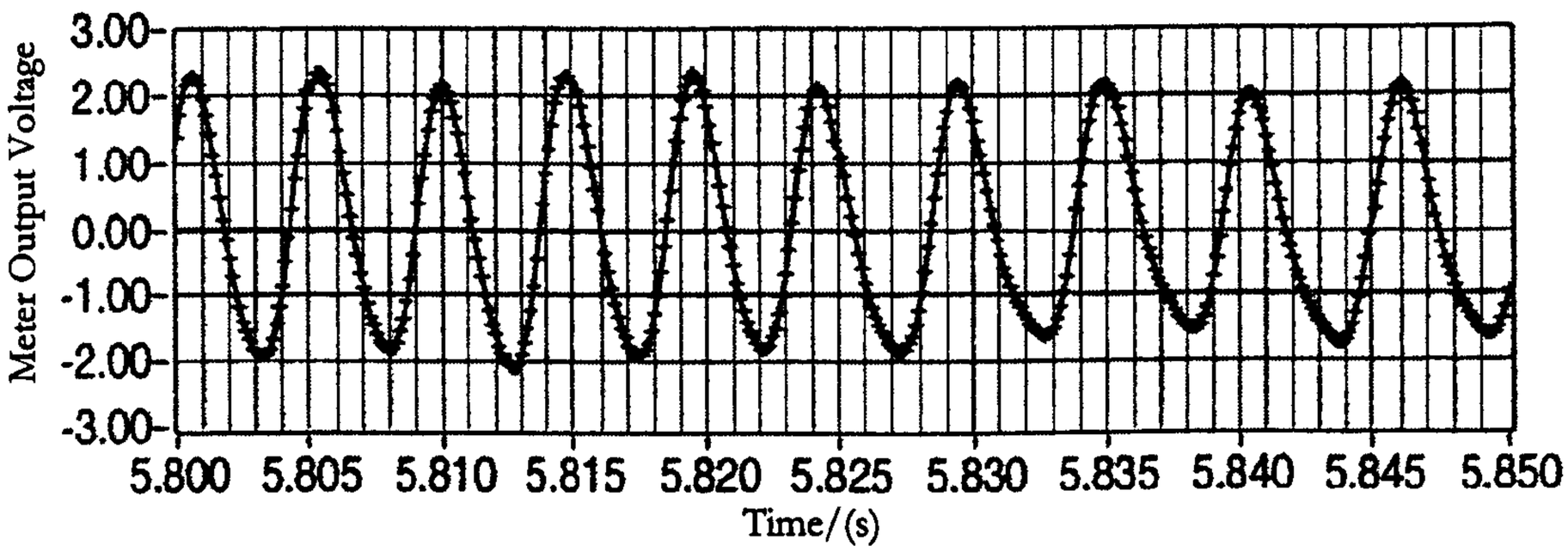

Figure 7. 1 Digitised turbine meter output signal during a step

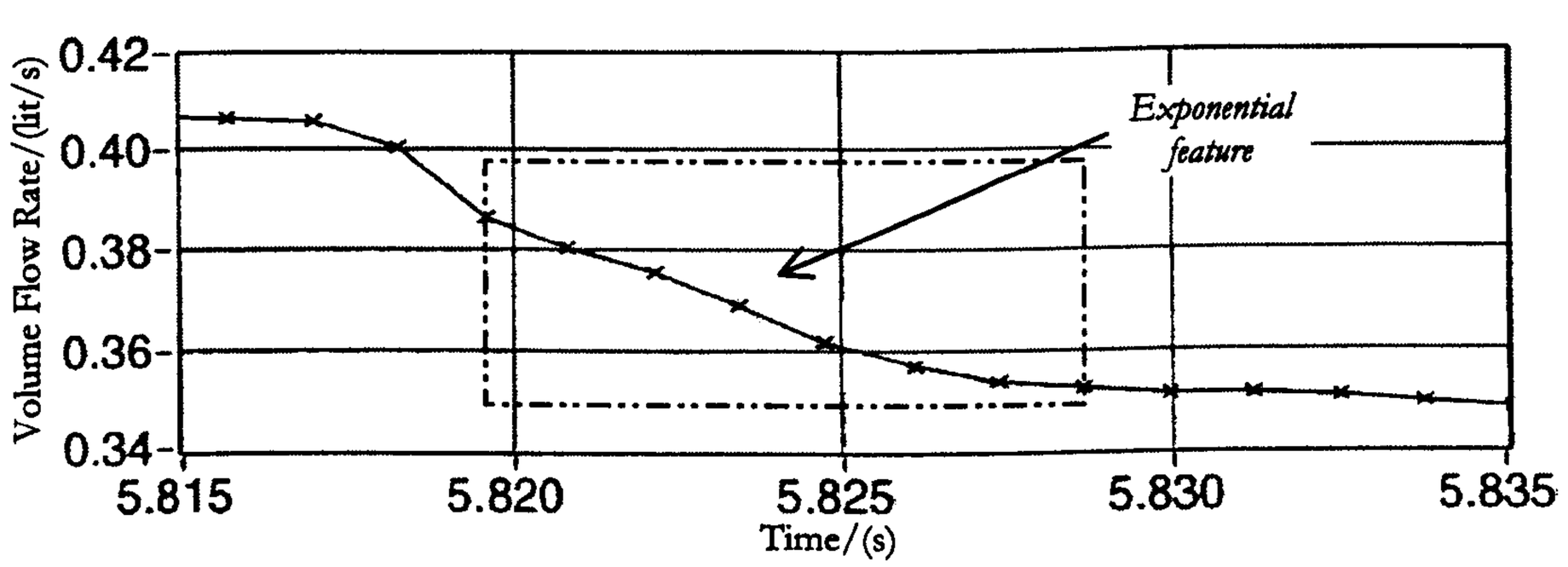

Figure 7. 2 Flow waveform showing the meter response to the step, processed from meter output signal shown in Figure 7. 1

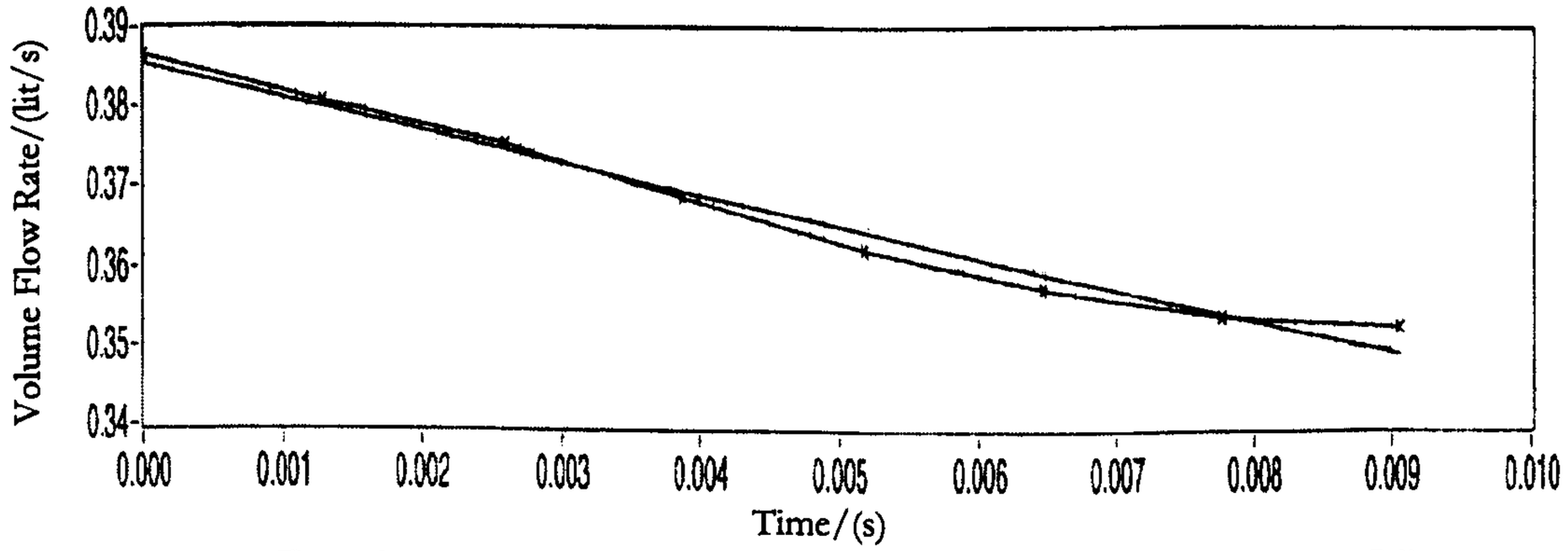

Figure 7. 3 Experimental response to a step change compared to a "best-fit" exponential change for meter flow waveform shown in Figure 7. 2

From the best-fit curve shown in Figure 7. 3, the quantity of $b(1+I_f/I_R)$ was found by using Eq. 4. 17. As shown in Table 7. 1, repeat tests under similar conditions suggested that the average value of the quantity $b(1+I_f/I_R)$, was 2.64×10^{-6} m^3 with an uncertainty of ±15 % (99 % confidence limits). Within this uncertainty, the tests did not show any difference between a step up and step down, neither did they show any change with flow rate (over a 2:1 range). (Note that all the above discussion is in terms of the response parameter $b(1+I_f/I_R)$, rather than the time constant, because the former is a function of the meter geometry and the fluid, while the latter also depends on the flow rate).

Test No.	Test Condition		$b(1+I_f/I_R)$ ($\times10^{-6}$ m^3)
	Flow rate before Step ($\times10^{-3}$ m^3/s)	Flow rate after Step ($\times10^{-3}$ m^3/s)	
1	0.325	0.390	1.96
2	0.325	0.390	2.87
3	0.325	0.390	2.70
4	0.440	0.490	2.93
5	0.420	0.480	2.46
6	0.420	0.480	2.09
7	0.410	0.350	3.44
8	0.400	0.350	2.35
9	0.395	0.340	2.99
10	0.495	0.440	2.70
11	0.490	0.430	2.04
12	0.490	0.440	2.63
13	0.485	0.250	3.64
14	0.485	0.250	1.90
15	0.485	0.250	2.94
		Average $b(1+I_f/I_R)$ = 2.64	

Table 7. 1 **Results of step response tests**

Having obtained an average value of $b(1+I_f/I_R)$ from experimental results, if the value of b is known, than a better estimation of λ (= I_f/I_R) could be obtained. To a first approximation, an estimate for $b(=I_R/\rho\bar{r}^2)$ from the rotor geometry by using Solidworks (as shown in Table 5. 1 Section 5.2.1) is 5.123×10^{-7} m^3. An alternative way to find for the true value of b would be running step flow tests on this meter with air, however, the accuracy of the result would be substantially reduced by the forces on the turbine, due to the electromagnetic pick-up (Cheesewright and Clark 1996). In view of the level of uncertainties already implicated from the water flow step tests, air flow step tests were not considered for this meter. Hence, within the limitation of this work, the best estimate for b is the value obtained from the rotor geometry (5.123×10^{-7} m^3).

Using this value, the experimental value of λ was then found to be around 4.16. This value is comparable to the one obtained from Solidworks (=3.434), as shown in Table 5. 1 (Section 5.2.1).

7.2.2 Step response test summary

Comparisons made between the experimental and theoretical results in Section 7.1.3 concluded that geometrical values of b and λ obtained from Solidworks for this meter might be too large. It was expected therefore that the results of the step response tests would give a smaller value of λ; however, the experimental value of λ was approximately 20% larger than the one obtained from the geometry. The sparseness of the data points was the main limitation in providing a better determination of the true values of b and λ. Therefore, it was decided to continue with the "Solidworks" values of b and λ for this meter, for the subsequent modelling work.

7.3 Correction of Meter Reading

In the theoretical modelling presented in Section 5.2, the meter indicated flow ($\dot{V}_m$) was predicted from the time dependent true flow ($\dot{V}_a$) by using the "frictionless" liquid equation" (Eq. 4. 16);

$$b(1+\lambda)\frac{d\dot{V}_m}{dt} + \dot{V}_m\dot{V}_a = \dot{V}_a^{\,2} + b\lambda\frac{d\dot{V}_a}{dt}$$

In spite of the poor theoretical predictions for Meter B, the theoretical prediction for Meter D was reasonably acceptable; hence Cheesewright devised a method of attempting to correct the turbine meter reading using Eq. 4. 16. The alternative viewpoint was to try to predict the true flow ($\dot{V}_a$) (using the same equation) from the meter indicated flow ($\dot{V}_m$); hence the term "correction of meter reading". The following two sections review the procedures (Cheesewright 2001) required for these corrections.

7.3.1 Correcting the effect of averaging Δt

Before applying Eq. 4. 16 for the correction to allow prediction of the true flow, it is relevant to recall (from Section 6.2) that the "4 points per signal cycle" turbine meter output signal was not equally spaced in time and the signal needed to be re-sampled in order to obtain equal time intervals between each data point; this involved the averaging of Δt for each signal cycle of $\dot{V}_m(t)$. Within this procedure, the slope of $\dot{V}_m$ would be disrupted, hence a correction of this effect has to be made before $\dot{V}_a$ can be estimated from the logged data, time series of $\dot{V}_m$.

If the time series of $\dot{V}_m$ is written as,

$$\dot{V}_m(t) = \overline{\dot{V}_m}(1+\alpha\sin 2\pi f_p t) = \overline{\dot{V}_m} + \overline{\dot{V}_m}\alpha\sin 2\pi f_p t \qquad \textbf{Eq. 7. 1}$$

And the averaged value of $\dot{V}_m(t)$ over a data sampling interval δt as:

$$[\dot{V}_m]_{ave.}(t) = \frac{1}{\delta t}\int_{t-\frac{\delta t}{2}}^{t+\frac{\delta t}{2}} \overline{\dot{V}_m}\left(1+\alpha\sin 2\pi f_p t\right).dt \qquad \text{Eq. 7. 2}$$

$$= \frac{\overline{\dot{V}_m}}{\delta t}\int_{t-\frac{\delta t}{2}}^{t+\frac{\delta t}{2}}\left(1+\alpha\sin 2\pi f_p t\right).dt$$

$$= \frac{\overline{\dot{V}_m}}{\delta t}\left\{[t]_{t-\frac{\delta t}{2}}^{t+\frac{\delta t}{2}} + \alpha\int_{t-\frac{\delta t}{2}}^{t+\frac{\delta t}{2}}\sin 2\pi f_p t.dt\right\}$$

$$= \frac{\overline{\dot{V}_m}}{\delta t}\left\{\delta t + \alpha\int_{t-\frac{\delta t}{2}}^{t+\frac{\delta t}{2}}\sin 2\pi f_p t.dt\right\}$$

$$= \overline{\dot{V}_m}\left\{1+\frac{\alpha}{\delta t}\left[-\frac{1}{2\pi f_p}\cos 2\pi f_p t\right]_{t-\frac{\delta t}{2}}^{t+\frac{\delta t}{2}}\right\}$$

Hence, Eq. 7.2 can be written as:

$$[\dot{V}_m]_{ave.}(t) = \overline{\dot{V}_m}\left\{1-\frac{\alpha}{2\pi f_p \delta t}\left[\cos 2\pi f_p t\right]_{t-\frac{\delta t}{2}}^{t+\frac{\delta t}{2}}\right\} \qquad \text{Eq. 7. 3}$$

The cosine function term on the R.H.S in the above equation can be expressed as:

$$\left[\cos 2\pi f_p t\right]_{t-\frac{\delta t}{2}}^{t+\frac{\delta t}{2}} = \left\{\cos\left[2\pi f_p\left(t+\frac{\delta t}{2}\right)\right] - \cos\left[2\pi f_p\left(t-\frac{\delta t}{2}\right)\right]\right\}$$

$$= \left[-2\left(\sin 2\pi f_p t\right)\cdot\left(\sin 2\pi f_p \frac{\delta t}{2}\right)\right]$$

$$= \left[-\left(\sin 2\pi f_p t\right)\cdot\left(\sin \pi f_p \delta t\right)\right] \qquad \text{Eq. 7. 4}$$

Substitute Eq. 7. 4 into Eq. 7. 3:

$$[\dot{V}_m]_{ave.}(t) = \overline{\dot{V}_m}\left\{1+\left[\frac{\alpha}{\pi f_p \delta t}\left(\sin 2\pi f_p t\right)\cdot\left(\sin \pi f_p \delta t\right)\right]\right\}$$

$$= \overline{\dot{V}_m} + \overline{\dot{V}_m}\left[\frac{\alpha}{\pi f_p \delta t}\left(\sin 2\pi f_p t\right)\cdot\left(\sin \pi f_p \delta t\right)\right] \qquad \text{Eq. 7. 5}$$

Hence a ratio can be found for $\frac{\dot{V}_m(t)-\overline{\dot{V}_m}}{[\dot{V}_m]_{ave.}(t)-\overline{\dot{V}_m}}$, and this value can be used to correct for the averaging effect of each meter indicated data point, which yields the following correction factor:

$$\begin{aligned}\frac{\dot{V}_m(t)-\overline{\dot{V}_m}}{[\dot{V}_m]_{ave.}(t)-\overline{\dot{V}_m}} &= \frac{\overline{\dot{V}_m}\left(\alpha\sin 2\pi f_p t\right)}{\overline{\dot{V}_m}\left[\frac{\alpha}{\pi f_p \delta t}\left(\sin 2\pi f_p t\right)\cdot\left(\sin \pi f_p \delta t\right)\right]} \\ &= \frac{\alpha\left(\sin 2\pi f_p t\right)\cdot\left(\pi f_p \delta t\right)}{\alpha\left(\sin 2\pi f_p t\right)\cdot\left(\sin \pi f_p \delta t\right)} \\ &= \frac{\pi f_p \delta t}{\sin \pi f_p \delta t}\end{aligned} \qquad \textbf{Eq. 7. 6}$$

7.3.2 Estimation of $\dot{V}_a$ from $\dot{V}_m$

In Eq. 4. 16, in order to make the notation simpler, replace the following:

1. $x_i,(i=1\rightarrow n)$ as the time series of values of $\dot{V}_a$;
2. $y_i,(i=1\rightarrow n)$ as the time series of values of $\dot{V}_m$; and
3. approximate $\frac{d\dot{V}_a}{dt}$ by $\frac{x_i - x_{(i-1)}}{dt}$.

Now Eq. 4. 16 becomes:

$$x_i^{\,2} - y_i x_i - b(1+\lambda)\frac{dy_i}{dt} + b\lambda\frac{(x_i - x_{i-1})}{dt} = 0 \qquad \textbf{Eq. 7. 7}$$

Where y_i and $\frac{dy_i}{dt}$ can be obtained from the logged data. Therefore if a first value of x_i can be obtained, a forward time marching method can be used to solve for x_i at each step.

In order to obtain the first value of x_i, ideally the last term on the L.H.S. in Eq. 7. 7, $\frac{x_i - x_{(i-1)}}{dt}$, should be equal to zero; yet the logged data does not contain this information due to the pulsating flow condition. However, it is known that $\frac{x_i - x_{(i-1)}}{dt} = 0$ occurs just before $\frac{dy_i}{dt} = 0$. Hence 1 or 2 time steps just before $\frac{dy_i}{dt} = 0$ can be chosen to start the time marching step, taking the first value of $x_i = \frac{y_i}{2}\left(1 + \sqrt{1 + \frac{4b(1+\lambda)}{y_i^2}\frac{dy_i}{dt}}\right)$.

Eq.7. 7 can now be written as

$$x_i^2 - x_i\left(y_i - \frac{b\lambda}{dt}\right) - b(1+\lambda)\frac{dy_i}{dt} - \frac{b\lambda}{dt}x_{i-1} = 0 \qquad \textbf{Eq. 7. 8}$$

The solution for x_i is then given by

$$x_i = \frac{y_i}{2}\left[\left(1 - \frac{b\lambda}{y_i dt}\right) + \sqrt{\left(1 - \frac{b\lambda}{y_i dt}\right)^2 + \frac{4b}{y_i^2}\left((1+\lambda)\frac{dy_i}{dt} + \frac{\lambda x_{i-1}}{dt}\right)}\right] \qquad \textbf{Eq. 7. 9}$$

Where y_i (the time series of values of $\dot{V}_m$) is the logged meter output data; and b and λ are obtained from the Solidworks program using individual meter geometrical values (as shown in Table 5. 1). The above equation can then be programmed as a Labview sub-program and the time series of $\dot{V}_a$ can be obtained.

The following sections review the results of the correction of meter readings for all five meters. Comparisons will then be made with the experimental results which were presented in Section 6.4 and 6.5.

7.4 Correction Results

This section presents a number of results showing the effects of individual meter corrections which are compared to the corresponding experimental data. Each diagram consists of: the "actual flow" (━) inferred from the calibrated EM meter signal superimposed onto the mean flow as given by the weigh tank; the "meter indicated flow" (—) inferred from turbine meter output signal; and the "corrected meter flow" (—) inferred from the corrected meter signal, using the methods described in the previous section. Individual data points are not shown as they may overlap each other.

It should be noted that with the exception of Meter D at low frequency, whilst the correction produces changes in the right direction, there are very significant difference between corrected and actual flows.

7.4.1 Meter A

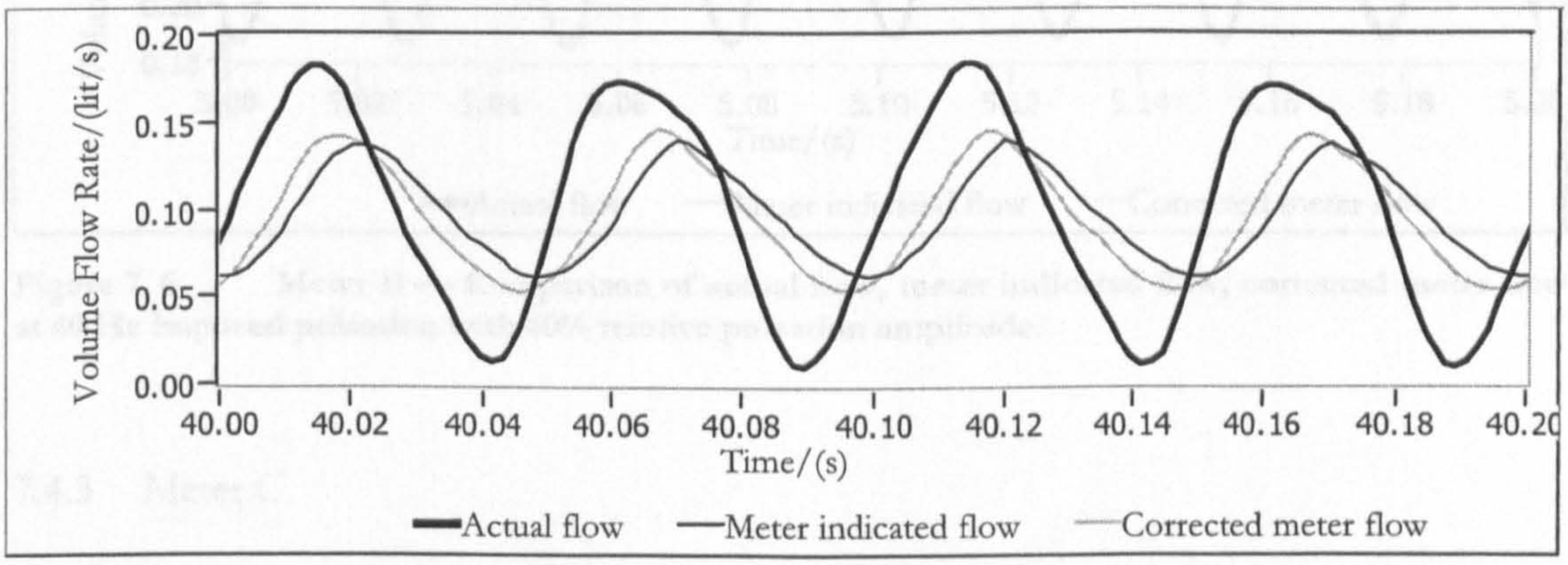

Figure 7. 4 Meter A — Comparison of actual flow, meter indicated flow, corrected meter flow at 20 Hz imposed pulsation with 90% relative pulsation amplitude.

7.4.2 Meter B

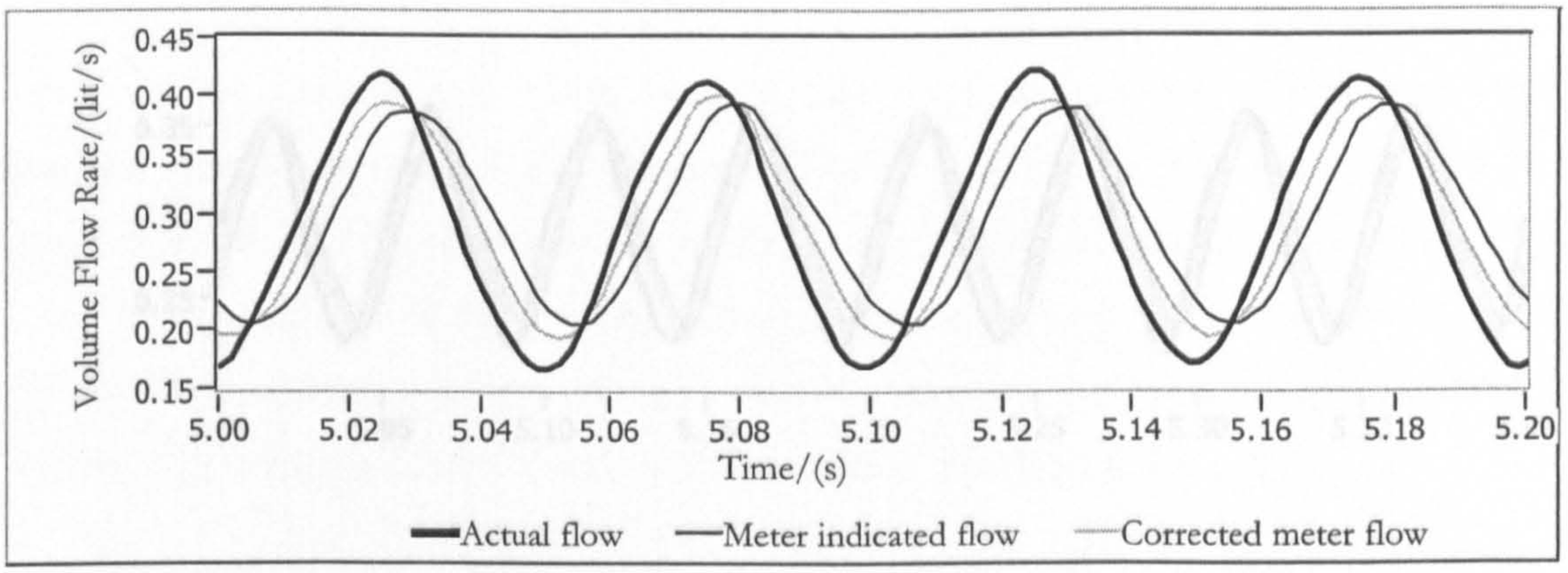

Figure 7. 5 Meter B — Comparison of actual flow, meter indicated flow, corrected meter flow at 20 Hz imposed pulsation with 40% relative pulsation amplitude.

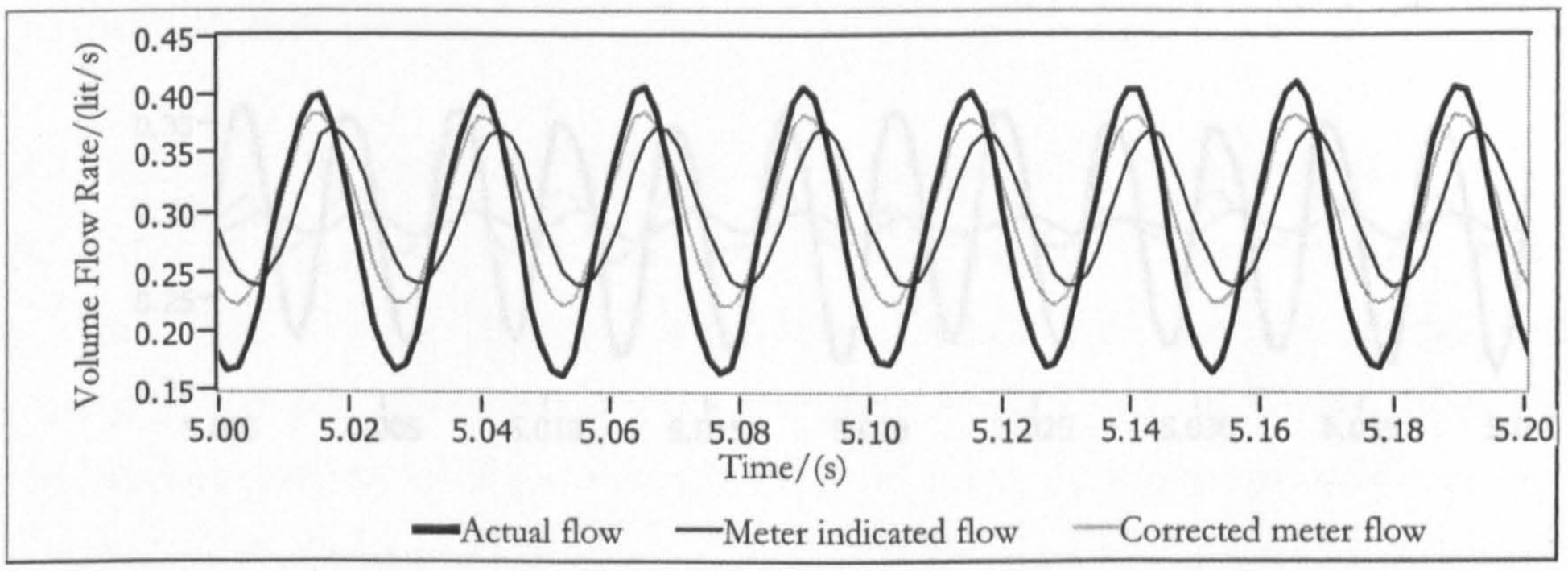

Figure 7. 6 Meter B — Comparison of actual flow, meter indicated flow, corrected meter flow at 40 Hz imposed pulsation with 40% relative pulsation amplitude.

7.4.3 Meter C

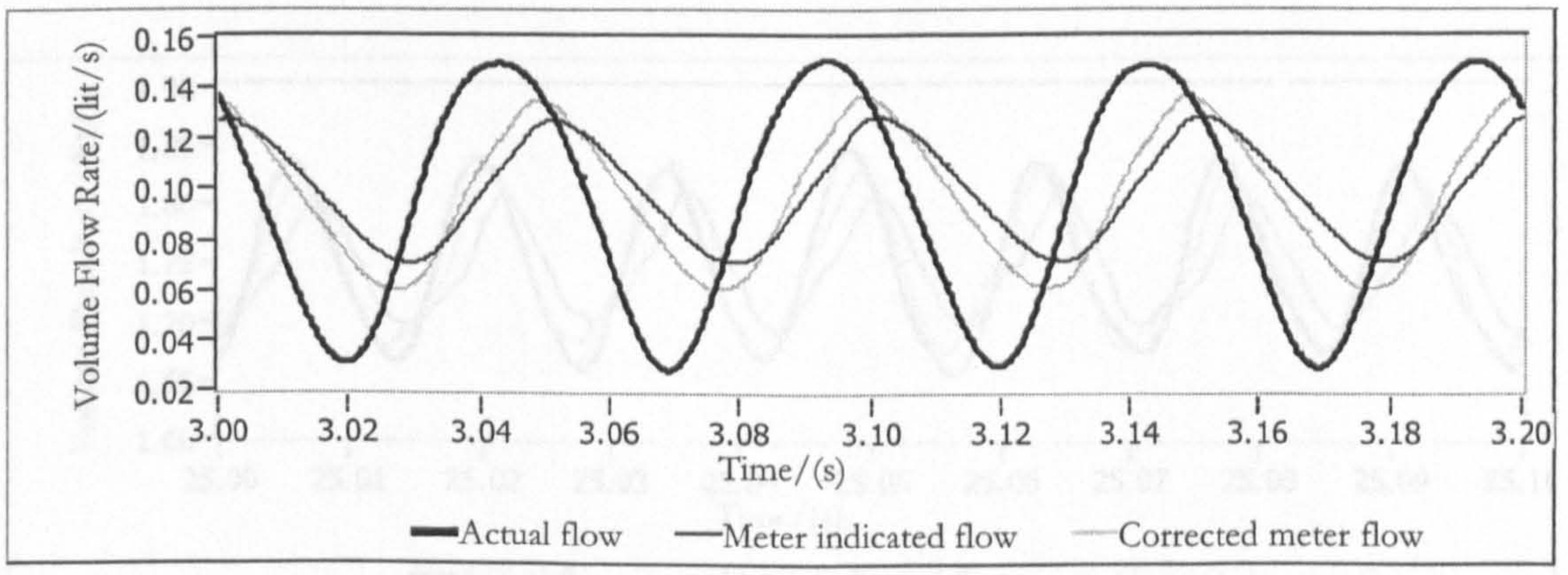

Figure 7. 7 Meter C — Comparison of actual flow, meter indicated flow, corrected meter flow at 20 Hz imposed pulsation with 65% relative pulsation amplitude.

7.4.4 Meter D

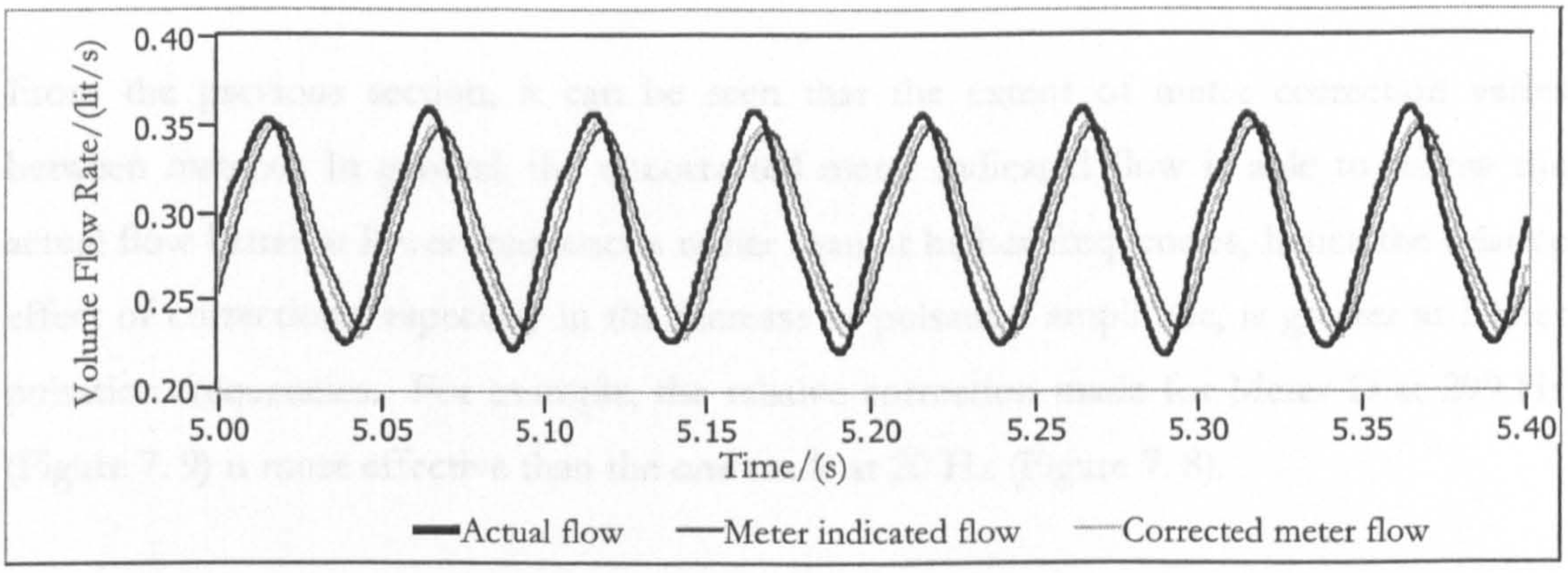

Figure 7. 8 Meter D — Comparison of actual flow, meter indicated flow, corrected meter flow at 20 Hz imposed pulsation with 23% relative pulsation amplitude.

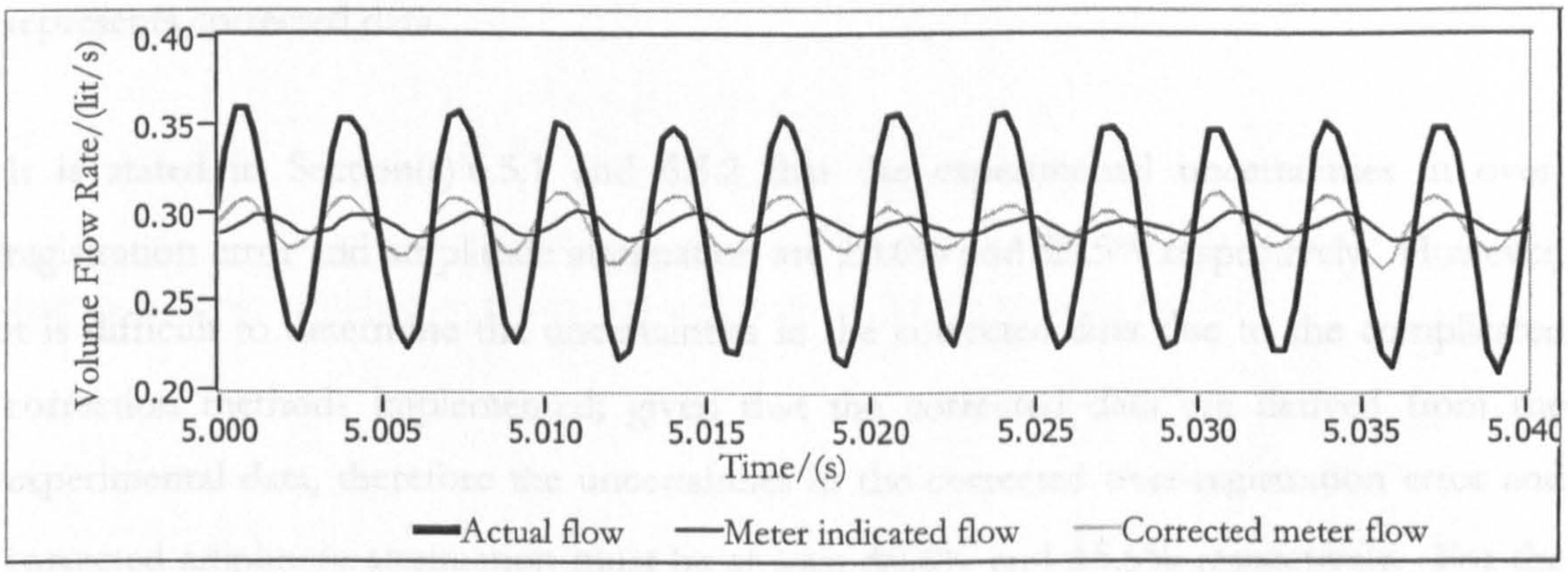

Figure 7. 9 Meter D — Comparison of actual flow, meter indicated flow, corrected meter flow at 299 Hz imposed pulsation with 22% relative pulsation amplitude.

7.4.5 Meter E

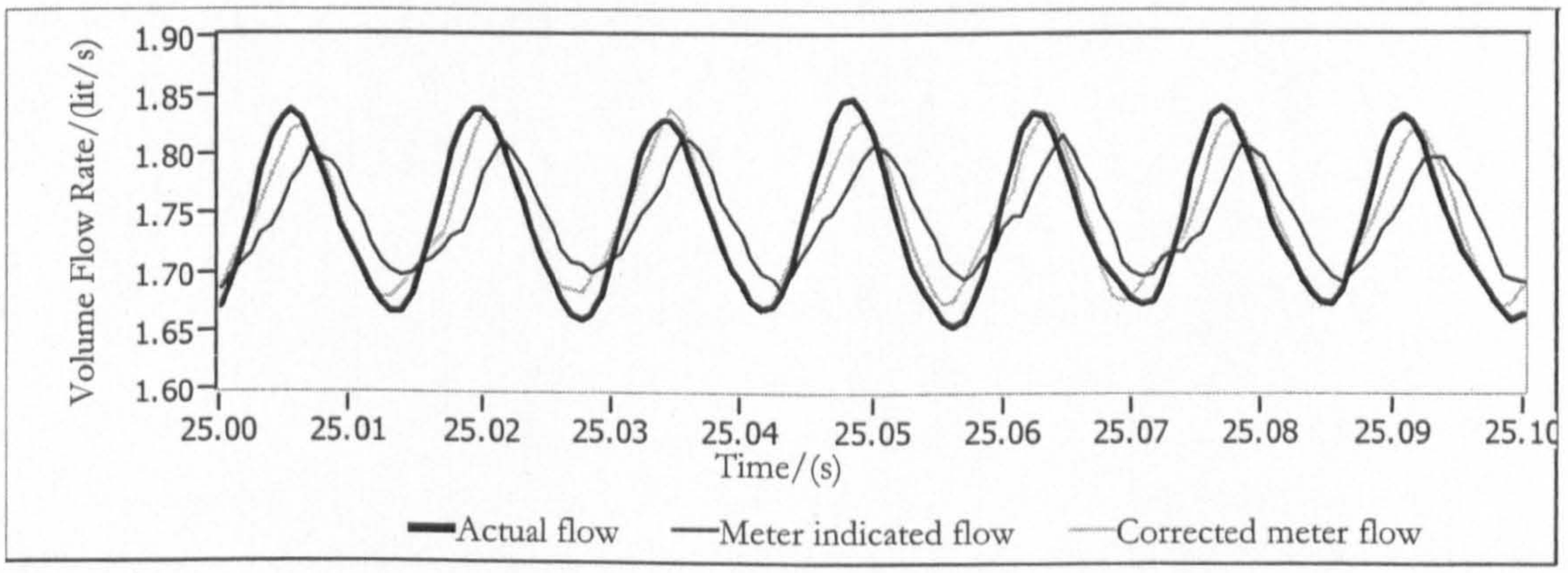

Figure 7. 10 Meter E — Comparison of actual flow, meter indicated flow, corrected meter flow at 70 Hz imposed pulsation with 5% relative pulsation amplitude.

7.5 Review of Meter Reading Corrections

From the previous section, it can be seen that the extent of meter correction varies between meters. In general, the uncorrected meter indicated flow is able to follow the actual flow better at lower frequencies rather than at higher frequencies, hence the relative effect of corrections, especially in the increase in pulsation amplitude, is greater at higher pulsation frequencies. For example, the relative correction made for Meter D at 299 Hz (Figure 7. 9) is more effective than the one made at 20 Hz (Figure 7. 8).

This section reviews the whole series of meter correction results for each meter (Figures 7. 11 to 7. 20). In each figure, the prefixes "E" represents experimental data and "C" represents corrected data.

It is stated in Section(s) 6.5.1 and 6.5.2 that the experimental uncertainties in over-registration error and amplitude attenuation are ±0.6% and ±5.5% respectively. However, it is difficult to determine the uncertainties in the corrected data due to the complicated correction methods implemented; given that the corrected data are derived from the experimental data, therefore the uncertainties in the corrected over-registration error and corrected amplitude attenuation must be at least ±0.6% and ±5.5% respectively. For the following figures, individual error bars are not included as data may overlap each other.

7.5.1 Correction of over-registration errors

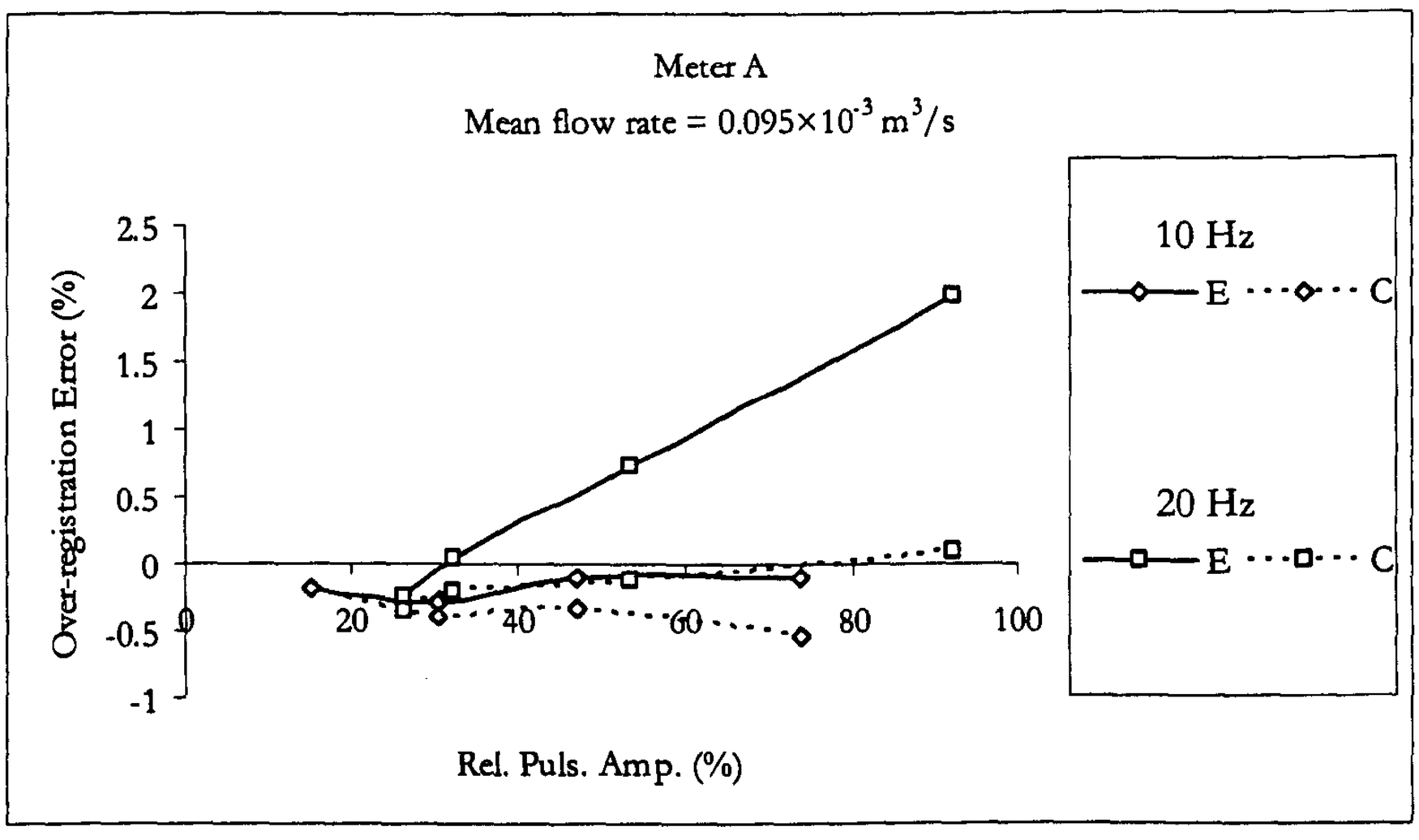

Figure 7. 11 Meter A – Correction of over-registration errors with differing pulsation amplitudes and two pulsation frequencies (for the experimental results shown in Figure 6. 32)

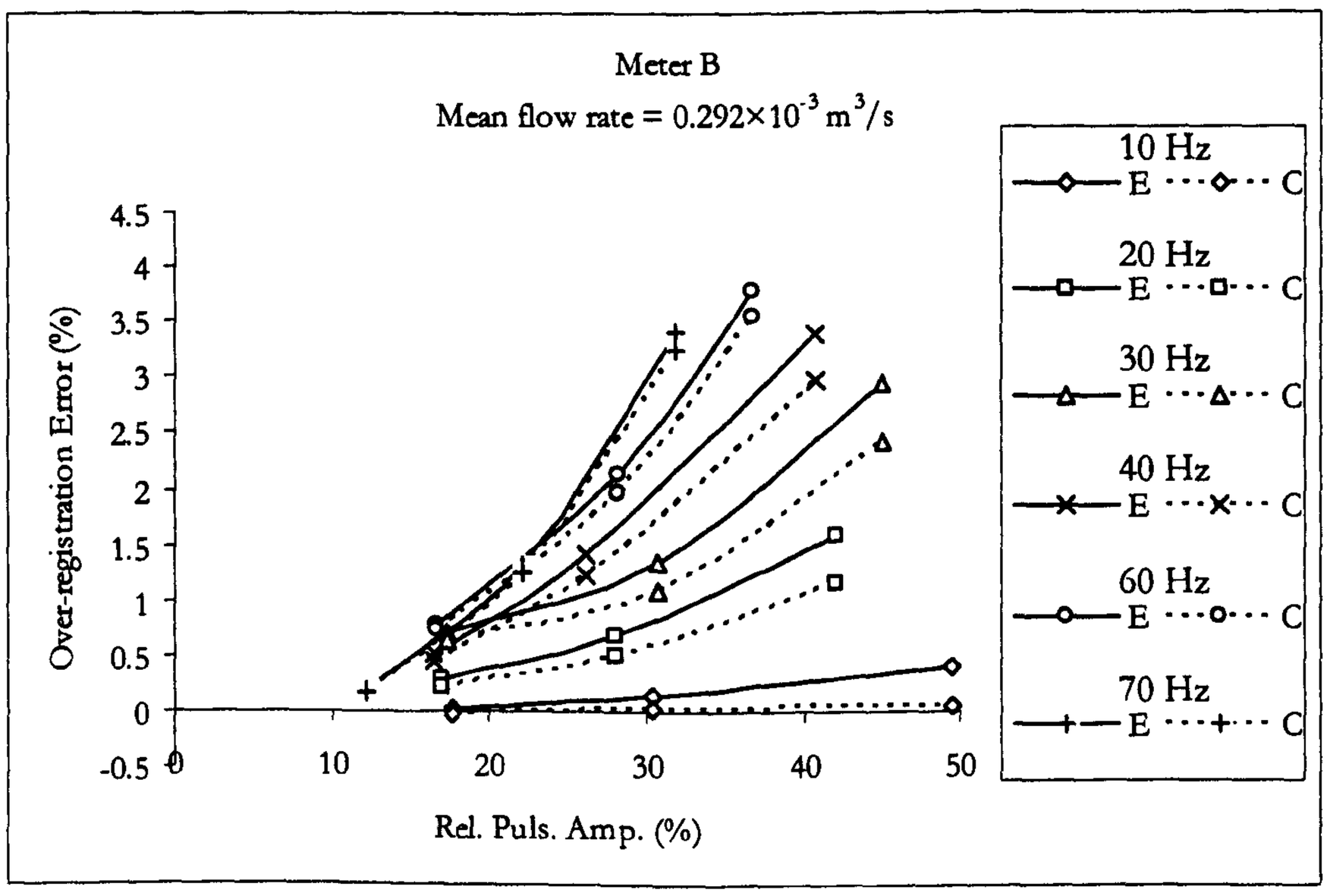

Figure 7. 12 Meter B – Correction of over-registration errors with differing pulsation amplitudes and pulsation frequencies (for experimental results shown in Figure 6. 33)

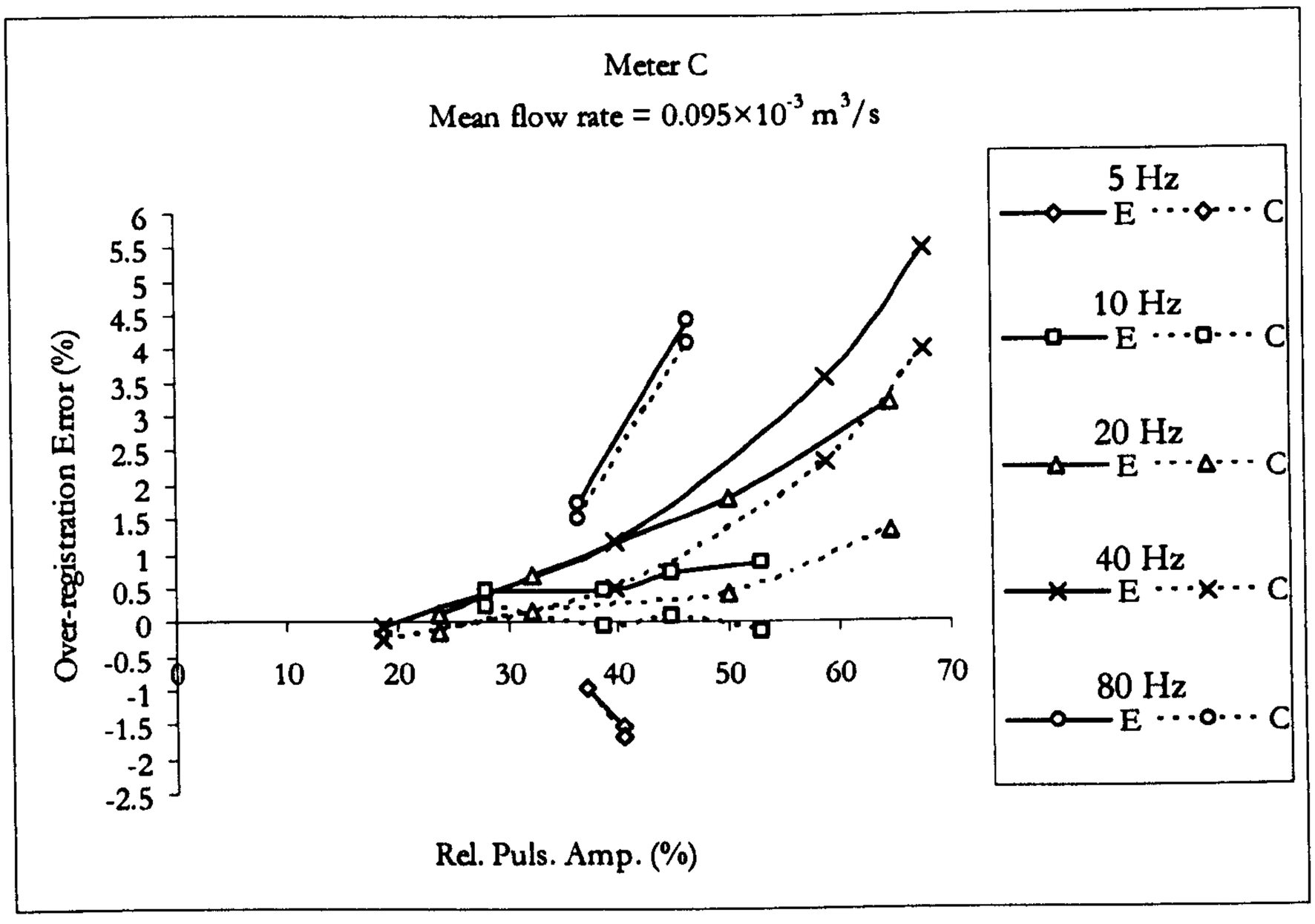

Figure 7. 13 Meter C — Correction of over-registration errors with differing pulsation amplitudes and pulsation frequencies (for experimental results shown in Figure 6. 34)

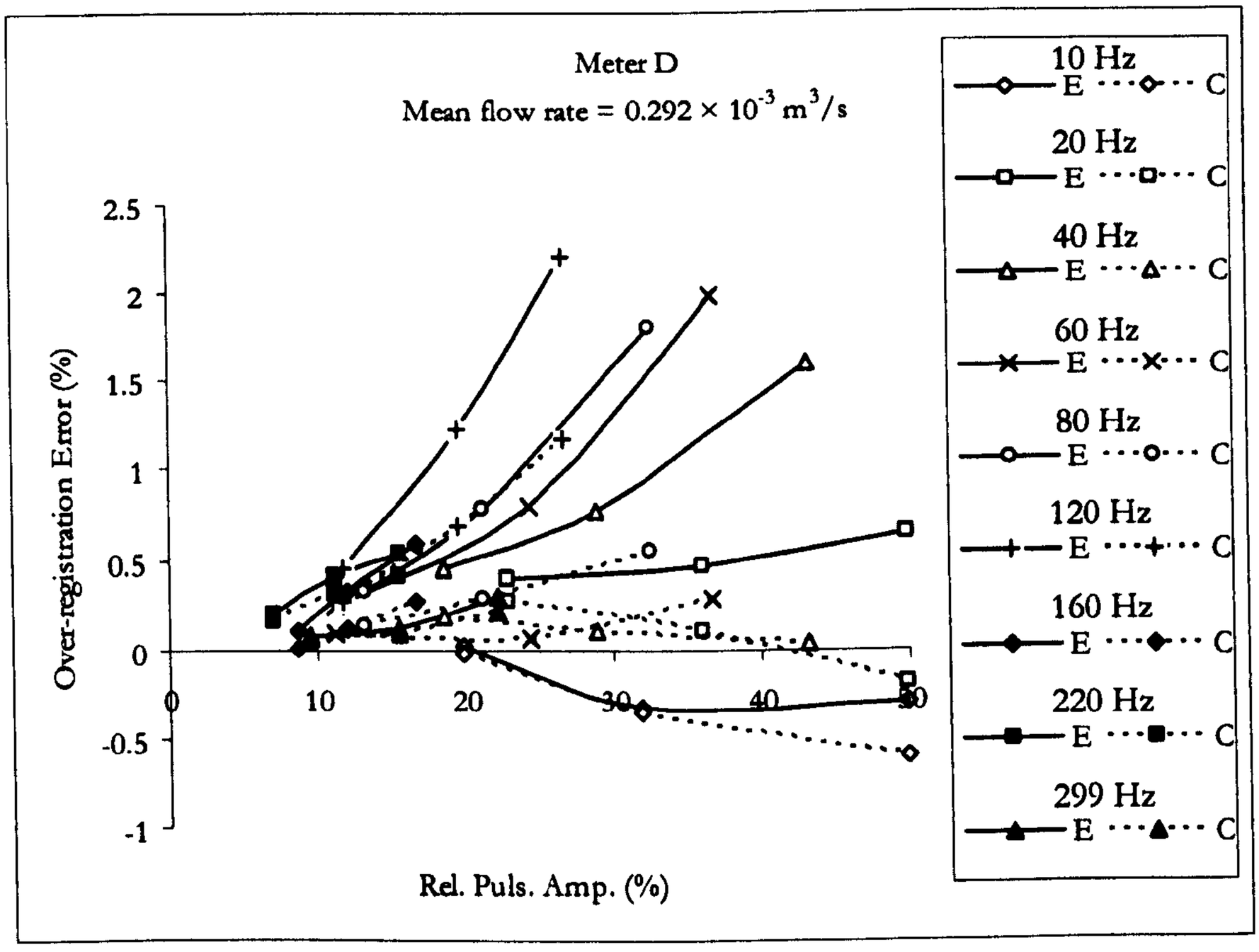

Figure 7. 14 Meter D — Correction of over-registration errors with differing pulsation amplitudes and pulsation frequencies (for experimental results shown in Figure 6. 35)

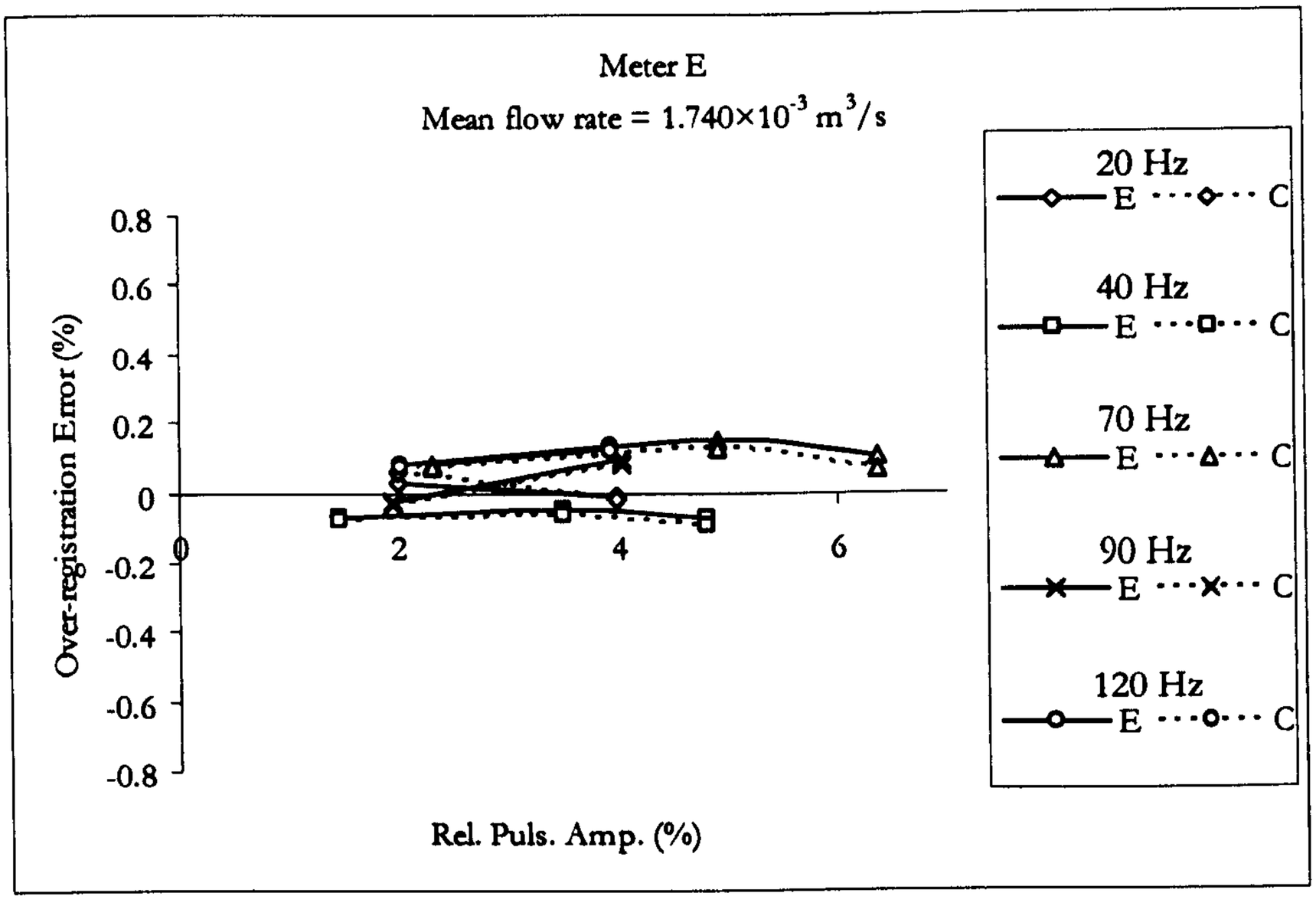

Figure 7. 15 Meter E — Correction of over-registration errors with differing pulsation amplitudes and pulsation frequencies (for experimental results shown in Figure 6. 36)

7.5.1.1 Comparisons of effectiveness of correction procedure on over-registration for "standard" pulsation cases

Similar to the presentation in Section 6.5.1.1, since there was a 20 Hz pulsation test for every meter, a comparison of reduction in over-registration errors can be made on all the meters at 20 Hz and it is shown in Figure 7.16.

At 20 Hz pulsation, it can be seen from Figure 7.16, depending upon the meter, that there are different levels of reduction in over-registration errors. Since the reductions achieved for meter E are negligible, meter E will be excluded from any comparison being made from Figure 7.16. The average relative reduction of individual meter over-registration errors is tabulated in Table 7.2. It can be seen from Table 7.2 that whilst meters A and C gained around 100% relative correction of over-registration errors, relative correction of meter D errors is 76%, but meter B resulted the least reduction of over-registration errors of 26%.

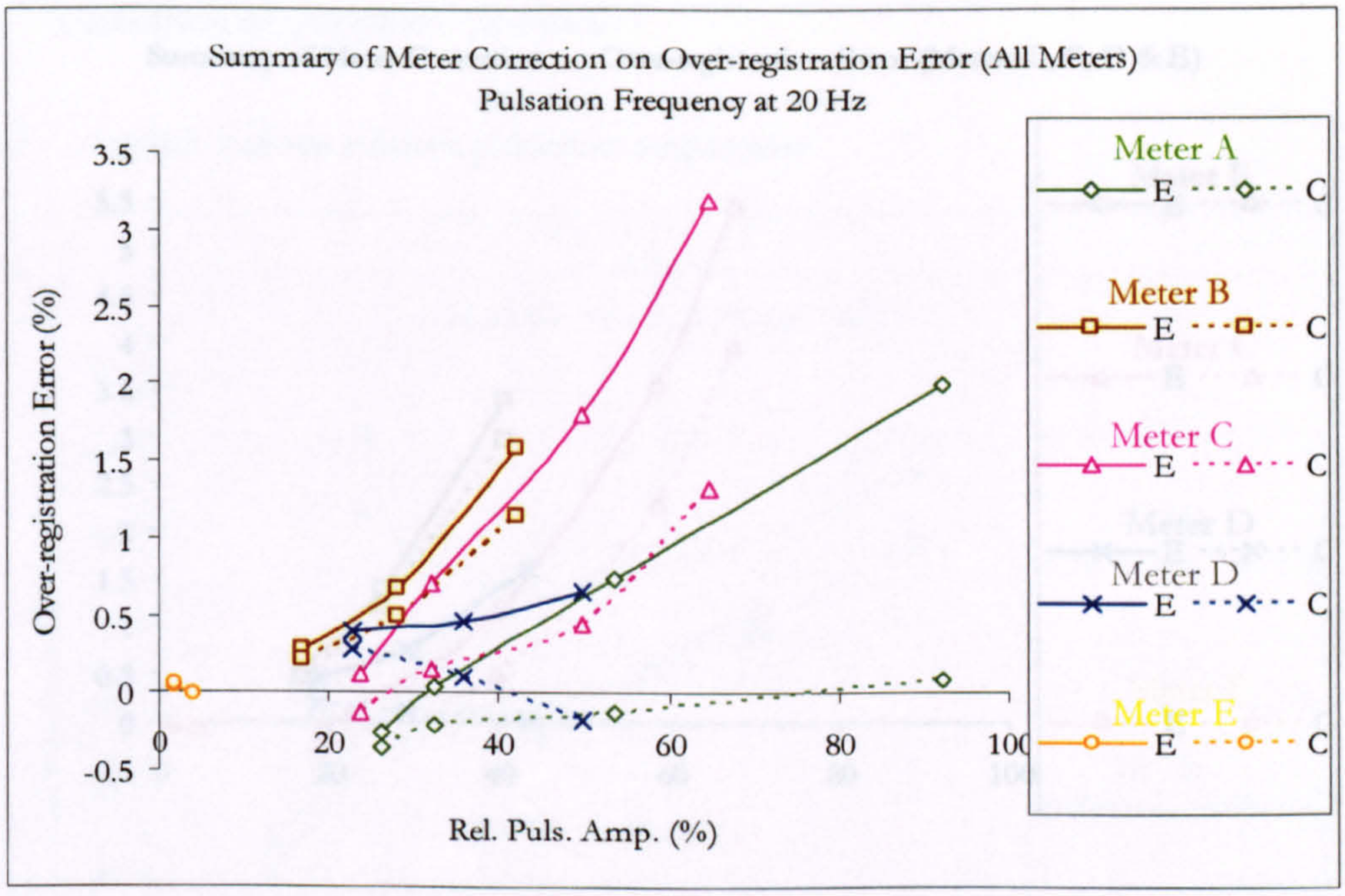

Figure 7. 16 A comparison of over-registration error for all meters at 20 Hz pulsation frequency with corrections (for experimental results shown in Figure 6. 40)

Meter	Average relative reduction of over-registration error (%) at 20 Hz
A	106
B	26
C	103
D	79
E	negligible reduction

Table 7. 2 Average relative reduction of over-registration error for meters at 20 Hz

On the other hand, by comparing the correction results at 40 Hz, another rank order can be observed (excluding meter A, not tested at 40 Hz). Figure 7.17 shows the results obtained for meters B, C, D and E. Again, since there are negligible errors resulted for meter E, this meter will be excluded from any comparison being made from Figure 7.17.

The average relative reduction of individual meter over-registration errors at 40 Hz is tabulated in Table 7.3. It can be seen that the relative reductions for meters B and C are almost half the values observed for 20 Hz (Table 7.2). However, the relative reduction for meter D error remains consistent with the one observed for 20 Hz.

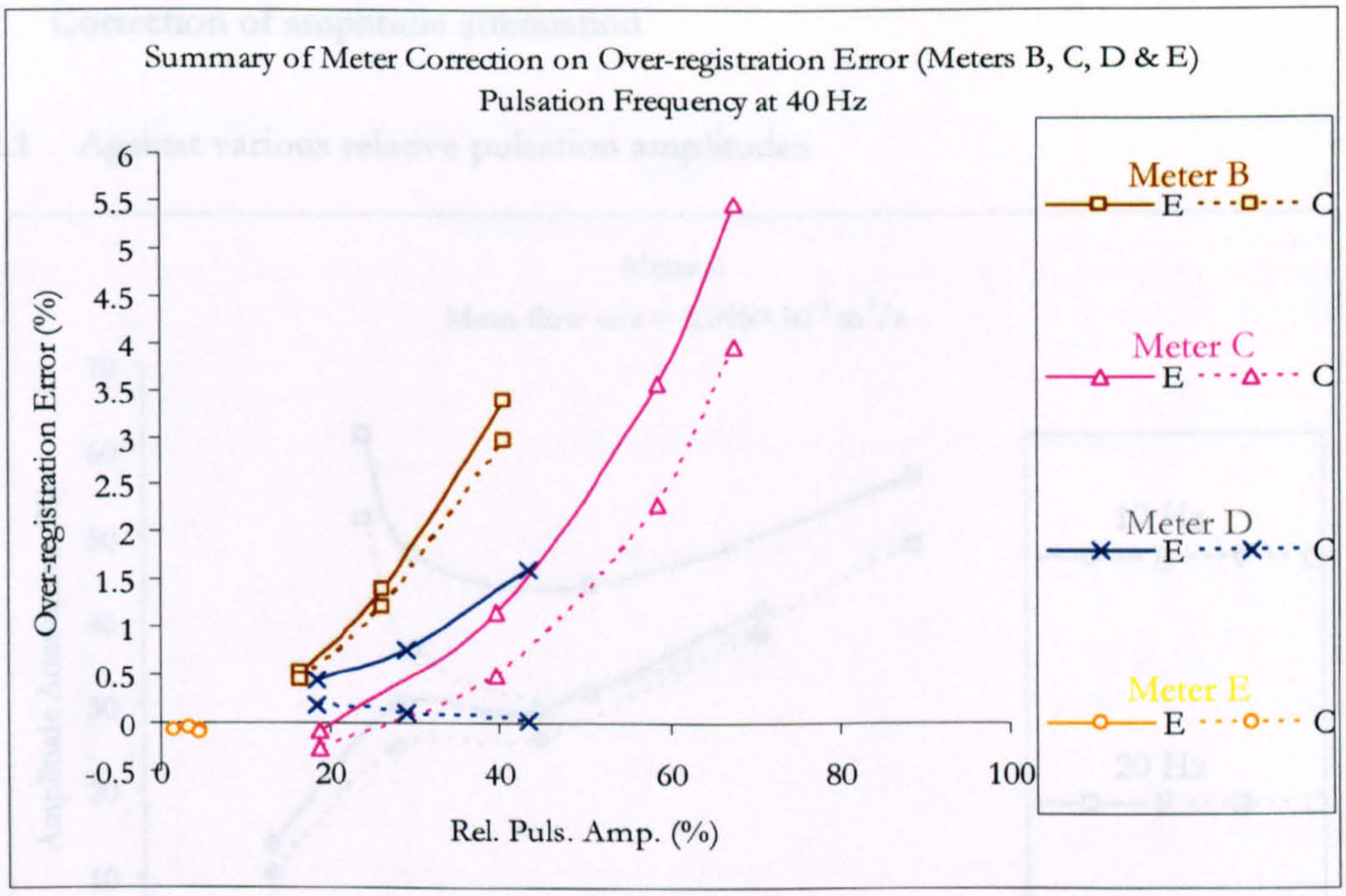

Figure 7. 17 A comparison of over-registration error for meters B, C, D and E at 40 Hz pulsation frequency with corrections (for experimental results shown in Figure 6. 41)

Meter	Average relative reduction of over-registration error (%) at 40 Hz
B	13
C	40
D	81
E	negligible reduction

Table 7. 3 Average relative reduction of over-registration error for meters at 40 Hz

7.5.2 Correction of amplitude attenuation

7.5.2.1 Against various relative pulsation amplitudes

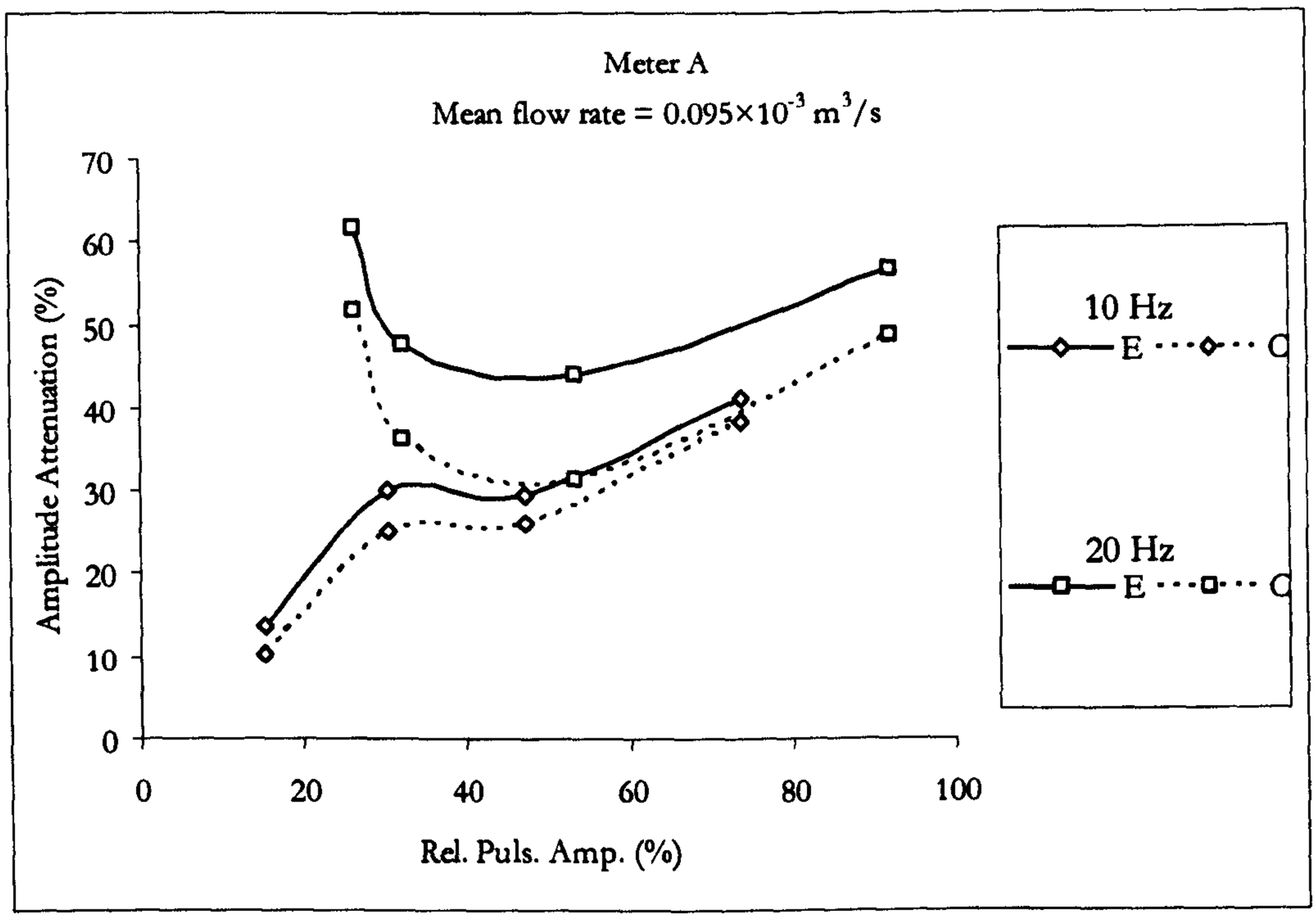

Figure 7. 18 Meter A – Correction of amplitude attenuations with differing pulsation amplitudes and pulsation frequencies (for experimental results shown in Figure 6. 42)

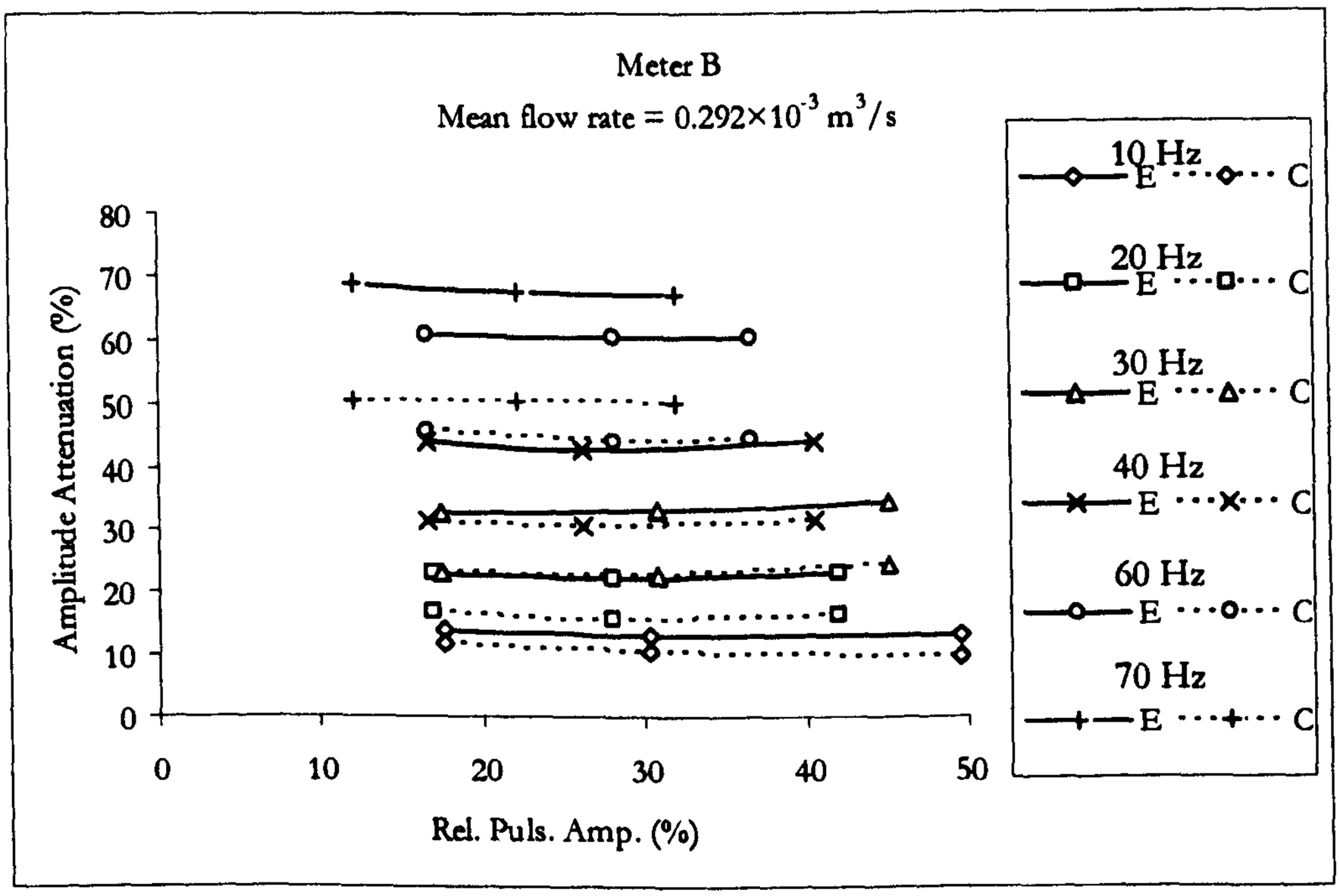

Figure 7. 19 Meter B – Correction of amplitude attenuations with differing pulsation amplitudes and pulsation frequencies (for experimental results shown in Figure 6. 43)

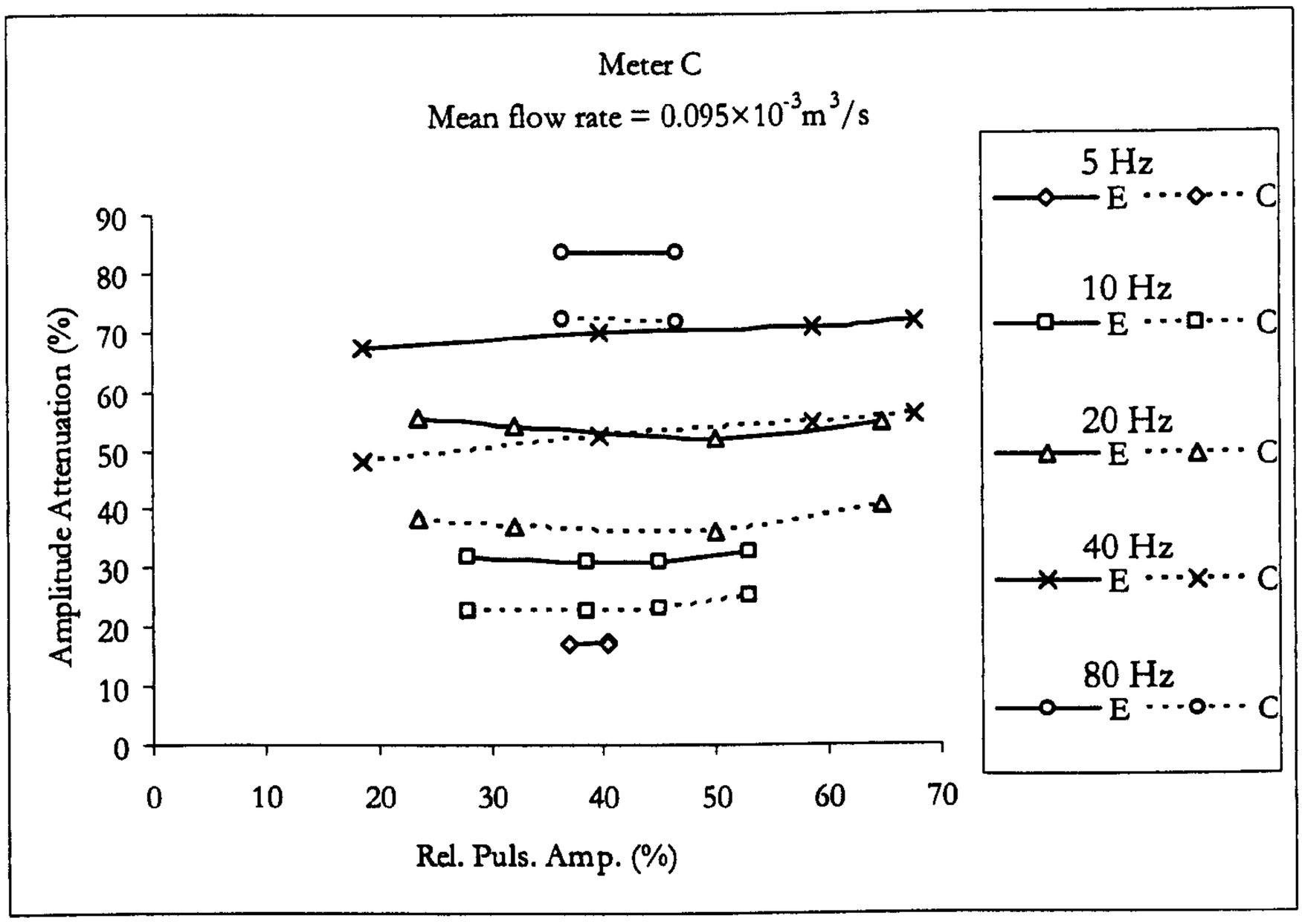

Figure 7. 20 Meter C — Correction of amplitude attenuations with differing pulsation amplitudes and pulsation frequencies (for experimental results shown in Figure 6. 44)

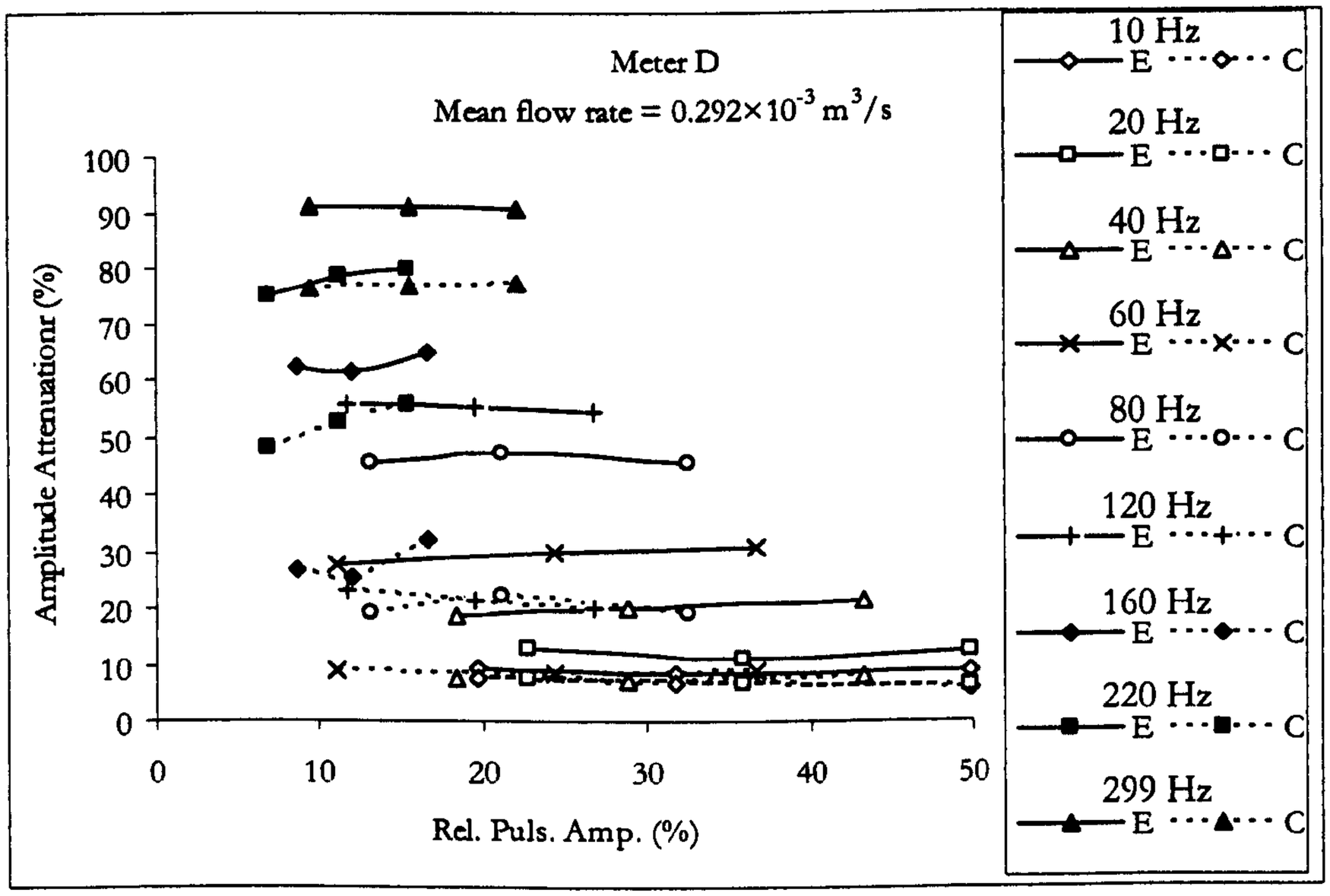

Figure 7. 21 Meter D — Correction of amplitude attenuations with differing pulsation amplitudes and pulsation frequencies (for experimental results shown in Figure 6. 45)

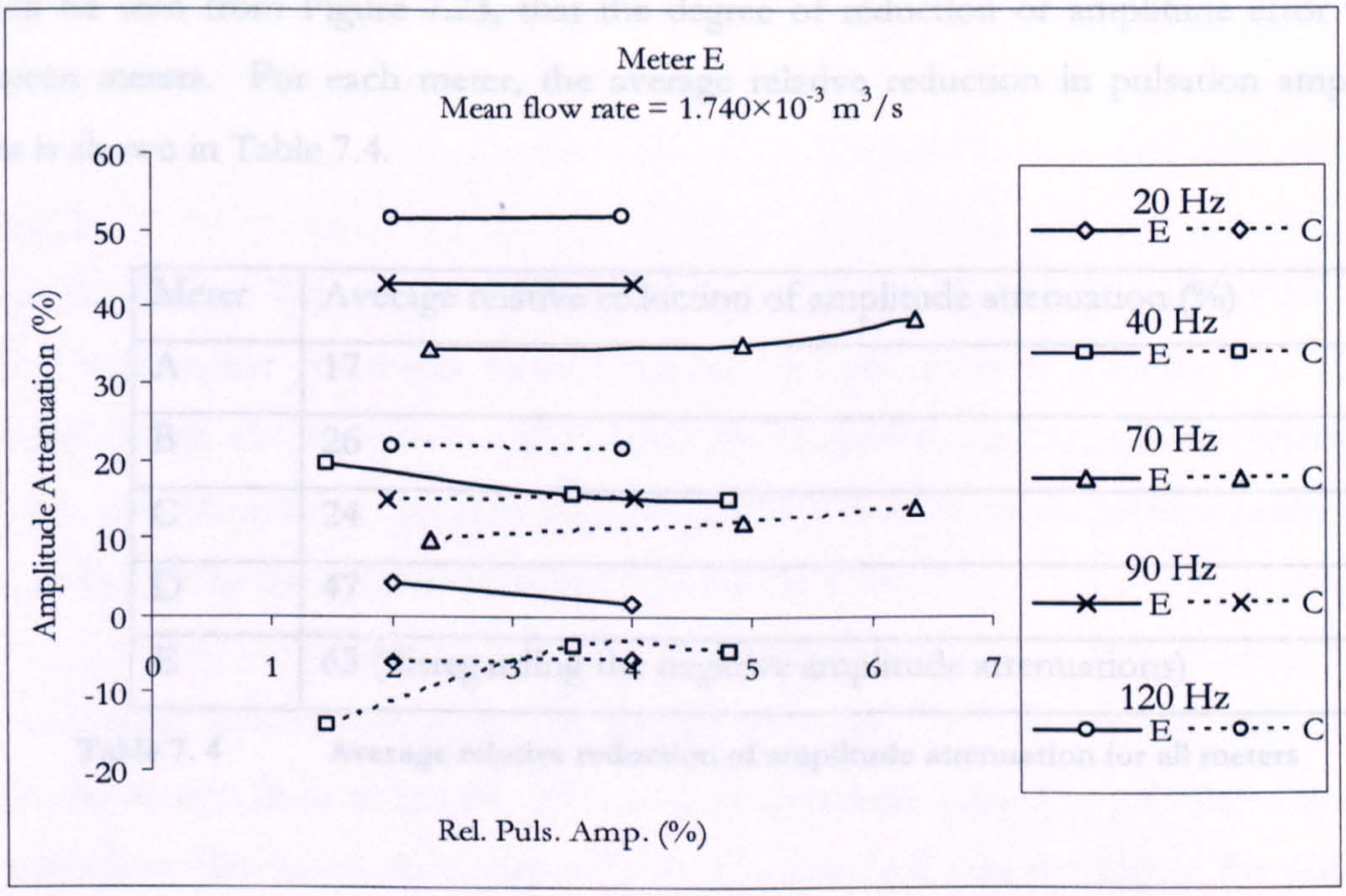

Figure 7. 22 Meter E — Correction of amplitude attenuations with differing pulsation amplitudes and pulsation frequencies (for experimental results shown in Figure 6. 46)

7.5.2.2 Comparison of effectiveness of correction procedure on amplitude attenuation for "standard" pulsation cases

The amplitude attenuation is strongly dependent on pulsation frequency as shown previously in Section 6.5.2.3, Figure 6.55; this allows an alternative view of the reductions for amplitude errors using the experimental results shown in Figure 7.23.

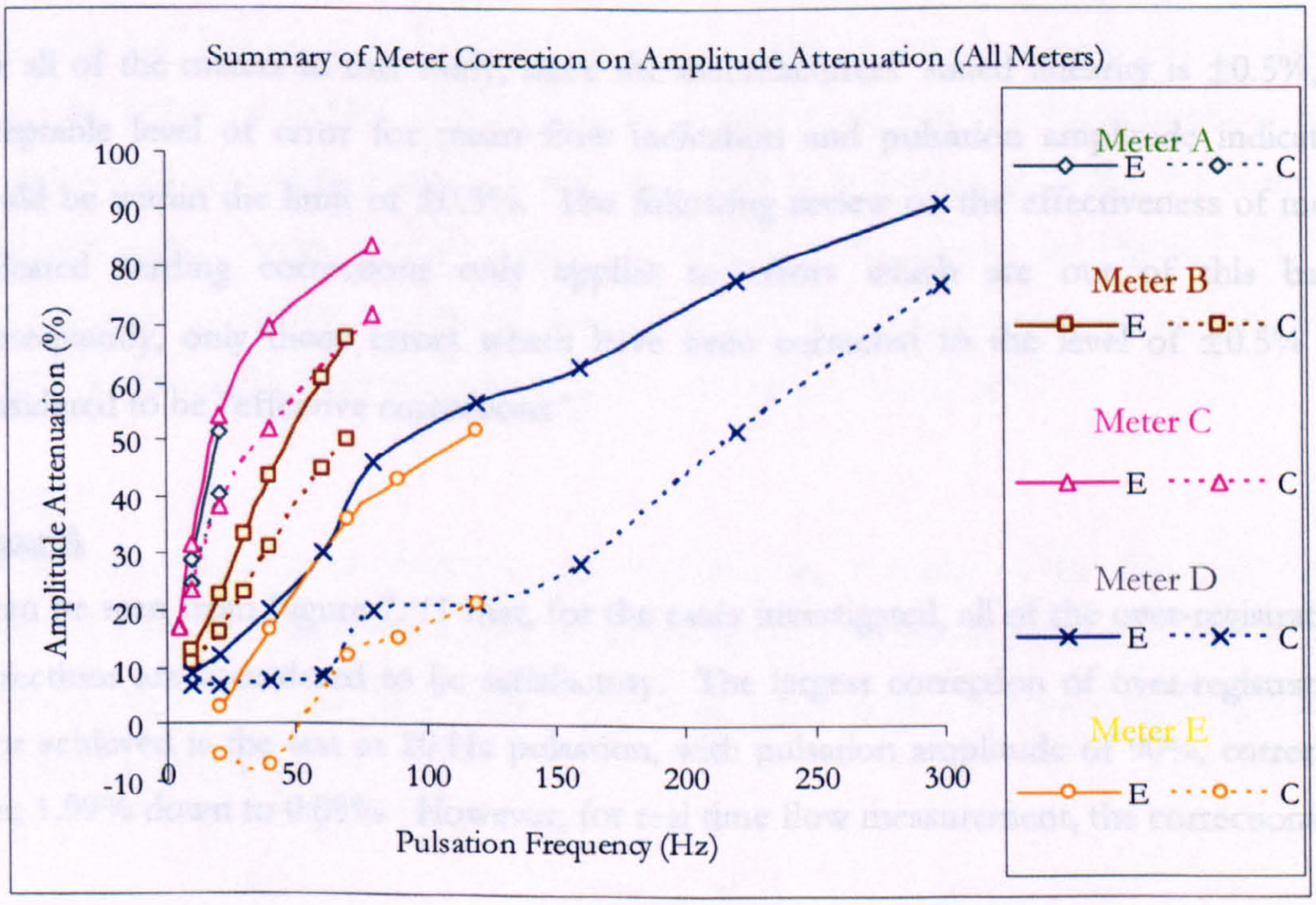

Figure 7. 23 A comparison of amplitude attenuation vs pulsation frequency for all meters

It can be seen from Figure 7.23, that the degree of reduction of amplitude error varies between meters. For each meter, the average relative reduction in pulsation amplitude error is shown in Table 7.4.

Meter	Average relative reduction of amplitude attenuation (%)
A	17
B	26
C	24
D	47
E	63 (disregarding the negative amplitude attenuations)

Table 7. 4 Average relative reduction of amplitude attenuation for all meters

7.5.3 General observations

It can be observed that the over-registration errors are reduced by the correction procedure. However, for the majority of cases, especially for meter B, the corrected values are still above the manufacturer's stated linearity of ±0.5%. It can also be observed that the errors in pulsation amplitude are reduced; however, following use of the correction procedure, the errors still remain relatively large.

For all of the meters in this study, since the manufacturers' stated linearity is ±0.5%, an acceptable level of error for mean flow indication and pulsation amplitude indication would be within the limit of ±0.5%. The following review on the effectiveness of meter indicated reading corrections only applies to errors which are out of this band. Subsequently, only those errors which have been corrected to the level of ±0.5% are considered to be "effective corrections".

Meter A

It can be seen from Figure 7. 11 that, for the cases investigated, all of the over-registration corrections are considered to be satisfactory. The largest correction of over-registration error achieved is the test at 20 Hz pulsation, with pulsation amplitude of 90%, corrected from 1.99% down to 0.08%. However, for real time flow measurement, the corrections of

amplitude attenuation are not that significantly effective. As seen from Table 7. 4, the relative reduction of amplitude attenuation is only 17%.

Meter B

It is observed from Figure 7. 12 that the majority of corrected mean flow values are above 0.5%, therefore the correction method applied on this meter is considered to be not effective. It can also be seen that the higher the frequency, the less relative correction is resulted. For example, as shown in Tables 7. 2 and 7. 3, at 20 Hz the relative correction is 26%, and at 40 Hz the relative correction is halved to 13%.

For real time flow measurement, as shown in Table 7. 4, the relative reduction of amplitude attenuation is only 26% and that the corrections applied to pulsation amplitude are inefficient. However, from Figure 7. 19, it is observed that the higher the pulsation frequency, the more the relative correction can be resulted. For instance, the amplitude attenuations at 60 Hz have been improved from 60% to 45% generally, that is equivalent to a relative increase of pulsation amplitude of 25%; whilst at 10 Hz, the amplitude attenuations have been improved from 13% to 11% generally, and this represents to a relative increase of pulsation amplitude of 15%.

Meter C

It can be seen from Figure 7. 13 that satisfactory corrections in over-registration errors are achievable for cases up to 40 Hz when the imposed relative pulsation amplitudes are below 50%. As shown in Tables 7.2 and 7.3, the relative reduction of over-registration error decreases with increasing frequency, and for pulsation frequency at 80 Hz, the corrected over-registration errors remain almost unchanged. As shown in Figure 7. 23, the corrections for pulsation amplitude attenuation are not adequate enough; as seen from Table 7. 4, the relative reduction of amplitude attenuation is only 24%.

Meter D

Overall, corrections were acceptable (Figure 7. 14); the majority of the over-registration errors are reduced within the region of ±0.5% apart from the 120 Hz cases above 20% pulsation amplitude and the relative corrections seem to be consistent with increasing pulsation frequency.

For real time flow measurement, it is observed from Figure 7. 23 that the corrections applied to pulsation amplitude are inefficient. However, disregard the comparison with meter E due to the relative low imposed pulsation amplitude applied during experimentation, meter D has the most relative reduction in amplitude error amongst meters A, B, C and D (as shown in Table 7.4).

Meter E

Since all of the mean flow errors are within the limit of ±0.5% for the cases investigated, the review on corrections of mean flow reading is not necessary. For amplitude attenuation, it is observed from Table 7.4 that meter E has the most relative reduction amongst other meters.